Атомная
энергия

Number 4, 1956

The Soviet Journal of

ATOMIC ENERGY

IN ENGLISH TRANSLATION

CONSULTANTS BUREAU, INC.

227 WEST 17TH STREET, NEW YORK 11, N. Y.

ATOMNAYA ENERGIYA

Academy of Sciences of the USSR

Number 4, 1956

The Soviet Journal

of

ATOMIC ENERGY

IN ENGLISH TRANSLATION

CONSULTANTS BUREAU, INC.
227 West 17th Street
New York 11, N. Y.

Printed in the United States

Annual Subscription $ 75.00
Single Issue 20.00

THE SIX-METER SYNCHROCYCLOTRON OF THE INSTITUTE OF NUCLEAR PROBLEMS, ACADEMY OF SCIENCES USSR*

D. V. Efremov, M. G. Meshcheryakov, A. L. Mints, V. P. Dzhelepov, P. P. Ivanov, V. S. Katyshev,** E. G. Komar, I. F. Malyshev, N. A. Monoszon, I. Kh. Nevyazhsky, B. I. Polyakov, A. V. Chesinoi

The chief characteristics of the six-meter synchrocyclotron of the Institute of Nuclear Problems of the Academy of Sciences, USSR, which provides proton acceleration to an energy of 680 Mev, are described.

INTRODUCTION

The construction of powerful high-energy accelerators for heavy particles became feasible with the announcement by V. I. Veksler (1944) and McMillan (1945) of the phase stability principle in connection with particle motion in cyclic resonance accelerators.

In order to further research in the physics of high-energy particles and gain experience in synchrocyclotron acceleration techniques a large five-meter synchrocyclotron was built at the Institute for Nuclear Problems of the Academy of Sciences, USSR; using this machine it was possible to accelerate deuterons to an energy of 280 Mev and α-particles to an energy of 560 Mev. In 1950, protons with an energy of 500 Mev were obtained with this machine [1-3]. The construction of the accelerator was preceded by studies on a working model which clarified a number of questions connected with the start-up and operation [4].

Studies of the operation of this machine and experience acquired in carrying out research with it made it possible in 1953 to modify the accelerator so that it became feasible to accelerate protons to an energy of 680 Mev. The average current in the outermost orbit in this operation was 0.3 μamp. A general view of the six-meter synchrocyclotron is shown in Fig. 1.

In rebuilding the machine a new vacuum system was installed, the diameter of the pole-pieces of the electromagnet was increased to six meters and a new radio-frequency resonance system was developed. The six-meter synchrocyclotron provides intense beams of positive and negative π-mesons with energies up to 400 Mev and neutrons with energies up to 600 Mev. By making certain minor changes in some of the components of the radio-frequency system in this machine it is also possible to obtain deuterons with energies of 420 Mev and α-particles with energies up to 840 Mev [5], [6].

The Electromagnet

It is well known that the stable motion of ions in the gap of an electromagnet is limited to the region in which the index denoting the decay of the magnetic field intensity in the radial direction

$$n = \frac{d \ln H}{d \ln R} < 0.2,$$

*Reported at the All-Union Conference on the Physics of High-Energy Particles, May 14, 1956.

**Deceased.

so that for n = 0.2 there is observed a parametric resonance between the free vertical and radial oscillations of the ions being accelerated.

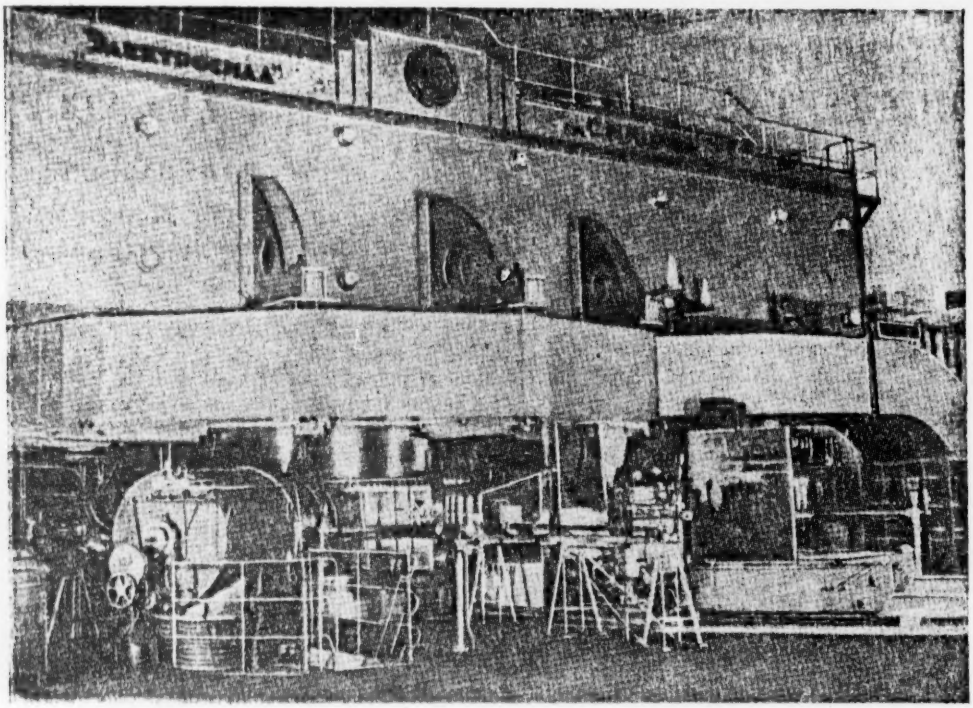

Fig. 1. General view of the accelerator.

In actual accelerators, because of the limitation of the vertical dimension of the aperture of the dee, the region in which parametric resonance may arise determines the maximum radius of the region of magnetic field in which the acceleration of ions is feasible. This was kept in mind in designing so as to obtain the largest possible stable orbits for the accelerated ions.

In the five-meter magnet the pole tips were fabricated from soft iron in the form of solid discs. The pole tips now in use, which are six meters in diameter, are welded together from several pieces.

The pole tips simultaneously serve as the upper and lower walls of the vacuum chamber located in the gap between the poles of the magnet. The gap space between the pole tips at the center of the chamber is 600 mm. The magnetic field intensity at the center of the vacuum chamber is 16,600 gauss. The length of the electromagnet is 18 m, height about 10 m and weight 7,000 tons. The yoke was made from ordinary carbon steel. The exciting winding of the electromagnet consisted of air cooled copper straps. The direct-current generator required to obtain the nominal field intensity had a power rating of 1000 kw. The current in the exciting winding was stabilized to within ± 0.1 %.

A great deal of laborious computational and experimental work was devoted to the magnetic field corrections in the acceleration region. In addition to the use of shims at the periphery of the pole pieces a great deal of effort was made to insure the coincidence of the surface at which the radial component of the magnetic field was zero with the median plane of the acceleration chamber.

In carrying out the work on the correction of the magnetic field configuration it was found necessary to develop apparatus suitable for accurate magnetic measurements; an instrument for measuring the decay of the magnetic field in the radial direction [1], an instrument for determining the azimuthal asymmetry of the magnetic field [7], and apparatus for determining the location of the surface at which the radial component of the magnetic field vanishes.

As a result of these studies and the corrections of the magnetic field of the six-meter synchrocyclotron the radius of the region in which stable motion of the accelerated ions could be guaranteed reached a value of 279 cm.

The machine also had a number of auxiliary non-symmetrical exciting windings fed from a separate generator thus making it possible, while the machine was in operation, to vary the location of the plane containing the trajectory of the accelerated particles; this feature was used in determining the optimum operating conditions.*

The decay of the magnetic field intensity in the radial direction from the center out to the limiting radius needed for focusing the particles in the vertical plane was 4.9%. The displacement of the center of the outermost orbit did not exceed 2 cm. Careful adjustment of the magnetic field of the accelerator made it possible to accelerate protons to an energy of 680 Mev [8]. To enhance ion focusing in the initial acceleration stage steel cones were placed at the center of the pole tips.

Means were also provided for relatively fast changes of the polarity of the electromagnet (15 min) thus making it easy to get an output of π^+ or π^- mesons of various energies through the collimators in the apertures in magnet supports.

Resonance System and Radio-Frequency Generator [9]

The design of the rf system for this machine was dictated by the necessity of obtaining an accelerating voltage of some 15 kv and a frequency change from 26.5 to 13.6 mc for proton acceleration. In this connection it is necessary that the metal rotor of the variable condenser, which determines the frequency, be located in a region of weak magnetic field in order to avoid high eddy currents. On the other hand the removal of the rotor to a location at which the leakage field of the magnet is weak is undesirable because it is impossible to keep the system compact. Therefore extensive precautions were taken to see that the variable condenser, which was located at a point at which the field intensity is 600-800 gauss, is well shielded magnetically. Inside the shield the field intensity is no greater than 30 gauss. It turned out, however, that under these conditions the distance from the center of the pole pieces to the variable condenser is approximately equal to a half-wavelength at the high-frequency end of the operating region. Thus to tune up the system in this region it was necessary to raise the upper resonance frequency both by changing the wave impedance and by constructional changes which resulted in a slight increase of the current paths in the system. The expansion of the operating range on the low frequency side was accomplished by increasing the wave impedance of the system in the immediate neighborhood of the variable condenser. This part of the system can be considered a "lumped" inductance.

The radio-frequency resonance system consists of the dee with its grounded frame, the variable condenser and the line which connects them. Close to the variable condenser the latter assumes the form of a coaxial line; it is connected to the dee through a smooth transition section (Fig. 2).

The rotor of the variable condenser, which consists of 6 discs with 10 fins in each is braced against the inner conductor of the coaxial line by insulators and is electrically connected to it by a semicylindrical (6 pairs of cylinders) condenser with a capacity of 20,000 μf. The shaft and rotor are held firmly by metal bearing-supports which are located radially at the center of gravity of the system. To keep the reactance of the supports high over a wide range of frequencies they are made in the form of cylindrical spirals, i. e. chokes; these are fabricated from special hollow steel tubing which is water cooled and copper-plated to reduce the radio-frequency resistance. The inductance of these bearing supports is in parallel with the line and increases the upper frequency of the operating range to some extent.

The present design provides a wide range of operating frequencies with relatively small values of current and voltage in the variable condenser. It has been feasible to use an accelerating voltage amplitude of more than 15 kv and an accelerating-cycle repetition rate of about 100 cps.

The semicylindrical condenser effectively shunts the ball bearings of the rotor and its contact brush which is a slotted bronze collar which rides on the steel shaft of the rotor. Although the peak current through the condenser reaches 3,000 amp the current through the bearing and contact brush does not exceed 100 amp. The

*The control of the location of the plane also made it possible to reduce smoothly by a factor of several thousand the intensity of the external proton beam; this was necessary in order to carry out several physics experiments.

apparatus has been operated without any trouble for more than 10,000 hours without replacement of bearings.

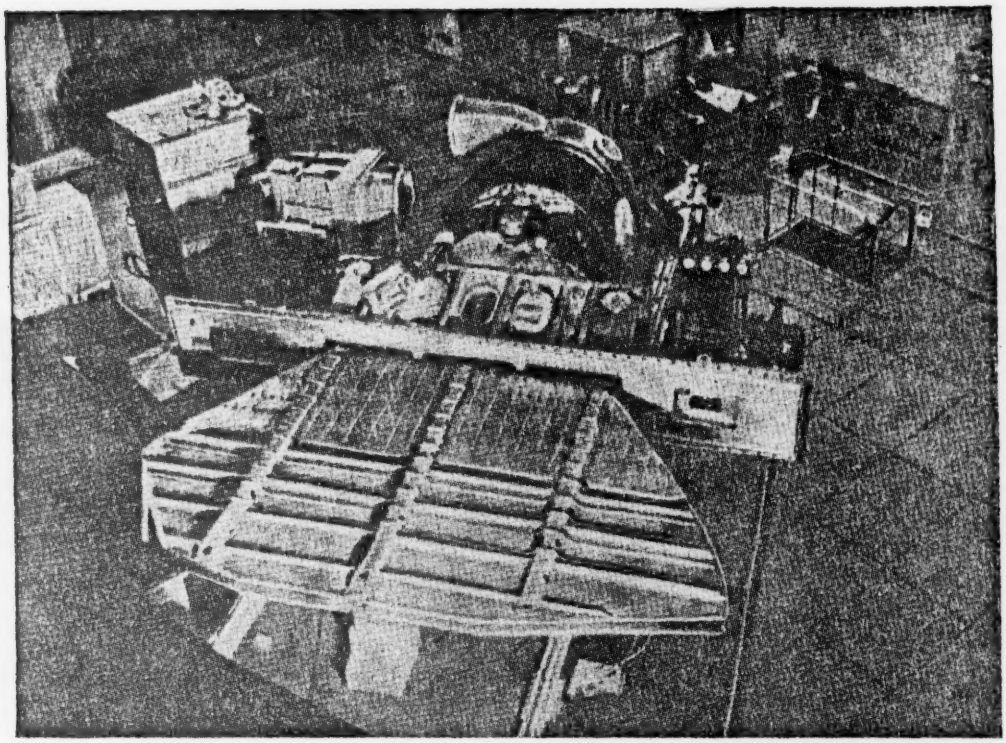

Fig. 2. The dee removed from the vacuum chamber.

The rotor design permits the capacity of the resonance system of the radio-frequency generator to be varied and gives optimum values of the system impedance over a wide range of frequencies.

Parasitic oscillations were virtually suppressed by using a "band-pass" oscillator system in which positive feedback occurs only in a specified frequency region; this system allows wide, independent control of the absolute magnitude of the positive feedback in the extreme high and low frequency regions. The system makes use of a series of LC circuits between the plate and the cathode input and between the input grids and cathode of two ultrahigh frequency oscillator triodes (GU-12A) which are of the grounded type and also employs output inductances, interelectrode condensers, and cathode chokes.

The operation of the resonance system and the radio-frequency generator have been described in a separate report [6].

The radio-frequency system can be cut off during the non-operating part of the cycle by a thyratron unit which controls the grid of the oscillator [9]. The system can be operated so that the acceleration cycle is controlled by a frequency which is several times smaller than the modulation frequency; it is also possible to obtain single acceleration pulses, thus allowing the system to trigger a Wilson cloud chamber or some other detection device. All modes of operation are controlled by a special timer unit [10] which maintains strict time sequence between the pulses which trigger the ion source, the thyratron control system and the other components. Use of the timer also makes it possible to synchronize the operation of the accelerator with that of other instruments and devices being used in the various nuclear research projects. All the counting sequences are controlled by the frequency-change cycle of the radio-frequency oscillator which drives the resonance system. The switching of the radio-frequency voltage during each cycle is accomplished by means of a photoelectric system in which a light beam incident on a photoelectron multiplier is interrupted by the fins on the rotor of the variable condenser.

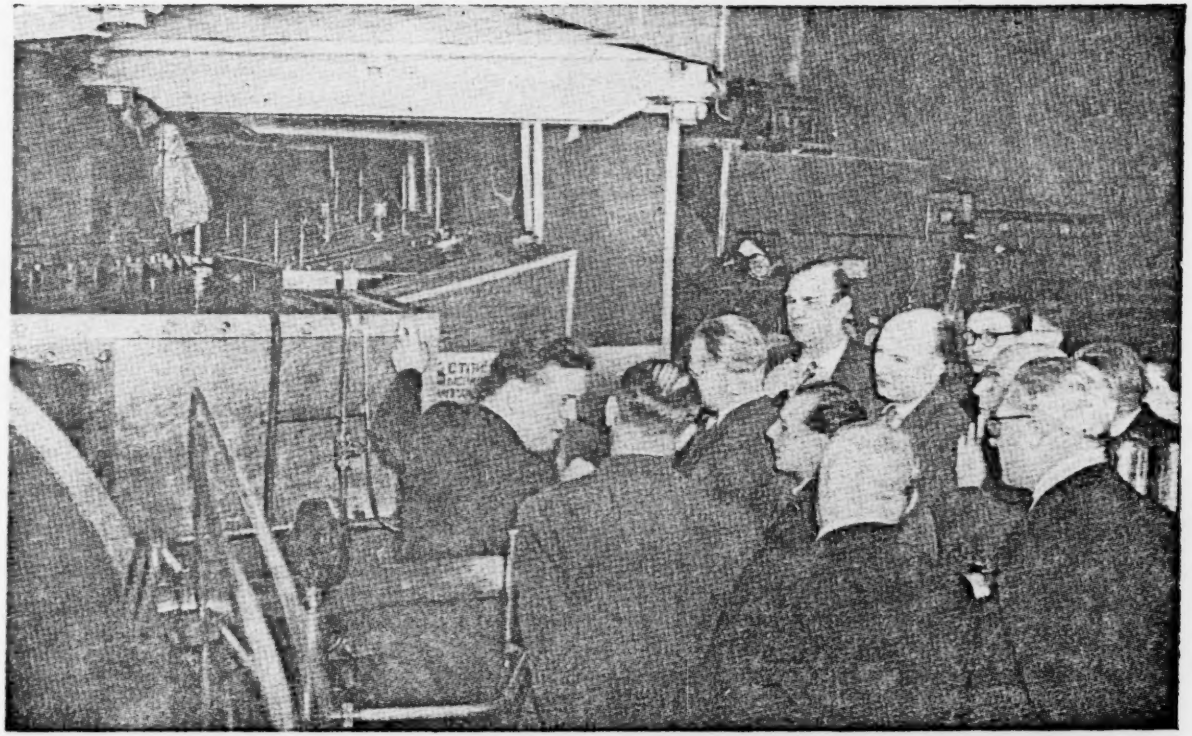

Members of the International Conference on the Organization of an Eastern Institute of Nuclear Research at the Academy of Sciences USSR examine the 680 Mev synchrocyclotron (March 1956).

Vacuum System

The operating stability of the accelerator as well as the intensity of the accelerated ion beam at the output are determined to a large degree by the vacuum conditions in the volume of the chamber and frequency varying device. The accelerator vacuum chamber has the form of a rectangular parallelepiped 675 x 675 x 100 cm^3.

This chamber is built from brass plates 100 mm in thickness. The steel top and bottom of the chamber also serve as the pole tips. The vacuum seal between the brass plates of the chamber and the pole pieces, as in the other vacuum apparatus, is achieved by means of rubber gaskets.

Following appropriate conditioning of the chamber the minimum pressure of the residual gas is $2 \cdot 10^{-6}$ mm Hg. With the introduction into the ion source of the working gas the pressure does not exceed $6\text{-}7 \cdot 10^{-6}$ mm Hg. The volumes of the chamber, the resonance line and the variable condenser are contiguous. The total volume in which a high vacuum is maintained is about 35 m^3. The vacuum chamber is evacuated by two oil-jet pumps with a total capacity of 80,000 liters per second at a pressure of $1 \cdot 10^{-5}$ mm Hg. The housing of the variable condenser is evacuated by an auxilary pump with a capacity of 10,000 liters/sec at a pressure of $1 \cdot 10^{-5}$ mm Hg. The baffles of the high vacuum pumps are cooled to a temperature of $-20°$ C to freeze out the oil vapors.

The quality of the vacuum gaskets is such that under normal conditions the increase in the chamber pressure which arises due to the leakage of air from the outside and outgassing from the inner surfaces amounts to 0.2-0.3 mk/hour.* If a preliminary vacuum of the order of 10^{-3} mm Hg is maintained in the chamber then the operating vacuum for the conditioned accelerator can be reached in 25-30 min after opening the vacuum valves on the oil-jet pumps.

The vacuum chamber of the accelerator is provided with various devices which are used to introduce targets into the chamber and to locate them at a given radius. This operation is carried out remotely without disturbing the operating vacuum in the chamber.

Ion Source and Particle Extraction

The ion source in the six-meter synchrocyclotron is the usual arc type with a thermal tungsten cathode. A cold cathode was also used quite successfully. In this case a considerably greater stability in the magnitude of the ion current is achieved at normal intensities. In the cold cathode source the discharge is excited by the radio-frequency field in the dee by secondary electron emission from an aluminum or beryllium cathode.

Extraction of the proton beam from the vacuum chamber into the external region is accomplished by excitation of radial oscillations of the accelerated particles in the outermost orbit and the ejections of protons through a magnetic channel [11]. The ion current in the external beam is 5-7% of the current in the circulating beam. A large of number of beams of neutrons and charged π-mesons of both sign is also extracted. The extraction of each beam is accomplished by means of special devices located in the accelerator. A separate report [12] is devoted to information on the extraction of particle beams from the vacuum chamber.

Arrangement of the Accelerator Facilities

All the accelerator facilities are located in two buildings. The first building contains the equipment which cannot be separated from the accelerator by any appreciable distance if efficient operation is to be achieved. In this building there is a laboratory with experimental and monitoring apparatus which is used in research on the external particle beams.

In order to provide the most favorable conditions for carrying out research with the accelerator the control room of the accelerator is isolated from the main laboratory by two concrete shielding walls with thicknesses of 4 and 2 m and a ceiling 1.5 m thick. The passage of the particle beams through the 4-meter wall which separates the accelerator room from the measurement enclosure is allowed by a porthole with collimators (Fig. 3).

The electric power facilities and the water cooling installation for the resonance system and the radio-frequency generator, and the control console for all circuits and components of the accelerator are located in the second building.

*[Probably equals 10^{-6} mm Hg/hour.—Translators note].

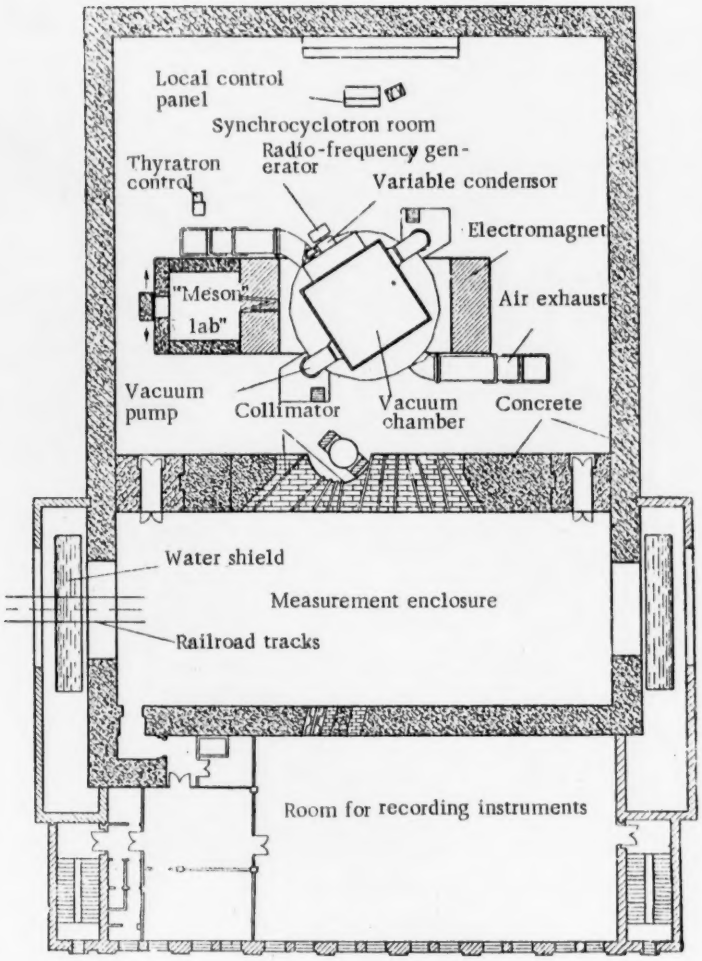

Fig. 3. Plan of the six-meter synchrocyclotron building.

Control of the Synchrocyclotron

Because of the radiation which accompanies the operation of the machine the presence of personnel in the main room in the immediate vicinity of the accelerator is not possible. The monitoring functions involved in the operation of the machine and the control of the facilities are carried out remotely by the attending engineer and technician who remain in a room containing the control console in the second building (Fig. 4). For this purpose there are provided a number of instruments and devices which permit automatic remote control of the facilites.

The synchrocyclotron and its facilities have operated without trouble for many thousands of hours without requiring any significant shutdown for repairs or modification.

Main Trends of Nuclear Research

In the research which is being carried on at the synchrocyclotron of the Institute of Nuclear Problems of the Academy of Sciences USSR most attention is being devoted to the nucleon energy region 380-660 Mev and

to the following three types of nuclear processes: the elastic scattering of protons by protons, neutrons by protons, and neutrons by neutrons; the production of charged and neutral π-mesons in nucleon-nucleon collisions, and the interaction of π-mesons with nucleons. Experimental investigations are also being devoted to a study of the interaction of nucleons and π-mesons with nuclei. A discussion of these investigations is beyond the scope of the present report and is to be found in appropriate papers.

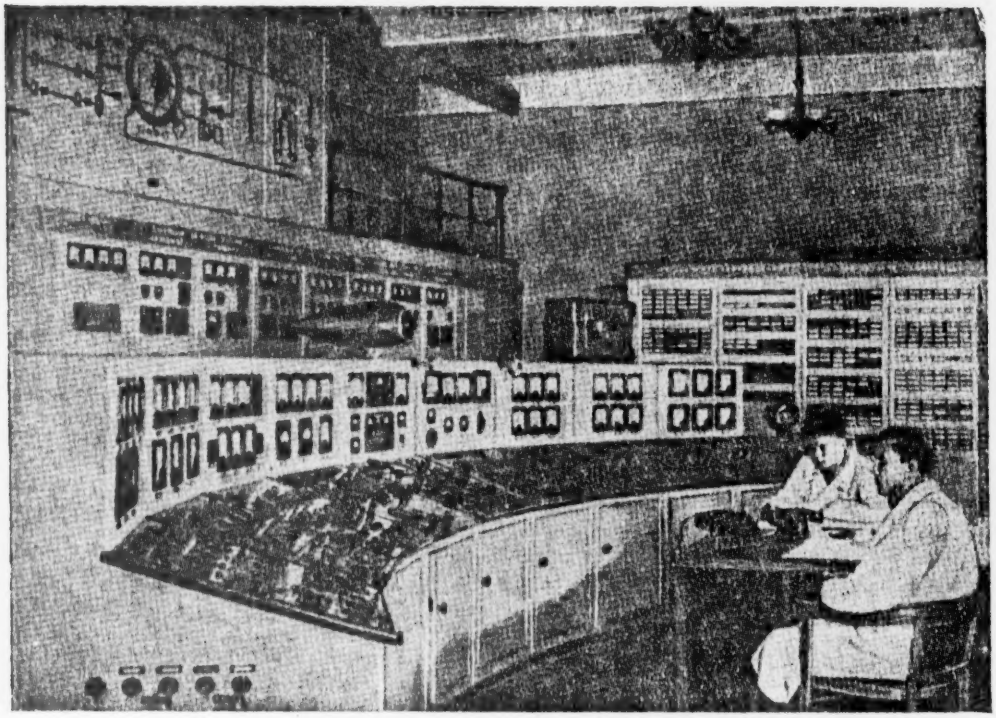

Fig. 4. Main control console.

SUMMARY

At the synchrocyclotron of the Institute of Nuclear Problems, which at the present time is the largest machine of its type in the world, research in the energy region up to 700 Mev is being carried on by many physics and chemistry institutes of the Academy of Sciences USSR.

The accelerator is operated regularly from 100-105 hours per week. It is possible to carry out research on 13 external beams of protons, neutrons, and π-mesons of high energy.

The construction of this accelerator is the result of the combined efforts over a number of years of a large group of scientists, engineers, and technicians. Many plants participated in the construction of these facilities, particularly manufacturers of electrical equipment.

The design and development of the various components of the six-meter synchrocyclotron involved a good deal of research in the realms of physics, radio-engineering, electronics, power engineering and vacuum techniques. As a result of this research it has been possible to avoid a great deal of the difficulties involved in the start-up operation, although certain of these remained and were overcome in the initial operating stages.

It is apparent that the synchrocyclotron acceleration technique is extremely convenient in this region of particle energy. The experience acquired in operating actual synchrocyclotrons and calculations which have been made indicate that the upper limit on the energy for this method of accelerating protons is approximately 1,000 Mev.

LITERATURE CITED

[1] M. G. Meshcheryakov, A. V. Chestnoi, V. P. Dzhelepov, V. S. Katyshev, A. A. Kropin, V. P. Dmitrievsky, et al. (Report Inst. Nuc. Prob., Acad. Sci. USSR) (1951).

[2] L. M. Gurevich, N. K. Kaminsky, I. G. Klyatskin, I. Kh. Nevyazhsky, B. I. Polyakov, N. K. Titov, and V. F. Trubetskoi (Rep. RAL . Acad. Sci. USSR) (1947-1950).

[3] D. V. Efremov, E. G. Komar, and N. A. Monoszon (Report NIIEFA) (1950).

[4] M. G. Meshcheryakov, G. I. Budker, V. P. Dmitrievsky, V. S. Katyshev, A. A. Kropin, and A. V. Chestnoi, et al. (Report Inst. Nuc. Prob., Acad. Sci. USSR) (1947-1949).

[5] M. G. Meshcheryakov, A. V. Chestnoi, V. P. Dzhelepov, V. S. Katyshev, M. F. Shulga, and V. T. Dmitrievsky (Report Inst. Nuc. Prob., Acad. Sci. USSR) (1954).

[6] A. L. Mints, I. Kh. Nevyazhsky, and B. I. Polyakov, Certain Characteristics and Information Concerning the Radio Frequency System of the Six-Meter Synchrocyclotron (Report to the All-Union Conference on the Physics of High Energy Particles) (Moscow, 1956).

[7] M. P. Zeldovich, and S. M. Rubchinsky (Report RAL Acad. Sci. USSR) (1949).

[8] A. V. Chestnoi, V. S. Katyshev, V. P. Dmitrievsky, A. A. Kropin, B. I. Zamolodchikov, T. N. Tomilina, and V. B. Mukhina (Report Inst. Nuc. Prob., Acad. Sci. USSR) (1953).

[9] A. D. Vlasov, G. P. Grudinskaya, G. I. Zhileiko, B. T. Zarubin, B. G. Kulman, V. M. Lupulov, I. Kh. Nevyazhsky, and B. I. Polyakov (Report RAL Acad. Sci. USSR) (1948-1955).

[10] M. M. Veisbein, G. I. Kiryanov , and A. K. Kotlyakov (Report RAL Acad. Sci. USSR) (1954).

[11] V. P. Dmitrievsky, V. I. Danilov, Yu. N. Denisov, V. S. Katyshev, A. A. Kropin, and A. V. Chestnoi, Extraction of the Proton Beam from the Six-Meter Synchrocyclotron (Report to the All-Union Conference on the Physics of High-Energy Particles) (Moscow, 1956).

[12] V. P. Dzhelepov, V. P. Dmitrievsky, V. S. Katyshev, M. S. Kozodaev, M. G. Meshcheryakov, K. I. Tarakanov, and A. V. Chestnoi, The High-Energy Particle Beam from the Six-Meter Synchrocyclotron and its Utilization (Report to the All-Union Conference on the Physics of High-Energy Particles) (Moscow, 1956).

Received May 29, 1956.

HIGH ENERGY PARTICLES FROM THE SIX-METER SYNCHROCYCLOTRON AND THEIR UTILIZATION*

(REVIEW ARTICLE)

V. P. Dzhelepov, V. P. Dmitrievsky, V. S. Katyshev,** M. S. Kozodaev
M. G. Meshcheryakov, K. I. Tarakanov, and A. V. Chestnoi

The problem of increasing the efficiency of utilization of the six-meter synchrocyclotron at the Institute of Nuclear Problems, Academy of Sciences USSR is reviewed. The method by which a large number of particle beams is obtained and collimated is described; using these beams it is possible to carry on several simultaneous experiments. Characteristic beam data are presented.

INTRODUCTION

Accelerators which produce particles with energies of several hundreds of millions of electron volts offer wide possibilities for carrying on research on the most important problems of contemporary nuclear physics, for instance studies of the structure and properties of elementary particles, clarification of the nature of their interaction, determination of the characteristics of their exchange reactions and so on.

High energy accelerators represent large scale industrial efforts and require the expenditure of large sums for their construction and operation. Thus the question of the efficient utilization of these machines assumes major importance.

The present paper is devoted to a short description of the approach to this problem which has been adopted at the synchrocyclotron of the Institute of Nuclear Problems, Academy of Sciences USSR [1] which accelerates protons to an energy of 680 Mev.

Basic Methods of Increasing the Efficiency of Utilization of the Accelerator

The chief objective of the scientific research at the six-meter synchrocyclotron is the study of elastic and inelastic nucleon-nucleon interactions in the 300-660 Mev energy region and the scattering of π-mesons by nucleons and deuterons. Since the cross sections for the majority of these processes range from several millibarns to some tens of millibarns the acquisition of accurate quantitative data entails the expenditure of a considerable amount of accelerator operating time.

The efficiency and scope of the utilization of the synchrocyclotron in nuclear research with high-energy particles depends to a large degree on the rational solution of two problems: the extraction from the accelerator vacuum chamber of intense beams of various types of high energy particles and the reduction of the background caused by the accompanying radiation.

*Presented at the CERN symposium on high energy accelerators and meson physics (Geneva, June 1956).
**Deceased.

In this connection we may make mention of the following features of the facilities at the six-meter synchrocyclotron:

a) the beams of high energy protons, neutrons, and π-mesons are extracted from the accelerator chamber through the shielding wall in thirteen directions;

b) there are a measurement enclosure and a special laboratory, shielded from the background radiation, for work with π-meson beams;

c) it is possible to carry on simultaneous experiments with several beams of the same or different particles;

d) the experimental equipment is operated automatically by remote control;

e) nuclear events are recorded by means of a multichannel electronic system.

The High Energy Particle Beams

In principle it is possible to obtain beams of high-energy particles from any point in the orbit of the accelerated protons. The realization of this possibility, however, depends strongly on the design of the accelerator.

It is important that the accelerator vacuum chamber and its side walls be free from any devices which might hinder the extraction of the particle beams. The extent to which this condition has been realized may be seen from Figs. 1 and 2.

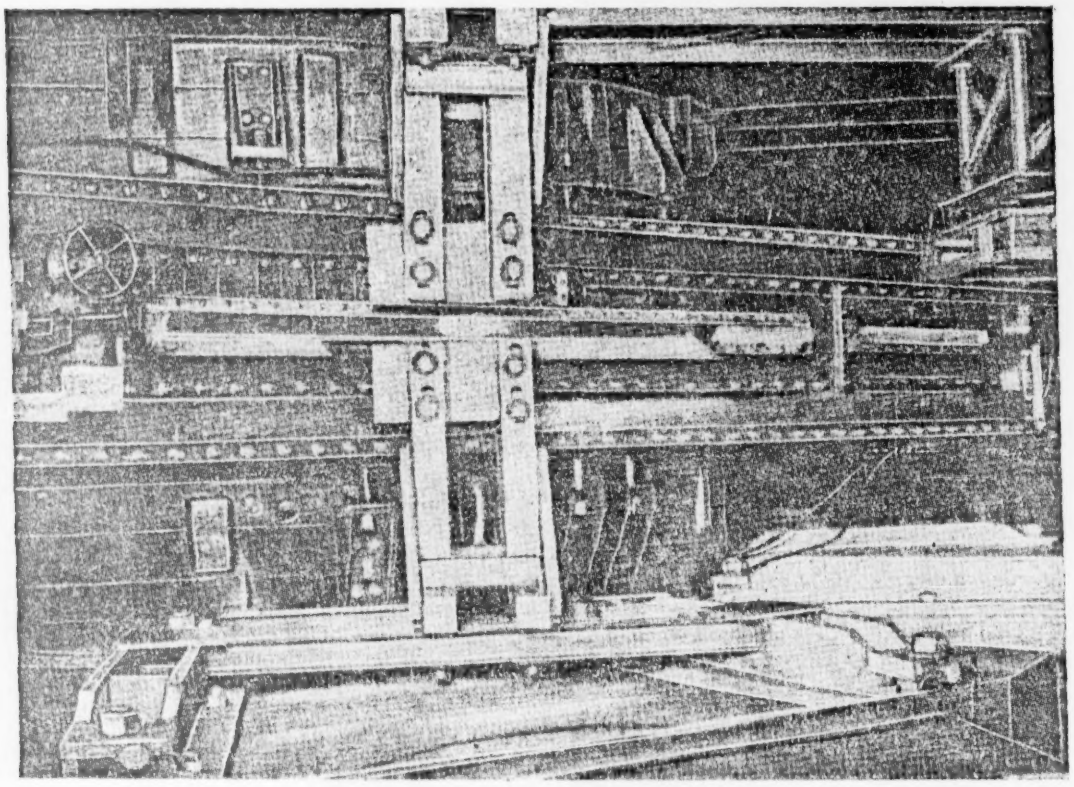

Fig. 1. The vacuum chamber of the synchrocyclotron showing the side from which the proton, neutron and π-meson beams are extracted.

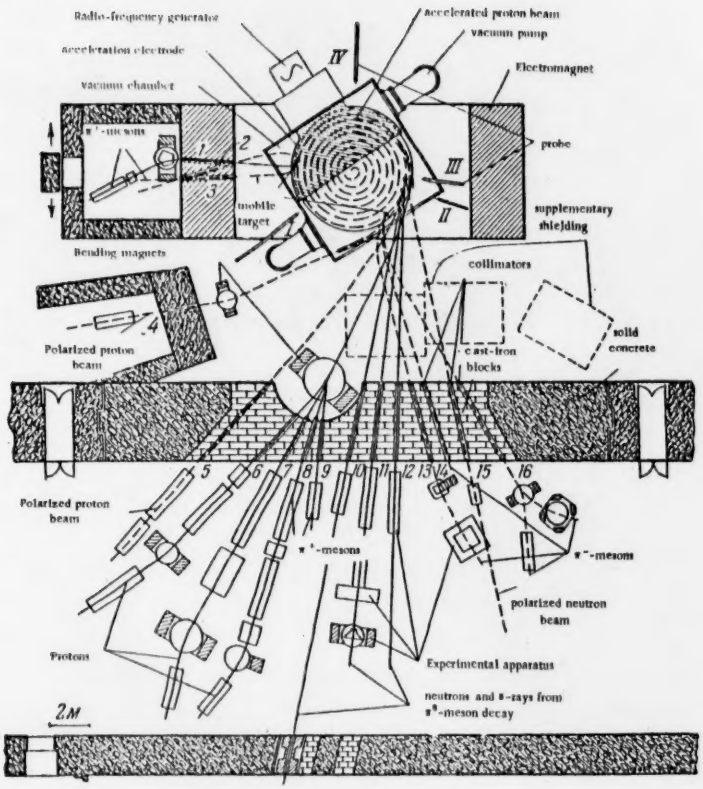

Fig. 2. The high-energy particle beams from the six-meter synchrocyclotron.

The first of these shows the front wall of the chamber. Almost the entire length of this wall, at the level corresponding to the proton orbit, is provided with a window for the extraction of the particle beams; these are duraluminum diaphragms approximately 1 mm thick.

In Fig. 2 is presented a general diagram of the accelerator chamber which shows the particle-beam configuration, the shielding layout and the measurement apparatus.

Most of the high energy particle beams which are ejected into the atmosphere are directed into the measurement enclosure which contains the experimental apparatus. The collimators are located in the porthole through the four-meter concrete shielding wall. The latter are steel pieces of square cross section, 3.6 m long, which have circular openings through the center, the diameters of which vary from 10 to 150 mm. The space between the collimators is filled with cast-iron blocks, providing good shielding for the porthole as well as the possibility of making changes in the arrangement of the collimators. Fig. 3 shows a longitudinal section through the building which houses the synchrocyclotron and the supplementary shield of concrete blocks which is in front of the four-meter wall of the measurement enclosure (in Fig. 2 this shield is indicated by dotted lines). The figure also shows a collimator of circular shape located in one of the neutron beams which is designed for work with circular scatterers.

Shielding of Synchrocyclotron Operating Personnel From Accelerator Radiation

An idea of the amount of shielding for the measurement enclosure and the room containing the recording and detection apparatus can be obtained from the following data. The general radiation level in the measurement enclosure for proton energies of 680 Mev with currents at the external target of 0.2-0.3 μamp varies from

0.1-0.2 mC/sec (in the right side of the enclosure) to 1.5-3 mC/sec (in the left side of the enclosure in which there is a dome in the ceiling to allow the operation of a crane); the corresponding fast-neutron intensity (energies of 0.5 Mev and above) varies from 1-2 neut./cm^2 sec to 60 neut./cm^2 sec. The flux of neutrons with energies higher than 50 Mev is less than 5 neut./cm^2 sec [2].

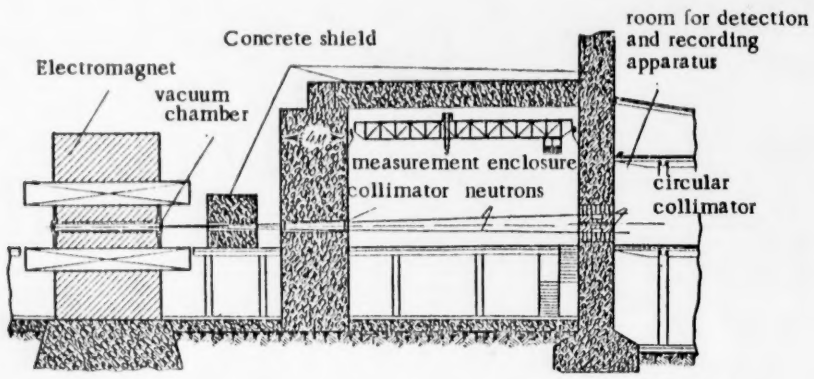

Fig. 3. Radiation shielding for the six-meter synchrocyclotron.

In the room which contains the recording instruments the radiation is negligibly small. This is indicated by the fact that when the accelerator is operated at high intensities the Geiger-counter count in any part of the room is not greater than double the cosmic-ray background [2].

Characteristics of High-Energy Beams Extracted From The Accelerator Chamber

Unpolarized proton beams. For obvious reasons great effort was expended in increasing the intensity of the external proton beam. An earlier method of proton extraction based on the scattering of protons by a uranium target was replaced by a new scheme developed experimentally at the Institute of Nuclear Problems, Academy of Sciences USSR [4] and the Nuclear Physics Laboratory of the University of Liverpool [5] in which radial oscillations of the particles are excited by a local inhomogeneous magnetic field.

The local magnetic field inhomogeneities are obtained by placing an iron mass in the vicinity of the last accelerator orbit. An exciter unit is used to start the radial oscillations. In the vicinity of the exciter the magnetic field intensity falls off radially. The adjustment of the precession of the centers of curvature of the particle orbits is achieved by means of a second excitation region ("regenerator") in which the magnetic field intensity along the radius increases rapidly.

The magnetic field configuration in the excitation zone and the radial extent of this zone must be chosen so as to provide a sufficiently large jump in the last orbit (about 40 mm [6]) while not causing any perturbation of the stable particle motion in the vertical plane.

The extraction of the particles from the chamber was accomplished by means of a magnetic channel consisting of two iron plates of varying cross section.

In order to control the angular spread of the external proton beam, following the magnetic channel there is a focusing device which reduces the beam spread in the horizontal plane [7]. At a distance of 7 m from the magnetic channel the beam diameter is approximately 8 cm. The angular spread of the external beam is less than $\pm$ 0.5°.

The total intensity of the external beam and the flux at various distances from the chamber along the particle trajectory was determined from the induced β-activity in the reaction $C^{12}(p, pn)\,C^{11}$. These measurements showed that the total proton current at egress from the magnetic channel is $7 \cdot 10^{10}$ protons/sec; this is 5-6% of the average particle current in the vicinity of the last orbit.

Using a bending magnet the external beam can be directed into one of the three collimators (6, 7, or 8) located in the concrete shielding wall (Fig. 2). Thus, on the one hand, the space in which experimental instru-

ments for proton studies can be located is enlarged considerably, while on the other, most favorable conditions for operation of the instruments are created.

The proton flux in the measurement enclosure, at a distance of 15 m from the output window of the chamber, is $(1\text{-}2)\cdot 10^8$ protons/cm^2 sec. The energy spread in the proton beam is very small. The deviation of particle energy from the mean value $E_{av} = 657$ Mev, as determined by range measurements in copper, was no greater than $\pm$ 5 Mev [8].

Because of the high intensity of the external proton beam, it was possible, outside of the accelerator chamber, to obtain a beam of π-mesons with energies up to 400 Mev at fluxes of 60 mesons/cm^2 sec (at energies about 240-270 Mev). In these experiments a target of liquid hydrogen or polyethelene is placed in the proton beam, in front of the bending magnet (Fig. 2). The momentum and direction analyses of the π-mesons are carried out in the measurement enclosure through collimators 8 and 9. At energies of 300 Mev the energy spread of the π-mesons in these beams was $\pm$ 5 Mev [9]. In Fig. 4 is shown a typical π^+-meson energy spectrum obtained from proton-proton collisions at 657 Mev [9]. (The π-meson emission angle is 24° in the laboratory system).

Neutron Beams, γ Rays and Polarized Proton Beams. As in all other particle accelerators, at the six-meter synchrocyclotron neutrons are obtained by proton bombardment of internal targets (usually beryllium), which are placed on probes (Fig. 2, probe III) in the vicinity of the outermost orbit. Four narrow "rays" are obtained from the wide beam of neutrons emitted by the target through the use of collimators 10, 11, 12 and 15. The first three

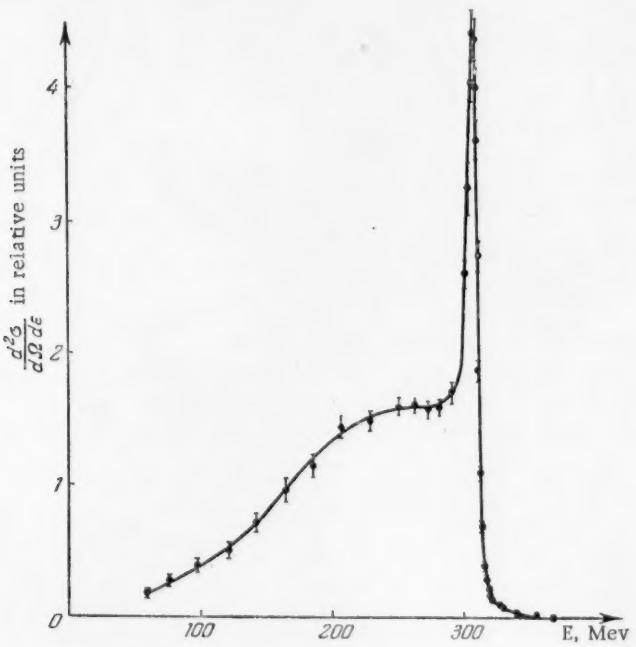

Fig. 4. Energy spectrum for π^+-mesons in (p-p) collisions.

neutron beams are unpolarized. At incident proton energies of 680 Mev the flux of neutrons with energies greater than 400 Mev at the location of the experimental apparatus is approximately $2\cdot 10^4$ neut./cm^2 sec. The fourth neutron beam (collimator 15, emission angle 18°) is partially polarized. It has been shown experimentally that the polarization is approximately 15% [10]. The energy spectrum of neutrons emitted through collimator 11 (emission angle 0°) is presented in Fig. 5 [11]. The spectra of the neutrons emitted through the other collimators are similar although the maxima are shifted somewhat toward the low energy region.

The beam emitted through collimator 15 exhibits the largest shift in the main maximum and this amounts to about 80 Mev [11].

In addition to the four neutron beams there are obtained from the same target four high energy γ-ray beams which arise in the decay of the neutral π-mesons which are produced. The γ-ray flux for energies higher than 10 Mev in the measurement enclosure is about $2 \cdot 10^3$ quanta/cm^2 sec (collimator 11). The energy distribution is shown in Fig. 6 [12]. The study of these γ-rays serves as a means of obtaining information on the nature of the interaction of π^0-mesons with matter.

Since experiments with polarized nucleon beams are of great interest, two beams of polarized protons are also extracted from the six-meter synchrocyclotron. One of these, which passes through collimator 4, consists of protons which experience diffraction scattering on beryllium nuclei within the vacuum chamber. The beam is polarized to about 60% [13]; the proton energy is 635 ± 15 Mev. The other beam, which passes through collimator 5, is comprised of protons which are quasi-elastically scattered by nucleons in the beryllium nuclei. The polarization of this beam is about 30% [13]. The intensities of both beams are approximately equal and are about $4 \cdot 10^4$ protons/cm^2 sec.

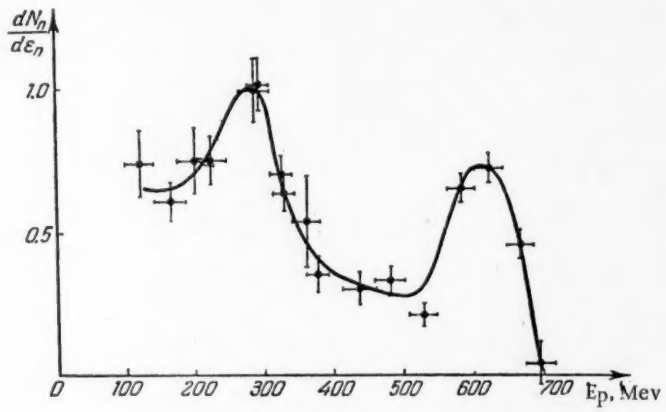

Fig. 5. The neutron energy distribution.

The π-meson Beam. In order to create the most favorable conditions for work with negative π-mesons, a "meson laboratory" was built directly behind one of the vertical supports of the yoke of the magnet. The iron in the yoke was about 3 m thick and provides good shielding against the direct radiation from the accelerator chamber. The concrete walls and ceiling of the laboratory, which are 1 m thick, serve as shields against scattered neutrons and γ-rays.

To provide an exit for mesons into this laboratory there are three collimators (1, 2, 3) in the magnet yoke; by means of multiple magnetic shields the magnetic field in these collimators is reduced from 1600 to 1-2 gauss.

π-mesons which are produced in a beryllium target (10 mm in thickness) located inside the accelerating electrode (dee) are directed into these collimators. The target is controlled remotely. By changing its azimuthal and radial coordinates in conjuction with appropriate changes in the direction of the magnetic field in the magnet gap it is possible to obtain π-mesons of both signs and of various energies. Thus there are available π^--mesons with energies ranging from 140 to 410 Mev and π^+-mesons with energies from 140 to 245 Mev. The π^- flux in the "meson laboratory" varies with energy from 200 to 2-3 mesons/cm^2 sec [14]. The background radiation level in this laboratory is quite high, however; the general radiation level is 1-2 mC/sec, thermal neutron level 500 neut/cm^2 sec, and neutrons with energies $E_n > 50$ Mev, 3 neut/cm^2 sec [14]. The thickness of the concrete shielding should be increased to 1.5-2 m to reduce this background.

In carrying out experiments with Wilson cloud chambers and diffusion chambers the meson flux should not exceed 20-30 particles/cm^2 sec and the background of spurious radiation must be extremely low. In this work π-mesons with energies from 150 to 400 Mev are utilized; these enter the measurement enclosure through

collimators 13, 14, and 16. The intensities of these π-meson beams vary from 40 per cm^2 sec (E_π = 230 Mev) to 1-2 per cm^2 sec (E_π = 400 Mev). The energy spread is ± 6 Mev for E_π = 230 Mev [15]. The meson source is a second mobile target the positioning mechanism of which is located on the front wall of the accelerator vacuum chamber.

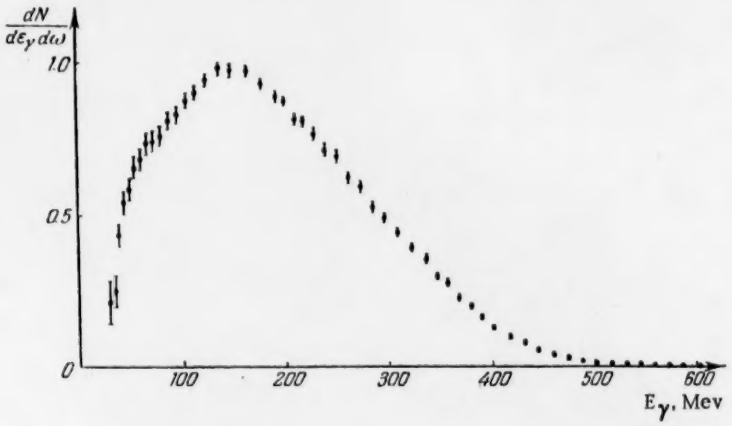

Fig. 6. The energy distribution for γ-rays from the decay of π^0-mesons produced in the collision of 670 Mev protons with carbon nuclei.

In concluding this description of the particle beams we may note that the difficulty of locating the charged π-meson beams was substantially reduced through the use of a scheme in which a current-carrying wire under tension is employed to determine the particle trajectories [16].

Irradiation of Samples Inside the Synchrocyclotron Chamber

In addition to the mobile targets located in the chamber the accelerator is provided with four probes by means of which it is possible to introduce (or extract) into the vacuum chamber samples of various materials for irradiation by the proton beam accelerated to the desired energy. A similar method of sample irradiation is widely used in radiochemical research.

Simultaneous Operation With Several Particle Beams

In the experiments with high energy particles several different techniques are employed: electronic particle detection (scintillation counters and Čerenkov counters in conjunction with photomultipliers), thick-layered emulsions, magnetic spectrometers, Wilson cloud chambers, diffusion chambers, bubble chambers and so on.

At the disposal of the experimenters there are ten electromagnets with pole diameters ranging from 30 to 100 cm, powered by a system which is capable of operating five magnets simultaneously. There are also available several thousand concrete blocks weighing up to 50 kg for the construction of local shields.

The arrangement of the experimental apparatus in the measurement enclosure is shown in Fig. 7. All terminal equipment for the detection apparatus (counting circuits, recorders, mechanical registers, etc.) and the remote control panels for the experimental equipment and the magnet-current regulator, which are located in places unsafe for personnel (the measurement enclosure and the "meson laboratory") are placed in a special detection apparatus room which is separated from the measurement enclosure (see Fig. 3) by a concrete wall 2 m in thickness. The equipment located in these two rooms is interconnected by a system of radio-frequency, high voltage, and control cables. The use of a patching system allows any of the detection instruments to be used in combination with the experimental equipment in any part of the measurement enclosure.

When the machine is in operation no one is permitted in the measurement enclosure; the doors are self-latching. Scientific personnel engaged in nuclear research at the accelerator remain in the room containing the detection apparatus while the machine is in operation. As has been indicated earlier the background

radiation level in this room is extremely low thus allowing people to remain for an unlimited time.

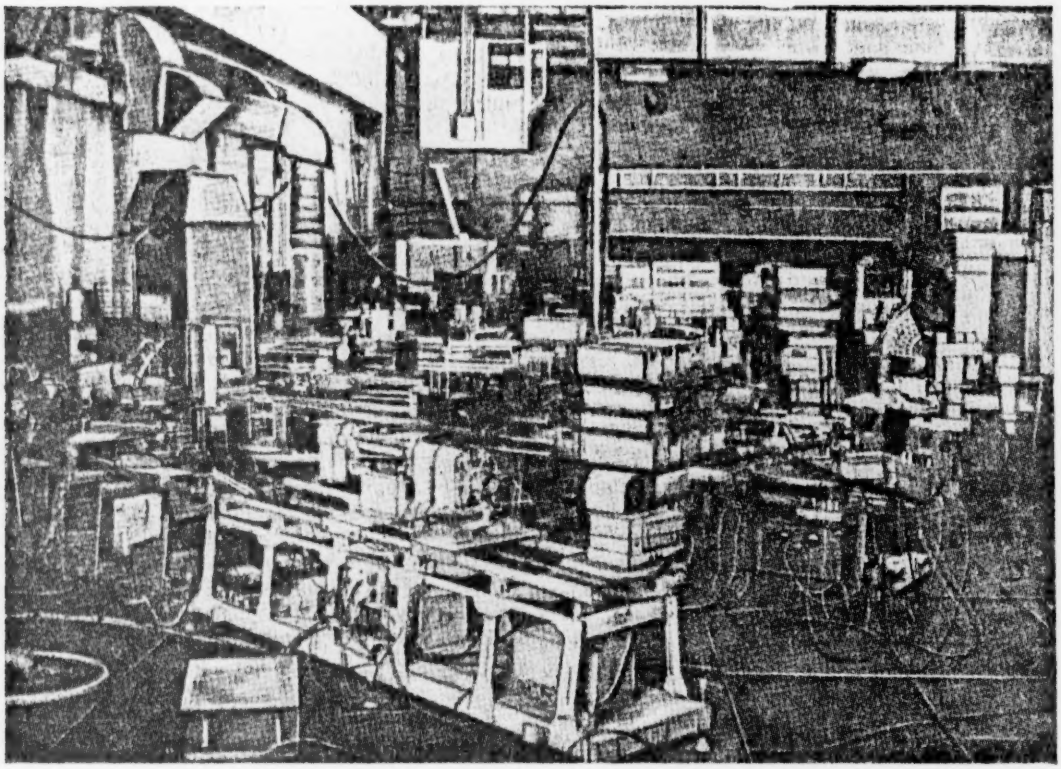

Fig. 7. The measurement enclosure with experimental equipment in place.

The present system of collimators and shielding is arranged so that most advantage can be taken of parallel (simultaneous) operation of groups of experimental instruments with several beams of the same or of different particles. For instance over a long period of time there were conducted experiments with 10-12 instruments on four neutron beams and two polarized proton beams. It is also possible to conduct simultaneous experiments with two cloud chambers (a Wilson chamber and a diffusion chamber) with the negative π-meson beams which enter the measurement enclosure.

In this connection we may note that it has been feasible to pulse the accelerating voltage of the six-meter synchrocyclotron [1]; this allows an interruption of the radio-frequency oscillations at the appropriate instant of time and thus particlesemerge from the accelerator in bursts at times when the chambers are prepared for detection.

In working with Wilson cloud chambers and diffusion chambers on experiments with maximum energy π-mesons, the flux of which is quite low, to increase the intensity of the pulsed π-meson beam, use is made of the so-called "storage technique" [17]. This technique is based on the following: for several acceleration cycles (three-four) protons are accelerated only out to a radius of 160-180 cm (with a corresponding energy of 240-300 Mev); then on the fourth or fifth cycle the accelerating voltage is applied over the entire frequency range (25-14 mc) as a result of which the protons are accelerated out to the limiting radius (278 cm) at which the target is located. By this means it has been possible to increase three-fold the intensity of the π-meson beam and hence to enhance the operating efficiency of the detection chambers.

SUMMARY

The extraction from the synchrocyclotron chamber of a large number of high-energy particle beams creates the possibility of carrying on research on a wide front.

By carrying on several experiments simultaneously, by the use of a multichannel electronic system and through the use of remote control of apparatus located in spots which are unsafe for personnel it has been possible to increase substantially the utilization factor of the machine and to keep non-operating time to a minimum. The later is not greater than 7-8% and is determined chiefly by the time required for changes in the experimental apparatus and modification of the machine.

LITERATURE CITED

[1] D. V. Efremov, M. G. Meshcheryakov, A. L. Mints, V. P. Dzhelepov, P. P. Ivanov, V. S. Katyshev, E. G. Komar, I. F. Malyshev, N. A. Monoszon, I. Kh. Nevyazhsky, B. I. Polyakov, and A. V. Chestnoi, The Six-Meter Synchrocyclotron of the Institute of Nuclear Problems. Report to the All-Union Conference on the Physics of High Energy Particles (Moscow, 1956).

[2] V. N. Mekhedov, M. M. Komochkov, K. O. Oganesyan, and A. M. Rozanova, Report Inst. Nuc. Probs., Acad. Sci. USSR (1954).

[3] J. L. Tuck, and L. C. Teng, Phys. Rev. 81, 305 A (1951).

[4] V. P. Dmitrievsky, V. I. Danilov, Yu. N. Denisov, N. L. Zaplatin, V. S. Katyshev, A. A. Kropin, and A. V. Chestnoi, Report Inst. Nuc. Probs., Acad. Sci. USSR (Jan., 1955).

[5] A. V. Crewe, J. W. G. Gregory Proc. Roy. Soc. Ser. A, 232, 242 (1955).

[6] V. P. Dmitrievsky, Dissertation, Inst. Nuc. Probs., Acad. Sci. USSR (1953).

[7] V. I. Danilov, V. P. Dmitrievsky and A. V. Chestnoi, Report Inst. Nuc. Probs., Acad. Sci. USSR, (1954).

[8] V. P. Zrelov, Report Inst. Nuc. Probs., Acad. Sci. USSR (1955).

[9] M. G. Meshcheryakov, B. S. Neganov, V. P. Zrelov, I. K. Vzorov, and A. F. Shabudin, J. Exptl.-Theoret. Phys. (in press).

[10] V. P. Dzhelepov, Yu. M. Kazarinov, and Yu. N. Simonov, Report Inst. Nuc. Probs., Acad. Sci. USSR (1955).

[11] V. B. Flyagin and V. S. Kiselev, Report Inst. Nuc. Probs., Acad. Sci. USSR (1955).

[12] Yu. D. Bayukov, M. S. Kozodaev, and A. A. Tyapkin, Report Inst. Nuc. Probs., Acad. Sci. USSR (1955).

[13] M. G. Meshcheryakov, G. D. Stoletov, and S. B. Nurushev, Report Inst. Nuc. Probs., Acad. Sci. USSR (1955).

[14] A. E. Ignatenko, V. V. Krivitsky, A. I. Mukhin, B. Pontecorvo, and A. A. Reut, Report Inst. Nuc. Probs., Acad. Sci. USSR (1954).

[15] V. P. Dzhelepov, V. G. Ivanov, M. S. Kozodaev, V. T. Osipenkov, N. I. Petrov, and V. A. Rusakov, Report Inst. Nuc. Probs., Acad. Sci. USSR (1955).

[16] J. J. Thomson, Phil. Mag. 6, 13, 561 (1907).

[17] T. N. Tomilina and M. F. Shulga, Report Inst. Nuc. Probs., Acad. Sci. USSR (1956).

Received May 17, 1956.

THE 10 BEV PROTON SYNCHROTRON OF THE ACADEMY OF SCIENCES USSR*

V. I. Veksler, D. V. Efremov, A. L. Mints, M. M. Veisbein,
F. A. Bodopyanov, M. A. Gashev, A. I. Zeidlits, P. P. Ivanov,
A. A. Kolomensky, E. G. Komar, I. F. Malyshev, N. A. Monoszon,
I. Kh. Nevyazhsky, V. A. Petukhov, M. S. Rabinovich, S. M. Rubchinsky,
K. D. Sinelnikov, A. M. Stolov

A short description is given of the basic parameters and specifications of the 10-Bev proton synchrotron. The various aspects of the design and construction of the accelerator have been considered in greater detail in a series of reports delivered to the accelerator section of the All-Union Conference on the Physics of High Energy Particles.

INTRODUCTION

The development of contemporary nuclear physics is directly connected with the progress of accelerator technology. Thus it is natural that physicists try to achieve particle acceleration to the highest possible energy. A proposal for the construction of a 10-Bev proton accelerator was presented to the Academy of Sciences USSR. At that time in the Soviet Union there had been accumulated, as is known, experience in the construction and operation of electron and proton accelerators in the energy region of hundreds of millions of electron volts. This experience was used as a basis for the development and construction of the gigantic 10-Bev accelerator.

The combined efforts of scientists and engineers with many fields of specialization were required in the construction of this machine.

The physics questions involved in the accelerator design were explored at the P. N. Lebedev Physics Institute Academy of Sciences, USSR [1], the design and basic accelerator facilities were worked out at the Scientific Research Institute for Electro-Physical Apparatus, Ministry of the Electrical Industry, USSR and in the Electronics Laboratory of the Academy of Sciences, USSR, and the design of the linear accelerator used for injection was carried out at the Kharkov Physico-Technical Institute of the Academy of Sciences, Ukrainian SSR.

Special mention should be made of the support and guidance of the late Academician S. I. Vavilov in the early years of the development of the 10 Bev synchrotron and of the constant assistance given by the director of the P. N. Lebedev Physics Institute Academy of Sciences, USSR, D. B. Skobeltsyn.

The construction of the accelerator was carried out at the newly built Electrophysical Laboratory of the Academy of Sciences USSR which is presently converted to the Joint Institute for Nuclear Research. The accelerator is now finished and is undergoing prove-in tests.

The present paper contains a short description of the accelerator. The various aspects of the design and construction of the machine have been presented in more detail in a number of reports to the accelerator section of the All-Union Conference on the Physics of High Energy Particles.

*Presented at the All-Union Conference on the Physics of High Energy Particles, Moscow, 1956.

The Chief Characteristics of the Accelerator

As is the case with all other accelerators already built or under construction for proton energies greater than 1000 Mev the machine described here is a proton synchrotron.

As is known the synchrotron acceleration method uses the "self-phasing" properties of particles moving in a varying magnetic field in a constant (or almost constant) equilibrium orbit. The frequency of the accelerating voltage must be varied in proportion to the particle velocity. The motion of the particles takes place in a chamber located between the pole pieces of a ring magnet. The magnet consists of four quadrants (average radius 28 m) separated by eight-meter straight sections. The particle injection system is located in one of these straight sections and two others contain the accelerating electrodes. Particle extraction is accomplished in one of the straight sections.

The protons undergo preliminary acceleration to an energy of 8.5-9 Mev in a linear accelerator and then travel 10 m along a straight path. Along the straight path the beam is focused by a double magnetic correction system, a magnetic lens and a compensating condenser. Then the beam is turned through an angle of 75° in a focusing bending magnet and is introduced into the synchrotron chamber. The aperture in the vacuum chamber is 200 x 36 cm. The overall length of the chamber is 204 m.

Calculation shows that the adjustment of the beam for entry into the chamber must be made with an accuracy of several minutes of angle. This adjustment is realized by means of an electrostatic inflector which consists of five deflection plates to which is applied a stabilized dc voltage regulated to within 100 kv. The particles are injected into the chamber when the magnetic field intensity in the gap is 150 gauss. Acceleration is terminated when the magnetic field intensity reaches a value of 13,000 gauss. The particles receive energy increments in two drift tubes located in two diametrically opposite straight sections. The effective amplitude of the accelerating voltage can be changed from 3 to 8 kv. The acceleration cycle lasts for approximately 3.3 sec. The cycles are repeated at 12 second intervals.

At the end of the acceleration cycle the beam can be directed at suitable targets and used either in the immediate vicinity of the accelerator magnet (near the straight sections and near windows in the magnet yoke) or in a special enclosure.

The determination of the basic parameters was made on the basis of work on synchrotron theory carried out at the P. N. Lebedev Physics Institute Academy of Sciences USSR [3]. This work was used in setting up an approach to determining the basic accelerator parameters, in exploring various sources of particle loss, in choosing the optimum injection condition and the required magnetic field configuration and in solving many other problems arising in the design, construction and start-up of the machine. A number of important questions connected with injection and particle energy loss due to resonance build-up of oscillation were solved on a working model which delivered a proton beam with energies up to 180 Mev [2], [3].

The synchrotron theory which was developed is well known in this country and is used in many laboratories in calculations on new accelerators. We shall limit ourselves here to a qualitative description of the particle motion which is derived from the more exact theory.

The motion of particles in cyclic accelerators can be analyzed into three components:

1) Motion in a constant equilibrium orbit at the resonance rotational frequency. A particle in an equilibrium orbit is in resonance with the frequency of the accelerating field at all times.

2) Slow oscillations about the equilibrium orbit which are associated with the deviation of the particle from exact resonance. These are called radial phase oscillations since deviations from resonance lead to a change in the phase of the radio-frequency field which accelerates the particle in each passage through the gap. The period of the phase oscillations varies from 500 to 1500 μsec; this is from 100 to 2,000 times larger than the rotational period. As it is usually stated, in departing from the equilibrium orbit the particle moves along an instantaneous orbit which oscillates about the equilibrium orbit.

3) Fast oscillations about the instantaneous orbit with periods from 7 to 2 μ sec.

Thus the motions of particles in the synchrotron may be pictured in the following way. The instantaneous orbit executes slow oscillations about the stationary equilibrium orbit, which passes through the center of the accelerator chamber. The particles, in turn, execute fast oscillations about the instantaneous orbit.

In order for the equilibrium orbit to remain fixed the changes in the magnetic field strength and the frequency of the accelerating field must be correlated. An error in the frequency Δf shifts the orbit radially. An investigation of the present machine shows that a relative error $\pm$ 0.1% in frequency causes a radial shift of as much as $\Delta r = \pm$ 6 cm.

The radial phase oscillations are usually damped during the acceleration process; in the present case their amplitude falls from 50 cm at the beginning to 1 cm at its termination. The difficulty of starting up the machine arises, in particular, from the fact that the amplitude of radial phase oscillations, due to any type of perturbation, may increase so much as to result in the loss of particles from the beam.

In a synchrotron it is necessary to take special measures for the suppression of harmonics of the magnetic field which are caused by ripple in the rectified current which is supplied to the magnet winding. This situation arises because the frequency of the radial phase oscillations occuring during acceleration changes continuously and may fall into resonance with these perturbations. In particular, resonance with the second harmonic (1200 cps) can lead to a considerable loss of particles. The loss of particles can result not only from ripple in the voltage applied to the magnet winding but also from fluctuations in the frequency or amplitude of the electric accelerating field. Both theoretical considerations and experience have shown that oscillations excited by noise are particularly dangerous because of the relatively long period of acceleration. It is well known that the noise shifts are proportional to $\sqrt{t}$ where t is the acceleration time.

Free-oscillation theory and a calculation of all possible perturbations on the particle motions were of great value in setting up specifications. An investigation was made of simple and parametric oscillations, the coupling between radial and vertical oscillations, and the effect of non-linearities; using these results a cetain effective region was selected which is free from resonances: $0.55 < n < 0.75$.

On the other hand, free-oscillation resonances, which are dangerous in the acceleration period, can, in certain cases, be utilized to increase the injection efficiency. Thus the region of resonance values for n at the edge of the magnet can be used for injection and it is found that the possibility of changing the magnetic field configuration by means of supplementary windings is of great value in this connection.

Among the main scientific-engineering problems whose solutions were needed in the construction of the machine there were the construction of an electromagnet and its supply system, a vacuum chamber and evacuation system, a radio-frequency acceleration system and an injector. It was necessary to perform a great deal of theoretical and experimental work which will have general value in the construction of large cyclic accelerators. Here we would include the development of electromagnet calculations and methods for correcting and stabilizing magnetic fields, the extension of the theory and construction of high-power converter equipment, progress in methods for keeping the frequency of the accelerating voltage correlated with the magnetic field intensity, methods for amplifying radio- frequencies over wide ranges,and so on.

The Electromagnet and Its Supply System

The dimensions and weight of the electromagnet, as well as the capacity of its power system, increase sharply with an increase of the energy of the accelerated particles. Assuming the best value of the magnetic field intensity, the tolerances on the deviations of the magnetic characteristics from specifications and the accuracy with which the frequency of the accelerating voltage is related to the magnetic field, the weight of the magnet increases in porportion to the maximum particle energy raised to about the 2.5 power, while the energy stored in the magnetic field goes as the fourth power. Hence the construction of synchrotrons of the usual type for high particle energy encounters, first of all, the engineering and economic difficulties associated with the building of a large electromagnet and its power system.

A reduction of the dimensions and weight of the electromagnet and the capacity of the power system can be realized only by increasing the maximum intensity of the magnetic field and by assuming more stringent requirements in the accuracy of construction and adjustment of all components. Any sizeable increase in the magnetic field strength above that which has been mentioned does not yield any economic advantage since saturation effects tend to increase the weight of the magnet and the capacity required of its power system. Furthermore, the difficulties associated with the magnetic field corrections become worse. Thus a reduction in the weight of the magnet and the capacity of the power system can be accomplished chiefly by stricter tolerances.

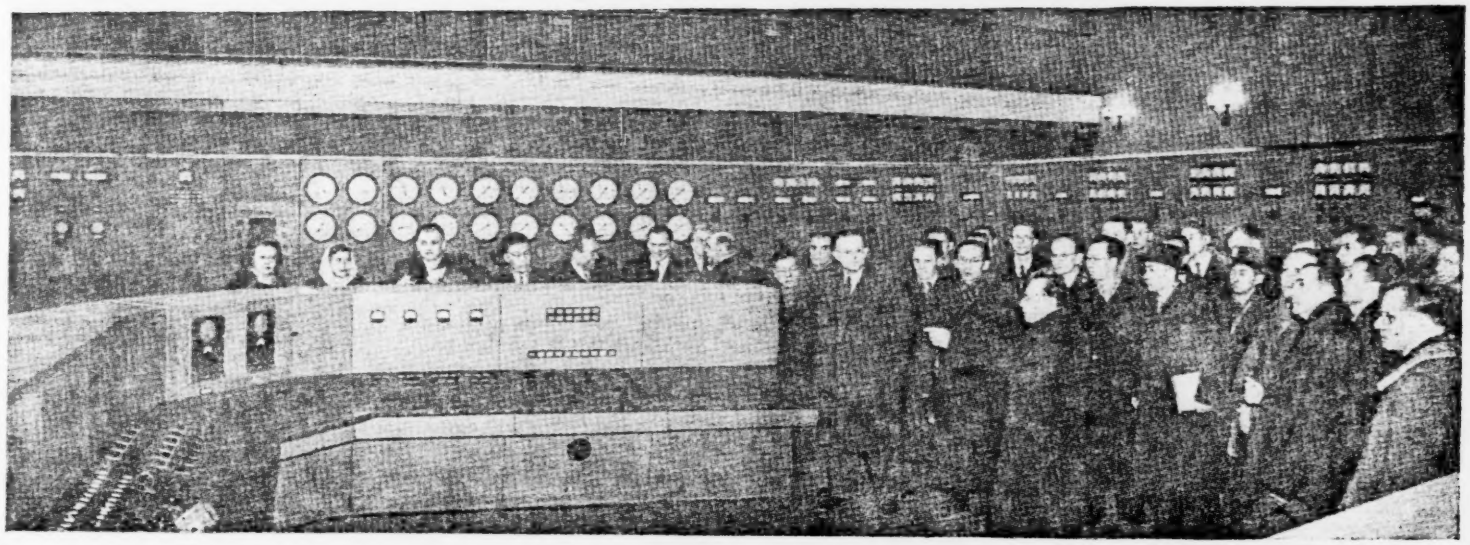

Members of the International Conference for the Organization of an Eastern Institute of Nuclear Research inspect the central control console of the 10 Bev proton synchrotron at the Electrophysical Laboratory of the Academy of Sciences, USSR.

The tolerances and the relative dimensions of the aperature in the 10 Bev accelerator are smaller than those of similar accelerators. The relatively high tolerances impose strict requirements on the quality of the manufacture and assembly of the magnet and require special methods for precision correction of the magnetic field.

The following systems for correction of the field have been designed and developed: a demagnetization system for eliminating the distortions due to the residual fields, a compensation system for dynamic distortions of the field, a system for locating the median plane of the magnetic field, a system for controlling the field index, a system for correcting azimuthal inhomogeneity and a system for expanding the operating region of the field at high field strengths, thus ameliorating saturation effects. The results of preliminary tests on the magnetic field of the monitored electromagnet indicated that all these correction systems work satisfactorily [4, 5].

Each of the four quadrants of the magnet consists of 12 units. The weight of each unit is about 750 tons. A general view of the magnet is shown in Figs. 1 and 2. The outer diameter is 72 m. The weight of the magnet and its windings is 36,000 tons [6].

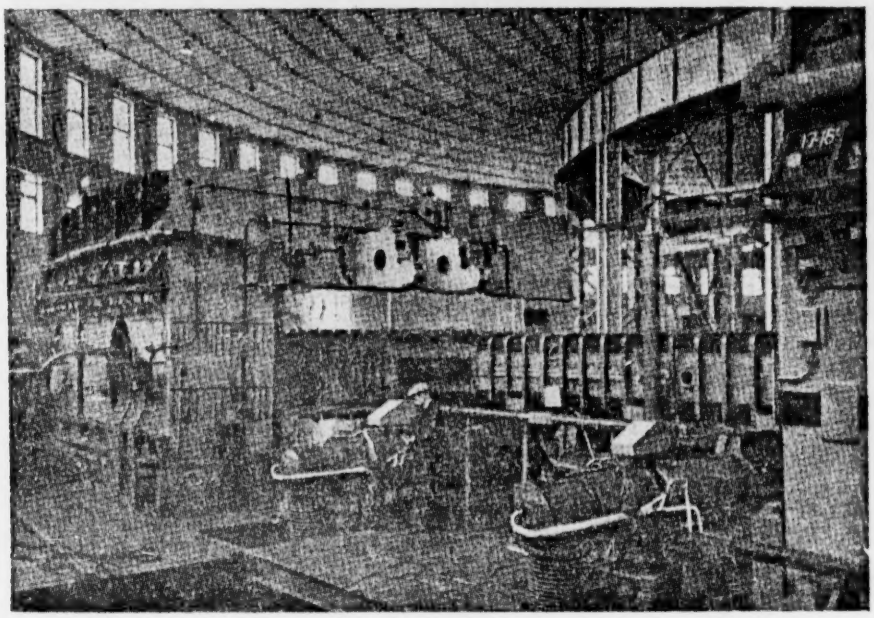

Fig. 1. General view of the outside of the ring magnet.

In the power system for the magnet, use is made of a system in which energy is stored in rotating fly-wheels. The conversion of mechanical energy into electrical energy is accomplished by alternators which are connected to ion tubes (ignitrons). In the period during which the magnetic field is increasing the power system supplies energy to the magnetic field in the magnet and the ignitrons operate as rectifiers while the alternators work as generators. After the maximum intensity of 13,000 gauss is reached the ignition converters are switched over to inverter operation and the energy stored in the magnet is returned to the alternators. In this case the alternators become motors and convert the energy of the magnetic field into kinetic energy of the fly-wheel. In this system the only power required from the line by the electric motors is that needed to make up for losses.

The data on the power system are as follows; maximum power – 140,000 kva, maximum current – 12,800 amp, maximum voltage – 11,000 volts, number of units operated in parallel – 4 (Fig. 3), number of ignitrons – 96.

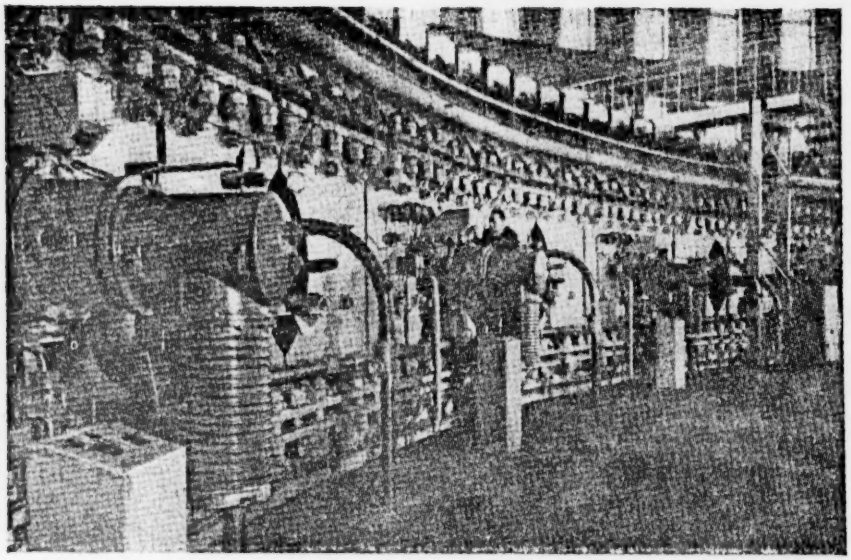

Fig. 2. General view from inside the ring magnet.

The extremely large peak power of the apparatus entails the use of a large number of ignitrons operated in parallel. In this mode of operation a whole series of problems arises connected with the need for distributing the load equally over all tubes. Furthermore the need for the greatest possible reduction of dangerous harmonics of the magnetic field leads to the necessity of applying to the electromagnetic windings a rectified voltage with extremely small ripple.

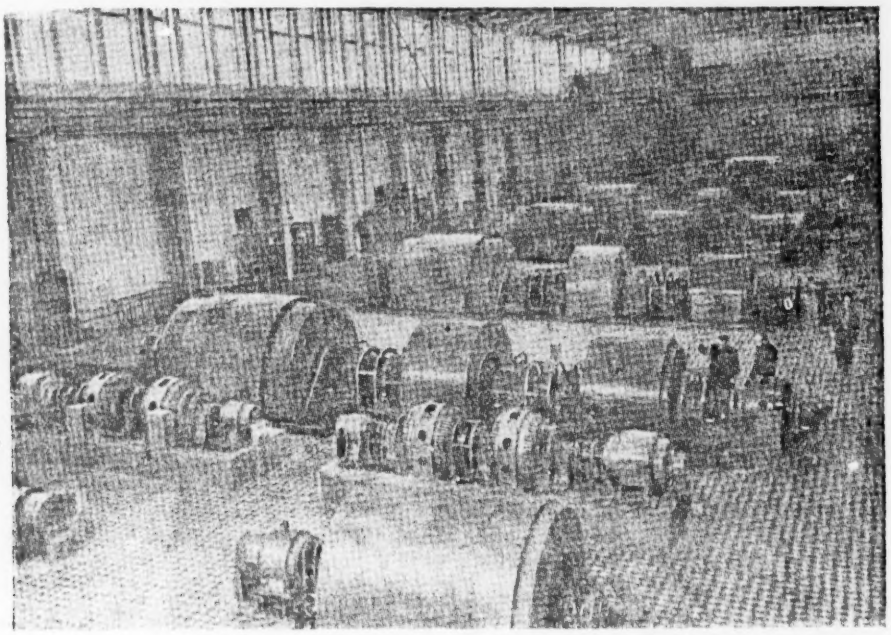

Fig. 3. General view of the synchronous-machine room.

This problem was solved through the use of alternators making use of two systems of three-phase winding on each machine, shifted 30° in phase with respect to each other. Each system of windings feeds a bridge rectifier [7]. For further reduction of ripple in the magnetic field a special system was developed for reducing the pulsating part of the magnetic flux in the operating gap of the field.

In the development of the supply system a good deal of attention was paid to the reduction of the effect of accidental outages. These disturbances (arc-backs, phase jumps, etc) are particularly troublesome in the inverter mode since they tend to make the system unstable. It was found necessary to take special measures to bring the system into stable operation artificially after these disturbances were eliminated.

In Fig. 4 is shown a general view of the room in which the ignitron converters are located.

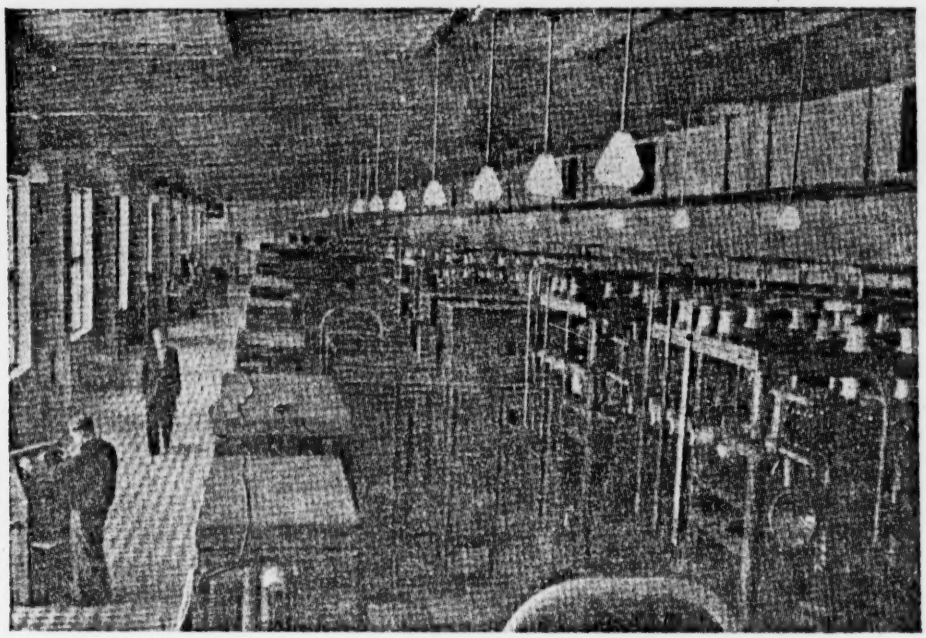

Fig. 4. General view of the ignitron room.

The Vacuum System

One of the chief difficulties involved in the construction of the vacuum chamber for the synchrotron was its great size (the chamber volume is about 160 m^3), the high required vacuum(10^{-6} mm Hg) and the existence of a varying magnetic field which excluded the possibility of using massive metal parts in the construction.

The solution to this problem was found in the utilization of a double vacuum system consisting of an inner high-vacuum chamber and an external fore-vacuum chamber. Using this system the horizontal surfaces of the high-vacuum chamber, which are saturated by the magnetic flux, can be thin sheets of stainless steel 0.15 mm in thickness. These sheets are separated by insulating sections the dimensions of which are such as to make negligible the magnetic field distortions caused by eddy currents.

The horizontal parts of the high-vacuum chamber are fastened directly to the pole shoes of the electromagnet. The pole shoes of the electromagnet also serve as construction members of the fore-vacuum chamber and are sealed by sheets of textolite and rubber. The side walls of this chamber are of duraluminum with sheet-rubber covering. The vacuum maintained in the fore-vacuum chamber is usually of the order of 1 mm Hg.

To avoid mechanical injury to the high-vacuum chamber by accidental pressure surges in the fore-vacuum chamber there is a protection system with interlocks and gauges [8].

The high-vacuum system is evacuated by 56 oil-diffusion pumps. Each pump has a capacity of 5,000 liters per second [9]. The high-vacuum system is furnished with traps which are connected to a central liquid nitrogen supply system.

The fore-vacuum chamber is evacuated by 16 type VH-6 pumps.

The Radio-Frequency System and Control of Particle Injection and Acceleration

The design and construction of the radio-frequency system for proton acceleration and a system for control of the injection and acceleration of particles required the solution of a number of new problems in the fields of radio-engineering and electronics. Heretofore, in general, the problem has been the design of a radio-frequency system in which it is possible to vary the frequency of the electric field over wide limits, thus providing the required increase in the energy of the particles. In general, a system consisted of a frequency-modulated oscillator and wide-band radio-frequency amplifiers which were used to drive the accelerator elements.

It was suggested that the most effective form for the accelerator elements for high-energy synchrotrons would be short drift tubes. This system of acceleration was tried on the 180 Mev synchrotron model and was adopted for use in the 10 Bev machine.

The specifications called for an oscillator the frequency of which could be varied in the course of an acceleration cycle from 0.182-1.5 mc and which would exhibit the proper functional dependence on the intensity of the magnetic field in the gap with an accuracy better than $1 \cdot 10^{-3}$. In developing this oscillator a comparison was made of the various schemes for wide-range frequency modulation. The method which was finally selected was one in which the modulation characteristic is stabilized by negative feedback through a precision frequency discriminator. The final model of the oscillator has a frequency range of 0.15-1.5 mc.

The stability of the modulation characteristic of the oscillator, as determined from 100 hours of operation is better than $\pm 7 \cdot 10^{-4}$.

Experimental measurements which have been performed indicate that the relative level of spurious frequency-oscillations in the region 600-2,000 cps, at frequencies corresponding to harmonics of the supply line, is less than $5 \cdot 10^{-7}$ and that the spectral density of noise frequency-modulation in this same range is less than 0.05 cycles^2/cycle.

The frequency of the oscillator is controlled by the intensity of the magnetic field in the gap of the magnet. Two methods of frequency control have been investigated. The first makes use of an auxiliary magnet which is in series with the main magnet so that the same exciting current flows through both; this magnet is located at a place which is free from radiation. The coil of the oscillator, which contains a ferrite core, is located in the gap of the auxiliary magnet. The changing magnetic field intensity causes corresponding changes in the magnetic permeability of the ferrite core and hence in the oscillator frequency. The second scheme makes use of a device which integrates the value of the magnetic field; this consists of a pick-up coil located in the gap of the auxiliary magnet or main magnet and an electronic integrator, the output voltage of which is used to control the frequency of the oscillator. In both schemes a correlation better than $\pm 10^{-3}$ between the frequency of the accelerating field and the intensity of the magnetic field is achieved through functional conversion of the signal used to control the frequency of the oscillator [10, 11].

The frequency-modulated signal from the oscillator is amplified to 20,000 v in wide-band multistage amplifiers with a power of 200 kw. This method of amplification is used in all stages with the exception of the output stage, which determines the electric power requirements from the supply line. The final amplifier stage is a tuned amplifier.

The tuned circuit of the final stage makes use of a system the capacity of which (1,500 μf) is determined by the drift tube and whose inductance is the coil with the ferrite core. In maintaining automatically the correlation between the tuned circuit and the frequency of the amplified oscillations, the magnetic permeability of the core of the coil, under the influence of the magnetizing winding, changes by a factor of 100. The current

flowing through the magnetizing winding is controlled by changes in the voltages obtained from a coil which detects the difference between the frequency of the tuned circuit and the frequency of the electric accelerating field.

It was found feasible to use a tandem system in switching the radio-frequency amplifiers so that the voltages applied to both accelerating electrodes are added. By virtue of this arrangement it is possible, with two accelerating electrodes, located in opposite straight sections, to reduce by a factor of two the rf power and also to cut in half the weight of the ferrite (to 2 tons) as compared with an arrangement in which there is only one accelerating electrode.

In designing the inductance with the ferrite core, which is in the circuit of the output stage of the radio-frequency amplifier, it was necessary to study the behavior of ferrites in strong radio-frequency fields.

As a result of this work it was decided to build the variable inductance in the form of a section of coaxial line partially filled with ferrite. This construction was tested and then used in the circuit of the final stages of the radio-frequency amplifiers [12 - 14].

The solution of the problem of obtaining signals for switching the injector and the radio-frequency accelerating voltage, etc., required the development of new types of magnetic-field analyzers.

The accuracy required for the switching system which switches the injector and the radio-frequency accelerating field in the synchrotron is ±10, which corresponds to a relative accuracy in the strength of the magnetic field $\pm 3 \cdot 10^{-4}$ and an absolute accuracy of $\pm 4 \cdot 10^{-2}$ gauss. To obtain an indication of the instantaneous values of the magnetic field intensity, use was made of a system in which the variations of the field intensity were transformed to frequency changes in an oscillator. Pulses are obtained which have a direct relation to the instantaneous value of the changing frequency and consequently to the magnetic field intensity. As a result, pulsed signals are obtained which assure an accuracy in the switching system for the injector and accelerating field which is better than $\pm 3 \cdot 10^{-4}$ [15].

For precision measurements of the instantaneous frequency of the radio-frequency accelerating voltage a new method was devised which yielded a relative accuracy better than $5 \cdot 10^{-4}$.

The use in the synchrotron of a time-varying magnetic field also necessitated the development of new methods of dynamic measurements of magnetic field intensity. It was found necessary to build special apparatus for measurements of the instantaneous field in the range from 150-13,000 gauss with an accuracy of $1 \cdot 10^{-4}$. For this purpose the most effective scheme was one in which use was made of nuclear magnetic resonance.

It is not possible in the present paper to consider other important parts of the installation: the linear accelerator, the input system, electron optics and a number of others.

In conclusion we should note that the construction of the accelerator involved the participation of a large number of scientific research institutes and plants of the Ministries of Electrical Engineering and Electronic Manufacturing as well as a number of planning, building and construction organizations, all which contributed much to this important project. At the present time adjustment operations are being carried out at the synchrotron and in the near future we expect to proceed to the complicated job of starting up this accelerator.

LITERATURE CITED

[1] V. I. Veksler, A. A. Kolomensky, V. A. Petukhov, and M. S. Rabinovich, Physical Principles in the Construction of the 10 Bev Proton Synchrotron (Report to the All-Union Conference on the Physics of High-Energy Particles Moscow 1956).

[2] L. P. Zinovyev and V. A. Petukhov, Experimental Research on a Model of the 10 Bev Proton Accelerator, Ibid.

[3] I. S. Danilkin and M. S. Rabinovich, Certain Questions in the Theory of Cyclic Resonance Accelerators as Applied to Experiments with the 180 Mev Synchrotron, Ibid.

[4] A. A. Zhuravlev, E. G. Komar, I. A. Mozalevsky, N. A. Monoszon, and A. M. Stolov, Magnetic Characteristics of the 10 Bev Proton Synchrotron, Ibid.

[5] M. D. Veselov, A. A. Zhuravlev, I. A. Mozalevsky, E. A. Myae, A. M. Stolov, and S. V. Fedukov, Methods and Results of an Experimental Investigation of the Magnetic Field of the 10 Bev Proton Synchrotron, Ibid.

[6] E. G. Komar, H. A. Monoszon, N. S. Streltsov, and G. M. Fedotov, Certain Construction Features of the Electromagnet for the 10 Bev Proton Synchrotron, Ibid.

[7] M. A. Gashev, E. G. Komar, N. A. Monoszon, A. M. Stolov, and F. M. Spevakova, The Power Supply for the Electromagnet of the 10 Bev Proton Synchrotron, Ibid.

[8] E. G. Komar, I. F. Malyshev, Ya. L. Mikhelis, and A. V. Popkovich, The Vacuum Chamber of the 10 Bev Proton Synchrotron, Ibid.

[9] S. A. Vekshinsky, The Vacuum Pumping System for the Accelerator, Ibid.

[10] A. L. Mints, M. S. Rubchinsky, M. M. Veisbein, F. A. Vodopyanov, A. A. Kuzmin, and V. A. Uvarov, Systems for Correlating the Frequency of the Accelerating Field and the Intensity of the Magnetic Field in Proton Synchrotrons, Ibid.

[11] F. A. Vodopyanov, The Radio-Frequency Generator In the System of f-H Correlation in the 10 Bev Proton Synchrotron, Ibid.

[12] Yu. M. Lebedev-Krasin, The Accelerating Elements of the Proton Synchrotron and Basic Questions in the Application of the Radio-Frequency Voltage, Ibid.

[13] I. Kh. Nevyazhsky, G. N. Drabkin, V. F. Trubetskoi, and A. S. Temkin, The Use of an Inductance With a Ferrite Core in the Power-Amplifier Stage of the 10 Bev Proton Synchrotron, Ibid.

[14] L. M. Gurevich, B. M. Gutner, G. M. Drabkin, and N. K. Kaminsky, Automatic Tuning of the Output Stage of the Radio-Frequency Generator in the 10 Bev Proton Synchrotron, Ibid.

[15] A. L. Mints, S. M. Rubchinsky, M. M. Veisbein, A. A. Vasilyev, Control Systems for Particle Injection and Acceleration in the Proton Synchrotron, Ibid.

Received May 29, 1956

BASIC FEATURES OF A PROJECTED 50-60 BEV STRONG-FOCUSING PROTON ACCELERATOR*

V. V. Vladimirsky, E. G. Komar, A. L. Mints, L. L. Goldin, D. G. Koshkarev, N. A. Monoszon, S. Ya. Nikitin, S. M. Rubchinsky, S. V. Skachkov, N. S. Streltsov, E. K. Tarasov

The basic features of a projected 50-60 Bev strong-focusing proton accelerator are described. The critical energy is eliminated by changing the dependence of orbit length on momentum. The weight of the magnetic system, consisting of 120 sectors is less than 22,000 tons, the peak power is approximately 100,000 kva, the mean radius is 236 m.

The limiting proton energy was chosen on the basis of the following considerations. We are attempting to achieve an energy sufficient for multiple meson-production and the production of anti-particles of all known types of elementary particles. At the same time, in the design, it is convenient to utilize specifications and data already developed in connection with the construction of the USSR 10 Bev accelerator, especially the unique power system. For a maximum particle energy of 50-60 Bev the kinetic energy in the center-of-mass system in the collision of a proton with a single nucleon is about 9 nucleon masses, the peak power of the magnet supply is about 100 kva and the weight of the magnetic system is less than 22,000 tons.

One of the important questions which arises in the design of this type of machine is the problem of phase stability in the region of the transition energy. In the present design use is made of a system which introduces changes of the particle orbit length so as to avoid a critical energy altogether [1]. The compensation system is based on the utilization of forced oscillations of those particles whose momentum deviates from the equilibrium value. These forced oscillations arise as a result of periodic azimuthal changes in the magnitude of the magnetic field: the sign of the field is reversed in every eighth magnet and its magnitude is one-half that in the regular magnets (Fig. 1). The space period of the compensating magnets in azimuth is slightly less than the period of the free radial proton oscillations. Under these conditions the largest amplitude of the radial displacement occurs in the compensating magnets and the change of arc length can be shown sufficient to compensate for the average change in arc length in all the remaining magnets. The critical energy condition is eliminated at the expense of a 20% increase in the length of the orbit.

The choice of the compensation system determines the choice of the rather high frequencies for the transverse particle oscillations: 13.75 per turn for the radial oscillations and 12.75 for the vertical. The mean opening angle of the beam $2 \cdot 10^{-3}$ radian represents a compromise between the desire to reduce the weight and power requirements of the machine and an attempt to keep practical tolerances on the field errors. The maximum field at the orbit will be 10,000-12,000 gauss, the length of the orbit 1483m. The basic orbit parameters are given in Table 1. Tolerances for the magnetic field are given in Table 2.

The magnetic field gradient in the turning magnets is relatively small, hence these magnets can be made without a return path. The compensating magnets, however, have return paths. A profile of these magnets is shown in Fig. 2. In order to allow free access to the chamber the magnet yokes for all magnets are C-shaped.

*Reported to the All-Union Conference on the Physics of High-Energy Particles. May 14, 1956.

The magnets are very heavy hence it is impossible to make them of one piece. Each magnet will consist of five stacks of weight 38 tons including the windings. The construction of the regular magnets is shown in Fig. 3. The total weight of iron in the magnet yoke is 17,000 tons. The total weight of the magnet including structural members is 22,000 tons.

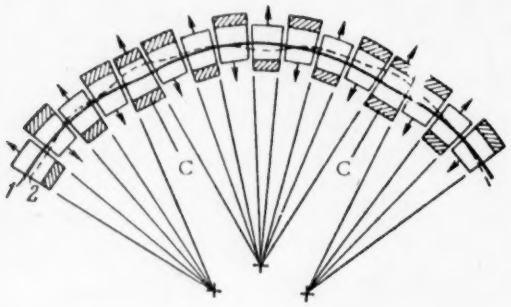

Fig. 1. Arrangement of the magnets in the accelerator. C) compensating magnets; ↓ ↑ direction of increasing magnetic field; 1) equilibrium trajectory; 2) non-equilibrium periodic trajectory for $p > 0$ (the amplitude of deviations from equilibrium is exaggerated.

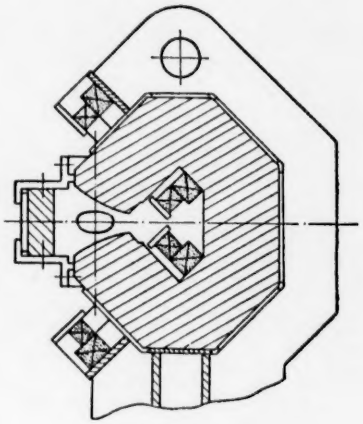

Fig. 2. Construction of the compensating magnets.

TABLE 1

Total number of magnets	120
Number of compensating magnets	15
Number of radial oscillations per turn	13.752
Number of vertical oscillations per turn	12.744
Length of the radial focusing magnets	10.99 m
Length of the vertical focusing magnets	10.69 "
Gap length between magnets	1.518 "
Radius of curvature of the regular magnets	166.1 "
Radius of curvature of the compensating magnets	−296.6 "
Distance from the chamber axis to the asymptote of the hyperbolic pole pieces of the regular magnets	404.0 mm
Internal half-height of the chamber	60 "
Internal half-width of the chamber	100 "
Utilization factor for the magnetic field	0.805
Logarithmic derivative of orbit length with respect to momentum	$-8.2 \cdot 10^{-4}$
Opening angle of the beam	$2 \cdot 10^{-3}$ radian
Amplitude of the radial oscillations caused by compensation	40 mm

TABLE 2

Allowable momentum deviations $\Delta p/p$	0.5%
Field tolerances $\Delta H/H$	0.25%
Gradient tolerances $\Delta \text{grad}/\text{grad}$	0.3%
Tolerance on magnet displacement	1.0 mm
Tolerance on vertical displacement (amplitude of 13th harmonic)	0.5 "

Data on the magnet power supply is given in Table 3.

Peak powers of the order of 100 kva will be obtained from generators with flywheels. The nominal capacity of each unit is 37 kva. There is a 12-phase ignitron inverter system. In order to reduce the ripple

in the rectified voltage it is planned to use a filter and a special scheme for reducing ripple by negative feedback.

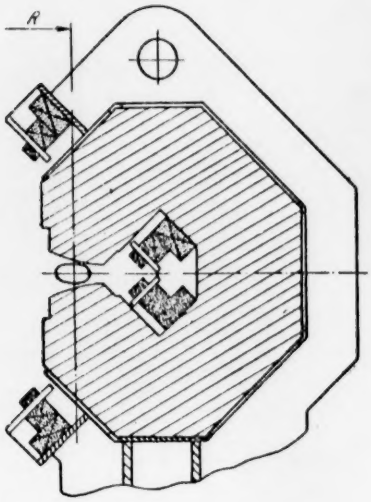

Fig. 3. Construction of the regular accelerator magnets.

The injector will be a 100 Mev linear accelerator. The magnetic field at injection is 90 gauss. Any deviation of particle momentum from the nominal value leads to compensating radial oscillations and causes the frequency of the free transverse oscillations to approach the approximate resonance value. This situation determines the allowable momentum deviations $-5 \cdot 10^{-3}$.

The accelerating system is supplied with an rf voltage the frequency of which is 30 times greater than the rotational frequency of the particles. The basic data on the radio-frequency system is given in Table 4.

As can be seen from Table 4 in the terminal acceleration cycle the tolerance for frequency deviations is very small. In this last cycle however, the frequency change is small and thus the problem is not too serious.

We are considering a design in which the frequency is controlled by the beam. This system will be tested in a 7 Bev accelerator which is under construction.

TABLE 3

Growth time for the magnetic field	3.8 sec
Number of cycles per minute	6
Maximum exciting current	12,000 amp
Maximum voltage	8,000 v
Resistance of exciting winding at 15° C	0.31 ohm
Maximum inductance of exciting winding	1.8 henry
Peak power	96,000 kva

TABLE 4

Frequency of the accelerating field at the beginning of the acceleration cycle	2.624 mc
Frequency of the accelerating field at the end of the accelerating cycle	6.068 mc
Tolerance on the deviations (slow) of the frequency from the specified frequency $\Delta f/f$	
beginning of cycle	$2 \cdot 10^{-3}$
end of cycle	$2.6 \cdot 10^{-6}$
Corresponding accuracy of magnetic field $\Delta H/H$	
beginning of cycle	$2.5 \cdot 10^{-3}$
end of cycle	10^{-2}
Frequency of small synchrotron oscillations F	
beginning of cycle	5150 cps
end of cycle	24 cps
Tolerance on resonant harmonics $\delta f/f$	
beginning of cycle	$31 \cdot 10^{-7}$
F = 50 cps	$4 \cdot 10^{-8}$
end of cycle	$12.5 \cdot 10^{-9}$
Tolerance on noise modulation of the frequency	$4.8 \cdot 10^{-3}$ cps^2/cps

In the accelerator under design the protons acquire approximately 100 kev per turn. The sum of the accelerating voltages is 200 kv. As accelerating elements we propose to use transformers with ferrite cores. The power of the radio-frequency source will be about 500 kw.

LITERATURE CITED

[1] V. V. Vladimirsky and E. K. Tarasov, "On the possibility of eliminating the critical energy in a strong-focusing accelerator." Collection: Certain Questions in the Theory of Cyclic Accelerators (Acad. Sci. USSR Press, 1955).

Received May 29, 1956

LUMINESCENT CHAMBER

E. K. Zavoisky, M. M. Butslov, A. G. Plakhov and G. E. Smolkin

This paper gives a more detailed description of the components of the luminescent chamber and their development since the time at which an earlier report [1] was published; new experimental data are also presented.

One of the basic components of the chamber (Fig. 1) is the electron-optical image-converter (EIC), which utilizes the principle of the cascade electron-optical light amplifier. Although this principle was reported in the literature long ago [2], the only successful experimental realization of the idea up to the present time has been that of M. M. Butslov.* A multicascade EIC of this type has an electron multiplication factor η_e which is no smaller than that of multipliers with resolving powers (at the screen) of $d \approx 10^{-2}$ cm and makes it possible to detect photographically one electron emitted from the input cathode.

The diagram of the EIC is shown in Fig. 1. The converter consists of an input section and several amplifier cascades which are coupled by optical contact through thin transparent sheets. There is a fluorescent screen 1 on one side of the sheet and a photocathode 2 on the other. The electron image is kept in focus in the multiplier cascades by the homogeneous magnetic field of the solenoid 3. In the input section electrostatic focusing is employed. With appropriate voltages on the photocathode 2 and the diaphragm 4, an electrostatic lens is formed. Electrode 5 provides fine focusing of the electron image on the screen 1.

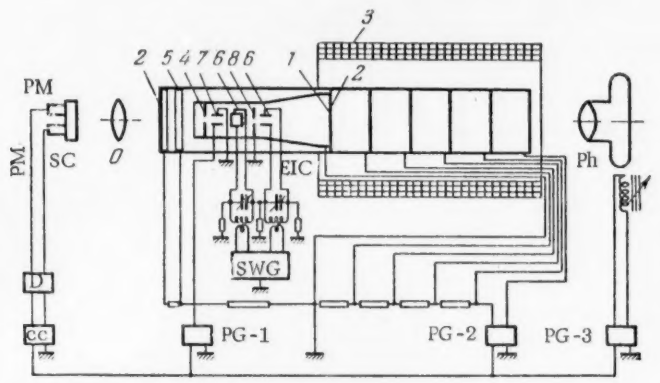

Fig. 1. Diagram of the luminescent chamber. SC) Scintillation crystal; O) objective; EIC: 1) fluorescent screen; 2) photocathode; 3) solenoid; 4) diaphragm; 5) focusing electrode; 6) deflection plates; 7) 8) pulsed electron gate; Ph) photographic apparatus; PG-1) pulse generator for the electron gate; PG-2) pulse generator for the high voltage; PG-3) pulse generator for control of the photographic apparatus; SWG) sweep generator.

*The EIC described in [3] has only one amplifier cascade and an amplification factor of less than 100.

In the space between the diaphragm and the screen there are two pair of deflection plates 6 which provide the high-frequency sweep. Electrodes 7 in conjunction with the diaphragm 8 comprise a pulsed electron gate. Fig. 1 shows a set-up which incorporates a radio-frequency generator and resonance circuits for the deflection plates as well as a pulse generator PG-1 for the gating section.

Because there is no time delay this pulse scheme is an improvement over the analogous arrangement using a magnetic deflection system described in [4]. It provides a sweep "frame" with a resolving time of 10^{-8} sec and a continuous radio-frequency sweep with a resolving time $3 \cdot 10^{-12}$ sec [5].

Fig. 1 also shows the arrangement of the high-voltage power supply for the EIC. In dc operation, the supply for all sections is obtained from a single high-voltage source through voltage dividers. In recording the tracks of cosmic particles and other random phenomena, a pulsed supply is used for the output section in order to reduce the background. For this purpose a gating electrode such as that described above is used in the output section of the EIC. More frequently, however, use is made of a high-voltage pulse supply from a special electrical set-up. * In the figure this unit is designated by PG-2. The pulse length was varied to fit the emission time of the output screen. **

In recording tracks of relativistic particles and other weak signals, even with pulsed supplies on the output section it is impossible to eliminate the background due to the inherent noise of the EIC. To reduce this background a pulsed supply was used on the electron gate 7-8 in the input section; this is PG-1. The length of this pulse is determined by the electron time-of-flight in the interelectrode gap ($\approx 5 \cdot 10^{-9}$ sec) and the duration of the signal itself. For example in working with CsI(Tl) $\tau \approx 3 \cdot 10^{-6}$ sec. In this case the noise of the photocathode is completely supressed. It is, of course, also possible to pulse all the other sections of the EIC.

Synchronization of the gating pulses was accomplished by means of a scheme consisting of a photomultiplier PM, a discriminator D and a coincidence circuit CC with a resolving power of $4 \cdot 10^{-8}$ sec. Following the operation of the pulse generators the film in the photographic apparatus was shifted automatically.

The operation of the luminescent chamber is strongly dependent on certain important properties of the crystal such as light output, transparency to its own luminescence, and also the relative degree of correspondence between the crystal luminescence spectrum and the spectral sensitivity of the photocathode. Unfortunately it was necessary to use crystals of NaI(Tl), CsI(Tl), anthracene and other low quality crystals. However, even in these it was shown experimentally that the amount of light emitted along the track of the charged particle is adequate for detecting even relativistic particles.

This can be shown from an elementary calculation. A typical relativistic singly-charged particle loses, in a CsI(Tl) crystal, about 5 Mev per cm of track.

The number of photons emitted in this segment of track into an angle 4π is

$$F = \frac{5 \cdot 10^6}{\epsilon} \approx 1{,}4 \cdot 10^5,$$

where ϵ is the energy required for the emission of one light quantum in CsI(Tl) which is taken to be ~ 35 ev [6]. The number of quanta incident on the photocathode of the EIC is determined by the solid angle intercepted by the objective

$$s = \frac{F}{16} B^2 \frac{k^2}{(1+k)^2} \cdot g.$$

Here B and k are the relative aperature and the magnification of the objective, g is the ratio of the corresponding solid angles in the crystal and in air – this may reasonably be taken as $1/n^2$ where n = 1.79, the index of refraction of a CsI crystal. Typically b = 1/2 and k = 1 so that we get $s \approx 170$ photons/cm.

*A detailed description of suitable circuits, developed by the authors, will be given elsewhere.

**It is assumed that the limitation on the emission time of the screen is the speed of the photographic apparatus and not the resolving time of the instrument.

The spectrum of the CsI(Tl) emission is almost entirely contained within the spectral sensitivity curve of a cesium-antimony photocathode. Taking the quantum efficiency of the photocathode to be $\delta = 10^{-1}$ [7], we obtain the number of electrons emitted from 1 cm of length of the image of the track on the photocathode $m \approx 17$. Since the resolving power of the EIC is $d \approx 10^{-2}$ cm it is easily seen that the image of the track will consist of different points with spaces between them. Each point corresponds to one electron at the input of the EIC. The space l between the points is

$$l = \frac{1}{m} = \frac{16(1+k)^2 \cdot n^2}{F \cdot B^2 \cdot k^2 \cdot \delta}.$$

The useful thickness of the crystal is determined by the depth of focus of the objective and can be computed from the formula

$$\Delta = \frac{d \cdot \sqrt{n^2 [k^2 B^2 + 4(1+k)^2] - k^2 B^2}}{k^2 B}.$$

All other conditions being equal the gaps in the track are a function of the ionizing power of the particle. It is convenient to use this relation in conjunction with the range-energy relation in the crystal to identify the

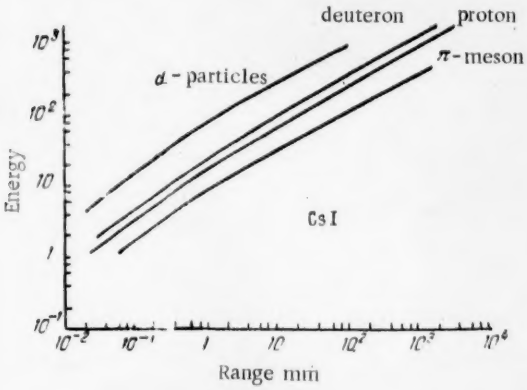

Fig. 2. Range-energy curve for a CsI crystal.

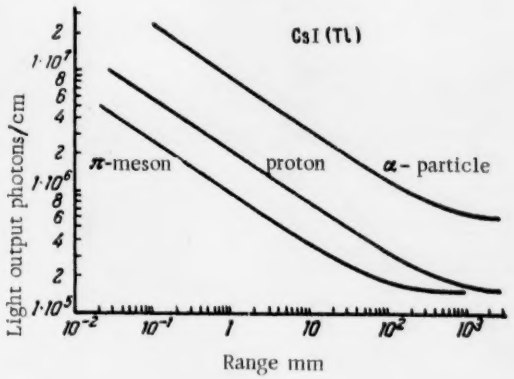

Fig. 3. Range-light output curves for a CsI(Tl) crystal.

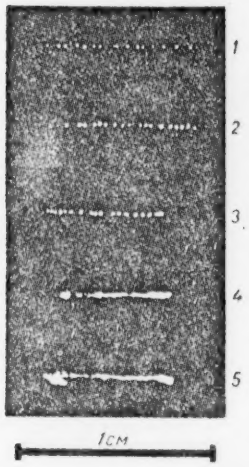

Fig. 4. Photographs of proton tracks in a CsI(Tl) crystal.

particle. In the case of strongly ionizing particles which produce heavy tracks* the spaces which are used for identification purposes are obtained from the optical density of the negative along the track. In Fig. 2 and Fig. 3 are shown range-energy curves and range-light output curves for CsI(Tl) which have been calculated for this purpose. The calculation was based on the well-known Bethe formula for energy loss by ionization. In the low-energy region, where the particle velocity remains comparable to that of a k-electron in an atom, data on energy loss in silver [8] and experimental results on atomic stopping power of the elements were used [9]. Finally we present photographs (Fig. 4) of proton tracks in a CsI(Tl) crystal obtained with the neutron beam of the synchrocyclotron of the Institute of Nuclear Problems, Academy of Sciences USSR. The tracks are arranged in

*We may note that for $l = d$ and even for $l < d$ the tracks are not heavy. Only for $l \ll d$ do the points become fused into a heavy track. The reason for this seems to be fluctuations in the light flux and the quantum efficiency of the crystal and photocathode.

order of increasing ionizing power of the particles; 1) is the track of a 200 Mev proton, 2) and 3) are tracks of slower protons (the lineal density of points in tracks 1, 2, and 3 are in the ratio 2:3:4), 4) is the track of a proton coming to rest, 5) is apparently the track of a slow proton produced in a star. At the end of its path it undergoes a 15° deflection and an intermittent increase in ionization density. It is possible to see the spacing between crystal nuclei in the tracks of the slow protons.

The authors wish to express their gratitude to I. V. Kurchatov for his constant interest and assistance in this work.

LITERATURE CITED

[1] E. K. Zavoisky, G. E. Smolkin, A. G. Plakhov and M. M. Butslov, Proc. Acad. Sci. USSR 100, 241 (1955).*

[2] Ardenne, Elektr. Nachr. Techn. 13, 230 (1936).

[3] Eckart, Ann. Physik 14, 1 (1954).

[4] Courtny – Pratt, Research 2, 287 (1949).

[5] E. K. Zavoisky, S. D. Fanchenko, Proc. Acad. Sci. USSR 100, 661 (1955).

[6] G. Birks, Scintillation Counters (Foreign Lit. Press, Moscow, 1955).

[7] S. Yu. Lukyanov, Photoelements, (Acad. Sci. USSR Press, Moscow-Leningrad, 1948).

[8] Bogaardt and Vigneron, J. phys. radium 11, 652 (1950).

[9] Segre, Exper. Nucl. Phys. 1 (1952).

*[Consultant's Bureau translation – Report PC-9].

PLANE-PARALLEL SPARK COUNTERS FOR THE MEASUREMENT OF SMALL TIMES

M. V. Babykin, A. G. Plakhov, Yu. F. Skachkov, and V. V. Shapkin

Descriptions are given of the construction and the results of investigations of the characteristics of plane-parallel spark counters filled with argon and diethyl ether vapor.

INTRODUCTION

In recent years there has been greater and greater development of spark counters with plane-parallel electrodes. The interest in these counters is due to the fact that they have quite a number of advantages in comparison with counters of other types. They are primarily distinguished by their high resolving power in time.

In a number of papers [1-4] measurements have been made of the time lag of the discharge in two counters placed close together and both traversed by the same fast ionizing particle. The values obtained for the half-width of the curve of the relative time lags agree well with each other, giving the amount $(5\text{-}6)\cdot 10^{-9}$ sec.

For further reduction of the spread of the time lag of the discharge there are at least two possibilities: increasing the overvoltage on the counters and decreasing the distance between the electrodes. Besides these, there is an important influence on the development of the discharge from the nature of the working gas and of the organic additive.

The discharge in a plane-parallel spark counter is localized in a small volume. This fact makes it possible to judge the place of traversal of the counter by the particle to an accuracy of about the size of the gap between the electrodes. In order to observe the spark, one of the electrodes can be made of glass with a semitransparent conducting film.

Under suitable conditions plane-parallel spark counters have good counting characteristics: the slope of the plateau amounts to several percent per 100 v, and the amplitudes of the output pulses of spark counters reach some hundreds of volts, so that the necessity for preamplifiers in the counting circuits is eliminated.

Along with their obvious superiorities, spark counters have important shortcomings, which to a considerable extent limit their application. As the first of these shortcomings we must note the large dead time. To obtain good counting characteristics one must use quenching circuits with $10^{-3}-10^{-4}$ sec duration of the quenching pulse, or else corresponding quenching resistances. Besides this, the counters are very sensitive to the temperature and have limited service life (after $10^{6}-10^{8}$ pulses, washing out and refilling is necessary).

But in spite of this, owing to their high time-resolving power, spark counters are used in the solution of many problems of nuclear physics and for studies of cosmic rays. They are most of all useful for measurements of the energy of fast charged particles by time of flight, and of the lifetimes of excited states of nuclei.

Together with measurement of the lifetime of excited states of nuclei, data can be obtained on the angular correlation of $\gamma-\gamma$, $\beta-\gamma$, or $\alpha-\gamma$ processes, if spark counters are used that have semitransparent electrodes, which allow the place where the particle passes to be located very accurately.

Construction of the Spark Counters

The basic problem that we set ourselves in our study of plane-parallel spark counters was the improvement of their time characteristics, i. e., the reduction of the time lag of the discharge relative to the instant of passage of the charged particle through the counter, and the reduction of the dead time of the counters.

As was indicated above, the lag of the counter can be reduced by a considerable shortening of the distance between its electrodes. But along with this it is necessary to increase the pressure of the working gas and the organic additive, in order to produce a satisfactorily operating counter with adequate efficiency. Thus in the development of counters with the smallest possible gaps one has to deal with relatively high pressures, which to a considerable degree determines the construction.

To increase the allowable counting rate a special spark counter was constructed, with one of its electrodes made in the form of small sections insulated from each other and connected with the source of voltage through high resistances. The limiting counting rate of such a counter increases in proportion to the number of sections.

The spark counters are relatively simple in construction. Figure 1 shows a cross section and Fig. 2 an outside view of a telescope of two plane-parallel spark counters with semitransparent electrodes. The body of the telescope is made of steel. Through a lead plug there is screwed into the body a valve 4, through which the counter is pumped out and filled. The porcelain insulator 3 for the electric lead is also screwed into the body and gasketed with lead. The end surfaces of the body are ground and then carefully worked onto it. The electrodes 1 are recessed below the ends by the amount of the gaps, in the present case 0.2 mm.

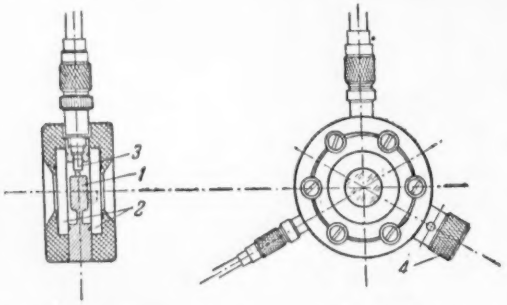

Fig. 1. Construction of a telescope of two plane-parallel spark counters.

The side walls 2 of the telescope are made of optical glass of thickness 5 mm. On the insides of the glass faces are applied circular semitransparent conducting layers to act as the second electrodes. The conducting layers are applied with tin chloride vapor. The resistance of such a layer amounts to 50 to 100 ohm/cm.

The packing between the ground faces of the body and the glass is provided by rubber rings, which are fitted into grooves in the faces. In the assembly the rubber is forced into the grooves and the glass comes firmly against the metal. Since the metal electrodes are set in 0.2 mm below the ground faces and the semiconducting electrodes deposited on the glass are in the planes of the ground ends, the gap between the electrodes has this value. The parallelism of the electrode planes is maintained within 0.002 mm with ease.

The metal electrodes are in one piece with the body and are grounded, while a voltage of either polarity, of 2000 to 3000 volts is carried by the leads through the insulator to the electrodes on the glass, the connection being through a paper resistor of 50 to 100 meg. The insulation of the electrode from the grounded body is provided by the glass itself; a separation of 6 to 8 mm along the surface of the glass is found to be quite sufficient.

Owing to the great brightness of the spark and the good transparency of the conducting layer, the operation of the counter can be observed visually in a lighted room. The possibility of directly observing and photographing the discharge in counters with transparent electrodes is a great advantage and permits the use of new electron-optical methods both for the study of the discharge itself and also for the solution of several other technical and physical problems [5].

The counters were filled with chemically pure argon at pressures of 3 to 10 atmos. Diethyl ether was used as the organic additive, at partial pressures varying over a wide range. Counters containing alcohol vapor were also tested, but under these conditions they work distinctly less well than the counters with ether

Before the filling with the working mixture, the counters were pumped out to about 10^{-4} mm Hg. It must be noted that changing the degree of evacuation within wide limits does not effect the quality of the counter. The edges of the metal electrodes were rounded and polished, and the electrodes on the glass were made of somewhat larger diameter in order to place their edges away from the opposing electrodes. In order

to make a good counter it is necessary to prepare the electrodes carefully and wash them well before assembly. Besides this, it is necessary to make sure that there are no scratches on the surfaces of the electrodes and that after assembly there does not remain even the smallest grain of dust.

The construction that has been described for the counter telescope, because of the massiveness of the walls, is good only for the registration of γ-quanta and high energy charged particles. But it can be used for the study of the question of the time lag of the discharge in the counters themselves in the registration of cosmic rays or cascade γ-radiation. In the later case, a preparation of Co^{60} can be inserted through the side opening in the body of the telescope and placed on the axis of the telescope between the metal electrodes [5].

Spark counters can also be adapted to the registration of electrons, protons, and α-particles of relatively small energies, if the electrodes are made of thin foil or micromesh. Spark counters can also be made that are effective in counting neutrons.

Counting Characteristics

In order to study the counting characteristics in their dependence on various conditions, namely on $p\delta$ (the product of pressure and gap size) and on the ether vapor content, a special counter was constructed with a movable electrode, the construction being that shown in Fig. 3.

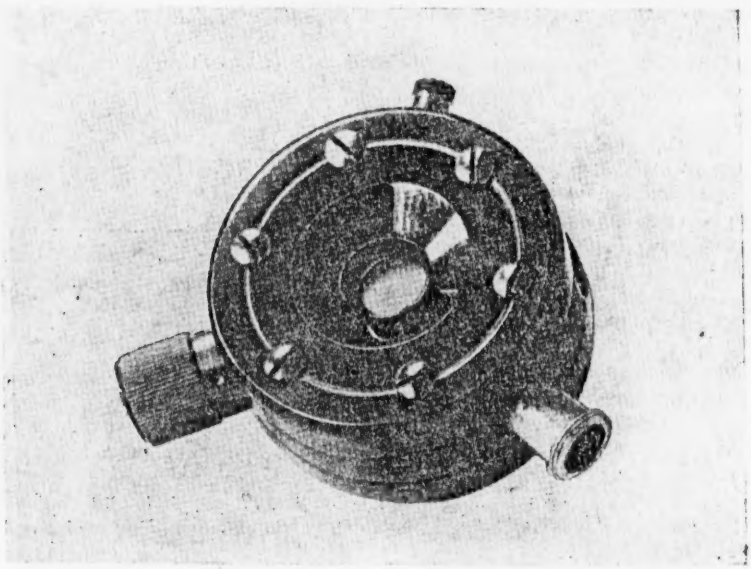

Fig. 2. External view of the telescope.

The steel electrode 1 is attached to the movable rod on a steatite insulator, and was carefully ground and polished together with the sleeve of the body. The displacement of this electrode along the axis of the counter was accomplished by a micrometer, so that the gap could be varied from 0 to 1 mm with an accuracy of 0.01 mm.

A sylphon was used to attach the moving part, its ends being welded to the rod and the body. The operating voltage was supplied through an insulated lead and the resistance R(150 meg). The stationary electrode was supplied by the glass with a conducting layer 2. This electrode was fixed in the plane of the flange of the second part of the counter body.

The registration of the discharges was carried out in two ways: by means of a photomultiplier and directly by a counter of electric pulses.

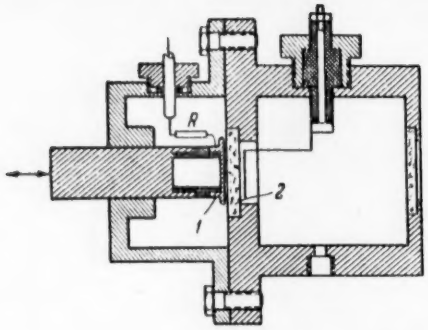

Fig. 3. Construction of counter with movable electrode. 1) movable electrode; 2) semi-transparent electrode.

As the working gas in the counter, argon was used at a pressure of 6 atmos. The organic additive was diethyl ether, whose partial pressure was viaried from 60 to 400 mm Hg.

The study of the dependence of the counting characteristics on the voltage was made with the γ-radiation of Co^{60}.

Figure 4 shows the dependence of the counting characteristics on the gap size for two pressures of the ether vapor (60 and 400 mm Hg). With widening of the gap their slope decreases, and the length of the flat part increases.

The variation of the slope in its dependence on the pressure of the vapor of the organic additive, for gap width 0.3 mm, is shown in Fig. 5. The rather decided slope of the counting characteristics at small pressures of ether vapor (60 mm Hg) indicates that at a small concentration of the organic additive in the counter a large number of false pulses is observed, although the background on the counter in the absence of a source is very small. This is probably explained by the weak absorption of ultraviolet radiation at low concentrations of the organic additive. When the pressure of the ether vapor is increased to 400 mm Hg, the absorption of the photons is increased, and the number of false counts falls; this leads to an improvement of the counting characteristic.

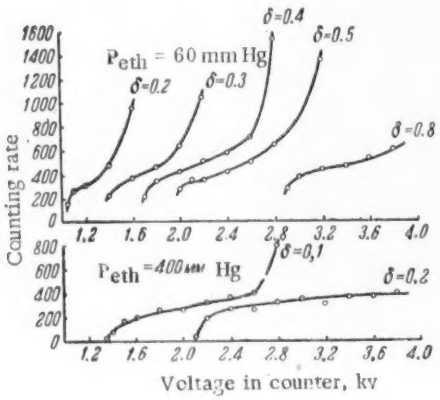

Fig. 4. Dependence of counting characteristics on gap size.

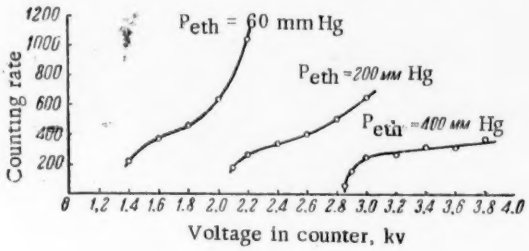

Fig. 5. Dependence of counting characteristics on on pressure of ether vapor.

The slope of the flat part of the characteristic, equal to 13% per 100 v at 60 mm Hg pressure of ether vapor, becomes 4% per 100 v at 400 mm Hg pressure of the ether vapor.

An important feature is that the pressure of the organic additive has a strong influence on the counting threshold. From this same Fig. 5 it is seen that with increase of the pressure of the ether vapor the characteristics are shifted into the region of high operating voltages. A change of the pressure of the ether vapor by 200 mm Hg causes a shift of the operating voltage by about 700 v. This makes it possible, by increasing the pressure of the vapor of the organic additive, to increase the field in the gap of the counter, which decreases the lag.

Spark counters, as is known, have a limited service time. This is due to the fact that in the process of operation the organic additive is decomposed, the electrodes become covered with a film, and the counter stops operating.

To determine the service time of a spark counter with a transparent electrode a special experiment was arranged.

The counter counted 10^8 pulses. On disassembling it, it was found that the surfaces of the electrodes were covered with a rather solid brown film, probably formed as a result of the decomposition of the ether and the sputtering of the material of the electrodes.

The metal electrode can easily be restored by washing. Washing of the semitransparent electrode also leads to removal of the film, but after prolonged operation of the counter the resistance of the conducting layer increases, which indicates its progressive destruction.

For many experimental problems, where the intensity of the radiation is not great, this service life of the plane-parallel spark counter is quite adequate.

Obviously, to increase the service life one can use halogen additives instead of organic additives. It has been found that with a halogen additive (bromine vapor) a spark counter can operate normally.

Time Characteristics of Plane-parallel Spark Counters

As was already indicated in the introduction, the main interest in spark counters is due to the fact that they give a small spread of the time lag of the discharge relative to the instant of passage of the charged particle. This permits them to be used for the measurement of small time intervals.

As an example of such a measurement there is shown in Fig. 6 a sweep photographic image of the sparks from two counters which were traversed by the same cosmic-ray particle. This photograph was obtained by a method for measuring small times by a sweep representation in an electron-optical image converter, as described previously [6].

Fig. 6. Sweep photograph of sparks in two counters, caused by a single cosmic ray particle. Sweep period $6.6 \cdot 10^{-9}$ sec, distance between counters 14 mm.

From photographs so obtained one can determine the relative lag of the discharges in two counters.

An attempt was made to determine the spread of the lags with cosmic rays.

The relatively small number of cases we have measured permits us to draw the conclusion that the spread of the lags does not exceed $4 \cdot 10^{-10}$ sec.

A more detailed study of this question can be found in the following paper [5].

From the photograph shown in Fig. 6 it can be seen that the length of the front and the duration of the whole spark are of great importance for the time measurements. To determine the length of the front and the duration of the spark, the sweep picture of the spark was subjected to microphotometry.

Figure 7 shows a microphotogram of the spark front. The intensity of the spark reaches half value after $1.5 \cdot 10^{-10}$ sec.

In the top of Fig. 8 there is shown a complete microphotogram of the same spark, from which it is seen that the total duration of the spark amounts to $2 \cdot 10^{-9}$ to $3 \cdot 10^{-9}$ sec; at the bottom is shown a microphotogram of part of the sweep picture of a spark, which brings out distinctly the structure of the spark, with a period of $4 \cdot 10^{-10}$ sec, corresponding to an oscillatory discharge process with wavelength 12 cm.

The data presented show that plane-parallel spark counters used with the previously described method for time measurement can find successful application for the solution of a wide range of problems of nuclear physics.

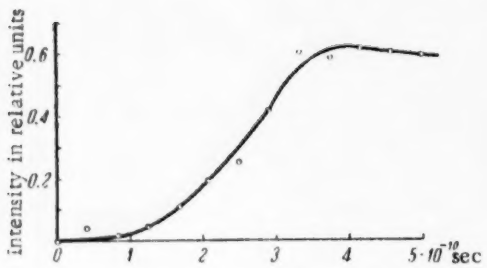

Fig. 7. Microphotogram of the front of the sweep photograph of a spark.

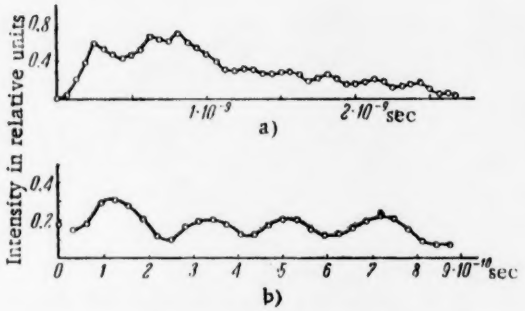

Fig. 8. Microphotograms: a) Sweep picture of a spark; b) part of a spark, with well marked structure.

The Sectioned Counter

For the solution of many problems of nuclear physics, counters are needed that admit large loads. The spark counters known up to the present have at best a counting rate of 10^4 pulses per sec. The counting rate of a spark counter with given electrode area can be increased by sectioning. At the same time this improves the time characteristics of the discharge in the counter; namely, it reduces the total duration of the spark and shortens its front. For this purpose a sectioned counter was built, with one of its electrodes consisting of 49 elements.

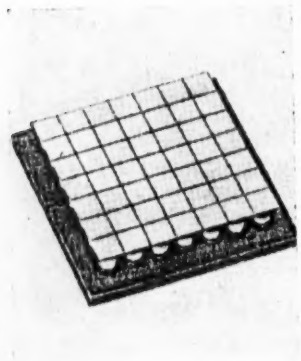

Fig. 9. The sectioned electrode of the counter.

Figure 9 shows a photograph of the sectioned electrode of the counter. The electrode was prepared in the following way. In a metal plate of dimensions 25 × 25 × 2 mm, at the corners of a square lattice with spacing 3 mm, there were drilled 49 holes of diameter 2 mm. Into the holes were soldered porcelain tubes, the ends of which had first been coated with silver and copper. To the free ends of these tubes was soldered a thin metal plate 21 × 21 × 0.2 mm, into the inner side of which there had previously been cut grooves (width 0.2 mm, depth 0.16 mm) forming a square lattice with the same spacing as before. Then the outer side of this plate was cut completely through to form separate sections. The sharp edges of the sections were rounded.

To provide a resistance between the solid plate and the sections, the porcelain tubes were filled with a semiconducting compound.

The other (common) electrode was a conducting layer on glass. When a particle passes through the counter, there is a spark discharge between one of the sections and the conducting layer. The number of photons from this spark is about 10^7. Its light can be registered by a photomultiplier or an electron-optical converter. At the time of the discharge a potential difference occurs between adjacent sections, approximately equal to the operating voltage. To prevent discharges between the sections, the gap width was chosen equal to the distance between them.

The resistances in the sections of the counter were chosen experimentally. Their size was chosen equal to 80 ± 30 meg, and corresponded to the smallest value of RC at which the spark discharge in the sections still did not go over into an arc.

The counting characteristic plotted against voltage has a rather steep slope. The breadth of the flat part of the characteristic covers 150 to 200 volts at a steepness of 10 to 15% per 100 v. Such a worsening of the counting characteristic by sectioning is due to the interaction of the sections, as was established by a comparison of the counting characteristics of a single insulated section and combinations of two, four, and more sections, and is clearly explained by ions getting from one section into others because of diffusion and the fringing fields of neighboring sections.

Tests were also made on the optical coupling between sections of the counter. In the discharge a brightly glowing channel is formed – a streamer. The ultraviolet radiation of the streamer produces a photoelectric effect at the electrodes of the counter. The probability of occurrence of false counts in neighboring sections is increased, if the spark jumps near the edges of the sections. This effect shows up especially strongly at large overvoltages on the counter, i. e., in the upper region of the counting characteristic. Paired sparks at the edges of adjacent sections are observed visually.

The paired sparks at the edges of the sections, produced by the photoelectric effect, cannot be separately registered by the counting circuit, which has a resolving time of 10^{-7} sec, since they follow each other at time intervals of the order of 10^{-9} sec.

The number of paired, triple, quadruple, and other multiple sparks is considerably increased if the pressure of the organic filler – ether – is reduced.

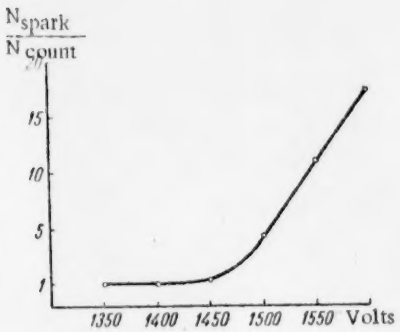

Fig. 10. Ratio N_{spark}/N_{count} as function of voltage. N_{spark} – number of sparks, determined photographically; N_{count} – number of counts on the registering device.

To determine the relation between the number of sparks in the counter and the number of recorded pulses and its dependence on the voltage, a simultaneous count was conducted of the pulses and of the sparks photographed by means of the electron-optical image converter. To make it possible to count the number of sparks on the photographs not more than 100 pulses were registered at each value of the voltage, and at voltages in the higher part of the plateau not more than 20. The results are presented in Fig. 10, which shows the dependence of the ratio of the number of sparks to the number of registered pulses on the voltage across the counter. In the middle of the plateau this ratio is equal to 1.3. Consequently, in the middle of the plateau 30% of the sparks turn out to be false.

In Fig. 11 are shown three photographs of the counter in operation, taken by means of the electron-optical image converter: a) corresponds to the beginning of the plateau, b) to the middle, and c) to the end.

In the first two photographs the edge effect is not noticeable; in the third it is clearly visible.

The sectioned counter was tested at extreme load. The limiting counting rate was $1.6 \cdot 10^5$ pulses per sec. In unsectioned counters the counting rate did not exceed 10^4 pulses per sec.

In the sectioned spark counter a broad plateau could not be obtained because of the optical and ionic connection between adjacent sections. But this shortcoming can be avoided by more refined construction and by a suitable choice of the filler for the counter.

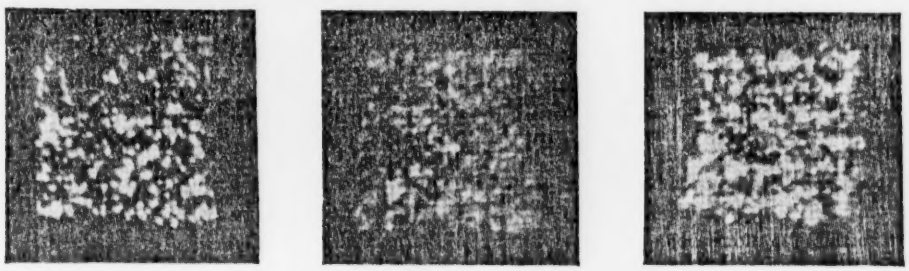

a) b) c)

Fig. 11. Interaction of the elements of the sectioned counter at various voltages: a) 1350 v, b) 1450 v, c) 1600 v.

CONCLUSION

In this research it has been established that it is possible to construct plane-parallel spark counters with high time resolution, good counting characteristics, high efficiency for counting charged particles, and comparatively long service life.

The authors consider it their pleasant duty to express their sincere thanks to Corresponding Member of the Academy of Sciences of the USSR E. K. Zavoisky for his valuable advice and his constant interest in this work.

LITERATURE CITED

[1] I. W. Keuffel, Rev. Sci. Instruments 20, 3, 202 (1949).

[2] L. Madansky and R. W. Pidd, Rev. Sci. Instruments 21, 5, 407 (1950).

[3] R. W. Pidd and L. Madansky, Phys. Rev. 75, 8, 1175 (1949).

[4] E. Robinson, Proc. Phys. Soc. 66, 397 A, 7 (1953).

[5] E. K. Zavoisky and G. E. Smolkin, Atomic Energy 1956 No. 4, 46 (T. p. 495).*

[6] E. K. Zavoisky and S. D. Fanchenko, Proc. Acad. Sci. USSR 100, 4 (1955).

Received March 29, 1956.

*T. p. = C. B. Translation pagination.

INVESTIGATION OF THE TIME-RESOLVING POWER OF PLANE-PARALLEL SPARK COUNTERS

E. K. Zavoisky and G. E. Smolkin

A study has been made of the resolving power of plane-parallel spark counters with small working gap and high pressure of the gas mixture. It is shown that the resolution time of such counters may reach 10^{-10} sec.

I

The most remarkable property of plane-parallel spark counters is their high resolving power in time. It has already been shown in papers published earlier [1, 2] that the resolution time of such counters can reach $5 \cdot 10^{-9}$ sec. It is shown below that it can be reduced at least to 10^{-10} sec.

As is well known, the resolution time of Geiger-Müller counters has a value of the order of 10^{-7} sec. Such a sharp difference between the time-resolving powers of the two gas-discharge counters is due first of all to the shape of the electric field in the gap between the electrodes. In the plane-parallel spark counter the field is everywhere homogeneous and is large enough for the initiation of ionization by collision and the formation of electron-photon avalanches, which lead to the spark discharge. Therefore in this case there is not required the so-called "drift time" for the primary electrons that are formed in the volume of the counter when ionizing particles pass through.

Besides this basic factor, there are a number of others on which the time resolution of the plane-parallel spark counter depends in an essential way. Such factors are: the size of the gap between the electrodes, the applied potential difference, the gaseous filling of the counter, and, finally, the ionizing power of the radiation to be counted.

In this connection it is necessary to point out that the resolution time indicated above, of $5 \cdot 10^{-9}$ sec [1, 2] was obtained by the use of counters with a gap of 2.5 mm between the electrodes. The filling was a mixture of argon with saturated vapor of xylol [1] and of alcohol [2]. The total pressure of the gas mixture did not exceed 60 cm Hg.* The potential difference applied to the counter was of the order of 2000 to 3000 volts. The attempts of some authors to reduce considerably the gap between the electrodes and thus to lower the resolution time of the counters have not led to the desired result [3].

In this regard the counters described in reference [4] represent a significant advance. The distance between the electrodes in these counters approaches tenths of a millimeter and the operating voltage across the counter is 2000 to 4000 volts. Thus the intensity of the electric field here exceeds by more than an order of magnitude that in the counters of the earlier construction. The filler used in these counters is a mixture of argon with ether vapor, which has a considerably higher pressure at saturation than the vapors of alcohol and xylol.

At the same time, the reduction of the gap between the electrodes does not lead to a lowering of the counting efficiency, since the total pressure of the gas mixture reaches 10 atmos and more. All this cannot fail to have an effect on the time resolving power of the counters, to the study of which the present paper is devoted.

*[cm Hg appears in the original – translator's note].

II.

The study of the inertial behavior of the counters was conducted by measuring the relative lag of the spark discharges in two counters in the registration of $\gamma - \gamma$ incidences from a radioactive Co^{60} source. As is well known, the nucleus of Co^{60} goes over by β-decay into an excited state of the nucleus Ni^{60*}, which then emits two cascade γ-quanta with energies 1.17 Mev and 1.33 Mev. The lifetime of the nucleus Ni^{60*} in the level 1.33 Mev has a value $\sim 7.5 \pm 2.5 \cdot 10^{-13}$ sec [5], so that it is entirely permissible to treat the emissions of the cascade γ-quanta as simultaneous.

Figure 1 shows the arrangement of the experimental apparatus. Two plane-parallel spark counters are placed in the common chamber 1; the electrodes 2, 4 are of steel and 3, 5 are glass with a transparent conducting surface. Such a surface can be obtained by treating the surface with tin chloride vapor. The transparency of the glass electrode is about 75%, and its surface resistance is $\sim$ 100 ohm/cm. The diameter of the electrodes is 10 mm. The space between them is 0.2 mm. The gaps between electrodes of both counters connect with the common chamber 1. The chamber was filled with saturated ether vapor and argon to a total pressure of 13 atmos. The voltage across the counters was fed through the steatite insulators 6. The noninductive and noncapacitive resistance R, made of black paper, was of the order of 100 meg.

The radioactive preparation on the special brass holder 7 was located in the center between the counters. It had the shape of a cylinder of diameter 2 mm and height 2 mm. The preparation was introduced into the recess 8, separated from the volume of the counter by a thick-walled brass tube, which made it possible to insert and remove the source without disturbing the apparatus.

The diagram also shows the apparatus necessary for the taking of the counting characteristics of the counters, and also for controlling the operation of the counters during the measurements. This consists of the photoelectric multiplier FEU-19, the coincidence circuit CC with resolution time 10^{-7} sec, and mechanical registering devices Reg_1, Reg_2 and Reg_3. The multipliers operated with the light scattered from the walls of the chamber, which fell on the cathodes of the photoelectric multipliers through the glass windows 11 and the light ducts LD. The inside walls of the chamber were painted a light color. The opaque partition 12 prevented any possible optical connection between the photomultipliers.

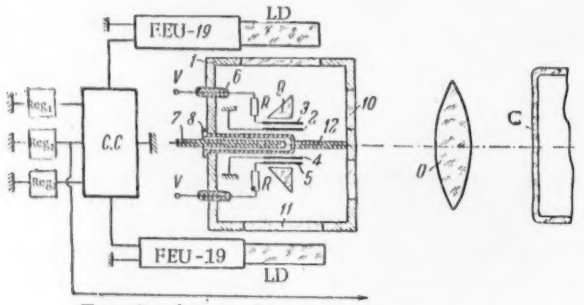

Fig. 2 shows the counting characteristics of both counters used in the work. It can be seen that they are, to a sufficient degree identical, and that they have a rather broad plateau, extending to 4000 v. The slope of the curves in the middle of the plateau amounts to less than 1%. Figure 3 shows also the curve of the dependence of the number of coincidences on the potential difference applied to the counters.

The absolute value of the counter efficiencies g_1 and g_2 for γ-quanta were determined from the data from the simultaneous registration of the number of coincidences n_{12} and the numbers of counts in the channels n_1 and n_2, by the well known formulas

$$g_1 = \frac{n_{12}}{n_2 \Omega_1} \quad \text{and} \quad g_2 = \frac{n_{12}}{n_1 \Omega_2},$$

where $\Omega_1 = \Omega_2 = 0.14$ steradian are the corresponding solid angles subtended by the counters.

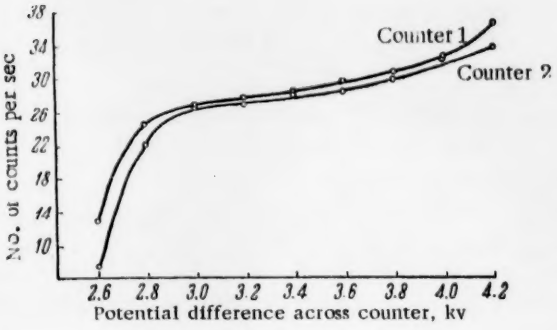

Fig. 2. Counting characteristics of the plane-parallel spark counters.

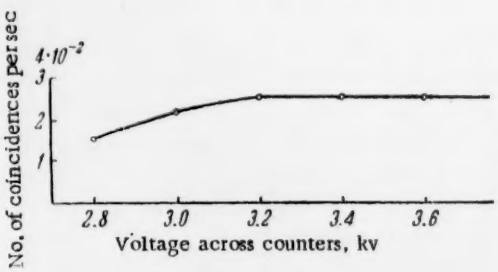

Fig. 3. Dependence of number of coincidences on voltage across counters.

For example, for potential difference 3400 v across the counters, one can find from the counting characteristics the numerical values of the quantities $n_1 = 28.5$, $n_2 = 28.2$, and $n_{12} = 0.025$ counts per second. Consequently,

$$g_1 \approx g_2 \approx 0.63 \cdot 10^{-2}.$$

From these same data the absolute value of the intensity N of the radioactive preparation was determined by the formula

$$N = \frac{n_1 n_2}{n_{12}} = 3.2 \cdot 10^4 \text{ disint./sec.}$$

A check of the circuit for accidental coincidences due to the load on the counters and to scattering of the γ-quanta at the walls of the counters showed that the number of such coincidences was negligibly small in comparison with the number of genuine coincidences.

III.

The measurement of the relative time lags of the spark discharges in the counters was carried out by recording them with a sufficiently sensitive electron-optical image converter, using a high-frequency sweep of the electron image [6, 7].

For this purpose the spark discharges in both counters were projected by means of the prisms 9 and the objective O onto the photoelectric cathode of the converter C (cf. Fig. 1). The light passed from the prisms to the objective through the glass windows 10 of the chamber 1. Since the discharge in a counter is localized in a very small volume, it was imaged on the photoelectric cathode (and consequently also on the screen) as a point image of light. This point image of the spark was swept out by means of a high-frequency field of wavelength $\lambda = 1.5$ m along an arc of a circle of diameter d = 10 mm.

The length of the whole circumference corresponds to the period of the high-frequency field, $T = 5 \cdot 10^{-9}$ sec. In practice, however, the total duration of the spark discharge turned out to be a bit more than the period of the high-frequency field. This could lead to an overlapping of the sweep and undesirable difficulties in finding the fronts of the sparks. Therefore we used a modulated high-frequency field. The wave length of the modulating voltage was 6 m.

The registering part of the apparatus (the electron-optical converter and the photographic camera) operated on a standby basis: the camera remained open all the time, but the electron image of the converter was shut off by a special shutter. Only upon a coincidence of discharges in both counters * was the shutter opened, and the

*This refers to coincidences with the resolution time of the coincidence circuit CC, equal to 10^{-7} sec.

image appeared on the screen of the converter and was photographed on motion picture film. After this the shutter was closed again, and the film was automatically advanced by one frame. The pulse length of the electronic shutter was $\sim 8 \cdot 10^{-5}$ sec. At a counter load equal to 28 counts per second, this shutter completely excluded the possibility of the occurrence of exposures with three sparks, despite the rather considerable inertia of the fluorescent screen of the converter. The synchronization of the pulse shutter was accomplished by means of the photomultipliers FEU-19 and the coincidence circuit CC.

In Figure 4 are shown two typical pictures of coincident spark discharges, obtained by the method described. The measurement of the relative time lag from these photographs was carried out by simple superposition of the images, which is easily done with an ordinary enlarger adapted for this purpose.

We now consider the accuracy of the measurements and the possible sources of error. The electric field intensity near the photoelectric cathode of the electron-optical converter was 1.7 electrostatic units. Consequently the resolution time of the converter, due to the electron optics [8], was equal to $6 \cdot 10^{-12}$ sec. The geometrical resolving power of the converter was 10^{-2} cm. Consequently the instrumental resolution time of the device, due to the period and amplitude of the high-frequency sweep, was equal to

$$\Delta t = \frac{T \cdot 10^{-2}}{\pi \cdot d} = 1.7 \cdot 10^{-11} \text{ sec}$$

The difference of the path lengths of γ-quanta falling in the center and at the edge of a counter and the path difference due to the size of the radioactive preparation amount together to not more than 0.4 cm. This can produce a delay of the order of $1.3 \cdot 10^{-11}$ sec.

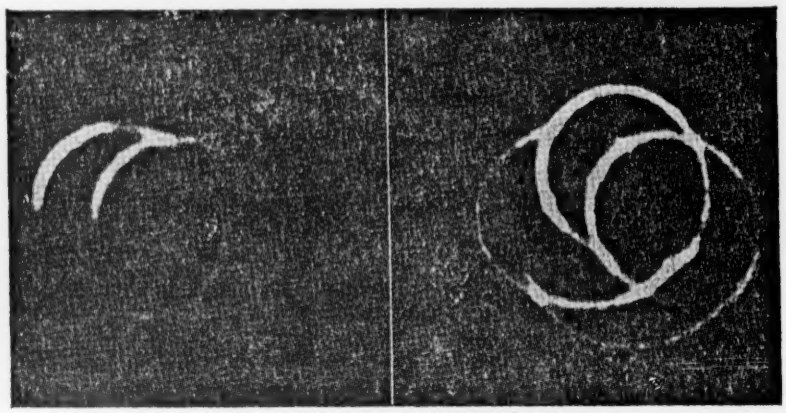

Fig. 4. Two typical pictures of coincident spark discharges in the counters.

The difference of the optical paths of the rays from the counters to the photoelectric cathode of the electron-optical image converter was not more than 0.5 cm, which corresponds to a time $\sim 1.7 \cdot 10^{-11}$ sec. But this constant delay can only displace the center of gravity of the distribution curve relative to the origin of coordinates, and does not increase its half-width.

The largest error occurs in the treatment of the photographs. It is due mainly to the uncertainty arising in identifying the fronts of the sparks, and is in size about $5 \cdot 10^{-11}$ sec.

It must also be noted that the spectrum of the electrons emitted by the walls of the counter under the action of the γ-quanta from the Co^{60} source is very broad. Together with the slow electrons and the electrons of moderate energies, there are present in it a considerable number of electrons with relativistic energies, right up to the maximum energy of the γ-quanta. Now, a relativistic electron moving at right angles with the plane of the counter ordinarily forms a very small number of secondary electrons in the gap between the electrodes.

At a pressure of 13 atmos and gap width 0.2 mm this number is about 5. This circumstance cannot fail to have an influence on the results of the measurements, for there is no doubt that the delay in the operation of the counter will be the smaller, the greater is the density of ionization along the path of the particle being counted.

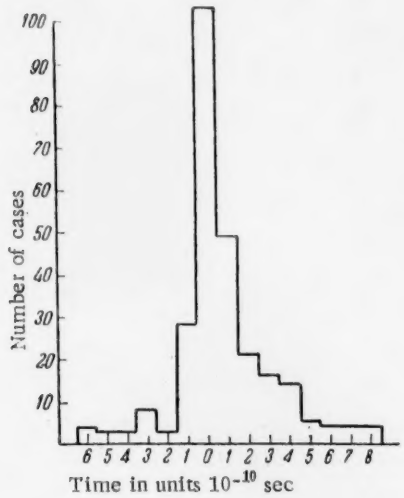

Fig. 5. Histogram of the lag distribution of the plane-parallel spark counters.

The results of the measurement of the resolving power of the counters are shown in Fig. 5, in the form of a histogram of the distribution of 269 cases of the relative time lags, obtained with a potential difference of 3600 volts across the counters. The half width of the distribution curve is about 10^{-10} sec.

Thus the time-resolving power of plane-parallel spark counters exceeds the resolving power of even scintillation counters. Therefore it is of interest to apply them in cases where this property can be advantageous, for example in measuring the lifetimes of short-lived isomeric states of atomic nuclei, the lifetime of the positron and of heavy metastable particles, in measurements of the energy of particles by time of flight, and in other cases. With the counters one can use the usual coincidence circuits with sufficient time-resolving power.

In conclusion it must be noted that according to our estimates the resolution time of spark counters found in our work is still not the limiting value, and may be reduced to 10^{-11} sec.

LITERATURE CITED

[1] J. W. Keuffel, Rev. Sci. Instruments 20, 3, 202 (1949).

[2] E. Robinson, Proc. Phys. Soc. 66, A 397, 73 (1953).

[3] R. W. Pidd and L. Madansky, Phys. Rev. 75, 8, 1175 (1949).

[4] M. V. Babykin, A. G. Plakhov, Yu. F. Skachkov, and V. V. Shapkin, Atomic Energy No. 4, 38 (1956) (T. p.487).*

[5] F. R. Metzger Bull. Am. Phys. Soc., Series II, 1, 1 (1956).

[6] E. K. Zavoisky, G. E. Smolkin, A. G. Plakhov, and M. M. Butslov, Proc. Acad. Sci. USSR 100, 2, 241 (1955).

[7] E. K. Zavoisky and S. D. Fanchenko, Proc. Acad. Sci. USSR 100, 4, 661 (1955).

[8] E. K. Zavoisky and S. D. Fanchenko, Proc. Acad. Sci. USSR 108, 218 (1956).

Received March 29, 1956.

*T. p. = C. B. Translation pagination.

APPLICATION OF THE PHOTOMULTPLIER FEU-12 TO SCINTILLATION SPECTROSCOPY

Iu. A. Nemilov, V. M. Ovchinńikov, A. N. Pisarevsky, and E. D. Teterin

An investigation was made of the spectral response and other characteristics of the FEU-12 photomultiplier having grid-type dinodes and developed by G. S. Vildgrube.

1. Introduction

The use and importance of the scintillation method in the technique of experimental physics have increased considerably during recent years. The scintillation method has been especially widely applied in nuclear spectroscopy. Photomultipliers used in scintillation spectrometers must satisfy the following requirements:

1. High amplitude resolution capability which is basically determined by:
   a. High effective photocathode sensitivity*
   b. Correspondence between the spectral sensitivity of the photocathode and the luminescent spectrum of the phosphor used.
2. Adequate over-all sensitivity.
3. Stability of the over-all sensitivity of the photomultiplier for continuous and intermittent operation.
4. Fast build-up of the photomultiplier steady-state performance after switching.
5. Linear light output characteristic over a wide range of scintillation amplitudes.
6. Low internal noise.
7. A pentode type output – input characteristic.
8. Over-all sensitivity independent of the load within wide limits.
9. Minimum influence of intense nuclear radiation on the over-all sensitivity of the photomultiplier.
10. Minimum sensitivity to external electromagnetic fields and maximum resistance to vibrations.
11. High overload capacity.

The combination of all the enumerated requirements constitutes a severe set of specifications which is far from being satisfied completely by existing photomultiplier systems. For example, the widely used photomultiplier FEU-19, which has high sensitivity, enables one to obtain satisfactory resolution only within a limited energy interval of the radiation being investigated, even under conditions of careful selection of samples having photocathodes of high quantum otuput and application of a special type of voltage dividers. Outside of this, FEU-19 hardly meets any of the remaining requirements. All this narrows down considerably its application to

*By effective sensitivity is meant the integrated sensitivity as measured at the output of the first dinode.

scintillation spectrometers. The defects of the FEU-19 are a natural consequence of the application of antimony-cesium emitters as the basic component of the multiplier system

In this communication we examine the application of the FEU-12 multiplier, developed by G. S. Vildgrube et al., to spectroscopy in the light of the above mentioned requirements.

2. Some Construction Characteristics of FEU-12

The FEU-12 has a semitransparent sectionalized type cathode 50 mm in diameter. The photocathode is followed by a focusing system in which one electrode can be used for cutting off or modulating the electron stream. Then follows the grid type multiplier system consisting of twenty dinodes (according to the characteristic of the electron stream FEU-12 is a linear system). The multiplying system terminates in a reflection type collector. The multiplier bulb is fitted into a standard cathode-ray tube socket. The maximum diameter of the multiplier is determined by the diameter of the socket. The photocathode, modulator and collector terminals are made directly in the bulb and do not increase the over-all dimensions of the equipment because of their "button" type construction. The dinode insulation and fastenings are ceramic. The unusual ruggedness of the system distinguishes favorably the FEU-12 from other types of multipliers.

FEU-12 is constructed with antimony-cesium or bismuth-silver-cesium photocathodes. The dinode system is stamped from a special alloy activated in the photomultiplier production process.

The general view of the photomultiplier is shown in Fig. 1.

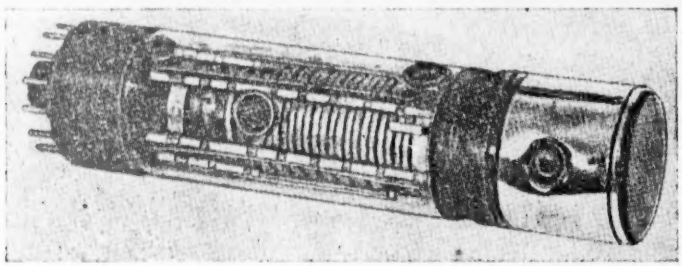

Fig. 1. General view of the FEU-12.

3. Some Static Characteristics

The basic static characteristics of the photomultiplier are:

1. Light characteristic;
2. Input and output volt-ampere characteristic;
3. Spectral characteristic of the photocathode;
4. Zonal characteristic of the photocathode referred to the output;
5. Over-all sensitivity of the photocathode.

The light characteristic indicates the dynamic measurement range that may be expected without changing the supply system all other conditions remaining unchanged. The static light characteristic of the FEU-12 is shown in Fig. 2. It is linear up to medium output currents exceeding 50 ma. The photomultiplier will yield such a current for a long time.

In Figs. 3a and 3b are shown the volt-ampere input-output characteristics. These are quite similar to those of pentodes. The first characteristic reaches saturation at 25 volts, the second at 40 volts for all the investigated samples. The pentode nature of these characteristics precludes such undersirable phenomena as generally take place in multipliers having characteristics with a pronounced maximum. The pentode nature of the input characteristic is secured by the focusing system of electron collection and for the output characteristic by the use of a

reflection-type collector. In systems using direct collectors (for example FEU-19), there is unavoidably obtained an output volt-ampere characteristic having a pronounced maximum due to the flight of electrons past the last dinode directly into the collector.

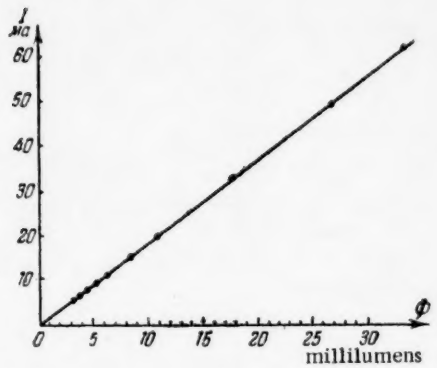

Fig. 2. Static light characteristic of one of the FEU-12 samples.

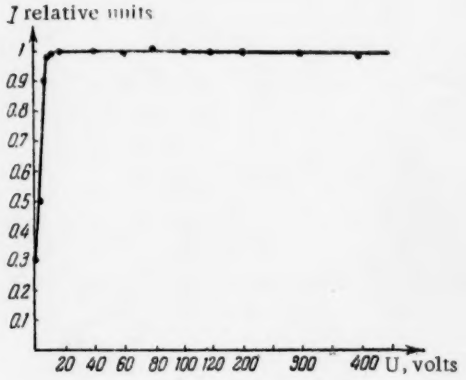

Fig. 3a. Volt-ampere input characteristic of FEU-12 (multiplier No. 99).

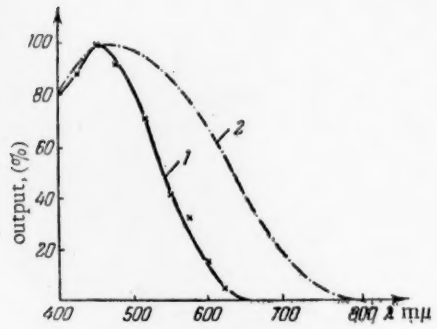

Fig. 4. Average spectral characteristics of photocathodes Bi-Ag-Cs and Sb-Cs. 1) Photocathode Sb-Cs. 2) Photocathode Bi-Ag-Cs.

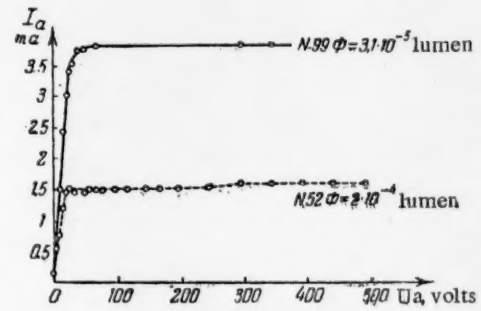

Fig. 3b. Volt-ampere output characteristics (anode characteristics) of FEU-12.

In Fig. 4 are shown the average spectral characteristics for the Sb-Cs and Bi-Ag-Cs photocathodes of the investigated photomultipliers. The characteristic of the Bi-Ag-Cs cathode extends into the region of longer wave lengths compared with the Sb-Cs photocathode, i. e. it is more "broad banded".

The zonal characteristic of the photocathode was measured for three sample multipliers according to the location of the maximum of the α-spectrum. A small CsI(Tl) crystal (2.5 mm diameter, 1.5 mm high) on which was placed a point source radiator was used for this purpose. For the poorest of the three samples the sensitivity spread over the photocathode area did not exceed 10% if the entire photocathode area was considered and 5% if only 2/3 of the photocathode area from the axis of the element was considered.

The over-all sensitivity of the photocathode for the investigated samples varied from 30 to 80 μa/lumen. Out of 25 samples tested 80% of the multipliers had a sensitivity exceeding 45 μa/lumen (when tested with a type A source of a color temperature 2848°).

The gains of the measured samples are within the limits 10^5 to 4×10^6 at an over-all voltage of 1600 volts distributed equally between the electrodes of the multiplier. If necessary the gain can be increased to 10^6 to 10^7 at the expense of raising the working voltage: FEU-12 withstands without damage an increase in the applied voltage up to 2000-2500 volts.

In concluding the description of the static characteristics, it should be noted that the parameters which are determined by the geometry of the multiplier were practically alike for all the investigated samples.

4. Application of FEU-12 In The Scintillation Spectrometer. Selection of Power Supply.

The multipliers were used in several different scintillation γ-spectrometers (single, paired and others). The widest application of the multiplier in spectrometer work is its use in a single spectrometer. We shall therefore discuss only this type.

In the spectrometer the multipliers were used in combination with crystals NaI(Tl) and CsI(Tl). In the table are shown the relative outputs in crystals and photocathodes of both types.

TABLE

Relative Signal Outputs Obtained With Different Photocathodes and Crystals

Photocathode	Crystals	
	CsI(Tl)	NaI(Tl)
Sb-Cs	1	3
Bi-Ag-Cs	1	1.5

The values shown in the table are average results for crystals of medium quality and different multipliers. In some cases deviations from these values reached 50%.

Photomultipliers with Bi-Ag-Cs photocathodes can be used in combination with phosphors of a luminescence spectrum displaced toward the green region.

The question of how to select the correct power supply for the multiplier is sufficiently important to merit special discussion. For example, for FEU-19 this question is very decisive. An important advantage of FEU-12 is the fact that it does not require any special selection of a power supply and it will operate with uniform voltage distribution among all the electrodes. The dependence of the resolution on the input voltage arrangement was investigated for several photomultipliers. The results show that the best resolution is obtained with voltages between electrodes in ratios of 2-3 : 1 : 1 : ... 1 (Fig. 5). This arrangement proved optimum from the standpoint of resolution as well as of signal to noise ratio for all the investigated samples. No special adjustments of the voltage distribution were required.

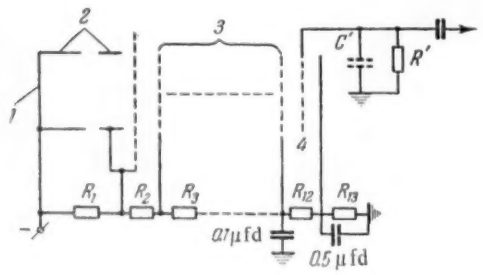

Fig. 5. Diagram of the FEU-12 electrode arrangement and the system of voltage distribution among the electrodes: R_1 = 2 to 3, $R_2 = R_3 = \ldots = R_{13} = 1$.
1) Photocathode 2) focusing electrodes 3) dinode grids 4) collector.

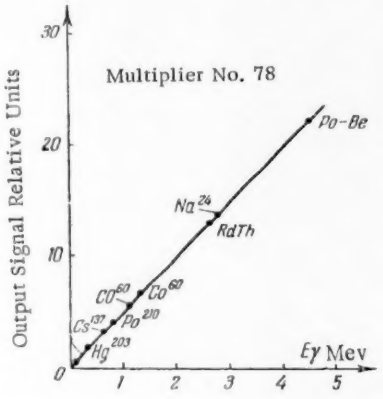

Fig. 6. Linearity test of the FEU-12 operation (in combination with a CsI(Tl) crystal)

Fig. 6 shows results of a linearity test of the multiplier in combination with a CsI(Tl) crystal. A similar result was obtained with a NaI(Tl) crystal. No deviations from linearity were observed in any of the tested samples.

The signal amplitudes obtained from the multipliers were 40 to 50 volts; in some samples it was possible to obtain signal outputs up to 100 volts by increasing the over-all supply voltage to 2000-2400 volts.

The resolution of the photomultipliers was tested with a NaI(Tl) crystal. For all photomultipliers with an over-all photocathode sensitivity higher than 45 μa/lumen the resolution, as measured by the width of the Cs^{137} peak at half its height, was at least 13%. For a good quality NaI(Tl) crystal and multiplier with Sb-Cs photocathode (E = 54 μa/lumen) the resolution obtained for the Cs^{137} line was 8%. Figures 7 and 8 show γ-spectra of some isotopes taken with average quality crystals and photocathodes of medium sensitivity. The law $\Delta \sim \sqrt{E}$ (Δ denotes resolution, E energy of γ rays) is well maintained for the energy range where the size of the crystal does not influence resolution. The law $\Delta \sim \sqrt{\epsilon}$ (ε denotes over-all sensitivity of the photocathode) is well maintained in multipliers with photocathodes of near spectral characteristics. The fullfillment of the latter relationship indicates good uniformity in the system geometry of the various samples.

5. Internal Noises. Stability. Constancy of Parameters. Sensitivity to Electromagnetic fields.

With the optimum power supply arrangement shown in Section 4 the threshold of practically complete noise suppression did not exceed 15 kev (on the NaI (Tl) crystal scale) for any of the tested samples. For most of the samples this threshold was below 10 kev, and for some 4 to 5 kev (all measurements were made in a metal enclosure with the plus side of the high voltage supply grounded).

If a metal shield is placed over the front portion of the bulb and held at the photocathode potential, the threshold of noise suppression is reduced by a factor of about 1.5. The effect of the screen is especially strong at higher supply voltages. At supply voltages higher than 2000 volts the threshold of nose suppression increases and the signal-to-noise ratio deteriorates.

A very important parameter of the equipment is its stability of operation and constancy of parameters between measurement cycles. Many photomultipliers do not meet these, we may say, most important tests.

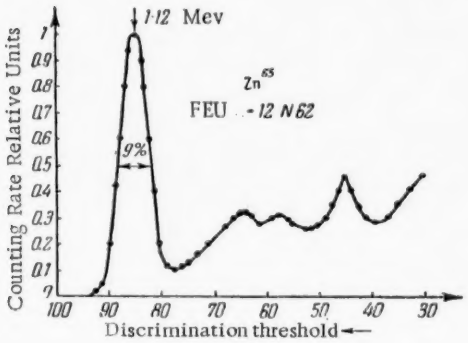

Fig. 7. Gamma spectrum of Zn^{65}. CsI(Tl) crystal 30 mm diameter, 20 mm high.

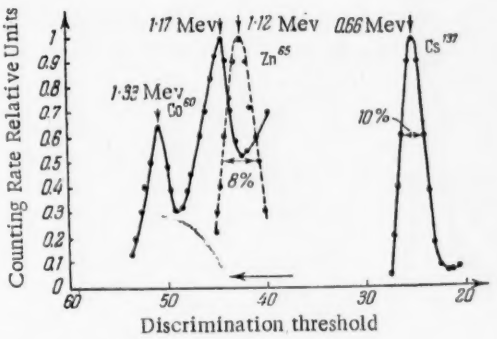

Fig. 8. Gamma spectra peaks of Co^{60}, Zn^{65}, Cs^{137}. NaI(Tl) crystal 30 mm diameter, 12 mm high.

Figure 9 shows the stability curve of FEU-12 (according to the position of the Cs^{137} peak) during 8 hours of continous operation (before each measurement the recording system was calibrated with a control pulse of standard amplitude). The deviation from the initial position of the peak did not exceed 1 to 1.5% and no tendency to deviate toward one or the other side is observed. This operational stability is characteristic for all tested samples.

The FEU-12 exhibits very good stability of its parameters. Results of careful observations of one sample (selected at random) over five months are shown in Fig. 10. No deviations of sensitivity in excess of 5 to 10% have been observed in other samples operated over prolonged periods. It should be noted that many of these samples were acted upon by strong radioactive sources for a long time.

In view of the absence of sharp focusing in its electron beam the FEU-12 is less susceptible to the action of external magnetic fields than systems with concave emitters. The multipliers operated without ill effects in the immediate vicinity of a cyclotron magnet in a shield consisting of two layers of transformer steel 0.5 mm thick and permalloy 0.5 mm thick.

FEU-12 shows low sensitivity to the action of radioactive radiations. This statement is based on the fact that within permissible limits of current in the divider, there was no observable influence of γ-rays and neutrons outside the measured energy range on the position of the measured lines on the energy scale.

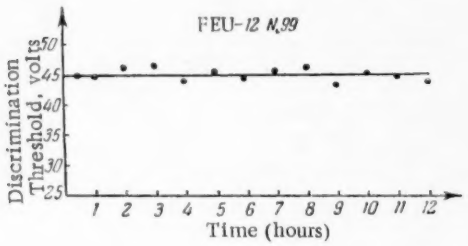

Fig. 9. Stability of FEU-12 in continuous operation.

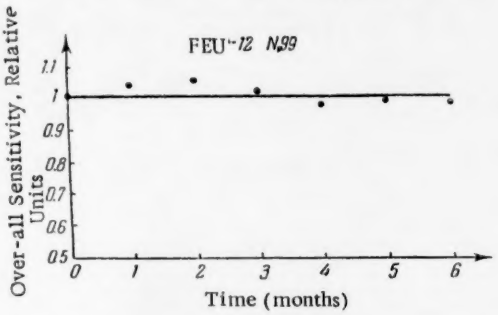

Fig. 10. The constancy of the FEU-12 over-all sensitivity.

No special study was made of the transition state following the switching on of the high voltage. However, no significant changes were observed in the counting speed in any interval on the energy scale 2 to 3 minutes after switching on the high voltage supply.

6. Additional Remarks. Other Capabilities of the Equipment

In collaboration with Mr. E. V. Ryabkov of the N. A. Vlasov Laboratory the authors determined the pulse build-up time at the output of the FEU-12 (by the method of delayed coincidences). The measured build-up time was 1.5 to 2×10^{-8} sec.

The following are some possible improvements which, it seems to us, should result in a further increase of resolving power: a shift of the spectral characteristics maxima of the photocathodes toward the short wavelength portion of the spectrum, and increased collection in the first section at the expense of some of its modernization in order to decrease the direct flight probability of electrons.

CONCLUSION

The investigation conducted leads to the following conclusions:

1. According to all of its characteristics the FEU-12 is completely suitable for application to scintillation spectroscopy.

2. The FEU-12 is especially attractive for work with high and strongly time-variant activities and when working in a background of strong activity in an extraneous energy range.

3. The high stability of the equipment and the constancy of its characteristics deserve special mention.

The authors consider it their pleasant duty to thank Mr. G. S. Vildgrube who made available to them photomultipliers and certain materials for technical tests.

LITERATURE CITED

[1] N. O. Chechik, S. M. Fainshtein, and T. M. Lifshits, Electron Multipliers (State Tech. Press, Moscow, 1954).

[2] G. Birks, Scintillation Counters (For. Lit. Press, Moscow, 1955).

[3] Nucleonics 12, 3 (1954).

Received March 14, 1956

ENERGY DISTRIBUTION OF GAMMA QUANTA FROM A POINT SOURCE OF GAMMA RADIATION IN AN INFINITE SANDY MEDIUM

V. V. Matveev, A. D. Sokolov, R. S. Shlyapnikov

Gamma spectra from point sources (Cr^{51}, Zn^{65}, Ra and MsTh) in an infinite sandy medium were studied with the aid of the scintillation spectrometer. The results obtained indicate that when gamma radiation passes through a thickness of sand there takes place an accumulation of soft scattered radiation of energy ~ 50 kev independently of the energy of the initial radiation.

INTRODUCTION

The most probable interaction processes between gamma quanta of energy up to several million electron volts (especially for substances of small Z) are photoelectric absorption and Compton scattering. In passing through layers of matter the gamma quanta, prior to absorption, may undergo a series of consecutive Compton scattering processes. This leads to the formation of secondary gamma radiation of energy smaller than that of the initial gamma quanta. There appear therefore in the energy spectrum of gamma radiation, passing through matter, photons of low energy.

In the case of nonmonoenergetic initial radiation the process of gamma radiation passing through matter is complicated by the fact that the spectrum of the radiation is changing with distance, the spectrum becoming harder since the probability of photoelectric absorption is greater for soft than for hard radiation. Depending on the medium, distance from the source and the energy spectrum of the primary radiation, the spectral change of the primary radiation and the accumulation of the secondary radiation, can make the spectrum of gamma quanta harder as well as softer.

A number of authors [1, 2] have computed the changes in intensity and spectral distribution of gamma quanta as a function of distance from point and flat sources of monoenergetic gamma radiation in an infinite absorption medium. References [3] and [4] deal with experimental verification of these computations, using water as the medium and radioactive isotopes Co^{60}, Cs^{137} and Hg^{203} as sources.

However, when solving certain practical problems it is necessary to know the changes taking place in the energy spectra of gamma radiation which has passed through thick layers of materials, such as sand, concrete or lead. This applies primarily to construction of geophysical equipment for the location and development of sources of radioactive ores, and also to gamma-ray shielding computations as well as other problems in radiometry.

Description of Experiment

1. Geometry of arrangement. The experiments were conducted in sandy soil. The geometry of the experiment is shown in Fig. 1. A recorder of gamma radiation was placed at a depth of 110 cm. Aluminum tubes were randomly installed at different distances from the source and in such a manner that a source of gamma quanta lowered into them was located on the same horizontal as the source. During measurements aluminum rods were placed inside the tubes in order to reduce the nonhomogeneity of the medium. The fact that the medium was limited on one side could not introduce any substantial distortions into the results, because measurements were made at distances not exceeding the depth to which the sources were lowered. The density of the sand in which the experiments were made was 1.6 g/cm^3.

2. The gamma spectrometer. A scintillation gamma spectrometer was developed and constructed for the experiments. The recorder of the gamma radiation was the counting head, consisting of a CsI (Tl) crystal (40 mm diameter, 15 mm high), an FEU-12 photomultiplier and an output cathode follower, mounted in the form of a separate output unit. Pulses from the cathode follower, were fed into a linear amplifier having a maximum output pulse of 100 volts. The gain of the amplifier was changed, depending on the recorded spectrum, between the limits of 3 and 150. After amplification the pulses entered a three channel analyzing system: 1) the general counting channel counted all the pulses and served to register the over-all gamma radiation intensity and to control the stability of the spectrometer operation; 2) the integrating counting channel; 3) the differentiation counting channel with a "window" width of 1.5 volts. The stepped voltage, common to the second and third channels, was varied from 0.8 to 100 volts.

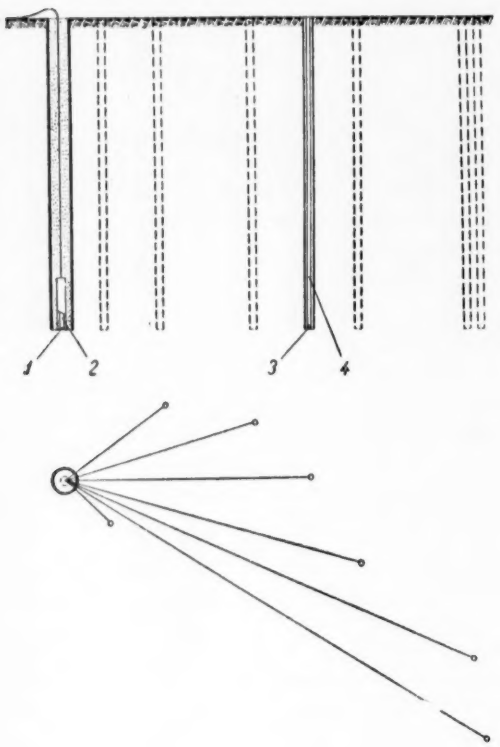

Fig. 1. Geometry of the experiment. 1) Crystal CsI 2) FEU-12; 3) Source of γ quanta; 4) Aluminum rod.

For maximum stability of the spectrometer operation, the supply voltage for the multiplier and also for the chains of voltage increments in the system were obtained from batteries, and the anode supply from electronically regulated rectifiers. The spectrometer was calibrated using gamma quanta emitted by radioactive isotopes Cr^{51} (323 kev), Cs^{137} (660 kev), Zn^{65} (1114 kev), Co^{60} (1.17 and 1.33 Mev) and ThC'' (2.62 Mev).

Results of calibration (Fig. 2) indicate that in this energy interval the deviation from linearity does not exceed 3%. The properties of the spectrometer used in this work result in half-width photoelectric peaks of 17.6% for 323 kev gamma quanta (Fig. 3, solid curve), 8.3% for 1114 kev (Fig. 4 solid curve) and 10.8% for the 660 kev radiation from Cs^{137}.

3. Sources of gamma radiation. To keep the system load within reasonable limits when making gamma radiation spectral measurements at different distances from the source, it is necessary to have a selection of sources of different intensities. There were therefore prepared for this work radioactive sources Cr^{51} and Zn^{65} having gamma radiation intensities ranging from 0.1 millicurie to 10 curie. For the investigation of the spectral changes in the gamma radiation from the uranium and thorium series elements in passing through layers of sand, there was available a selection of Ra and MsTh sources of various intensities. However, in this case it was not possible to select sources which completely meet the requirements of this work.

Experimental Results and Their Analysis

1. Energy distribution of gamma quanta in a sandy medium from a point source of monoenergetic gamma radiation. The energy distribution of gamma quanta from a point source of gamma radiation in sandy soil (see Fig. 1) was studied at distances from the Cr^{51} source of 5, 35, 45, 60, 70, and 80 cm (corresponding μR = = 0.83; 5.83; 7.49; 10; 11.7; 13.3) and from the Zn^{65} source at distances of 35, 70, 100 and 130 cm (corresponding μR = 3.4; 6.8; 9.6; 12.5).* The experimental results are shown in Fig. 3 for Cr^{51}, and in Fig. 4 for Zn^{65}.

*Translators Note: μ is the mass absorption coefficient, usually expressed in cm^2/gm.

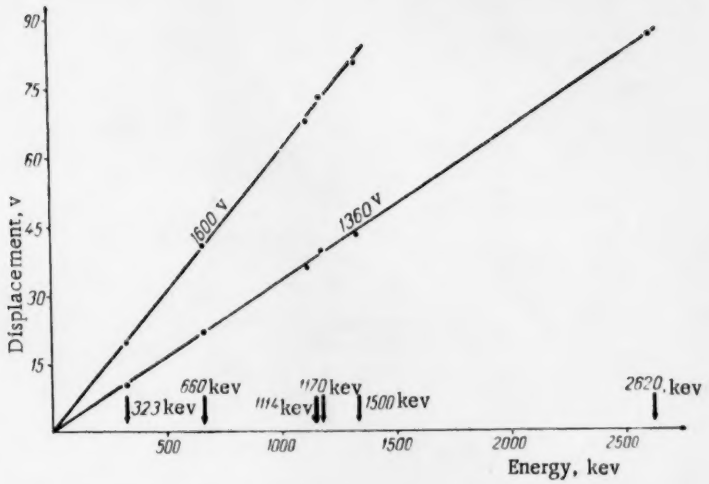

Fig. 2. Calibration of the spectrometer for two voltages on FEU-12.

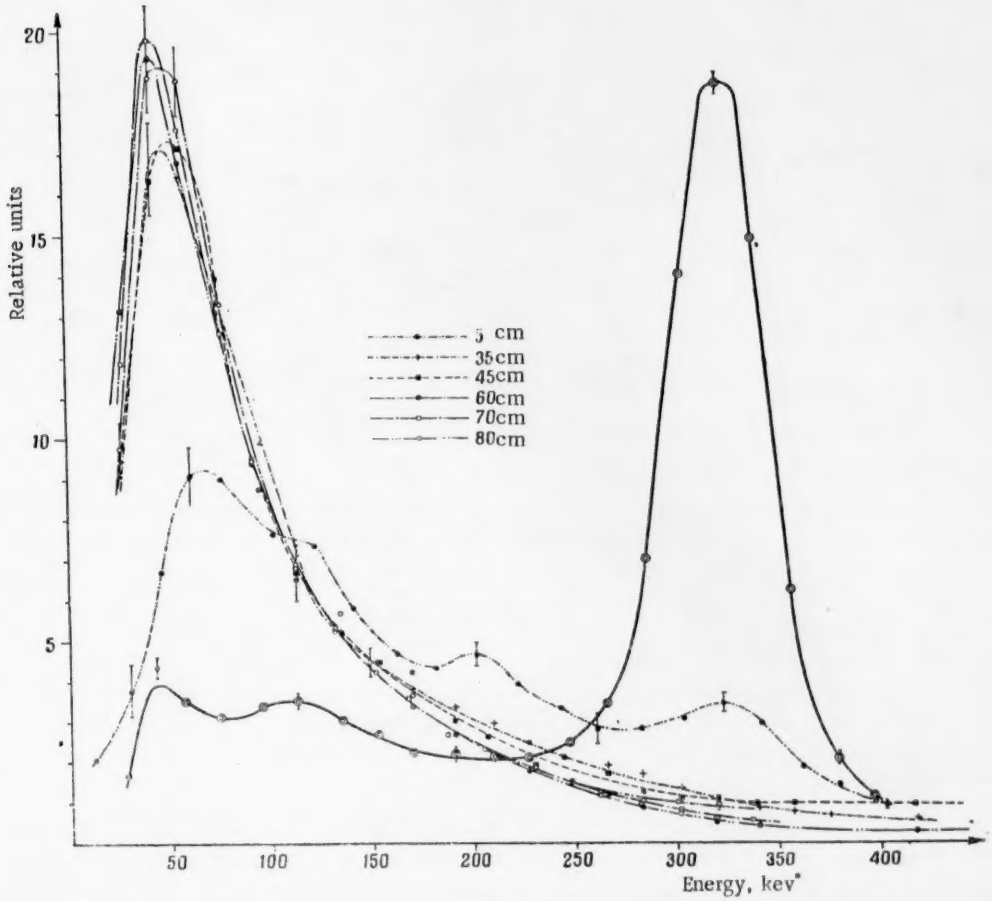

Fig. 3. Differential spectra of γ radiation from a Cr^{51} source.

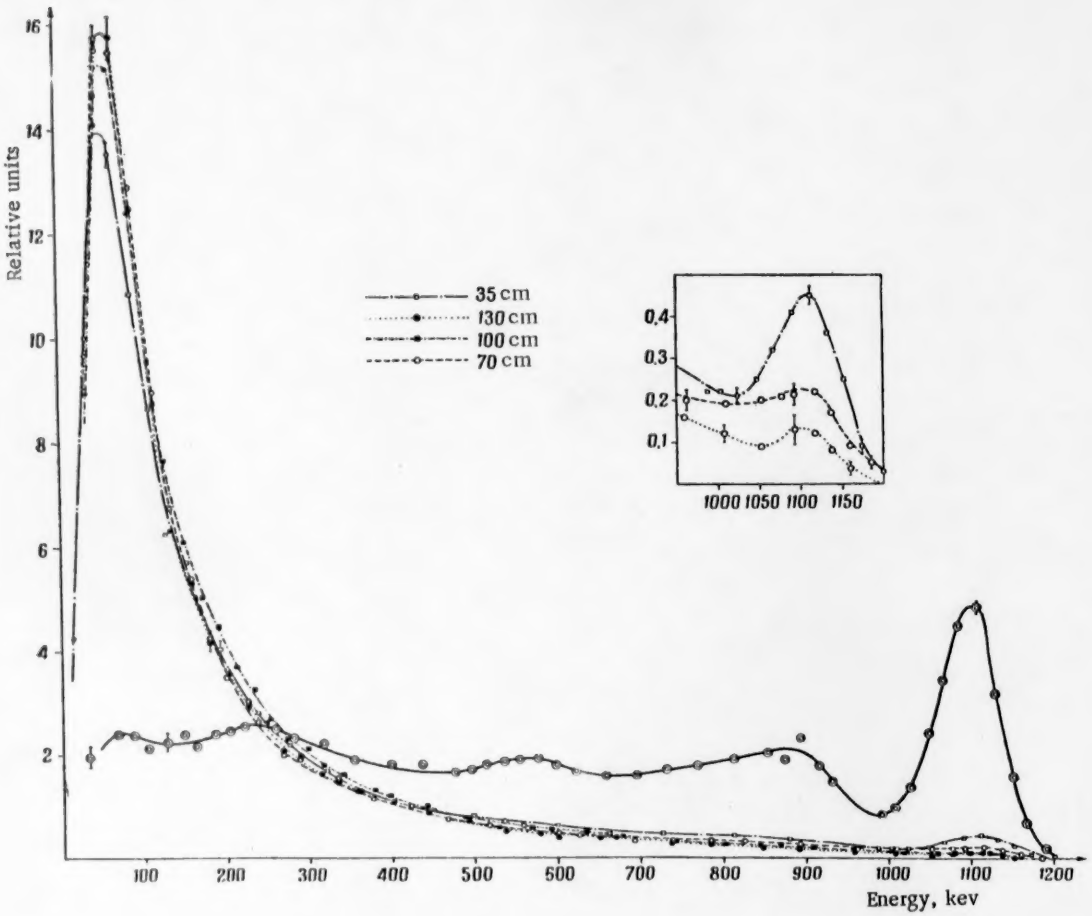

Fig. 4. Differential spectra of γ radiation, Zn^{65}.

For convenience in comparing the results obtained at different distances from the source, the spectra, normalized to the same area under the curve, are placed on the same drawing.

At $\mu R \geq 5$ the characteristics of the Cr^{51} and Zn^{65} spectra are similar, the major portion of the radiation being concentrated in quite a narrow energy interval with a maximum at 50 kev (the half width of the maximum ~ 140%, the width of the measuring equipment at 50 kev ~ 50%).

At relatively short distances ($\mu R < 5$) the primary radiation is predominant, although the secondary scattered radiation already comprises a considerable portion of the total. The gamma spectrum curve (see Fig. 3) taken at a distance of 5 cm ($\mu R = 0.83$) shows a peak at 205 kev, corresponding to gamma radiation which has undergone a single Compton scattering. (Computation yields a maximum at 210 kev for this case). The peak at ~ 120 kev in this curve is formed by the recoil electrons resulting from Compton scattering of 323 kev gamma quanta in the CsI (Tl) crystal. The ~70 kev peak in the curve is primarily due to the multiscattered secondary gamma radiation.

The results thus show that when gamma radiation passes through a thickness of sand, there takes place an accumulation of soft radiation of 50 kev independent of the energy of the primary gamma quanta.

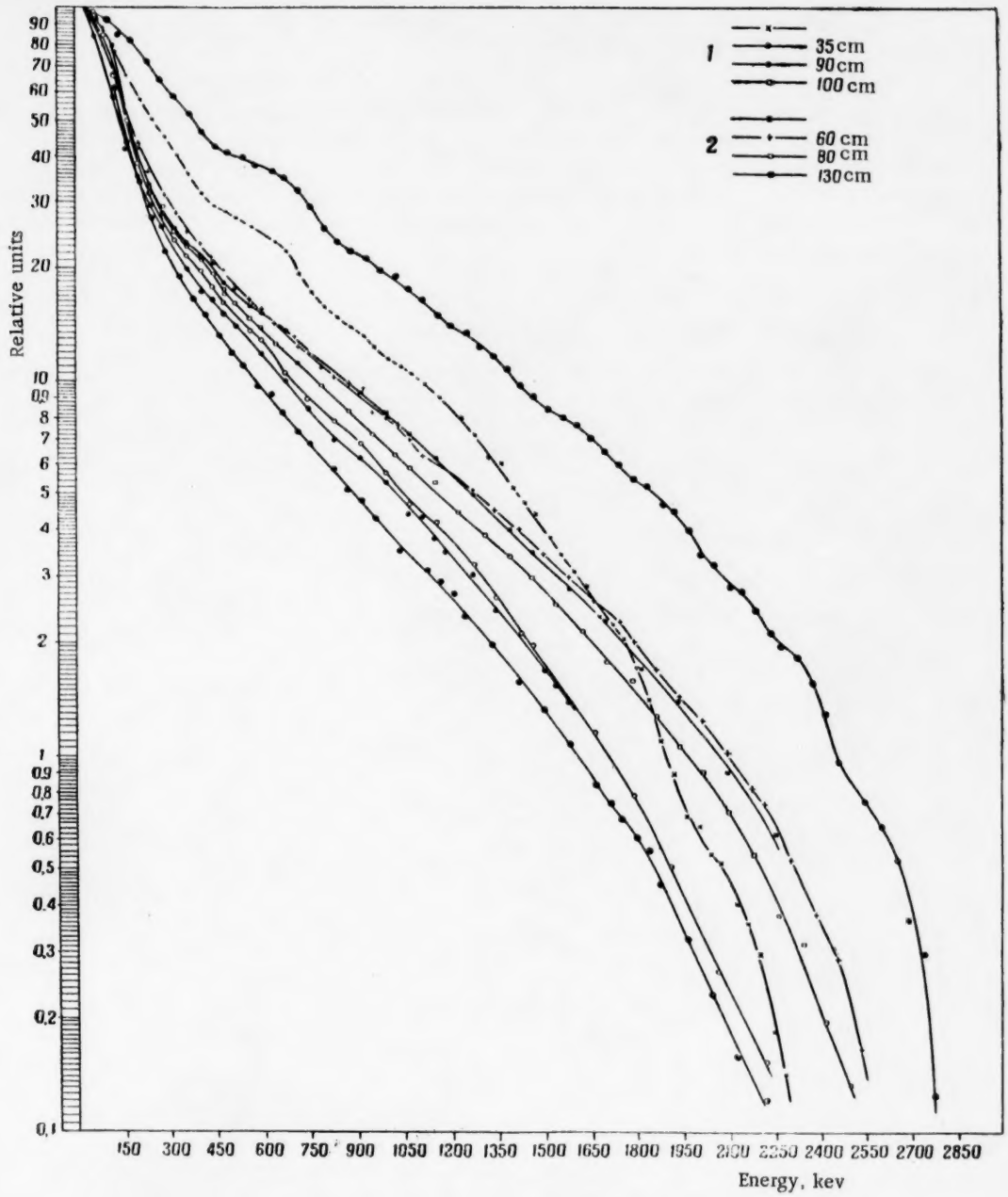

Fig. 5. Integral spectra of γ radiation from Ra(1) and MsTh (2).

In order to investigate the nature of spectral changes of gamma radiation in media composed of high Z material, similar experiments were made in lead using radiations of 323 kev and 1114 kev. However, the relatively large dimensions of the counting head which in this case introduce a nonuniformity in the medium, making it impossible to obtain a complete picture of the gamma quanta distribution in an infinite lead medium. The results therefore have no practical significance.

However, the obtained data show the existence of a weak maximum in the 200 kev region, the location of which does not depend on the energy of the primary radiation and which can be interpreted as a maximum corresponding to the secondary radiation scattered in lead.

2. Energy Distribution of Gamma Quanta in Sandy Mediums From a Point Source of Nonmonoenergetic Gamma Radiation. A study was made of the energy distribution in gamma radiation in sand from Ra and MsTh point sources. Measurements were made at distances of 35, 90 and 100 cm for Ra and at 60, 80 and 130 cm for MsTh. The data show that changes in the spectra of the gamma radiation take place in the same manner as in the preceding cases, i. e., in the soft portion of the spectrum there accumulates scattered radiation, ~ 50 kev, and the curves in this portion of the spectrum practically do not differ from each other. Differences in the hard portions of the spectra, though they exist, are not too well distinguished in the differential spectra, since the hard radiation comprises only a small portion of the total in Ra and MsTh. In this article are therefore presented not the differential but the intergral spectra (Fig. 5, 1 from Ra, 2 from MsTh), as a better pictorial presentation and as of interest in solving design problems and in utilization of geophysical and radiometric equipment.

In conclusion the authors wish to thank Professor I. I. Gurevich, Messrs. G. R. Golbeck, P. E. Stepanov and N. I. Laletin for their valuable advice during discussions in connection with this work.

LITERATURE CITED

[1] U. Fano, Nucleonics 11, 8, 9 (1953).

[2] L. V. Spencer, Phys. Rev. 88, 793 (1952).

[3] R. B. Theus, L. A. Beach and W. R. Faust, J. Appl. Phys. 26, 294 (1955).

[4] M. M. Weiss and W. Bernstein, Phys. Rev. 92, 1264 (1953).

Received March 12, 1956.

VAPORIZATION OF METALS BY FISSION FRAGMENTS

F. S. Laptev, B. V. Ershler

The number of atoms evaporating from the surface of a metal when it emits fission fragments or alpha particles was measured for U^{233} and Pu^{239}. This quantity depends considerably on the presence of an oxide layer on the surface of the metal and for U^{233}-emitting fission fragments changes from 24 to 1200 atoms for a change from an oxidized to a cleaned surface. For Pu^{239} with a cleaned surface the value is 3500 atoms per fragment. For alpha particles leaving Pu^{239} the value is 0.02. Approximate computations indicate that the number of atoms in the zone heated by the passing of the fragment to a temperature insuring evaporation of the metal is for uranium 5.6×10^6. The kinetic energy which the fragment imparts to the atoms of the lattice, apparently exceeds the value accepted in the literature at the present time.

When a heavy particle is stopped in a metal its kinetic energy is imparted to the electrons of the metal and to atoms of the lattice [1]. As a result there appears a higher temperature zone along the path of the particle. The existence of such zones was definitely demonstrated by disorder experiments with alloys of copper and gold when bombarded by fast neutrons, and also by a series of other experiments [2]. We found no experimental data in the literature on heated zones along tracks of fission fragments, although this case is of obvious interest. Valuable information concerning such zones can be derived by measuring the number of atoms evaporating from the surface of a metal as a fission particle departs from it. This work pertains to the determination of these quantities for U^{233} and Pu^{239}.

EXPERIMENTAL

In an aluminum enclosure 2 (see the figure) was fastened a 2×3 mm plate of the metal under study, above which was placed a metal screen 3. The enclosure was sealed into a quartz ampule evacuated to 10^{-4} mm of mercury. During irradiation with neutrons some of the fission fragments orginating in plate 1 emerged from the metal, atomizing a certain amount of it. Some of the U^{233} and Pu^{239} atoms evaporated in this manner settled on the screen; the number of these atoms could be determined by measuring the alpha activity of the screen. The number of atoms evaporated by one fragment was determined from the total number of fragments departing from the metal surface during irradiation and the total number of evaporated atoms.

The number of departing fragments was determined from the formula

$$Snvt\frac{R}{4}N\sigma_f,$$

where S is the surface of the sample; $\underline{nv}$ is the flow of thermal neutrons; $\underline{t}$ is the time of irradiation; R is the path length of the fission fragment in the metal (7.3×10^{-4} cm); N is the number of atoms in 1 cm^3 of metal; and σ_f is the fission cross section.

The number of evaporated atoms is equal to:

$$\frac{A\tau}{\ln 2} \cdot \frac{\omega}{2\pi},$$

where A denotes the α-activity of the screen; τ the half life of the evaporated element; and ω the solid angle subtended by the screen from the surface of the sample.

The background in the experimental arrangement for measuring the alpha activity of the screen was 0.8 pulse per min; this made possible measurements of alpha radiation from 5×10^{-10} g of U^{233}. Errors in the determination of alpha activity did not exceed ± 6%.

The following parameters were varied in these experiments: intensity of the neutron flux, duration of the irradiation, the nature of the contact between the irradiated metal and the aluminum holder to which it was fastened, and finally the distance between the screen and the sample. In addition, whenever it became apparent that the number of evaporated atoms depends substantially on the degree of oxidation of the metal surface, experiments were conducted with metal having an oxidized surface as well as with metal made as free as possible from oxides. Some results of such experiments are shown in the table.

TABLE

Number of Atoms Evaporated per One Fission Fragment Leaving the Surface of U^{233} and Pu^{239} Under Different Conditions

Exp. No.	Metal	Condition of surface	Irradiation time, hours	Neutron flux*, $\frac{\text{Neutr.}}{\text{cm}^2 \cdot \text{sec}} \cdot 10^{-2}$	Distance from screen to sample, mm	No. of fragments emitted from samples X 10^{-12}	No. of atoms knocked out by one fragment
1	U^{233}	Oxidized **)	24.0	0.7	0.0***)	12.0	37
2	U^{233}	»	11.0	1.3	0.4	10.0	13
3	U^{233}	»	9.0	1.3	0.4	8.2	11
4	U^{233}	»	17.0	0.7	0.6	5.7	56
5	U^{233}	»	20.0	0.7	1.5	8.6	35
6	U^{233}	»	42.7	0.7	1.5	18.4	20
7	U^{233}	»	50.7	0.7	1.5	22.0	7
8	U^{233}	Not oxidized ****)	2.0	0.28	1.0	0.10	1600
9	U^{233}	»	3.0	0.23	1.0	0.12	550
10	U^{233}	»	3.0	0.14	1.0	0.13	1000
11	U^{233}	»	46.5	0.0066	1.0	0.10	780
12	U^{233}	»	65.7	0.0019	1.0	0.041	2200
13	Pu^{239}	»	0.3	0.19	1.0	0.023	3990
14	Pu^{239}	»	5.0	0.11	1.0	0.020	2500
15	Pu^{239}	»	9.3	0.0047	1.0	0.014	4100

*The error in the determination of neutron flux did not exceed ± 1%.

**Cleaned of organic substances by a solvent.

***In this experiment contamination of the U^{233} screen surface was possible due to direct contact of the screen with the sample. Such experiments were set up to evaluate the magnitudes of the errors caused by the accidental contamination of the screen by contact with the sample.

****Mechanically cleaned to a metallic lustre.

As seen from the table the number of atoms evaporating with the departure of one fission fragment varies even in experiments conducted under identical conditions; nevertheless, there is clearly a sharp difference in the value of this number for metals covered with oxide as compared with those cleaned free of oxides. This difference exceeds considerably the accidental scatter for separate experiments; thus the average number of atoms caused to evaporate by one fragment from U^{233} in the presence of oxide on its surface is 24 (Experiments 2 to 7), and in the absence of oxide is 1200 (Experiments 8 to 12). Such a strong dependence of the measured

quantity on the presence of surface oxides explains the observed scatter in the data obtained under relatively similar conditions. This scatter in the case of "equally" clean surfaces could be due to the difference in the amount of oxidation still remaining.

It should be noted that the average number (3500 atoms for one fragment, Experiments 13-15) of evaporated atoms for Pu^{239} with its surface cleaned is so much higher than for the cleaned uranium that this difference cannot be caused by the accidental data scattering and that it indicates a difference in the behavior of the two metals when traversed by fission fragments.

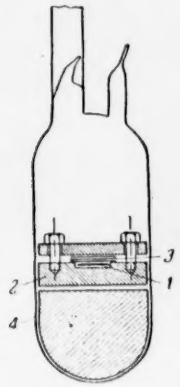

Fig. Arrangement for neutron irradiation of U^{233} and Pu^{239}.

We should point out that the evaporation observed in these experiments apparently cannot be caused by macroscopic heating of the entire sample under the action of fission taking place in it. Indeed, with macroscopic heating the number of evaporated atoms per fission fragment should be dependent on the intensity of the neutron flux and should, for example, fall off sharply with its decrease; actually a decrease in intensity by 2 orders of magnitude (from Experiments 8 to 12) practically does not change the number of evaporated atoms.

We have, in addition, obtained data on evaporation of plutonium upon emission from it of alpha particles. In this experiment a thin plutonium plate of 0.2 cm^2 area was kept in the sealed ampule under the aluminum screen for 1,5 and 7 months under a 10^{-4} mm vacuum. The number of atoms knocked out by one alpha particle was found from the alpha activity of the screen and from the computed number of alpha particles which have left the surface of the metal during the experiment. This turned out to be 0.02.

DISCUSSION OF RESULTS

Data on evaporation of metals by departing fission fragments are by therselves of interest and yet have not been published in literature until now. Besides, these data can be used for an approximate evaluation of certain parameters of the heated zones in metals, particularly the diameter of the zone in which, following the flight of the fragment, the temperature is raised to a value ensuring evaporation.

According to our measurements, the cylindrical crater which forms on the surface of the metal after the flight of the fragment, can hold 1200 metal atoms. Taking the depth of the crater as equal to its diameter,* we find for the latter the value $3.16 \cdot 10^{-7}$ cm. (The volume occupied by an uranium atom in the metal lattice is taken as 2.06×10^{-23} cm^3). The number of uranium atoms in the heated zone (the length of which is equal to 14.6×10^{-4} cm i. e., double the path length of the fragment) thus proves to be 5.6×10^6. Accounting for possible errors in our measurements, especially the approximation used in computing the diameter of the crater, it may be considered that this quantity was determined to within a factor of 2 to 3 and is apparently greater than the true value. Of considerable interest, however, is the fact that this value exceeds by a factor greater than 200 the number of atoms which, according to computations of Seitz [1], can be ejected from the corners of a uranium lattice by a pair of fission fragments.

Since exchange of energy between the excited electrons and the lattice nuclei must proceed at a slow rate because of the large difference between the masses of these particles, it must be assumed that the portion of the energy separated along the track which produces heating, local melting and evaporation of the metal is transmitted mainly by collisions of the fragment with the atoms of the lattice. If we assume that each atom located in the zone under consideration acquires by such collisions a kinetic energy not less than the latent heat of melting and vaporization of uranium (equal to 111 kcal/mole [3]), we obtain from this the general amount of energy of 27 Mev as imparted by a pair of fragments (having been completely stopped in the process) by collision with the atoms of the lattice, this energy comprising 17% of the total kinetic energy of the fragments. This value is higher than the one generally accepted in the literature (3%) [1], the discrepancy apparently exceeding the possible error in such computation.**

*Such an approximation probably gives a high value for the diameter, since the depth of the crater can possibly be several times its diameter, as we hope to show later.

**It is possible that this discrepancy indicates considerable transmissions of energy along the path from the excited electrons to the atoms during the existence of the hot zone.

The observed difference in the evaporation of uranium compared with plutonium is probably connected with the smaller heat of evaporation and lower melting temperature of the latter. In this connection data on evaporation for other metals under similar conditions would be of great interest.

LITERATURE CITED

[1] F. Seitz, Discussions Faraday Soc. 5, 271 (1949).

[2] S. Siegel, Phys. Rev. 75, 1823 (1949).

[3] E. G. Rauh, R. J. Thorn, J. Chem. Phys. 22, 1414 (1954).

TOTAL NEUTRON CROSS SECTION OF Ra^{226}

M. I. Pevzner, L. S. Danelyan, Yu. V. Adamchuk

The complete cross section of radium was measured in the energy interval 0.022 to 50 ev by means of a mechanical neutron selector. Resonance was found at $E_0 = 0.537 + 0.006$ ev. The resonance parameters, with Doppler spread and resolution of the equipment taken into account, are presented: $\sigma_0 = (3600 \pm \pm 150)$ barn, $\Gamma = (0.029 \pm 0.001)$ ev, $\Gamma_n = (2.1 \pm 0.1) \cdot 10^{-5}$ ev.

INTRODUCTION

The structure and parameters of resonant levels for most of the elements of the periodic system have been recently studied thoroughly by methods of neutron spectroscopy. Results of these works are collected in a series of known reviews [1]. Comparison and analysis of these data enabled us to draw a series of interesting, conclusions, important for modern nuclear theory concerning the parameters of these levels, their dependence on the atomic weight, excitation energy and other nuclear characteristics. The few gaps in the present data are connected, as a rule, with the difficulty of obtaining the necessary quantities of the element and of the required purity, or with the difficulty of making measurements. Radium is one of the elements for which no data are available at the present time. At the same time radium consists of one isotope of even atomic weight (spin equal to zero), and therefore permits a single-valued interpretation of experimental results. We therefore, consider it appropriate to publish results of our work on the measurement of the total Ra^{226} cross section in the energy interval 0.022 to 50 ev performed in 1953.

Brief Description of Apparatus and Conditions of Experiment

The total cross section of radium was measured by the method of transmitting neutrons through a mechanical selector with a transverse rotor. The construction of the selector and the method of its use for measurements have been described [2].

The diameter of the samples was chosen to ensure optimum transmission with the available quantity of radium and was 6 mm.

During the measurments the container with the sample was set up on an adjustable table between two nickel collimators 100 mm long and 5 mm diameter. The shape of the neutron beams leaving the collimator was determined by activating a silver foil and subsequently exposing to it an x-ray film. The background, which is a very small fraction (0.5 to 3%) of the total in the thermal energy region, reached 25 to 30% in the energy interval of 3 to 50 ev.

Table 1 shows the resolving power of the selector used in our measurements for different energies (ΔE denotes the width of the resolving function at half-maximum points).

Samples

For the measurement of the total neutron cross section of radium the anhydrous sulfate $RaSO_4$ was prepared since the neutron cross sections of the combining elements of this salt are small and well known. For the thinnest sample, intended for measurements in the resonance region, the bromide salt $RaBr_2$ was selected. The radium sulfate was poured into and hermetically sealed in special containers, prepared from thin boronless glass tubes

TABLE 1

Energy E, ev	0.5	1.5	5	10	50
Resolution $\frac{\Delta E}{E}$	0.05	0.06	0.07	0.10	0.20

of 6 mm inside diameter. Radium bromide was poured into a brass container and hermetically sealed. The total amount of salt was determined by weighing before and after filling. The radium content was determined by measurement of gamma radiation after equilibrium has been established. Since due to the method of preparation the Ra salt contained an admixture of barium, the difference between the total weight of the salt and the weight of $RaSO_4$ was ascribed to $BaSO_4$. The Ba content as a percentage of the weight of Ra was different for different samples. To preclude the flow of radium emanation in case of damage to the containers they were placed in a hermetic aluminum case over which was placed a lead cylinder for protection against radiation. Figure 1 shows the glass and brass containers with the radium salt and the aluminum case.

In Table 2 are shown some characteristics of the samples used.

TABLE 2

Sample No.	Sample	Total weight of salt	Weight of radium	Number of radium atoms in 1 cm^2 of the sample
1	$RaSO_4$	5.2446	3.350	$34.5 \cdot 10^{21}$
2	$RaSO_4$	0.8288	0.493	$5.1 \cdot 10^{21}$
3	$RaBr_2$	0.2804	0.1612	$0.755 \cdot 10^{21}$

EXPERIMENTAL RESULTS AND DISCUSSION

In order to verify the correctness of the data reduction, measurements were made of complete cross sections of boron in a brass container and of barium carbonate in a glass container. The results indicated absence of systematic errors connected with the geometry of the experiment.

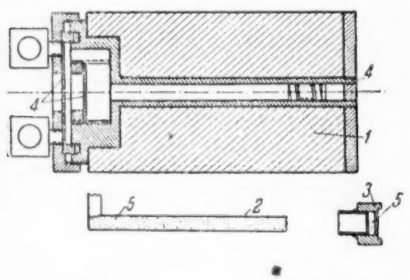

Fig. 1. Containers. 1) Lead; 2) glass; 3) brass; 4) duralumin; 5) radium salt.

In Fig. 2 is shown the complete cross section of Ra^{226} as a function of neutron energy in the interval 0.022 to 50 Mev. Measurements for the entire cross section curve were made several times using the thickest sample, No. 1 (transmission 0.25 to 0.4). Points in the resonance region were obtained using thin samples, Nos. 2 and 3. In measurements without any sample a similar empty container was placed in the path of the beam. From the experimentally obtained cross section were subtracted the cross sections of barium [1], sulphur [3] and oxygen [1].

In the region of thermal neutrons the cross section of radium varies as 1/v.

A resonance level was detected at 0.537 ev. The parameters of the level σ_0 and Γ, entering into the Breit-Wigner formula for an isolated level, were determined by the method of successive approximations, taking into account the Doppler widening and the resolution of the equipment [4]. We shall employ this method in cases where the Doppler width Δ is less than the width of the level and the resolution of the equipment does not seriously distort the shape of the resonance curve, i. e., when the half width of the resolution curve is less than or comparable with Γ.

For crystal structures of simple substances, for which the condition $\Gamma + \Delta \gg 2\Theta_{ac}$ holds, the thermal motion of the nuclei is accounted for as if the substance under investigation were in a gaseous state [5] (Θ_{ac} is the characteristic Debaiev temperature, which determines the acoustic oscillations spectrum of the crystal matrix). In cases of crystal structures consisting of several kinds of atoms the distortion in the shape of the

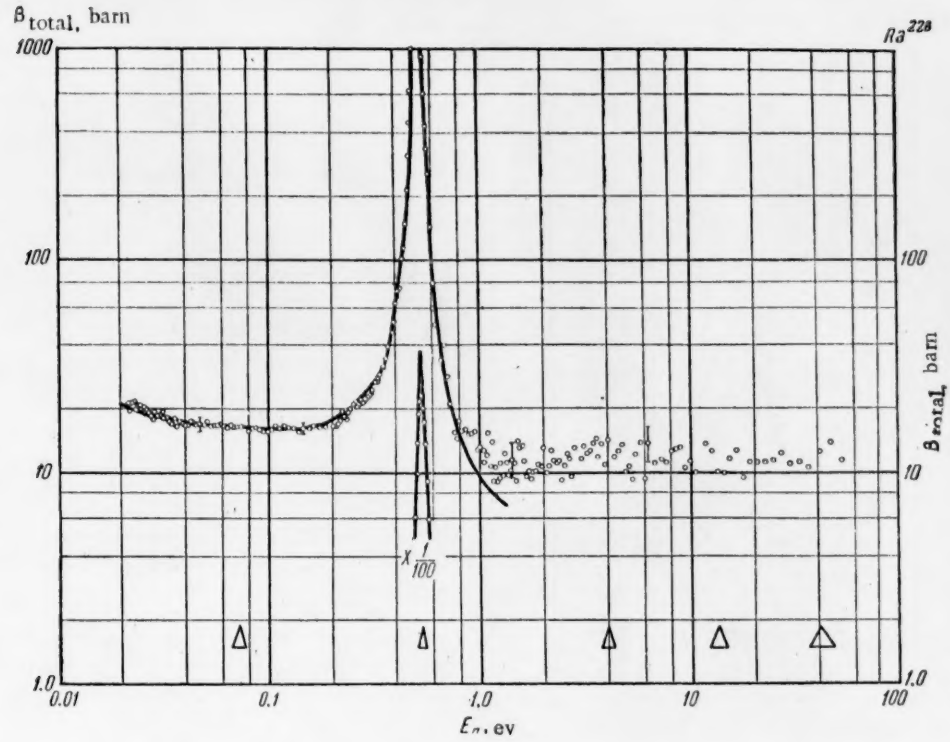

Fig. 2. Complete neutron cross section of radium

resonance absorption curve could also be caused by optical oscillations of the matrix, with a corresponding temperature Θ_{op}, and the condition of applicability of the formulas, correct for gases, will be different. The theory of this problem has not yet been developed. Frequently the crystal structure of the compound is characterized by a single temperature Θ determined experimentally from the thermal conductivity at low temperatures. Information on the characteristic temperatures of radium compounds is not available. If we take the value of Θ for the compound $RaBr_2$ as not higher than 150° K *, we can apply the relationship which is correct for the gaseous compounds. For the detected level the Doppler width Δ was 0.015 ev.

TABLE 3

Parameter designation	Experimental parameters of the level	Resulting values	Computed parameters	
			first approximation	second approximation
E_0, ev	0.537 ± 0.006			
σ_0, barn	2300	3170	3500	3600 ± 150
Γ, ev	0.045	0.032	0.0297	0.029 ± 0.001
$\sigma_0\Gamma^2$, barn · ev^2				3.0 ± 0.2
Γ_n, ev				(2.1 ± 0.1) · 10^{-5}

*For example, for KBr Θ = 177°K, for AgBr Θ = 140°K [6].

In accounting for the finite resolving power of the equipment, the resolution function was approximated by a triangle with the additional factor $(E\sqrt{E})^{-1}$, which accounts for the nature of the spectrum E^{-1} and the dependence of the sensitivity of the detector on the energy $E^{-1/2}$.

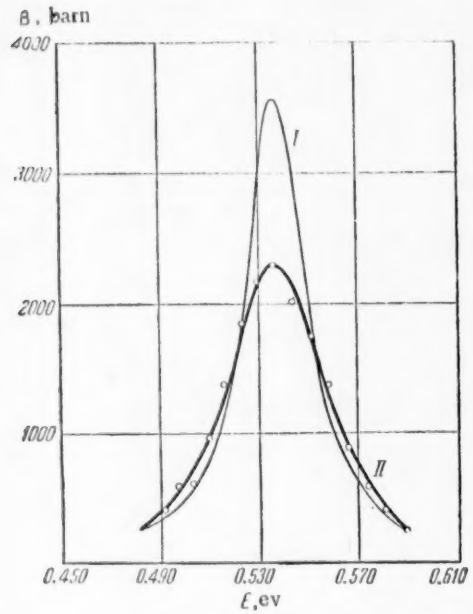

Fig. 3. Resonance region in the radium cross section. I) Theoretical Breit-Wigner Curve. II) Computed from the theoretical curve corrected for Doppler spread and resolution of the equipment.

The method of successive approximations was applied to thirteen experimental points in the resonance region obtained with the thin sample, No. 3.

Experimental and computed results of the values of the parameters in the resonance region are shown in Table 3.

The solid curve in Fig. 2 is computed according to the Breit-Wigner formula using parameters $E_0 = 0.537$ ev, $\sigma_0 = 3600$ barn, $\Gamma = 0.029$ ev, $\sigma_{scat} = 6.5$ barn. The absorption cross section for 0.025 ev computed according to the Breit-Wigner formula with above parameters is $\sigma(0.025\ ev) = (13.5 \pm 1.5)$ barn.

The resonance region is shown in Fig. 3.

In the energy interval of 2 to 50 ev there is observed a large scattering of experimental points. The accuracy of measurements in the energy region is 15 to 20%.

The obtained experimental data do not enable us to present reliable conclusions concerning the average interval between the levels of radium. Apparently this value is not smaller than 30 ev.

The magnitude of the radiation width for 0.537 ev $\Gamma_\gamma \approx \Gamma = 0.029$ ev agrees with the general law of variation of Γ with atomic weight [7, 8].

The authors thank the radiotechnical group under A. P. Tsitovich, who secured uninterrupted operation of the electronic equipment during measurements, A. M. Gonchukova and V. A. Chodakov for their help in the mathematical processing of the data, and V. I. Mostov for his participation in the discussions of the results.

LITERATURE CITED

[1] D. Hughes, Neutron Cross Sections, AECU-2040 (Russian edition with supplement: Atlas of Effective Neutron Cross Sections of the Elements edited by Yu.V. Adamchuk,(Acad. Sci. USSR Press, 1955). Also: D. Hughes, J. A. Harvey, Neutron Cross Sections (McGraw Hill Co., N. Y. 1955).

[2] V. I. Mostovoi, M. I. Pevsner, A. P. Tsitovich,"Physical investigations" Reports of the Soviet Delegation at the International Conference on the Peaceful Uses of Atomic Energy. (Acad. Sci. USSR Press, Moscow, 1955).

[3] L. J. Rainwater, W. W. Havens, J. R. Dunning, and C. S. Wu, Phys. Rev. 73, 733 (1948).

[4] V. L. Sailor, Phys. Rev. 91, 53 (1953).

[5] W. Lamb, Phys. Rev. 55, 190 (1939).

[6] F. Zeitz, Modern Solid State Theory (State Technical Press, Moscow-Leningrad, 1949). Chap. III.

[7] D. Hughes, J. A. Harvey, Nature 173, 942 (1954).

[8] H. H. Landon, Phys. Rev. 100, 1414 (1955).

Received March 13, 1956.

DIRECT MEASUREMENT OF THE ENERGY VARIATION OF η FOR U^{233}, U^{235}, AND Pu^{239} *

H. Palevsky, D. J. Hughes, R. L. Zimmerman, and R. M. Eisberg**

Brookhaven National Laboratory, Upton, N. Y. ***

A technique is described that measures directly the energy variation of η, the number of fission neutrons produced per neutron absorbed. When combined with total cross sections, the method is capable of giving fission cross sections as well. Results are presented in the energy region near thermal, of importance to reactor design, for U^{233}, U^{235}, and Pu^{239}. Comparison with η computed from total and fission cross sections shows good agreement for U^{233} and U^{235} but a disagreement outside experimental error for Pu^{239}. An auxiliary experiment demonstrates that ν, the number of neutrons per fission, is constant with energy in the region of interest for Pu^{239}, hence that the discrepancy cannot be ascribed to a ν variation.

1. Introduction

The variation with energy of η, the number of neutrons emitted per neutron absorbed by a fissionable material, is a quantity that is important to the understanding of the fission process as well as reactor dynamics. By definition,

$$\eta = \nu \frac{\sigma_F}{\sigma_a} \tag{1}$$

where ν is the number of neutrons per fission,
σ_F is the fission cross section, and
σ_a is the absorption cross section (radiative capture plus fission).

On the basis of the liquid drop model for fission (Bohr and Wheeler, 1939), the incoming neutron shares its energy with the other nucleons and the fission process takes place before the nucleus loses its excitation energy by radiation. The "prompt neutrons" emitted are "evaporated" from the highly excited fission fragments shortly after they separate. In such a model ν as a function of the incoming neutron energy is expected to be constant for slow neutrons because the kinetic energy of the neutron is small compared to the excitation energy of the compound nucleus. From such considerations it was first expected that η also would be constant with energy for low energy neutrons, because of the constancy of ν and the supposed high probability of fission relative to capture.

*Work performed under contract with U. S. Atomic Energy Commission.

**Now at University of Ninnesota, Department of Physics, Minneapolis, Minn.

***[The following is a reproduction of the original American paper, and not a re-translation from Russian – Publisher's note].

In 1944 at Los Alamos (McDaniel et al, 1944) resonances in the fission cross sections were observed whose parameters indicated that fission widths were comparable to radiation widths. From these experiments and the work at Columbia (Rainwater and Havens, 1945) on the total cross section measurements of the fissionable materials it was clear that the ratio of fission to absorption changed from level to level, hence that η would vary with energy.

At the time the present experiments were undertaken the variation is η with energy in the thermal region (needed for reactor calculations) had been obtained only from the ratio of fission to total absorption cross sections, involving the assumption of a constant ν. For U^{235} the variation of η deduced from such considerations, however was in gross disagreement with results of studies of the temperature coefficient of reactivity made at the start-up of the Oak Ridge and Hanford reactors. The present direct method for measurement of the η variation was developed to resolve this difficulty. The results were in agreement with the observed reactor temperature coefficients and it was later shown that the previous disagreement was a result of error in the early fission cross section measurements.

2. Principle of the Direct η Method

In this experiment the variation of η is measured directly. Under exactly the same experimental conditions two measurements are made: 1) the emission rate of fission neutrons from a thick foil of fissionable material as the incident neutron energy is varied, and 2) the change with energy of the flux of neutrons incident upon the foil. Thus one obtains directly from the ratio of two counting rates the change with energy of η. The fission neutrons are detected by means of proton recoils detected by a scintillation counter (Hornyak, 1952). A thick sample of the fissionable material is used, so that nearly all the incident neutrons are absorbed and a maximum counting rate is obtained in the scintillation detector. The incident flux is measured by a boron detector in the form of a BF_3 proportional counter that absorbs only a few percent of the incident beam. The boron cross section, in the energy range of the measurements, varies as 1/v (Carter et al, 1953; Egelstaff, 1954), and since the detector is "thin" the efficiency of the counter varies very nearly as the cross section.

The relationship between η and the measured counting rates, assuming the sample is black, is

$$\frac{C_F}{k_F} = \nu \frac{\sigma_F}{\sigma_a} \cdot \frac{C_B}{k_B} = \eta \frac{C_B}{k_B} , \qquad (2)$$

where C_F is the counting rate of the scintillation counter measuring the fission neutrons from the uranium, and C_B is the counting rate in the BF_3 counter measuring the incident flux. k_F and k_B are the efficiencies of the scintillation and BF_3 detectors, respectively. k_F is constant in the energy region of these measurements. k_B is proportional to $1/\sqrt{E_1}$ where E_1 is the incident neutron energy; therefore

$$\eta = \frac{k}{E_i} \cdot \frac{C_F}{C_B} , \qquad (3)$$

where k is a constant independent of the neutron energy. In these experiments no attempt is made to make an absolute determination of η, and the results are normalized at E = 0.0253 ev to the values of η given in the Brookhaven cross section compilation, BNL-325 (Hughes and Harvey, 1955).

In practice the sample is not quite "black" to the incident neutrons, and the absorption cross section is needed for computing a small correction for the number of neutrons not absorbed in the sample foil. However, since nearly all the incident neutrons are absorbed, the experimental results depend only in an insensitive way on the absorption cross section. In treating the experimental data small corrections are made for isotope impurities (1 to 3 percent), departure of the BF_3, counter response from the 1/v law ($\sim$ 1 percent), and for loss of neutrons scattered out of the foil ($<$ 1 percent).

The scattering correction, although very small in the thermal region, is important in the application of this method to higher energy measurements, where the absorption is smaller. For a black sample only those neutrons that are scattered back from the front face of the foil escape, all the other scattered neutrons being absorbed. A calculation shows that for a black sample the effective scattering cross section is only 15% of the true scattering cross section. This reduction in the scattering effect is of value for measurements at higher energies

where the scattering cross section becomes an appreciable part of the total cross section. The definition of the effective scattering cross section and a curve giving its value for various sample thicknesses is given in the appendix.

The energy of the incident neutrons is determined by a time-of-flight method using the Brookhaven slow and fast choppers to interrupt a beam of pile neutrons. The direct η measurement is not restricted by the method used for determining the incident neutron energy. Following the time-of-flight experiments at Brookhaven, similar measurements using a crystal monochromator for energy selection were reported from the Hanford laboratory (Leonard, 1955), and at the Geneva meeting in August 1955, several additional results using the same method were reported (Harvey and Sanders, 1956).

The direct η measurement offers a simple and accurate method for obtaining knowledge of the variation of η with energy. It is difficult to obtain from cross section measurements the variation of η in the region of resonances because good energy resolution is required for the proper interpretation of total and fission cross section data. The fact that η varies much more slowly with energy than does either σ_a or σ_F is the reason the direct measurement is the logical way to investigate this variation. Experimentally the direct method is attractive because the use of a thick sample yields the highest counting rate and at the same time gives a result that is fairly insensitive to the absorption cross section and sample thickness. These characteristics are in contrast to the cross section measurements where the samples must be thin in the resonance region to give the correct η variation. The present method also allows the use of the same apparatus to investigate all the fissionable materials, one foil being substituted for another when a measurement on a different isotope is required. Furthermore the alpha "pile up", which is a serious problem when materials of high specific activity are measured in ionization chambers, creates no difficulty in the direct η method.

3. Fission Neutron Detector

The fission neutrons are detected by means of proton recoils produced in a suspension of ZnS in lucite. This phosphor mixture is molded in the form of 2 in. diameter "buttons" approximately 1-1/2 in. in length. One end has a slight spherical depression to give intimate contact with the face of the RCA 5819 photomultiplier. The buttons are made by heating a mixture of 70 grams of lucite molding powders and 4 grams of 40 μ ZnS-Ag to 120°C in a die under 2500 lb/sq. in. pressure (Higinbotham and Handloser, 1954). A mechanically sturdy, nonhygroscopic cap is formed, which can be easily handled for mounting on the 5819 tube face.

The dimensions of the collimated neutron beam from the Brookhaven slow chopper are 1-1/2 in. x 3-1/2 in. Six 5819 photomultipliers are so located along the periphery of this area to surround the sample foil. The arrangement is shown in Fig. 1. The calculated fractional solid angle of the sample foil subtended by the six scintillation counters is 10%.

The operating point for the scintillation counter is determined by a compromise to satisfy two criteria. First, the efficiency of the counter for fission neutrons should be as large as possible. Second, the sensitivity of the scintillation counter for γ-rays from the (n, γ) process in the fission foil must be so low that less than one percent of the counts recorded are due to this process. From the work of Hornyak, 1952, and others at Brookhaven it was well established that the ZnS-lucite combination had low γ-ray efficiency; however, in order to be certain of the second criterion the following test was run. With the detector set up to perform the experiment, the fission foil is replaced by a gold sample that is of a thickness calculated to produce approximately as many (n, γ) events as are produced in the foil of fissionable material. Then a combination of counter voltage, amplifier gain, and discriminator bias is found so that the counting rate is about 0.1% of the counting rate with the fission foil in place. The extra factor of 1/10 is used because of the uncertainty about the number and energies of the γ's produced by (n, γ)reactions in gold and the particular isotope under investigation. Only a small loss of neutron efficiency results since the discriminator curve for γ-rays falls off much faster than the neutron curve.

Under the above operating conditions the over-all efficiency for counting fission neutrons from the U^{235} foil was approximately 10^{-3}, determined from a measurement of the incident flux and the known fission cross section of U^{235}. Therefore, since the solid angle is 10%, the efficiency of detection of fission neutrons incident upon the buttons is one percent. The probability for a 1 Mev neutron to make a recoil proton, of any energy, in the traversal of the button is about 1/4. Consequently only about 1/25 of the recoil protons produce a large enough light pulse to be counted above the discriminator level.

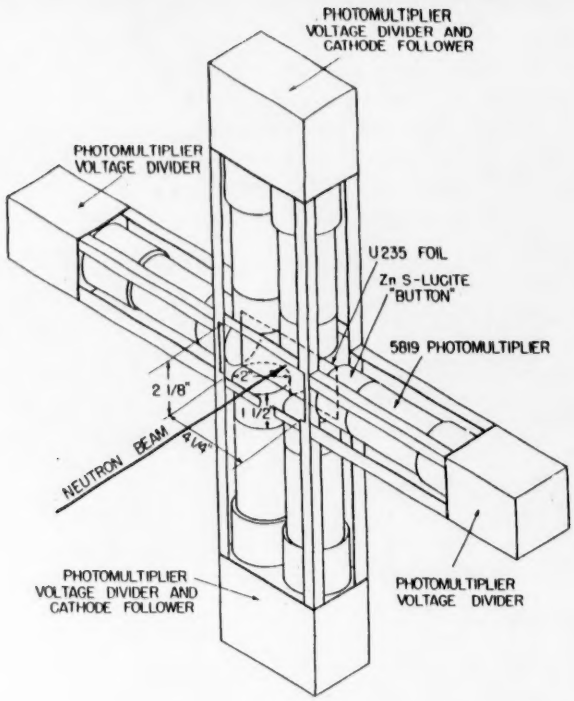

Fig. 1. Schematic drawing of the scintillation detector.

4. Results

By means of this direct method, measurements have been made with the Brookhaven slow chopper (Seidl et al, 1951) in the thermal region for U^{235}, U^{233}, and Pu^{239}. For Pu^{239} the fast chopper (Seidl et al, 1954) at Brookhaven was used to extend measurements through the 0.3 level. The results will now be presented and their connection with the cross section measurements for the same isotopes will be duscussed briefly.

4.1 U^{235}

The foils used were made of uranium metal enriched in U^{235} to a concentration higher than 90% and also contained minor amounts of U^{238} and U^{234}. Two sample thicknesses were used, 0.030" and 0.045". The data were taken in a series of repetitive cycles as follows:

C_1) The counting rate of a thin-walled BF_3 counter which gives the distribution in energy of the incident flux of slow neutrons.

C_2) The background counting rate pertaining to measurement C_1, obtained, at the slow chopper, by a 0.020" Cd foil inserted in the beam. This foil is essentially black to the incident neutrons in the energy range investigated in the experiment.

C_3) The counting rate of the fission neutrons detected by the scintillation counter.

C_4) The background counting rate pertaining to measure C_3, obtained by inserting a 0.020" Cd foil in the incident beam.

The variation in η is then obtained from the ratio

$$\frac{C_3 - C_4}{C_1 - C_2} = \frac{C_F}{C_B} \qquad (4)$$

Twelve cycles of data were taken, which permits one to demonstrate the general reproducibility of the results and also averages out the short term fluctuations in the sensitivity of the equipment. The statistical accuracy of the points varies from about one percent in the thermal region to about three percent at 0.16 ev. The corrections applied to the data are as follows: departure of BF_3 counter from 1/v, about 1.2%; U^{234} and U^{238} impurities, about 3.5%; and scattering correction, about 0.7%.

Figure 2 shows the combined results of the experiments performed with U^{235} at Brookhaven and Hanford. The Brookhaven data are normalized to $\eta = 2.08$ at thermal (E = 0.0253 ev), the value quoted in the Brookhaven compilation (Hughes and Harvey, 1955). The Hanford data are normalized to Brookhaven data in the energy region of 0.10 ev. The dashed line is computed from the ratio of σ_F/σ_a, Eq. (1), assuming ν constant, and using the most recent cross section data, given in BNL-325. The agreement between the direct measurement and the variation of η computed from fission and total cross sections is everywhere within one percent. U^{235} is the one fissionable isotope at present where the total and fission cross sections are known with sufficient precision so that the η variation deduced from these measurements has an accuracy comparable to the direct measurement.

The observed η variation in U^{235} is a good example of the accuracy obtainable by this new method of measurement. The change in η in the thermal region is very small ($\sim$ 1% from 0.01 to 0.1 ev). From the total and fission cross sections it is not possible to predict with certainty the sign of the slope of the η curve in the thermal region.

The resonance parameters of the 0.29 ev level give a ratio of radiative capture to fission cross section that is greater than that measured at thermal by spectrographic methods (Inghram, 1956). This fact had led to the belief that η would decrease with increasing energy in the thermal region. The results of the present η measurements at Brookhaven, however, showed the opposite to be true. This situation arises because contributions from at least two negative levels, in addition to those from the positive levels, are required to fit the cross section of U^{235} in the thermal region. From the observed variation of η and the total cross section an estimate may be made of the ratio of capture to fission for the negative levels (Harvey and Sanders, 1956).

4.2 U^{235}

The foil was made of uranium metal with a U^{233} content greater than 90% and a thickness of 0.025". The same experimental procedure was used in obtaining the U^{233} data as was outlined above for U^{235}. The corrections for isotopic impurities, scattering, and the departure of the BF_3 counters from 1/v were each about one percent.

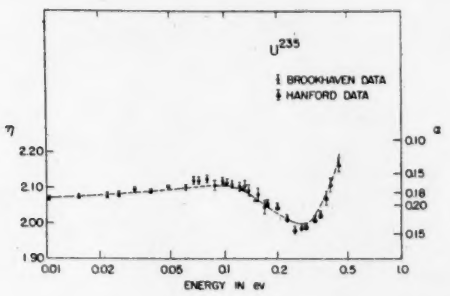

Fig. 2. η as a function of energy for U^{235}. The experimental data are normalized to $\eta = 2.08$ at thermal. The dashed line gives η as calculated from the absorption and fission cross sections assuming ν is constant.

Figure 3 gives the results of the measurements on U^{233} normalized to $\eta = 2.31$ at E = 0.0253. η is seen to be constant within statistical error ($\sim$ 1%) from 0.01 to 0.1 ev. The dashed line is computed from the curves drawn through the total and fission cross section data in the Brookhaven cross section compilation again with the assumption of a constant ν. The agreement between the two in this case is good within the large statistical errors in the fission cross section data, which would easily allow a $\pm$ 5% variation in η over this energy interval.

4.3 Pu^{239}

For the Pu^{239} measurement a 0.033" plutonium metal sample was used, which contained over 90% Pu^{239} and about one percent aluminum. The corrections for scattering and departure from 1/v are small ($\sim$ 1%). Below 0.35 ev the correction for isotopic impurities is also less than 1%. However, above 0.4 ev this correction rises rapidly and amounts to 28% at 0.7 ev.

Figure 4 shows the results of the measurements made with plutonium in the energy interval from 0.015 to 0.7 ev. Here, in marked contrast to U^{233} and U^{235}, η changes rapidly in the thermal region. The data from

thermal up to 0.15 ev were obtained with the slow chopper and normalized to $\eta = 2.03$ at thermal. The fast chopper was used to obtain the higher energy points and these were normalized to the slow chopper points in the neighborhood of 0.15 ev. The dashed line again is computed from BNL-325, assuming ν constant. From the direct η measurement the ratio of η at 0.3 ev to η at thermal is seen to be $0.75 \pm .02$. The cross section data assuming ν is constant gives for the same ratio $0.85 \pm .05$.

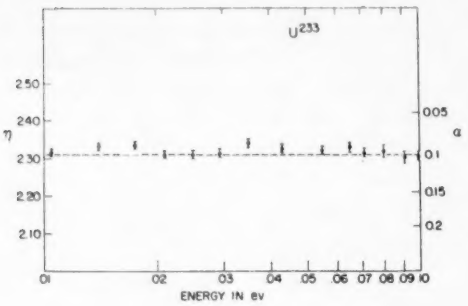

Fig. 3. η as a function of energy for U^{233}. The experimental data are normalized to $\eta = 2.31$ at thermal. The dashed line gives η as calculated from the absorption and fission cross section assuming ν is constant.

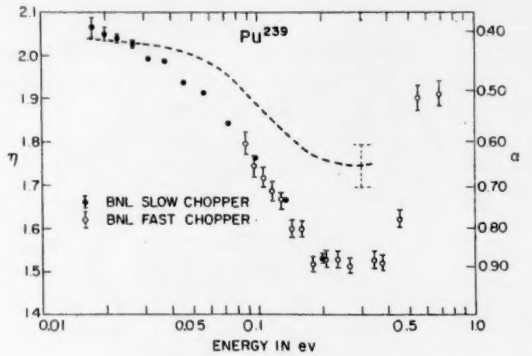

Fig. 4. η as a function of energy for Pu^{239}. The experimental data are normalized to $\eta = 2.03$ at thermal. The dashed line gives η as calculated from the absorption and fission cross sections assuming ν is constant.

The 12% disagreement between the direct measurement and the cross section results is seen to be outside the experimental error, and for this reason a series of experiments were performed to see if there was an unassigned source of systematic error. In order to check whether the experiment was dependent on the energy of the fission neutrons the bias on the scintillation counter was increased until the counting rate fell to one half of the value originally obtained. The slow chopper points were re-run with the higher bias settings and the results were in agreement with the first set of measurements. Next the shielding in the vicinity of the counters was re-arranged to make sure that scattered neutrons were not giving rise to spurious counts. No effect was found within an upper limit of 2%. As a final check the transmission of a 0.009" Pu foil was measured using the scintillation counter as a detector. The measured transmission agreed with the known cross section data again proving that the timed neutrons were of correct energy.

At first this disagreement was taken to imply that cross section measurements were in error. However recent theoretical (Bohr, 1956) and experimental (Pilcher, Harvey, and Seth, 1955) work have indicated that there is a possibility that a fissile nucleus can have more than one mode of fission. On the basis of such considerations it would be possible that ν might be different for the different levels. Therefore it was decided to investigate whether the assumption of the constancy of ν in the energy interval of the experiment was valid.

The measurement of the energy variation of ν was made by comparing the ratio of fission neutron to fission fragment counting rates in the thermal region and a small energy interval centered at 0.3 ev. The same counter as used in the η experiment was used to measure the fission neutrons, but a thin (0.001") foil was substituted for these measurements. In order to measure the fragment counting a gas scintillation counter containing 10 mg of Pu was constructed (Palevsky, Larsson, and Zimmerman, 1956). The neutron energies were selected by means of filters, using the beam of pile neutrons collimated by the fast chopper in a stopped, open position. The thermal data were obtained by Open-Gd differences using $Gd(NO_3)_3$ dissolved in D_2O as a filter. The atomic concentration of Gd in the filter was 5×10^{-4} atoms/cm^2. The energy interval centered on the resonance was obtained by taking Gd-Pu differences using the same filter and a 0.009" Pu foil. Because the plutonium foils in both the fission fragment and fission neutron detectors were thin the result is fairly insensitive to the shape of the neutron spectrum. The result of this experiment is as follows:

$$\frac{\nu_{\text{thermal}}}{\nu_{0.3\text{ ev}}} = 1.015 \pm 0.025$$

where uncertainty in the neutron spectrum constitutes one percent of the error and the residual error is statistical. It is therefore clear that the discrepancy between the direct η measurement and the cross section derived values cannot be attributed to a change in ν. This same conclusion has been reached by means of similar ν measurements at Saclay (Auclair, Landon, and Jacob, 1955), Hanford (Leonard et al, 1956), Argonne (Bollinger et al, 1956), and Moscow (Pevsner et al, 1956).

The constancy of ν constitutes a definite advantage of the present direct η method because the η measurement gives at the same time the energy variation of α, the ratio of capture to fission cross sections. It also implies that the relative fission cross section can be obtained from the η measurement together with the absorption cross section (Eq. 1), thus avoiding the often difficult direct fission measurement.

5. Conclusions

For U^{235}, where the total and fission cross sections have been most accurately measured, the agreement between the direct η measurement and the energy variation of η calculated from the cross sections, assuming ν is constant, is excellent. Such a comparison for U^{233} does not have much meaning at present because the cross section data do not have sufficient statistical accuracy. In Pu^{249} the disagreement between the direct measurement and the cross section calculation is about twice the standard deviation of the error associated with the cross section measurements. It should be mentioned that direct η measurements performed by Sanders at Harwell (Harvey and Sanders, 1956) using a crystal spectrometer are in excellent agreement with the present measurements. In the Harwell measurements the fission neutrons were moderated in paraffin and detected by BF_3 counters. Because of the widely different nature of neutron sources and detectors in the two experiments, one would expect that the kinds of systematic errors arising in the Harwell experiments would be entirely different from those of the Brookhaven measurements. The excellent agreement of the results, therefore, indicates that the energy variation of η has been correctly determined. The discrepancy between η and the cross sections for Pu^{239} cannot be ascribed to a change of ν with energy because the recent experiments at various laboratories, performed to check this possibility, have all verified the constancy of ν.

Even though both η and the cross section for Pu^{239} have been measured at several laboratories it seems most likely at present that the discrepancy, which is about nine percent when based on world average values (Harvey and Sanders, 1956) of all quantities, is a result of combined experimental errors. It is important that further measurements be made in order to resolve this discrepancy so that the present η method can be pushed to higher energies with confidence, and perhaps be used to obtain fission cross sections as well.

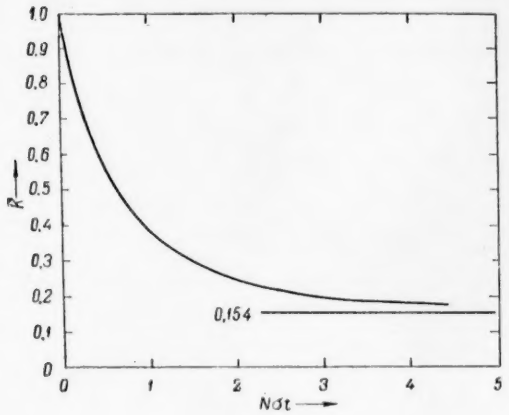

Fig. 5. $\bar{K}$, as a function of sample thickness $N\sigma t$. $\bar{K}\sigma_S$ is the effective scattering cross section.

Acknowledgements

The authors wish to thank Dr. T. I. Taylor of Columbia University for his assistance in taking the U^{235} data. We are also indebted to W. A. Higinbotham and J. A. Handloser of the Brookhaven Electronics Department for preparing the ZnS-lucite scintillation caps.

APPENDIX

The Effective Scattering Cross Section

The counting rate in the scintillation counter used to detect the fission neutrons from a fissionable material is proportional to the average neutron flux in the material. For a foil of thickness t the average flux is given by

$$\bar{F}(t) = \frac{\int_0^t F(x)\,dx}{\int_0^t dx} = F(0)\,\frac{1-e^{-N\sigma_a t}}{N\sigma_a t}, \qquad (5)$$

where $F(x) = F(0)e^{-N\sigma_a t}$ if there is no scattering in the foil. N is the number of nuclei per cm^3 and σ_a the absorption cross section. To include the effect of scattering let K(x) be the probability that a neutron scattered at the distance x will leave the foil without being absorbed. Thus $K(x)\sigma_s$, the effective scattering cross section, represents the fraction of the scattering cross section that is effective in contributing to the attenuation of the flux. We then have, including scattering,

$$\frac{d}{dx}F(x) = -F(x)N\sigma_a\left(1 + K(x)\frac{\sigma_s}{\sigma_a}\right). \tag{6}$$

Figure 5 shows the average value of K for various foil thicknesses in units of $N\sigma_a t$, computed from Eq. (6). The curve represents the numerical solution for K(x) of Eq. (6) and subsequent averaging over x.

LITERATURE CITED

Auclair, J. M., Landon, H. H., and Jacob, M. (1955) Compt. rendu 241, 1935.

Bohr, N., and Wheeler, J. A. (1939) Phys. Rev. 56, 426.

Bohr, A. (1956) Proceedings of the International Conference on Peaceful Uses of Atomic Energy, Paper P/911.

Bollinger, L. M., Cote, R. E., Hubert, P., Leblanc, J. M., and Thomas, G. E. (1956) Bull. Am. Phys. Soc. 1, No. 4.

Carter, R. S., Palevsky, H., Myers, V. W., and Hughes, D. J. (1953) Phys. Rev. 92, 716.

Egelstaff, P. A. (1954) J. Nuclear Energy 1, 57.

Harvey, J. A., and Sanders, J. R. (1956) Progress in Nuclear Energy Series I, Vol. 1, Chapter 1 (Pergamon Press, London).

Higinbotham, W., and Handloser, J. (1954) Rev. Sci. Instr. 25, 98.

Hornyak, W. F. (1952) Rev. Sci. Instr. 23, 264.

Hughes, D. J. and Harvey, J. A. (1955) Brookhaven National Laboratory Report 325 Neutron Cross Sections (Superintendent of Documents, Washington, D. C.).

Inghram, M. (1956) Proceedings of the International Conference on the Peaceful Uses of Atomic Energy, Paper P/596.

Leonard, B. R. (1955) reviewed by H. Palevsky, Proceedings of the International Conference on the Peaceful Uses of Atomic Energy, Paper P/587.

Leonard, B. R., Seppi, E. J., Friesen, W. J. (1956) Bull. Am. Phys. Soc. 1, No. 1.

McDaniel, B. D., Sutton, R. B., Anderson, E. E., and Lavatelli, L. S. (1945) Los Alamos Scientific Laboratory, University of California (unpublished).

Palevsky, H., Larsson, K. E., and Zimmerman, R. L. (1956) Rev. Sci. Instr. (in press).

Pevzner, M. I., Donelyan, L. S., and Adamchuk, Yu. V. (1956) private communication; Kalashinikov, V. I., Tebedev, V. I., Mikallyan, L. A. and Pevzner, M. I. (1956) private communication.

Pilcher, V. E., Harvey, J. A., and Seth, K. K. (1955) Phys. Rev. 100, 1248A.

Seidl, F. G. P., Palevsky, H., Randall, R. R., and Thorne, W. (1951) Phys. Rev. 82, 345.

Seidl, F. G. P., Hughes, D. J., Palevsky, H., Levin, J. S., Kato, W. Y., and Sjostrand, N. G. (1954) Phys. Rev. 95, 476.

FUEL BURN-UP IN NUCLEAR REACTORS

B. L. Ioffe and L. B. Okun

The paper describes the method of calculating fuel burn-up in nuclear reactors, taking into account the capture and multiplication of neutrons while slowing down. In the calculations, account is taken of the burn-up of U^{235} and the build-up and burn-up of Np^{239}, Pu^{239}, Pu^{240}, Pu^{241} and of the fission fragments.

INTRODUCTION

The economic characteristics of nuclear reactors designed for the production of electrical energy depend to an important degree on the quantity of raw material required to produce a given amount of electrical energy or, in other words, on the permissible degree of nuclear fuel burn-up.

If we assume that the problem of maintaining continuity of operation of reactor fuel elements has been solved, then the permissible extent of fuel burn-up will be determined by the initial excess reactivity in the reactor and by the laws of its decrease during the reactor's operation.

In this paper is considered the change in reactor reactivity with time (the kinetics of burn-up) for the case of extensive fuel burn-up. Numerical results are obtained for natural uranium systems with heavy water moderation.

Multiplication During Slowing Down

In burn-up kinetics a leading role is played by the accumulation of Pu^{239}, Pu^{240}, and Pu^{241}. These isotopes, and Pu^{239} in particular, have large neutron absorption and fission cross sections in the epithermal region. For this reason it is necessary to take into account in the kinetic equations not only the capture of neutrons in the epithermal range but also the deviation of the cross section from the 1/v law in the thermal region.

We will consider, to begin with, certain questions involved in calculation of the capture and multiplication of neutrons during the slowing down process.

Let us assume that the neutron spectrum (on the energy scale) has the form of the Maxwell distribution at the temperature T:

$$N(E)\,dE = N_T \frac{2}{\sqrt{\pi}} \gamma T^{-3/2} e^{-\frac{E}{T}} \sqrt{E}\,dE \qquad (1)$$

(N_T is the total number of thermal neutrons), which extends up to the energy E_{jo}* and of a Fermi distribution of slowing down neutrons f(E)dE, extending from the energy E_{jo} to the energy spectrum of fission neutrons. The "joining" energy E_{jo} is determined as the energy of intersection of the two spectra. In such an approximation, no account is taken of the influence of chemical binding (which becomes important near the joining energy) on the neutron spectrum. Comparison of the spectrum obtained with experimental measurements [1] shows that the

*The factor γ, which differs little from unity, takes account of the circumstance that the Maxwell spectrum must be normalized to unity in integration to E_{jo} rather than to infinity.

error introduced by such an approximation is comparatively small. The spectrum of the slowing down neutrons is determined by the equation

$$f(E) = \frac{l_s}{\xi v E} q(\tau) \varphi(E), \tag{2}$$

where l_s is the scattering mean free path, ξ is the mean logarithmic energy decrement, $d\tau = \frac{l_s l_t dE}{3\xi E}$, and $q(\tau)$ satisfies the equation

$$\Delta q = \frac{\partial q}{\partial \tau} + \frac{q(\tau)}{L^2(\tau)}, \tag{3}$$

where $L(\tau)$ is the diffusion length of neutrons of age τ.

In the Equation (3) it is assumed that the moderator does not contain any hydrogen, and that the total neutron absorption cross section is small compared to the scattering cross section, thereby assuring the applicability of the diffusion approximation. The existence of strong resonance absorption (for example by the resonance levels of U^{238} or Pu^{240}) is taken account of in equation (2) by the factor $\varphi(E)$, which represents the probability of escaping resonance absorption by the strong resonance levels, and which therefore cannot be included in L^2 in Equation (3).*

The initial conditions for the function $q(\tau)$ can be obtained through calculating the number of fast neutrons originating in the capture of thermal, as well as of slowing down neutrons, by the fissioning nuclei, and has the form

$$q(0) = \mu v_T \sum_i \nu_i' \sigma_{iT} p_i N_{iT} + \int_0^{\tau(E_{j_0})} \frac{k(\tau)}{L^2(\tau)} q(\tau)\, d\tau. \tag{4}$$

Here p_i is the concentration of the i^{th} isotope, σ_{iT} is the absorption cross section of thermal neutrons, ν'_i is the number of secondary neutrons per absorption, N_{iT} is the density of thermal neutrons at the location of the i^{th} isotope, μ is the fast neutron multiplication constant, $k(\tau)$ is the multiplication constant for neutrons of age τ. The thermal neutron cross sections entering into the first member of Equation (4) are assumed to have been averaged over the Maxwell spectrum in accordance with the equation

$$\sigma_T v_T = \overline{\sigma v} = \frac{\int_0^{E_{j_0}} \sigma v N(E)\, dE}{\int_0^{E_{j_0}} N(E)\, dE}, \tag{5}$$

where v_T = 2200 m/sec, is the standard speed of thermal neutrons. As is well known, in this averaging (see, for example, [2]) what is actually averaged are not the cross sections σ_a and the transport lengths l_t, but the magnitudes $\sigma_a v$ and the diffusion coefficients $D \sim l_t v$.

---

*The division of resonance capture into that by strong and weak levels is somewhat provisional. Subsequently we will include in φ only resonance capture in U^{238} and Pu^{240}, the remainder being included in the term $q(\tau)/L^2(\tau)$ in equation (3).

The Equations (3) and (4), together with the equation for thermal neutrons

$$D\Delta N_T - \frac{N_T}{T_c} = -q(\tau_{jo})\varphi(E_{jo}) \tag{6}$$

(T_c is the thermal neutron lifetime) determine fully the conditions for reactor critical size, and for the neutron density distribution in the reactor.

If the reactor does not have a reflector, the solution of Equations (3), (4) and (6) can be obtained through the substitutions

$$q(\mathbf{r}, \tau) = q(\tau)\, e^{i\bar{\varkappa}\mathbf{r}},$$

$$N_T(\mathbf{r}) = N_T(0)\, e^{i\bar{\varkappa}\mathbf{r}},$$

which gives

$$q(\tau) = q(0)\, e^{-\int_0^{\tau} \frac{d\tau}{L^2(\tau)} - \varkappa^2\tau}, \tag{7}$$

$$\left(\varkappa^2 + \frac{1}{L_T^2}\right) N_T(0) = \frac{\varphi}{D}\, q(0)\, e^{-\int_0^{\tau_{jo}} \frac{d\tau}{L^2(\tau)} - \varkappa^2\tau_{jo}}$$

where L_T is the diffusion length for thermal neutrons (calculated through averaging over the Maxwell spectrum by the method described above), while φ is the total resonance escape probability (by strong levels) in neutron slowing down to the energy E_{jo}. The substitution of Equation (7) into (4) leads to the characteristic equation for determining the Laplacian of the system $\varkappa^2$:

$$1 + \varkappa^2 L_T^2 = \frac{k_T e^{-\int_0^{\tau_{jo}} \frac{d\tau}{L^2(\tau)} - \varkappa^2\tau_{jo}}}{1 - \int_0^{\tau_{jo}} k(\tau) \frac{d\tau}{L^2(\tau)}\, e^{-\int_0^{\tau} \frac{d\tau}{L^2(\tau)} - \varkappa^2\tau}}, \tag{8}$$

where

$$k_T = \mu\eta\varphi\theta \tag{9}$$

is the thermal neutron multiplication constant.

From the equations (1), (2) and (7) we can determine the joining energy E_{jo}

$$e^{-\frac{E_{jo}}{T}} = \frac{\sqrt{\pi}}{2}(1 + \varkappa^2 L_T^2)\, \frac{l_s(E_{jo})}{\xi l_{cT}} \left(\frac{T}{E_{jo}}\right)^2 \times \times \left(\frac{E_{2200}}{T}\right)^{1/2}, \tag{10}$$

where l_{cT} = mean absorption length at the given temperature, while E_{2200} is the neutron energy corresponding to a neutron speed of v_T = 2200 m/sec. Now it is easy to deduce the burn-up equation for any isotope. Let ρ_i be the number of nuclei of the i^{th} isotope. The number of neutrons captured by the nuclei of this isotope per unit time are determined by the expression

$$N_T v_T \sigma_{iT} \rho_i + \rho_i \int_{E_{j0}}^{E_0} v\sigma_i(E) f(E)\, dE \tag{11}$$

(E_0 is the fission spectrum energy). Strictly speaking, the neutron density in equation (11) should be considered as varying for the different isotopes although for convenience we will ignore this fact in our notation, assuming that the appropriate corrections have been included in the cross sections. Inserting the Equation (7) into the Expression (11), we obtain the equation for the burn-up of the i^{th} isotope:

$$\frac{d\rho_i}{dt} = -N_T v_T \sigma_{iT} \rho_i - N_T v_T \frac{\mu \sum_k \nu'_k \sigma_{kT} \rho_k}{1 - \int_0^{\tau_{j0}} k(\tau) \frac{d\tau}{L^2(\tau)} e^{-\int_0^{\tau} \frac{d\tau}{L^2(\tau)} - x^2\tau}} \times \tag{12}$$

$$\times \rho_i \int_{E_{j0}}^{E_0} \frac{l_s}{\xi} \cdot \frac{\sigma_i(E)}{E} \varphi(E) e^{-\int_0^{\tau} \frac{d\tau}{L^2(\tau)} - x^2\tau} dE + Q - \lambda_i \rho_i,$$

where Q is the number of nuclei of the given isotope formed as a result of neutron capture by the preceding isotope; λ_i is the disintegration constant (if the given isotope is radioactive).

It should be noted that for an infinite system an equation of the type (12) can be easily obtained also for the case of moderation by hydrogen since in this case the kinetic equation for slowing down can be solved exactly.

In the sequel we will be investigating thermal neutron reactors for which the magnitude $\int_0^{\tau_{j0}} \frac{d\tau}{L^2(\tau)} =$

$= \int_{E_{j0}}^{E_0} \frac{l_s}{\xi l_c(E)} \cdot \frac{dE}{E}$ can be considered to be fairly small. Then the equation (12) goes over into

$$\frac{d\rho_i}{dt} = -N_T v_T \sigma_{iT} \rho_i - N_T v_T \mu\varphi \sum_k \nu'_k \sigma_{kT} \rho_k \rho_i \int_{E_{j0}}^{E_0} \frac{l_s}{\xi} \sigma_i(E) \frac{dE}{E} + Q - \lambda_i \rho_i. \tag{13}$$

In equation (13) we neglected, as well, the magnitude $\kappa^2\tau$, small in comparison with unity and, in addition, assumed that resonance capture $1-\varphi$, determined in the initial U^{238}, occurs at higher energies than the captures occurring during slowing down. Since the more significant capture, while slowing down in Pu^{239}, occurs in the resonance at 0.3 ev, the last assumption is sufficiently accurate. (The error resulting from this appears only in the quadratic terms in the expansion with respect to $\int \frac{d\tau}{L^2}$). All further investigations of the kinetics of burn-up will be made with the aid of equations of the type (13).

The Kinetic Equations

Let us now write down the burn-up equation. We will take into account the burn-up of U^{235}, and the accumulation and burn-up of Pu^{239}, Pu^{240}, and Pu^{241} during which the burn-up of U^{238}, and accumulation of U^{236} and Pu^{242}, can be neglected. We will take Np^{239} into account approximately, taking advantage of the circumstance that the lifetime of Np^{239} is significantly smaller than the fuel reloading period.

The kinetic equations, written in the form of equation (13), have the form:

$$\left.\begin{aligned}
\frac{d\rho_5}{ds} &= -\rho_5 - \psi_5 \cdot f(s)\varphi_8\mu,\\
\frac{d\rho_{Np}}{ds} &= c_8 + (1-\varphi_8)\mu f(s) - \\
&\quad - \frac{\lambda_{Np}}{N_T v_T \sigma_{5T}} - \bar{\sigma}_{NpT}\rho_{Np},\\
\frac{d\rho_9}{ds} &= \frac{\lambda_{Np}}{N_T v_T \sigma_{5T}}\rho_{Np} - \bar{\sigma}_{9T}\rho_9 - \psi_9 f(s)\varphi_8\mu,\\
\frac{d\rho_0}{ds} &= \bar{\sigma}_{NpT}\rho_{Np} + \bar{\sigma}^{r}_{9T}\rho_9 + \psi^{r}_9 f(s)\varphi_8\mu - \\
&\quad - \bar{\sigma}_{0T}\rho_0 - \psi_0 f(s)\varphi_8\mu,\\
\frac{d\rho_1}{ds} &= \bar{\sigma}_{0T}\rho_0 + \psi_0 f(s)\varphi_8\mu - \bar{\sigma}_{1T}\rho_1,\\
f(s) &= \nu'_5\rho_5 + \nu'_9\bar{\sigma}_{9T}\rho_9 + \nu'_1\bar{\sigma}_{1T}\rho_1.
\end{aligned}\right\} \qquad (14)$$

In the equations (14) $\bar{\sigma}_{iT} = \sigma_{iT}/\sigma_{5T}$; $c_8 = \sigma_{8T}\rho_8/\sigma_{5T}\rho_5^0$; $ds = N_T v_T \sigma_{5T} dt$; ψ_5, ψ_9, ψ_0, $1-\varphi_8$ is the probability of neutron capture in U^{235}, Pu^{239}, Pu^{240} and U^{238} during slowing down; the index r (σ^{r}_{9T} and ψ^{r}_9) designates radiative capture. All isotope concentrations are to be expressed with reference to the initial concentration of U^{235}.

Let us exclude ρ_{Np} from the Equations (14), using the fact that $\lambda_{Np}/N_T v_T \sigma_{5T} \gg 1$. In doing so, since the corrections arising from taking Np^{239} into account are not great, we will consider the magnitude $N_T v_T$ independent of the time. Then the solution of the second of the equations (14) can be written in the form

$$\rho_{Np} = N_T v_T \sigma_{5T} e^{-(\lambda + N_T v_T \sigma_{NpT})t} \times \int_0^t e^{(\lambda + N_T v_T \sigma_{NpT})t} [c_8 + (1-\varphi_8)\mu f(t)]\, dt$$

or, approximately, if we neglect the terms $1/\lambda^3$ and $N_T v_T \sigma_{Np}/\lambda^2$,

$$\begin{aligned}
\rho_{Np} &= \frac{N_T v_T \sigma_{5T}}{\lambda}[c_8 + (1-\varphi_8)\mu f(t)] - \\
&\quad - \frac{N_T v_T \sigma_{5T}}{\lambda}[c_8 + (1-\varphi_8)\mu f(0)]e^{-\lambda t} - \\
&\quad - \frac{N_T v_T \sigma_{5T}}{\lambda^2}\cdot\frac{d}{dt}[(1-\varphi_8)\mu f(t)].
\end{aligned} \qquad (15)$$

In the case of natural uranium systems, the magnitude f(t) changes very little during the fuel reloading cycle. For this reason the third member in the equation (15) may be dropped, after which we get:*

$$\rho_{Np} = \frac{N_T v_T \sigma_{5T}}{\lambda} [c_8 + (1 - \varphi_8) \mu f(t)] - \frac{N_T v_T \sigma_{5T}}{\lambda} [c_8 + (1 - \varphi_8) \mu f(0)] e^{-\lambda t}. \tag{16}$$

The insertion of the Expression (16) into the Equation (14) gives:

$$\left.\begin{aligned}
\frac{d\rho_5}{ds} &= -\rho_5 - \psi_5 f(s) \varphi_8 \mu, \\
\frac{d\rho_9}{ds} &= c_8 + (1 - \varphi_8) \mu f(s) - \\
&\quad - [c_8 + (1 - \varphi_8) \mu f(0)] e^{-\frac{\lambda s}{N_T v_T \sigma_{5T}} s} - \\
&\quad - \bar{\sigma}_{9T} \rho_9 - \psi_9 \mu \varphi_8 f(s), \\
\frac{d\rho_0}{ds} &= \frac{N_T v_T \sigma_{5T}}{\lambda} \bar{\sigma}_{NpT} [c_8 + (1 - \varphi_8) \mu f(s)] + \\
&\quad + \bar{\sigma}^r_{9T} \rho_9 + \psi^r_9 \mu \varphi_8 f(s) - \bar{\sigma}_{0T} \rho_0 - \psi_0 \mu \varphi_8 f(s), \\
\frac{d\rho_1}{ds} &= \bar{\sigma}_{0T} \rho_0 + \psi_0 \mu \varphi_8 f(s) - \bar{\sigma}_{1T} \rho_1
\end{aligned}\right\} \tag{17}$$

(in obtaining these equations it is sufficient to insert into the third of the Equations (14) only the first member of the Expression (16).

Calculation of capture in Pu^{239} during slowing down can be carried out without taking into account the fuel self-shielding effect since, as follows from the results obtained below, the absorption length in the center of the 0.3 ev resonance, at the Pu^{239} concentrations of interest to us, is significantly larger than the dimensions of the fuel element. An even smaller fuel self-shielding effect is involved in the calculation of ψ_5. Then, with the aid of (13), we can write

$$\left.\begin{aligned}
\psi_9 &= \frac{l_s}{\xi} \cdot \frac{S_U}{S_{mod}} n_5 \rho_9 I_9, \\
\psi_5 &= \frac{l_s}{\xi} \cdot \frac{S_U}{S_{mod}} n_5 \rho_5 I_5,
\end{aligned}\right\} \tag{18}$$

where S_U and S_{mod} are the surface areas of the uranium and of the moderator in the lattice, l_s/ξ refers to the pure moderator, n_5 is the number of U^{235} atoms per unit volume of the fuel element at the starting time, and

$I_i = \int_{E_{j0}}^{E_0} \sigma_i(E) \frac{dE}{E}$ is the resonance integral. The expression for ψ^r_9 can be written in an analogous way.

Let us now calculate resonance absorption in Pu^{240}. It is known that Pu^{240} has a very strong resonance level at the energy 1.07 ev. For this reason, even for those small concentrations of Pu^{240} which occur in the cases of interest to us, resonance absorption at this energy has an extremely important effect on the multiplication constant of the system. In this case, a noticeable fuel self-shielding effect should occur in resonance absorption at this level. In this way an expression for ψ_0 must be obtained which is valid for small as well as for large concentrations of Pu^{240} in the fuel element.

*The authors are grateful to P. V. Vavilov, who obtained the equation (16).

As is known [3], [4], the probability of a neutron resonance capture in its moving through a distance l within a cylindrical fuel element of radius R is determined, for the case of a single resonance, by the expression

$$\psi = \frac{l_s}{\xi} \cdot \frac{\pi^2}{4} \cdot \frac{\Gamma}{E_r} \cdot \frac{R}{S_{\text{mod}}} \cdot \frac{l}{l_{cr}} e^{-\frac{1}{2}\frac{l}{l_{cr}}} \left[I_0\left(\frac{1}{2}\frac{l}{l_{cr}}\right) + I_1\left(\frac{1}{2}\frac{l}{l_{cr}}\right)\right], \tag{19}$$

where Γ is the level width, while l_{cr} is the absorption length in the center of the resonance. It is necessary to average this expression over all directions of neutron motion in the fuel element. Let us make such an average approximately, replacing l by the mean path of the neutron in the fuel element $\bar{l} = 2R$. This approximation has sufficient accuracy for practical cases, since in the limiting case of $\bar{l}/l_{cr} \gg 1$ the expression (19), after the substitution $\bar{l} = 2R$, differs from the exact expression only by 2%; in the case of the other limiting situation of $\bar{l}/l_{cr} \ll 1$, it simply coincides with the exact result.

As a consequence we obtain:

$$\psi_0 = \frac{l_s}{\xi} \cdot \frac{\pi}{2} \cdot \frac{\Gamma}{E_r} \cdot \frac{S_U}{S_{\text{mod}}} \cdot \frac{1}{l_{cr}} e^{-\frac{R}{l_{cr}}} \left[I_0\left(\frac{R}{l_{cr}}\right) + I_1\left(\frac{R}{l_{cr}}\right)\right]. \tag{20}$$

As it is to be expected that the mean distance between resonances in Pu^{240} is of the same order as in U^{238} (that is, 15-20 ev), the remaining resonances must be located significantly higher, and their inclusion in ψ_0 can be disregarded.

The existence of noticeable self-shielding by the fuel leads to an increase in the effective cross section of the plutonium isotopes for thermal neutrons. This is associated with the fact that Pu^{239} is not formed uniformly throughout the cross section of the fuel element: there is more of it at the peripheries of the element and less at the center. The non-uniform distribution of Pu^{239} is due to two causes: in the first place, fuel self-shielding from thermal neutrons; in the second, self-shielding of the fuel from resonance neutrons. As a consequence of these causes, the absorption of resonance, as well as thermal neutrons by U^{238} in the peripheral regions of the fuel element and, consequently, the concentration of the Pu^{239} produced, is larger.

As a result, Pu^{239} is most of all formed in regions of the largest thermal neutron density, and this, in turn, leads to a greater burn-up of Pu^{239} in comparison with that which would take place if it were formed uniformly throughout the cross section of the fuel element. This effect can be taken into account in the following way. The increase in the effective thermal cross section of Pu^{239} induced by fuel self-shielding is equal to

$$\zeta = \zeta_1 + \zeta_2 = \frac{\int \rho_9(R)\, N(R)\, R\, dR \cdot \int R\, dR}{\int \rho_9(R)\, R\, dR \cdot \int N(R)\, R\, dR},$$

(All integrals are taken from 0 to R_1, where R_1 is the radius of the fuel element.) The magnitudes ζ_1 and ζ_2 relate, respectively, to self-shielding from thermal and resonance neutrons.

At small burn-ups, when the concentration of Pu^{239} resulting from the absorption of thermal neutrons by U^{238} is proportional to the thermal neutron density N(R), ζ_1 has the form

$$\zeta_1 = \frac{\int N^2(R)\, R\, dR \int R\, dR}{\left(\int N(R)\, R\, dR\right)^2} = \frac{\overline{N^2}}{(\bar{N})^2} > 1.$$

(For large burn-ups, ρ_9 increases more slowly than N, and the effect being studied decreases). In the diffusion approximation $N(R) = I_0(R/L_U)$, where L_U is the diffusion length of the neutrons in the fuel element. Expanding ζ_1 in a series with respect to R_1/L_U, we obtain:

$$\zeta_1 = 1 + \frac{1}{192}\left(\frac{R_1}{L_U}\right)^4 .$$

The fuel self-shielding effect for resonance neutrons can be calculated if it is assumed that the concentration of Pu^{239} produced by resonance absorption in U^{238} is inversely proportional to the magnitude $\sqrt{R_1^2 - R^2}$. This dependence on R corresponds to resonance absorption in a ring-like fuel-element (the external radius of which is R_1, and the internal is R_2), proportional to $\sqrt{R_1^2 - R_2^2}$ [3]. The magnitude ζ_2, characterizing the increase in the effective cross section for thermal neutrons in Pu^{239} produced by resonance absorption in U^{238}, is equal to

$$\zeta_2 = \frac{\int \frac{N(R)\,R\,dR}{\sqrt{R_1^2 - R_2^2}} \int R\,dR}{\int \frac{R\,dR}{\sqrt{R_1^2 - R_2^2}} \int N(R)\,R\,dR} \geqslant 1.$$

Changes In Reactivity

The reactivity of the system is characterized by the effective multiplication constant, small changes in which are proportional to small changes in the Laplacian. The expression for the effective multiplication constant can be easily obtained starting with the equation (8). For this purpose let us employ the circumstance that absorption during slowing down takes place primarily in the energy region near to thermal energies. The factor $e^{-\varkappa^2\tau}$ can be taken out from under the integral sign in the denominator at the value $\tau_{jo} = \tau(E_{jo})$. The expression (8) assumes the form:

$$1 + \varkappa^2 L_T^2 = \tilde{k} e^{-\varkappa^2 \tau_{jo}}, \tag{21}$$

where

$$\tilde{k} = k_T \{1 - (1-\delta)(1 - e^{-w}) + \\ + \delta (1 - e^{-w})\,\varkappa^2 L_T\}, \tag{22}$$

$$w = \int_0^{\tau_{jo}} \frac{d\tau}{L^2(\tau)},$$

$$\delta = \frac{\int_0^{\tau_{jo}} k(\tau) \frac{d\tau}{L^2(\tau)} e^{-\int_0^{\tau} \frac{d\tau}{L^2(\tau)}}}{k_T \int_0^{\tau_{jo}} \frac{d\tau}{L^2(\tau)} e^{-\int_0^{\tau} \frac{d\tau}{L^2(\tau)}}}. \tag{23}$$

In case of low absorption during slowing down $\left(\int_0^{\tau_{jo}} \frac{d\tau}{L^2(\tau)} \ll 1\right)$ in the expression for δ one can drop, in both numerator and denominator, the factor $e^{-\int_0^{\tau} \frac{d\tau}{L^2}}$. To the extent that these factors are dropped in

both the numerator and denominator the value of δ practically does not change even for not very small $\int_0^{\tau_{jo}} \frac{d\tau}{L^2(\tau)}$. Then

$$\delta = \frac{\int_0^{\tau_{jo}} k(\tau) \frac{d\tau}{L^2(\tau)}}{k_T \int_0^{\tau_{jo}} \frac{d\tau}{L^2(\tau)}}. \tag{24}$$

The multiplication constant for thermal neutrons, k_T, can be written in the following way:

$$k_T = \mu \varphi_8 \varphi_0 \varphi_{ff} \times \frac{\nu_5' \sigma_{5T} \rho_5 + \nu_9' \sigma_{9T} \rho_9 + \nu_1' \sigma_{1T} \rho_1}{\sum_T \rho_8 + \sigma_{5T} \rho_5 + \sigma_{9T} \rho_9 + \sigma_{0T} \rho_0 + \sigma_{1T} \rho_1 + \Sigma \sigma_T \rho + (\sigma_T \rho)_{ff}} \tag{25}$$

In the Expression (25) $\varphi_0 = e^{-\psi_0}$, $\Sigma \sigma_T \rho$ is absorption in the moderator and in the construction materials, $(\sigma_T \rho)_{ff}$ is absorption by the fission fragments, $\varphi_{ff} = e^{-\psi_{ff}}$, ψ_{ff} is the probability of resonance absorption in the fission fragments. Poisoning due to the isotopes Xe^{135}, Xe^{133} and Sm^{149}, the concentration of which rapidly attains equilibrium levels, we will include in $\Sigma \sigma_T \rho$ and not in $(\sigma_T \rho)_{ff}$. The ratio of the value of k_T at the time s to its value at the beginning of the fuel reloading cycle is equal to

$$\frac{k_T(s)}{k_T(0)} = \frac{f(s)}{\nu_5'} \cdot \frac{1}{1 - A(s)} \varphi_0(s) \varphi_{ff}(s) \times \times \frac{1}{1 + \frac{c_{ff}}{(1 + c_8)(1 + \Sigma c)(1 - A)}}, \tag{26}$$

where

$$\left.\begin{aligned} A(s) &= \frac{1}{(1 + c_8)(1 + \Sigma c)} \times \\ &\times \{1 - \rho_5 - \bar{\sigma}_{9T} \rho_9 - \bar{\sigma}_{0T} \rho_0 - \bar{\sigma}_{1T} \rho_1\}, \\ \Sigma c &= \frac{\Sigma \sigma_T \rho}{\sigma_{5T} \rho_5^0 + \sigma_{8T} \rho_8}; \quad c_{ff} = \frac{(\sigma_T \rho)_{ff}}{\sigma_{5T} \rho_5^0}. \end{aligned}\right\} \tag{27}$$

Here, as previously, it is assumed that if the mean neutron densities are different in various materials, then the cross sections must be multiplied by appropriate factors.

The magnitudes ω and δ are simply expressed through prior introduction of the probability of neutron absorption during slowing down:

$$w = \psi_5 + \psi_9 + \frac{l_8}{\xi} \cdot \frac{S_U}{S_{mod}} \times \sigma_5 \rho_5^0 2 \sqrt{\frac{E_{2200}}{E_{jo}}} [c_8 (1 + \Sigma c) + \Sigma c], \tag{28}$$

$$\delta = \frac{(1 + c_8)(1 + \Sigma c)(1 - A)}{w} \times \frac{\nu_5' \frac{\sigma_{5T}}{\sigma_{5T}'} \cdot \frac{I_5'}{I_5} \psi_5 + \nu_9' \frac{\sigma_{9T}}{\sigma_{9T}'} \cdot \frac{I_9'}{I_9} \psi_9}{f(s)}. \tag{29}$$

To obtain the value of the effective multiplication constant, it is necessary to calculate the change in the multiplication constant induced by change in L^2 T, which appears on the left side of the Expression (21). Since

$$L_T^2(s) = \frac{L_T^2(0)}{1 - A(s)}, \tag{30}$$

then

$$\frac{k_{eff}(s)}{k_{eff}(0)} = \frac{\tilde{k}(s)}{\tilde{k}(0)} \left(1 - \frac{\varkappa^2 L_T^2(0) A(s)}{1 - A(s) + \varkappa^2 L_T^2(0)}\right), \tag{31}$$

where the connection between $\tilde{k}$ and k_T, determined in accordance with the Expression (26), is given by the Expression (22), while ω and δ must be substituted from the Expressions (28) and (29). The Formulas (26), (27), (28), (29) and (31) completely determine changes in the effective multiplication constant of the system, that is changes in the reactivity connected with fuel burn-up.

Calculation of Fuel Burn-up In Heavy Water Moderated Natural Uranium Reactors

A burn-up calculation will now be carried out for several concrete systems. We will investigate a reactor using natural uranium and moderated by heavy water. Cooling of the reactor is accomplished by a gas. A reactor of this type was investigated in the paper [5]. The temperature of the moderator (heavy water) in such a reactor is close to 70°C. We will consider the temperature of the neutron gas to be 410°K. Taking l_s = 2.9 cm for the scattering mean free path of neutrons in heavy water for energies above the joining energy E_{jo} (and almost for the whole important part of the energy spectrum for moderated neutrons), and ξ^{-1} = 1.91, we find that E_{jo} = = 6.5 T, or E_{jo} = 0.22 ev. At the temperature 410°K, and a joining energy of 0.22 ev, the mean values of the cross sections (in barns) over the Maxwell distribution, and of ν' are (see Appendix 1): σ_{5T} = 663, σ^f_{5T} = 551, σ_{9T} = 1220, σ^f_{9T} = 850, ν'_{5T} = 2.10, ν'_{9T} = 2.01, σ_8 = 2.75. In the absence of exact information about the cross sections of Pu^{241}, let us take for the averages of the Pu^{241} cross sections over the Maxwell distribution σ_{1T} = 1450, σ^f_{1T} = 1100, ν'_1 = 2.2; the absorption cross section of Pu^{240} at the speed v_T = 2200 m/sec we will take as* σ_{0T} = 475, and for the parameters of the resonance level [1] E_r = 1.07 ev, $\sigma_0 \Gamma^2$ = 330 barn × ev^2, Γ = 0.042 ev. The values of the resonance integrals from the joining energy E_{jo} = 0.22 ev to the energies of the fission spectrum are taken as: I_5 = 545, I^f_5 = 390, I_9 = 2500, I^f_9 = 1500.

The effective cross sections of plutonium must be increased (in comparison with the effective cross sections of U^{238} and U^{235}) to account for the higher neutron density in the locations where the isotopes of plutonium are produced. This correction, calculated in accordance with the method outlined above, turns out to be, in this case very small: only 2%.

Using the above cross sections, a numerical calculation of the concentrations of uranium and plutonium isotopes are carried out using the Formulas (17), (18), (20) for the case that the resonance capture probability of U^{238}, $1 - \varphi$ = 0.117 (the ratio of the uranium to the moderator areas S_U/S_{mod} being equal to 0.036). The results of the concentration calculations are given in the table in the form of the burn-up function Wt (in megawatt-days per ton of uranium). The magnitude of Wt is evidently proportional to the total number of fissions (per ton of uranium), therefore, if it is assumed that the fission energy for all fissionable isotopes is equal to 195 Mev, it can be written as

$$Wt = 6600 \int_0^s [\bar{\sigma}'_{5T}\rho_5 + \bar{\sigma}'_{9T}\rho_9 + \bar{\sigma}'_{1T}\rho_1 \quad + (\psi'_5 + \psi'_9)\varphi_8 \mu f(s)]\, ds.$$

*The assumed value of the cross section is obtained from the parameters of the resonance level (on the assumption that there are no levels with negative energies). It agrees with the data of paper [6], if it is noted that in the experiments of [6] the resonance level was effectively shielded.

In the table are also given the values of the function f(s) and resonance absorption in Pu^{240} – ψ_0.

s	Wt	p_5	p_9	p_0	p_1	ψ_0	f(s)
0	0	1.000	0	0	0	0	2.125
0.1	595	0.897	0.067	0.001	0.001	0.001	2.159
0.2	1190	0.804	0.129	0.007	0.001	0.004	2.195
0.3	1780	0.720	0.178	0.015	0.002	0.008	2.210
0.4	2380	0.644	0.217	0.025	0.005	0.012	2.207
0.5	3000	0.575	0.248	0.036	0.009	0.015	2.194
0.6	3560	0.513	0.272	0.048	0.013	0.018	2.174
0.7	4160	0.457	0.292	0.060	0.017	0.019	2.150
0.8	4780	0.406	0.307	0.073	0.021	0.021	2.123
0.9	5350	0.360	0.319	0.085	0.027	0.023	2.095
1.0	6000	0.318	0.328	0.096	0.032	0.024	2.069

On the basis of these facts, and in accordance with the equations (26), (29) and (31), a calculation was made of the variation of the effective multiplication constant. In these calculations of the multiplication constant, absorption by fission fragments was computed with the aid of data given in the literature for the production and cross sections of fission fragments (see Appendix 2), while wasted thermal absorptions were assumed equal to $\Sigma c = 0.118$. The results of the calculations are given in Fig. 1 (on curve 1). In examining the data of the table, and of Fig. 1, it is, first of all, important to notice the large role played by resonance absorption in Pu^{240} in causing a decrease in the effective multiplication constant. For example, with s = 0.75, it represents about 2%. Let us note that at these concentrations of Pu^{240} the resonance level is already shielded to a noticeable degree (because of fuel self-shielding ψ_0 has decreased by a factor of 2.5).

It is necessary to mention also that the magnitude f(s) changes very little in the range of variation of s of interest to us. This circumstance will later permit us to make a series of simplifications.

If the density of neutrons in the reactor along the height of the uranium fuel channel is not uniform, then the effective multiplication constant we have calculated will not determine the reactivity of the system since, at every instant, various points along the channel height will have different burn-up and, consequently, various values of k_{eff}. The reactivity of the system will be characterized by some mean value of the multiplication constant along the channel height. It is known that if the change in the multiplication constant δk_{eff} is small in comparison with $k_{eff} - 1$, then the effect of this change on the reactivity can be determined by perturbation theory through averaging the square of the neutron density. Then

$$\frac{\overline{k_{eff}(s)}}{k_{eff}(0)} = \frac{\int \frac{k_{eff}(s, z)}{k_{eff}(0)} N^2(z)\, dz}{\int N^2(z)\, dz}$$

We will investigate a reactor without an upper reflector in which the neutron density distribution varies with height according to a cosine law. In this case $k(s,z) = k(s_0 \cos z)$ and

$$\frac{\overline{k_{eff}(s_0)}}{k_{eff}(0)} = \frac{4}{\pi k_{eff}(0)} \int_0^{\pi/2} \cos^2 z \cdot k_{eff}(s_0 \cos z)\, dz = \frac{4}{\pi} \cdot \frac{1}{s_0^2} \int_0^{s_0} \frac{s\, ds}{\sqrt{s_0^2 - s^2}} \cdot \frac{k_{eff}(s)}{k_{eff}(0)}, \qquad (32)$$

where s_0 is the burn-up attained in the central region of the channel (with respect to height). The values of the multiplication constant averaged along the height, calculated in accordance with equation (32) as a function of the burn-up averaged along the height $\bar{s} = \frac{2}{\pi} s_0$ (in the recalculation to Wt), are shown in Fig. 1 (Curve 2).

The excess reactivity of the reactor in question is about 1.5%. As can be seen from Curve 2 (Fig. 1), in case of simultaneous reloading of all channels, a reloading cycle of approximately 1800 megawatt-days/ton can be attained (if it can be assumed that radial non-uniformity of the neutron density is sufficiently small).

The length of the reloading cycle can be significantly increased in steady state operation if the reactor contains, at a given time, fuel elements of various ages, that is, if the channels are continously reloaded. Let us study such a state. Let us assume that the distribution of the fuel elements according to burn-up (according to s) is uniform, that is, in any sufficiently small radial region the number of fuel elements in any given interval

Δs, the change with s is the same. Then, as before, we will assume that such a state is not realized along the channel height, and that reloading proceeds simultaneously. Then the mean value of the effective multiplication constant will be given by the formula*

$$\frac{\overline{k_{\text{eff}}(s_0)}}{k_{\text{eff}}(0)} = \frac{4}{\pi s_0}\int_0^{s_0} ds \int_0^{\pi/2} dz \cos^2 z \frac{k_{\text{eff}}(s\cos z)}{k_{\text{eff}}(0)} = \frac{4}{\pi s_0^2}\int_0^{s_0} ds \sqrt{s_0^2 - s^2}\frac{k_{\text{eff}}(s)}{k_{\text{eff}}(0)}, \qquad (33)$$

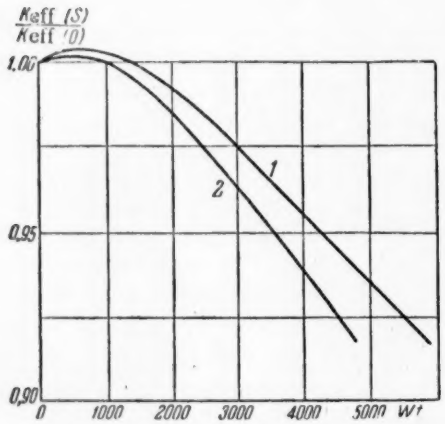

Fig. 1. Results of calculations of the effective multiplication constant. 1) Variation in the effective multiplication constant calculated in accordance with equation (31); 2) variation in the effective multiplication constant calculated in accordance with Equation (32).

where s_0 is the maximum burn-up in the central region (height-wise) of the fuel element. Averaging of k(s) (curve 1 in Fig. 1) gives the mean burn-up $\left(\bar{s} = \frac{2s_0}{\pi}\right)$, corresponding to an excess reactivity of 1.5% in a steady state operation equal to 3150 megawatt-days/ton, which is significantly larger than for the case of simultaneous reloading of all channels.

In order to determine the dependence of the effective multiplication constant on the more important parameter – resonance absorption in U^{238}, let us make calculations for various values of this parameter. In this case it is necessary to make certain simplifications. Using the circumstance that the function f(s) determining the number of fast neutrons changes little with the length of the reloading cycle, it is possible to set f(s) = f(0). In the burn-up equations let us calculate the resonance absorption in Pu^{240} without taking into account fuel element self-shielding. Doing so will introduce some error into our results (especially for large burn-up), however, the more important part of this error can be eliminated if in the calculation of the multiplication constant we determine resonance absorption in Pu^{240} by the correct Equation (20).

With these simplifications, the system of burn-up Equations (17) reduces to a system of linear differential equations which can be easily solved. The calculation was made for two values of resonance absorption:: 1) $1 - \varphi_8 = 0.08$ and 2) $1 - \varphi_8 = 0.16$.

Wasted absorption of neutrons in both cases is taken into account in the same way as in the exact calculation: $\Sigma_c = 0.118$. In this case it is necessary that, during the variation of $1 - \varphi_8$, the reactor volume is changed so that the system remains critical. It is also assumed that variation in the resonance absorption is produced by changing the dimensions of the lattice cell and not by a change in the size of the fuel element. Accordingly the remaining magnitudes, associated with absorption during slowing down, such as Ψ_5, Ψ_9, Ψ_0 will change in proportion to the change in $1 - \varphi_8$.

The values of the effective multiplication constant obtained through the Equations (26 - 29) and (31) are given in Fig. 2.

For a check, a calculation was made with the same parameters as for the exact case: $1 - \varphi_8 = 0.117$, $\Sigma c = 0.188$ (variant 3). The results are similarly given in Fig. 2. Comparison of these results with the results of the exact calculation shows use of the simplified method introduces a comparatively small error into the final results.

---

*Strictly speaking equation (17) cannot be used under steady-state conditions inasmuch as the number of fast neutrons [the function f(s)]in this case is not determined by fuel elements of one and the same age. However, since f(s) varies slowly, the error arising from this can be neglected.

It is necessary to note that changes in waste absorption of thermal neutrons alter the kinetics very little. Actually by differentiation of the Equation (26) it can be seen that a change in Σc of $\delta(\Sigma c)$ the $\frac{k_{eff(s)}}{k_{eff(0)}}$ changes by

$$\delta\left(\frac{k_{eff}(s)}{k_{eff}(0)}\right) = \frac{k_{eff}(s)}{k_{eff}(0)} \cdot \frac{A(s)}{1-A(s)} \cdot \frac{\delta(\Sigma c)}{1+\Sigma c},$$

and since $A(s) \leq 0.1$, a change in Σc by 0.05 will induce a change in the multiplication constant of only 0.5%. In this case, however, the increase in absorption improves the kinetics ($A < 0$), as is obvious from physical considerations.

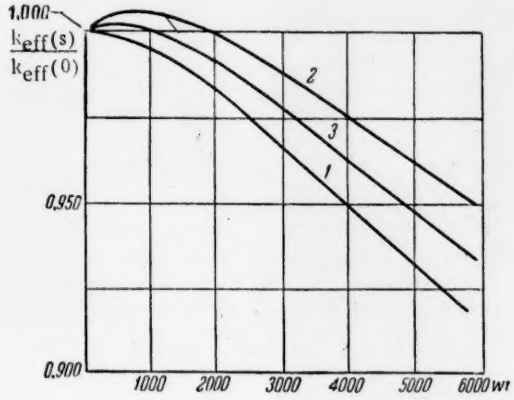

1—1—φ_8=0.08; 2—1—φ_8=0.16; 3—1—φ_8=0.117.

Fig. 2. Values of the effective multiplication constant.

In Fig. 3 is shown a graph of the dependence of the length of the fuel reloading cycle on $1 - \varphi_8$ for stationary operation, and for the case where fuel elements in the reactor have a uniform age distribution. It is assumed that the steady state prevails only along the radial direction, and that along the height direction simultaneous unloading of the whole channel is taking place. The mean values of the effective multiplication constant were determined from equation (33). As in the exact case, the excess reactivity was assumed to be 1.5%. As can be seen from figures 2 and 3, an increase in resonance absorption in U^{238} and, consequently, an increase in the number of Pu^{239} atoms formed per one atom of U^{235} destroyed (this magnitude represents, at the beginning of the reloading cycle, 0.74, 0.80, 0.87, respectively, for the first, third and second variants), does not importantly increase the length of the fuel reloading cycle. This fact is associated with the circumstance that with an increase in $1 - \varphi_8$ the absorption of thermal, and especially of resonance, neutrons in Pu^{240} is also increased, which decreases the multiplication constant to an appreciable degree.*

From this it follows that in an increase in the volume of the reactor in order to obtain a longer reloading period (in the scale of Wt), it is more profitable not to increase resonance absorption in U^{238}, but simply to leave a larger excess reactivity. In this case, however, the concentration of plutonium in the materials removed from the reactor will be decreased significantly, and its contamination by Pu^{240} increased.

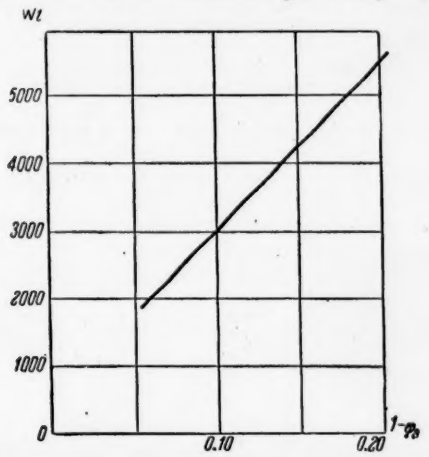

Fig. 3. Dependence of the length of the reloading period on $1 - \varphi_8$ for a steady state.

CONCLUSION

Numerical calculations of systems consisting of natural uranium and heavy water moderator showed that in the decrease of the reactor's reactivity, an important role is played by the accumulation of Pu^{240} due to its large resonance absorption at the 1.07 ev level.

It is demonstrated that the duration of the fuel reloading period is significantly increased (in comparison with the case in which the reactor is unloaded all at once)

*It is necessary to note that the undesirable effects of Pu^{240} can be weakened if resonance absorption is increased not by way of decreasing the lattice cell length, as was assumed in the given calculation, but by way of increasing the amount of uranium in the channel. Doing so would lead to strong shielding of the resonance level of Pu^{240}, and its effect would be smaller.

if the reactor operates in a steady-state condition, that is, if the fuel elements are unloaded continuously and, in each given moment in the reactor, there are to be found fuel elements of all ages, uniformly distributed with respect to extent of burn-up. In this case the fuel reloading cycle can be increased by a factor of 1.5 to 2.

In the heavy-water-moderated natural uranium reactors, operated in a steady state, studied above, burn-ups of the order of 3000-4000 megawatt day/ton can be attained.

If one seeks only to increase the extent of burn-up, then one should not, for a reactor of given volume, use a lattice with the largest resonance absorption probability, since it is more advantageous to have a larger excess reactivity. In this case, naturally, the power of the reactor will be smaller.

The lattice parameters (for example, spacing) determining the magnitude of the resonance absorption must be chosen by way of comparing two competing factors: an increase in the extent of burn-up (accompanied, however, by a decrease in the amount and quality of the plutonium) and a decrease in the power of the reactor.

In conclusion we wish to express our deep gratitude to A. N. Galanin for a series of valuable suggestions, B. I. Ilyichev for assistance in the calculations and to A. P. Birzgal for the numerical solution of the system of equations.

APPENDIX 1.

The Effective Cross Sections of the Fissionable Isotopes

The effective cross sections of the various isotopes of uranium and plutonium for thermal neutrons, as well as the number of secondary neutrons born per absorption of a thermal neutron, were assumed to be as given by Table 1. In Table 2 are given the corrections Δ for the departure of the cross sections from the 1/v law as functions of the neutron temperature, and of the joining energy:

$$\Delta = \frac{\overline{\sigma v}}{(\sigma v)_{v=2200}} - 1.$$

For U^{235}, $\Delta\sigma$ practically coincides with $\Delta\sigma^f$, and is almost independent of the joining energy; for this reason the values of $\Delta\sigma$ are given only as a function of the temperature. In calculating ν' for Pu^{239} it was assumed that the physical ν is independent of the energy, and therefore $\nu' \sim \frac{\sigma^f}{\sigma}$. The resonance integrals for U^{235} and Pu^{239} as functions of the joining energy are given in Table 3.

TABLE 1

Isotope	U^{235}	Pu^{239}	Pu^{241}	U^{238}	Pu^{240}
Absorption cross section σ in barns	690	1030	1450	2.75	475
Fission cross section σ^f in barns	574	740	1100	–	–
Number of secondary neutrons per absorption ν'	2.10	2.05	2.2	–	–

Note: For Pu^{241} these cross section values σ, σ^f and ν' were taken as averages over the Maxwell distribution.

All tables were based on the data of the International Conference on the Peaceful Uses of Atomic Energy, and of the compendium of neutron cross sections.

APPENDIX 2

Absorption In Fission Fragments

Assume that in the fission of the k^{th} nucleus (k = 5, 9, 1), with a probability ω_i, k, there is produced the i^{th} stable fragment having the absorption cross section σ_i. The concentration of these fragments will be determined by the following equation

TABLE 2

Corrections Δ for deviation of the cross sections from the 1/v law (in %)

U^{235}					
T (°K)	300	400	500	600	700
$\Delta\sigma=\Delta\sigma'$	2.1	4.0	5.4	6.1	6.7

Pu^{239}								
	$\Delta\sigma$				$\Delta\sigma'$			
joining energy E_{jo}/kT / T (°K)	5	6	7	8	5	6	7	8
300	5.8	6.7	7.3	7.6	4.7	5.5	6.0	6.4
400	13.2	15.8	18.3	19.7	10.9	13.0	14.9	16.1
500	24.8	31.2	37.2	40.3	19.5	24.5	29	32
600	45	59	64	65	36	47	51	52
700	82	96	98	99	66	77	79	80

TABLE 3

Resonance Integrals

Joining energy E_{jo} (ev)		0.13	0.20	0.30	0.40	0.48
U^{238}	I in barns	660	565	470	423	400
	II » »	494	404	334	292	272
Pu^{239}	I in barns	3200	2750	1550	715	605
	II » »	1950	1710	860	383	315

$$\frac{d\rho_i}{ds}=\sum_k w_{i,k}\bar{\sigma}'_{kT}\rho_k-\bar{\sigma}_i\rho_i, \tag{2.1}$$

which has the solution

$$\rho_i(s)=e^{-\bar{\sigma}_i s}\int_0^s e^{\bar{\sigma}_i s}\left[\sum_k w_{i,k}\bar{\sigma}'_{kT}\rho_k(s)\right]ds. \tag{2.2}$$

Absorption in the fragments is equal to

$$c_{jo}=\sum_i \bar{\sigma}_i\rho_i, \tag{2.3}$$

where the ρ_i must be substituted from (2.2) (burn-up of the fragments on account of resonance absorption is not considered).

In calculating the absorption it is convenient to take advantage of the circumstance that $\sum_k w_{i,k}\bar{\sigma}'_k\rho_k(s)$ changes slowly during the fuel reloading cycle, and for the majority of isotopes we may take $\omega_5=\omega_9$, so that

$$\rho_i(s)\approx(1-e^{-\bar{\sigma}_i s})\,w_5\bar{\sigma}'_5. \tag{2.4}$$

It is convenient to consider the fragments as falling into three groups: 1) large absorbers with $\bar{\sigma}_i \gg 1$; 2) weak absorbers with $\bar{\sigma}_i \ll 1$ and 3) medium absorbers with $\bar{\sigma}\sim 1$.

To the first group belong (except Sm^{149}, included by us in the initial multiplication constant) the following isotopes $_{64}Gd^{157}$, $_{63}Eu^{155}$, $_{48}Cd^{113}$, $_{62}Sm^{151}$. For them the sum of losses is equal to

$$\sum_{\text{I}} c_i = 0{,}6 \cdot 10^{-2}.$$

The principal components of the second group are the fragments: $_{38}Sr^{89}$, $_{43}Te^{99}$, $_{42}Mo^{95}$, $_{45}Rh^{103}$, $_{54}Xe^{131}$, $_{59}Pr^{141}$, $_{55}Cs^{133}$, $_{60}Nd^{145}$, $_{61}Pm^{147}$, $_{36}Kr^{92}$, $_{53}I^{129}$, $_{57}La^{139}$. The sum of the losses of the second group is equal to

$$\sum_{\text{II}} c_i = 3{,}8 \cdot 10^{-2}\, s.$$

Finally, to the third group belong: $_{63}Eu^{153}$, $_{60}Nd^{143}$, $_{36}Kr^{83}$. The absorption by this group is given in the table. All these data are obtained by using the Equation (2.4).

s	0.2	0.4	0.6	0.8	1.0	1.5
$\sum_{\text{III}} c_i \cdot 10^2$	0.47	0.89	1.27	1.64	1.97	2.70

Calculation by the exact formula (2.2) shows that the results differ by not more than 10%. This deviation evidently lies within the limits of reliability of our knowledge of absorption in fragments. Data about resonance absorption in the latter are significantly less reliable. It is known merely that the isotopes having significant resonance absorption include $_{45}Rh^{103}$, $_{47}Ag^{109}$, $_{42}Mo^{95}$, $_{62}Sm^{152}$, $_{55}Cs^{138}$. The total resonance integral for them corresponds to 60 barns per fission. We will assume that the actual resonance integral is equal to 150 barns per fission. Inexactness in resonance absorption will not greatly affect our results, since in our case with $S_U/S_{mod} = 0.036$, $\psi_0 = 1 \times 10^{-2}$s, that is, it does not exceed 1% even at the end of the fuel reloading period.

LITERATURE CITED

[1] Yu. G. Abov, Conference of the Academy of Sciences of the USSR on the Peaceful Uses of Atomic Energy, July 1-5, 1955, Meeting of the Division of Physico-mathematical Science (Acad. Sci. USSR Press, 1955).

[2] L. Landau, and E. Lifshits, The Mechanics of Continuous Media, 1st ed. (State Tech. Press, 1945).

[3] I. I. Gurevich, and I. Ya. Pomeranchuk, "Reactor building and reactor theory," Reports of the Soviet Delegation to the International Conference on the Peaceful Uses of Atomic Energy (Acad. Sci. USSR Press, 1955) p. 220.

[4] E. F. M. van der Held,"Computation of the effective resonance integral," Report No. 948,presented by the Netherlands to the International Conference on the Peaceful Uses of Atomic Energy, 1955.

[5] A. I. Alikhanov, V. V. Vladimirsky, P. A. Petrov, and P. I. Khristenko, Atomic Energy 1956, No. 1, 5 (T. p. 3)*

[6] B. Bentley, "Experimental reactors and the physics of reactors," Reports of Foreign Scientists to the International Conference on the Peaceful Uses of Atomic Energy, 1955, (State Tech. Press, 1956), p. 676.

[7] D. J. Hughes, and J. A. Harvey, Neutron Cross Sections(McGraw-Hill Co. 1955).

Received April 14, 1956.

*T. p. = C. B. Translation pagination.

HEAT TRANSFER AND THERMOPHYSICAL PROPERTIES OF MOLTEN ALKALI METALS

I. I. Novikov, A. N. Solovyev, E. M. Khabakhpasheva, V. A. Gruzdev, A. I. Pridantsev, M. Ya. Vasenina

An investigation was undertaken of heat transfer to molten sodium during turbulent flow in a round copper or nickel tube. An interpolation formula was obtained. Experiments were conducted to determine thermal resistance between liquid sodium and a solid wall of copper, nickel, and stainless steel. Methods were developed for measurement of viscosity, temperature conductivity and density of molten metals. Results are given for measurements of these physical parameters for molten alkali metals (sodium, potassium, lithium and the eutectic solution of sodium and potassium) in a broad interval of temperatures.

INTRODUCTION

Molten alkali metals, especially sodium, are very promising heat carriers for atomic power reactors. Their advantages are the following:

1) Molten alkali metals are characterized by large values of specific conductivity and specific heat and are, therefore, outstanding heat transfer media. For transfer of the heat produced in a reactor smaller weights of the molten alkali metals are needed than of other heat transfer materials. In addition, their hydrodynamical properties are similar to those of ordinary materials so that pressure losses in the heat transfer circuit are not excessively great.

2) Thanks to the high boiling point (t_b for sodium is 883°C) the working temperature of the heat transfer material in the power installation can be kept high and its pressure low. In this way high thermal efficiency can be assured with a relatively simple reactor cooling system.

3) Because of the low melting point (t_m for sodium is 97.8°C, and for the eutectic mixture of sodium and potassium it is −12°C) alkali metals can be liquified easily and maintained in the system in this state.

4) Molten alkali metals induce relatively little corrosion in the construction materials so that it becomes possible to use steel and other alloys.

5) The alkali metals are relatively poor neutron absorbers (Na, for example, has a lower absorption cross section than water).

Deficiencies of the alkali metals in power reactor applications are: the heat transfer medium becomes radioactive under neutron bombardment in the reactor; in particular this is true of sodium, on account of which it is necessary to shield the primary heat transfer circuit and, in addition, the medium is chemically reactive with water and with oxygen—this chemical reactivity, jointly with induced radioactivity, leads to the requirement that the power system have at least two circuits (the heat transfer medium and the working substance in the power cycle).

Considering the import which the alkali metals have for atomic energy, the authors carried out a series of experiments during 1950-1956 with the objective of studying the thermophysical and heat-transfer parameters of the molten alkali metals. The principal results of these studies constitute the content of this paper.

Heat Transfer

The first USSR experiments on heat transfer to molten metals [1], made as far back as 1938-1940, showed that the coefficients of heat transfer to molten metals cannot be computed by using equations valid for other liquids and gases. For a number of years these were the only data of this kind in the world's literature. Intensive investigation of the heat transfer properties of molten metals began only in recent years in connection with the development of atomic energy.

In a series of researches [3] completed by the Academy of Sciences USSR, it was established that the heat transfer coefficients for the alkali, as well as for the heavy, metals can be obtained from the same set of defining equations:

for clean heated surfaces

$$Nu = 4.5 + 0.014\, Pe^{0.8} \tag{1}$$

and for oxidized surfaces

$$Nu = 3 + 0.014\, Pe^{0.8}. \tag{2}$$

The first of these equations agrees well with Dwyer's equation [6]:

$$Nu = 4.9 + 0.018\, Pe^{0.8}, \tag{3}$$

obtained as a result of reliable experimental data obtained from experiments with heavy metals.

Basing his work on the experiments of Lyon, Werner, King and Tidball, Dwyer came to the conclusion that, for the alkali metals and their alloys, Lyon's equation [2] is valid

$$Nu = 7 + 0.025\, Pe^{0.8}, \tag{4}$$

which differs from the Equations (3) and (1).

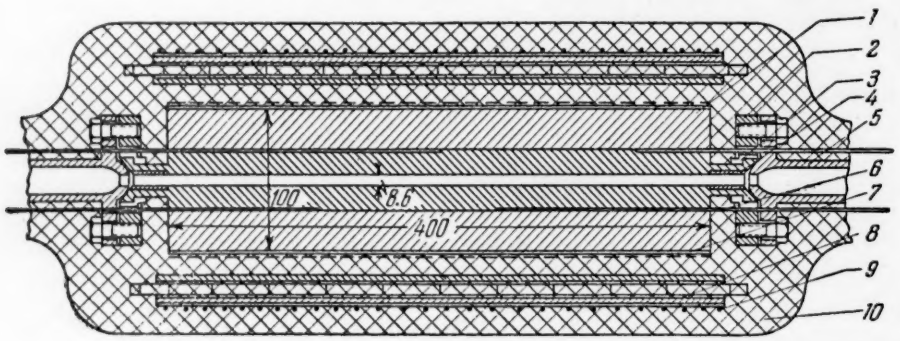

Fig. 1. The experimental heat exchanger. 1) Compound copper tube; 2) flange; 3) bearing; 4) stainless steel sleeve; 5) chamber frame; 6) thermocouple; 7) main heater; 8) calorimeter; 9) compensating heater; 10) asbestos insulator.

Thus, for example, the values of the heat transfer coefficients to liquid sodium and the Na-K eutectic, calculated according to Equation (1), differ from the ones given by Lyon's equation, on the average, by a factor of one and one-half. It was this deviation which caused the authors of this paper to make an experimental study of heat transfer to liquid sodium.

Experimental Methods. The experimental apparatus consisted of a closed circulating loop, composed of an experimental heat exchanger, cooler, pump, flow meter and a control valve.

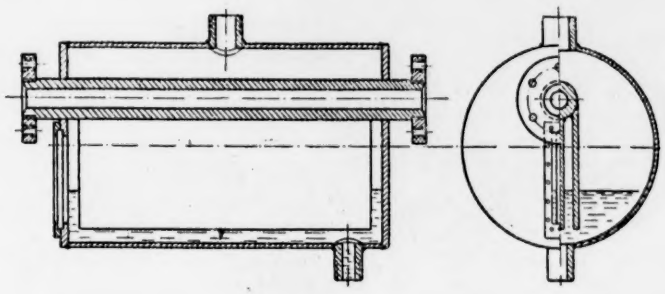

Fig. 2. Cooler

A massive copper pipe (rough cast) with an outside diameter of 100 mm, an inside diameter of 8.6 mm and a length of 400 mm, inside of which flowed the molten metal, served as the experimental heat exchanger, (Fig. 1). The heat exchanger consisted of two parts (external and internal), tightly placed, one inside the other, with a small conical angle. On the surface of the inner cylinder were placed seven thermocouples measuring temperature along the length. Two thermocouples were caulked on the end surfaces of the experimental heat exchanger. For compensation of losses from the side surface of the heat exchanger, over the primary heater were placed a calorimeter and a secondary heater. A zero indication by the calorimeter attested to the absence of heat losses.

To investigate the effect of surface conditions at the boundary of contact between the surface of the heat exchanger and the liquid metal, it was decided to experiment with various heating surfaces; copper (as in the experiments [3])and nickel (similar to the experiments [2]).

The temperature of the liquid sodium inside the working space was measured with the aid of two thermocouples mounted in special sleeves.

The cooler consisted of a thick copper tube with three thick copper plates welded to it. The tube was placed in a hermetically sealed hull partly filled with water (Fig. 2). Steam from the cooler was led into the condenser inside whose tubes water was circulated.

The circulation of the molten sodium was accomplished by a centrifugal pump especially built for the purpose (Fig. 3). The pump bearing was made of beryllium bronze and was lubricated with liquid sodium. The hermetic tightness of the arrangement was attained through location of the pump motor inside the body of the system, above the level of the liquid sodium. Special arrangements were provided for cooling the motor windings, and for protecting the motor and its bearing against contact with sodium or its vapor.

The flow rate of liquid sodium in the circuit was measured with the aid of an electromagnetic flow-rate meter.

Before the apparatus was filled with liquid metal it was checked for leak tightness, pumped out by a prevacuum pump, heated and filled with helium. During operation, a small excess helium pressure was maintained in the apparatus. Before and after each series of experiments the heat exchanger was checked through a special water circuit.

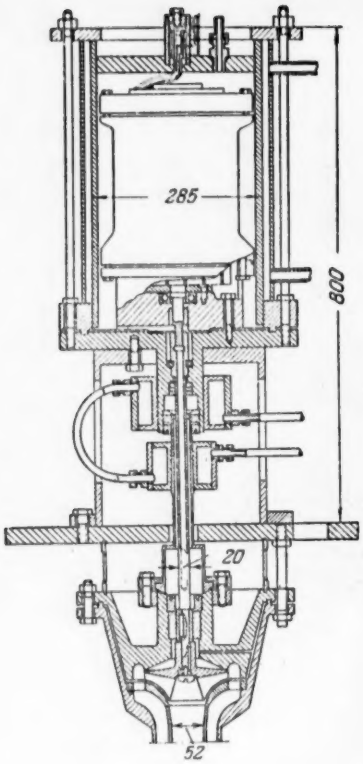

Fig. 3. Liquid metal pump.

Reduction of Experimental Data. The central part of the heat exchanger was used as the working volume. Doing so allowed exclusion of effects from the initial flow region and of end effects (heat losses from end surfaces). The heat transfer coefficient was computed according to the equation

$$\bar{\alpha} = \frac{Q}{F \cdot \vartheta} . \qquad (5)$$

The quantity of heat Q was determined from the introduced electrical power. To determine the temperature difference ϑ it was necessary to calculate the temperature of the liquid metal in the working part of the heat exchanger. For large values of the Peclet number (Pe > 300) heat overflow along the axis of the heat exchanger is negligibly small; heat brought to the rough copper casting is carried away from it by the liquid metal practically at one and the same cross section. Under such conditions, the temperature of the liquid sodium changed linearly with length and its value in the working space could be easily determined. For small values of the Peclet number, Pe, because of the large mass of the heat exchanger, heat overflow could result in nonuniform heating of the liquid. Under such conditions, after determining the heat transfer coefficient approximately (by assuming that the temperature of the liquid metal changes linearly along the length), the temperature distribution field was constructed, and the value of $\bar{\alpha}$ was then made more precise.

Estimates of heat overflow because of axial heat conductivity of the liquid metal showed that the influence of this effect is hundreds of times smaller than the influence of heat overflow through the heat exchanger walls.

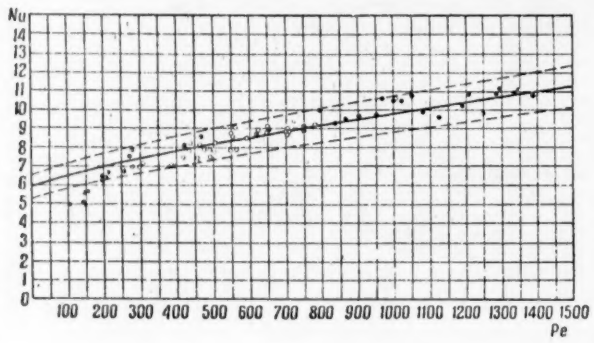

Fig. 4. Comparison of experimental results with copper and nickel surfaces [Nu = f(Pe)]. O copper surface; ● nickel surface.

Experimental Results. Two series of experiments were made on heat transfer to liquid sodium. In the first series of experiments heat exchange between sodium and a heated copper surface was investigated; in the second series, the inside surface of the same heat exchanger was covered with a nickel coating approximately 10 μ in thickness.

The experiments were conducted with sodium flow velocities from 0.8 to 11 m/sec, and temperatures from 140 to 340°C. Dimensionless moduli characterizing the conditions of heat transfer varied under these circumstances within the limits:

$$Re = 1.5 \cdot 10^4 - 2.1 \cdot 10^5,$$
$$Pr = (5 - 9) \cdot 10^{-3},$$
$$Pe = 100 - 1400.$$

It should be noted that in the experiments on both the copper and nickel heat exchange surfaces, during the initial period of apparatus operation, the values of the heat transfer coefficients obtained were considerably smaller in magnitude, and were unstable. After stable values of the heat transfer coefficients were reached, experiments with copper and nickel surfaces led to the same results (Fig. 4).

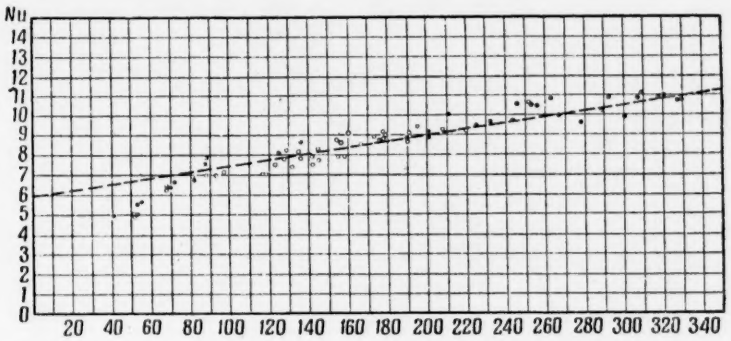

Fig. 5. Reduction of experimental data in the form of $Nu = f(Pe^{0.8})$. The values of $Pe^{0.8}$ are given along the abscissa.

Theoretical analysis shows that it is reasonable to reduce data on heat transfer, for heat transfer media with $Pr < 0.1$, according to the equation $Nu = a + bPe^n$, where the exponent n must be close to $n = 0.8$. In reducing the results of our experiments to the form $Nu = f(Pe)^{0.8}$ (Fig. 5) it was found that it is not possible to find a single formula (that is a single choice of the constants a and b) valid for all ranges of the number Pe. With $Pe < 200$, a significantly sharper drop in the Nu number for decreasing Pe numbers was observed.

For the range $200 < Pe < 1400$, the experimental data fit the empirical formula

$$Nu = 5.9 + 0.015\, Pe^{0.8}. \qquad (6)$$

with an accuracy of ± 10%.

In the region $Pe < 200$, there is still an insufficiency of experimental points to establish an approximating formula.

In Fig. 6 the data obtained by us are compared with the data of other authors. Values of the Nu number obtained by us turn out to be 20-30% lower than the data of Werner, King and Tidball [18] for heat transfer to the eutectic of Na-K (experiments with a heat exchanger of the "pipe inside a pipe" type), and agree well with the data by Mikheeva, Baum, Voskresensky and Fedynsky [3] and the data of Johnson [4], who studied heat transfer to the eutectic of Pb-Bi, and to mercury.

In Fig. 7 are compared the experimental data for the region $Pe < 300$ with the data published by Johnson et al. in 1954 [5]. In the coordinates of $Nu = f(Pe)$ these data agree well among themselves; this is evidence of the fact that with a decrease in the Pr number, a decrease in Nu number with lowering of Pe number begins in the region of large values of the Re number.

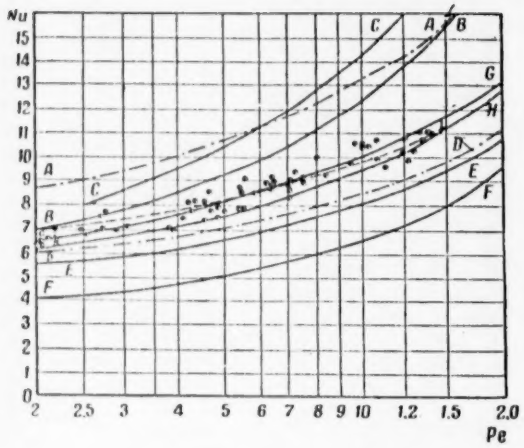

Fig. 6. Comparison of the experimental data. On the abcissa are given values of 10^2 Pe. A-A, Lyon's theory; B-B, Lyon's experiments with sodium and potassium; C-C, experiments by Werner, King and Tidball; D-D, theory of the laboratory of the Acad. Sci. USSR; E-E, experiments by the laboratory of the Acad. Sci. USSR (clean surfaces); F-F, experiments by the laboratory of the Acad. Sci. USSR (oxidized surfaces); G-G, Johnson's experiments with Pb-Bi; H-H, Dwyer's recommendations for heavy metals; I-I, MIFI data.

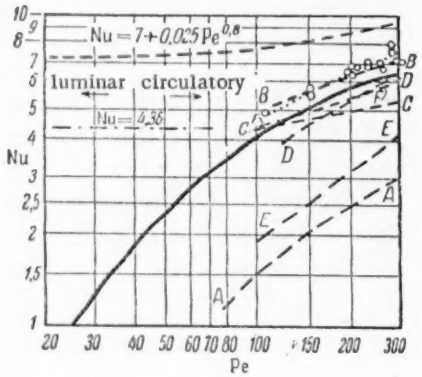

Fig. 7. Comparison of experimental data in the region of small Pe numbers.

The magnitudes of deviations in the values of heat transfer coefficients during the initial period of apparatus operation from the later, stable values, in various series of experiments, were different.

In experiments with a copper surface, a gradual increase in the heat transfer coefficient took place. On the basis of these data it was possible to assume that, during the initial period of operation, the heat transfer surface was covered with a poorly conducting oxide film which, with the passage of time, was removed by the sodium stream.

However, with heat transfer at a nickel surface during a period of 70 hours, temperatures of 150 to 250°C and with a rate of flow of the molten sodium of 3 m/sec, the heat transfer coefficients turned out to be 3-4 times smaller. Their magnitude increased sharply up to the stable values only when the temperature was raised to 350°C (the speed of metal flow increased in the process by a factor of two).

It is reasonable to assume that, under these conditions, it was possible to attain good thermal contact between the nickel surface and the liquid sodium. Subsequent lowering of the temperature and of the rate of flow did not lead to impairment of the thermal contact.

The Thermal Contact Resistance. As has already been mentioned, conditions at the boundary, "solid body-liquid heat transfer medium", have an influence on the process of heat transfer.

In the literature appears only the work of Moyer and Riemen which is devoted to the direct determination of the thermal resistance of the contact between sodium and stainless steel [7]. The precision of these experiments was not very high and, accordingly, it was decided to carry out experiments, if possible, with greater precision. For contact materials with liquid sodium, stainless steel, nickel and copper were employed.

The experiments were conducted using three experimental arrangements, somewhat different among themselves.

In arrangement No. 1 (Fig. 8), into a stainless steel tube 10 mm in diameter, 0.1 mm in thickness and 100 mm in length, from the lower end, was tightly inserted a metal rod (of copper, stainless steel or copper covered with a thin layer of nickel). The end of the rod was threaded through to the cooler. The upper part of the tube was filled with sodium. On the tube, on both sides of the surface of separation between the liquid sodium and the solid metal, five thermocouples of 0.14 mm nichrome-constantan wire were spot welded. The experimental tube was placed in an oven. The temperature field in the oven was smoothed out with the aid of a thick-walled steel screen.

TABLE

Index	Authors	Heat transfer medium	Surface material	Value of Pr
A-A	Bailey, Coup, Watson	Hg	steel	0.023
B-B	Trefsen	Hg	stainless steel	0.022
C-C	Stormquist and Borts	Hg, Hg + Na	steel	0.02
D-D	English and Barrett		Ni	0.017
E-E	Dudi and Unger	Hg	steel	0.022
F-F	" "	Hg + Na	"	0.022
—	Johnson, Hartnett, Glabauch	Pb — Bi	"	0.030
—	" " "	Hg	"	0.015
. . .	MIFI data	Na	Cu, Ni	0.006-0.008

The space between the screen and the tube was filled with diatomaceous powder. Ten thermocouples were welded to the screen for controlling radial heat overflow from the experimental tube.

In arrangement No. 2, two discs of dissimilar solid metals, with small openings for passage of the sodium, were inserted into a stainless steel tube. The thickness of the discs was 0.1 mm and the distance between them was 20 mm.

The tube was filled with liquid metal, and 12 thermocouples were welded to it (4 thermocouples to each part).

In arrangement No. 3, a stainless steel tube was filled to approximately one-half its length with metal discs 0.1 mm in thickness, with a distance between them of about 1.5 mm. The separating spiders were made of stainless steel.

During assembly of the various arrangements the metal surfaces were washed with dilute nitric acid, lye and distilled water and were carefully wiped off. The apparatus was then placed in the oven, heated and pumped out with a prevacuum pump for 2-3 hours.

Filling of the apparatus with liquid sodium was carried out with the aid of a special arrangement which assured filtration of the sodium through a porous glass filter.

Heat flow along the experimental tube was induced by an electrical heater located in the upper part of the apparatus. In the lower part of the tube a water cooler was located. The heater circuit included a voltage regulator.

The distribution of temperature along the tube was measured during the experiments. Since radial heat overflow into the surrounding medium, as well as the change in the heat transfer coefficient along the length of the tube because of temperature variation, were both negligible, the temperature plots were straight lines, which could be extrapolated to the boundary separating the liquid and solid metal and, in this way, used to detect as well as to compute the magnitude of the temperature drop across the contact (for the arrangements No. 1 and No. 2). Having determined the thermal current along the experimental tube with the aid of the measured temperature drop in the sodium, it was possible to compute the value of the thermal resistance of the contact $(\delta/\lambda)_x$ (Fig. 9).

In arrangement No. 2, the thermal resistance of the discs was taken into account.

In the arrangement No. 3, the thermal resistance of the contacts was determined from the relationship of the temperature gradients of the parts (the slopes of the straight lines), taking into account the thermal resistance of the discs themselves and of the spacing spiders (Fig. 10).

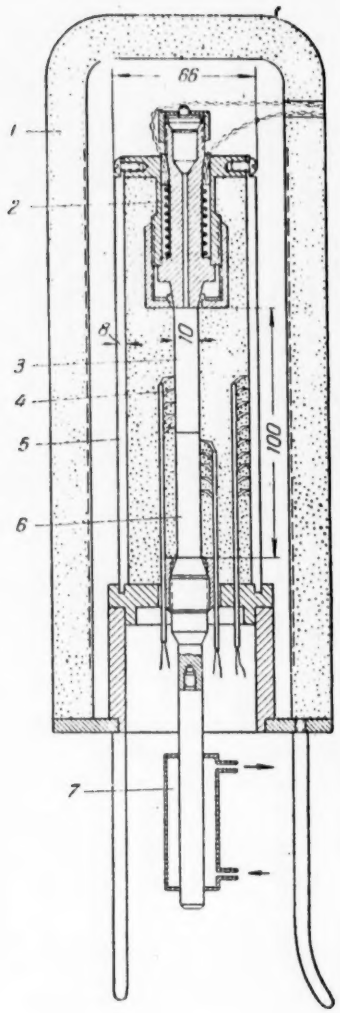

Fig. 8. Experimental arrangement No. 1. 1) oven; 2) electrical heater; 3) tube; 4) thermocouples; 5) screen; 6) rod; 7) cooler.

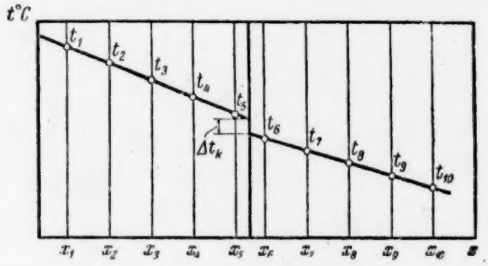

Fig. 9. Distribution of temperature along the tube in arrangement No. 1.

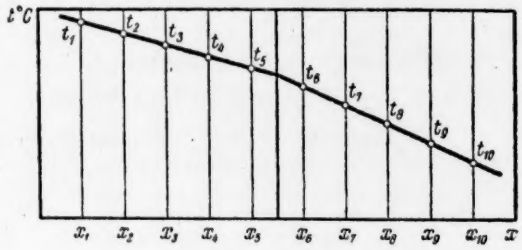

Fig. 10. Distribution of temperature along the tube in arrangement No. 3.

Results of measurments in all series of experiments showed that the thermal resistance of the contact is smaller than the maximum possible error of measurement, which was 5×10^{-6} m^2 hour °C/kcal. From this it follws that, even if a thermal contact resistance exists between stationary sodium and a clean surface of stainless steel, copper or nickel then in any case, it does not exceed the magnitude 5×10^{-6} m^2 hour °C/kcal. Such a thermal resistance could lower the heat transfer coefficient α (with $\alpha = 50{,}000$ kcal/m^2 hour °C) by about 20%.

Viscosity

Description of the Apparatus. For the measurement of viscosity the method of damped, torsional oscillations of a small pail, filled with liquid, was employed. The theory of the method was worked out in detail by E. G. Shvidkovsky [8]. The experimental arrangements are very simple (Fig. 11). A hermetically sealed cylinder is filled with the molten metal, suspended on a thin elastic filament, and permitted to undergo small torsional oscillations which are recorded on a moving photographic film. In comparison with the experimental arrangements described in the literature, several improvements were incorporated so that construction of the apparatus was simplified and the conduct of experiments made easier at sufficiently high precision of results (~ 1.5%). In particular, it was possible to dispense with the vacuum jacket, thereby simplifying the apparatus considerably. Protection of the metal against oxidation was assured by sealing the crucible hermetically, while the additional oscillation damping from air friction, not large in itself, was taken into account in the calibrating experiments.

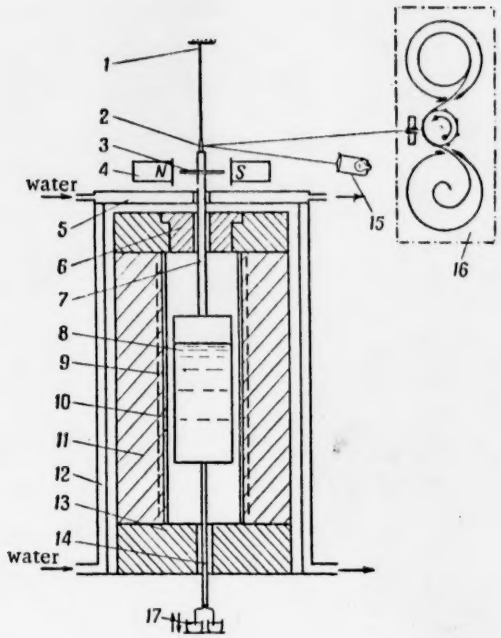

Fig. 11. Experimental arrangements. 1) suspension filament; 2) mirror; 3) iron rod; 4) electromagnet; 5) upper detachable cooler; 6) detachable diatomaceous plug; 7) suspension rod; 8) crucible; 9) electrical heater; 10) stainless steel tube; 11) zonolite filler; 12) side water shield; 13) diatomaceous washer; 14) porcelain straw with thermocouple; 15) light source; 16) photographic camera; 17) mercury baths.

The temperature was measured by a thermocouple whose junction was located in the crucible, and whose ends were led out through mercury contacts to a low resistance potentiometer. The mercury contacts were removed while photographic recording of the oscillations was in progress. The photographic recording was made on ordinary 24 mm movie film. The thickness of the curve recorded on the film did not exceed 0.1 mm, assuring an accuracy of amplitude measurement of 0.3-0.5%.

Much attention was paid to workmanship of the apparatus components since, otherwise, undesirable transverse oscillations would arise.

The torsional oscillations of the suspended system were not excited manually but, rather, with the aid of two electromagnets whose magnetic field was applied to a small iron rod inserted into the suspension rod. The current in the electromagnets, as well as their position, could be changed to alter the initial amplitude angle. Thanks to this arrangement oscillations were excited without shock, the initial angle was precisely controllable, the center of oscillation remained fixed and it was possible to brake the suspended system smoothly.

To decrease undesirable transverse oscillations, the upper part of the suspension rod was lightened and the filament shortened.

The oven was prepared to assure adequate homogeneity of the temperature field. To protect the suspension filament and the surrounding objects from heating, the oven was surrounded by a water cooler. All parts of the apparatus—the support for the suspension system, the oven, the photographic camera and the control panel—were placed on independent supports, allowing elimination of undesirable vibrations of the suspension system and of the camera.

The experimental apparatus turned out to be compact and convenient to use.

The manner in which the experiments were performed with this apparatus did not differ from that of analogous experimental arrangements reported in the literature. In the preliminary experiments the "null" parameters of the system were determined, that is, the internal radius of the crucible, the moment of inertia of the suspension system, the period and the logarithmic decrement of oscillation damping for the system with empty crucible. The dependence of the oscillation period on the temperature could be computed, without performing experiments, since all components of the system were made of a single material with a known coefficient of linear expansion.

The alkali metals oxidize quickly even in dry air and, because of this, filling the crucibles with clean metal presents definite difficulties. In our apparatus the metal being investigated is sucked through a thin copper capillary into a previously evacuated crucible. As was shown by control opening of crucibles after the experiments, the surface of the metal was fully clean.

Data reduction from the photographic records was carried out with the assistance of a large tool microscope. 30-40 complete amplitudes were measured. The harmonicity of the oscillations was checked, that is, it was determined whether the logarithm of an oscillation amplitude was a linear function of its order number.

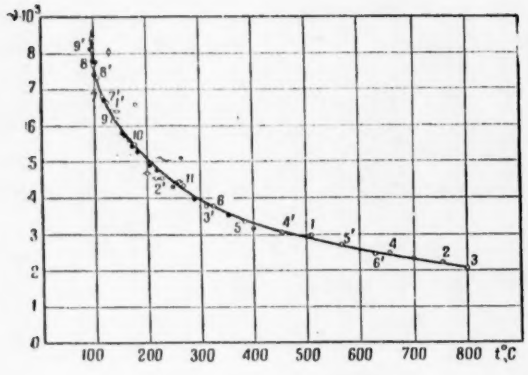

Fig. 12. The viscosity of sodium. O MIFI 1953; O L. M. H. (Liquid Metals Handbook, edited by Lyon) 1948; ● Chiong, 1936; ◒ Sauerwald, 1934; ◊ D'Ans and Lax, 1943.

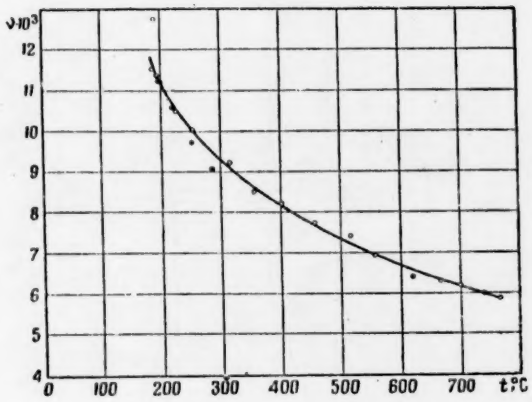

Fig. 14. The viscosity of lithium. O MIFI, 1953; ◑ Andrade, 1951.

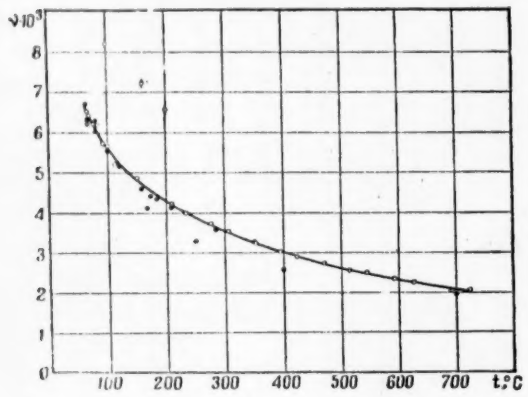

Fig. 13. The viscosity of potassium. O MIFI, 1953; ◑ L. M. H., 1948; ● Chiong, 1936; ◒ Sauerwald, 1934; ◊ D'Ans and Lax, 1943.

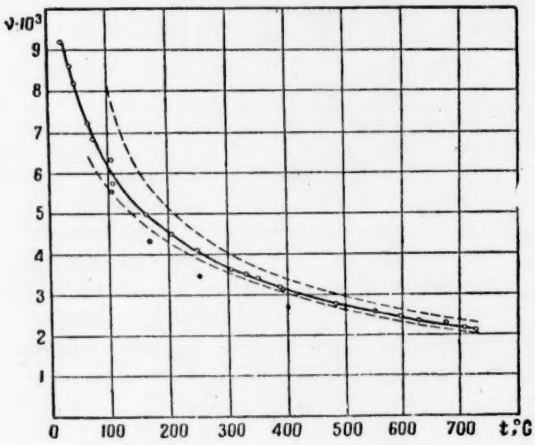

Fig. 15. Viscosity of the eutectic alloy (25% Na + + 75% K) O MIFI, 1953; ◑ L. M. H., 1948; the dashed curves - viscosity of the pure components according to MIFI data.

The viscosity calculations were made according to the formulas of E. G. Shvidkowsky [8]. It should be noted that the calculations take quite a bit of time.

Results of the Measurements. The kinetic viscosities of sodium, potassium, lithium and of the eutectic solution of sodium and potassium (25% Na, 75% K) were measured. With the exception of lithium, the viscosity was measured almost over the entire range of existence of the liquid state at atmospheric pressure. Previously, only mercury had been studied over so wide a temperature range. The results of the experiments are given in the graphs (Fig. 12-15). The accuracy of the experiments was ~ 1.5%. On the graphs are shown also the results of other investigations.

All measurements whose results are shown on the graphs were made only after attainment of a practically stationary thermal regime. Reproducibility was satisfactory. Experiments were performed while heating as well as while cooling. In addition, the experiments were performed on different days so that the metal cooled and then

was again heated. In the experiments with sodium two different types of crucibles were used. In all cases the experimental points fall satisfactorily on a single curve. This can be seen in the graph (Fig. 12) where, with each point, stands a serial number (the numbers stricken through refer to the crucible No. 2).

The results of our experiments with sodium agree satisfactorily with the results by Chiong [9], Sauerwald [12], and Lyon [18], and disagree with the data reported in the handbook by D'Ans and Lax up to 20%. For potassium (Fig. 13) our results agree with the data of Sauerwald and Chiong, and differ from the handbook data of Lyon [18] up to 15% in the middle of the interval, and from the handbook data of D'Ans and Lax up to 20%.

For lithium our data (Fig. 14) agree satisfactorily with the data of Andrade [11], who measured viscosity in not too wide a temperature interval (~ 100° above the melting point).

A similar deviation is found also for the eutectic alloy of sodium-potassium (Fig. 15) in comparison with Lyon's data.

Chemical analysis of the metals studied showed that they have a good level or purity.

Temperature Conductivity of the Alkali Metals

The necessity of a sufficiently dependable and precise method of measuring the thermal characteristics of the alkali metals up to 800°C and higher forced abandonment of a direct method of measuring the thermal conductivity λ, because the determination of this coefficient requires measurement of heat flow and which, at high temperatures, is associated with significant difficulties, frequently leading to large errors in the determination of λ. In this connection a number of advantages are displayed by dynamic methods of measuring temperature conductivity which is related to heat conductivity according to the well known equation $a = \frac{\lambda}{c\rho}$, where a is the coefficient of temperature conduction, λ is the heat conductivity, c is the specific heat, and ρ is the density.

In dynamic methods, heat flow through the specimen being studied is not measured, and the necessity of concern about good heat insulation of the specimen, or about taking account of heat losses, can be avoided. To determine temperature conductivity it is sufficient to know the change with time of the temperature, or of some parameter which depends linearly on the temperature, at one or two points of the specimen.

To measure the coefficient of temperature conductivity of the alkali metals we used Angstrom's dynamic method ("the method of temperature waves").

Description of the Apparatus. Construction of the apparatus employed for determining the temperature dependence of the coefficient of temperature conductivity of the alkali metals up to 800°C is shown in Fig. 16.

The metal being studied was placed into a vertically positioned, thin, stainless steel tube. The lower end of the tube was torch welded, the upper was connected to the top flange through a conical seal. On the outside of the upper part of the tube is wound a nichrome heater, fed through a circuit breaker by a stabilized ac source. It produced a temperature wave in the sample being studied with a fundamental period of 60-90 seconds. At approximate distances of 20 and 40 mm from the heater, two measuring thermocouples, made of nichrome and constantan wire 0.1-0.15 mm in diameter, were spot welded to the tube. In the stable thermal state, thanks to the exponential decrease of temperature along the length of the specimen investigated, the density gradient in the liquid metal (from above downward), at low amplitudes of the temperature wave, always remains positive and, therefore, convection in the liquid metal could arise only near the impulse heater. The existence of convection in the liquid metal, above the measuring thermocouples, had no effect on the results.

The upper flange was provided with some free volume to catch overflow of metal from the tube on heating. To eliminate the possibility of metal boiling, its free surface was always maintained at an excess pressure of an inert gas (helium or argon, introduced through the tube). Throughout the whole length of the specimen were distributed twenty radial copper screens for the purpose of interfering with radiative propagation of the temperature wave. The upper flange, together with the tube, was suspended on porcelain straws in the upper part of an evacuated quartz tube 800 mm in length and with a diameter of 65 x 70 mm. The upper (hot) end of the quartz tube was sealed, while the lower (cold) was hermetically attached to a steel plate through which the thermocouples and the feed for impulse heating were led out. The quartz tube, together with the assembly, was placed in a tube-like oven suitable for experiments at temperatures from 50° to 800°C.

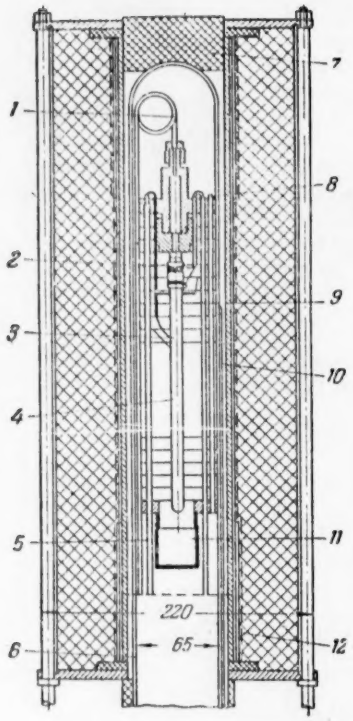

Fig. 16. Construction of the apparatus. 1) copper capillary tube; 2) nichrome impulse heater; 3) thermocouples; 4) thin-walled stainless steel tube filled with the material being investigated; 5) porcelain support straws; 6) quartz tube; 7) diatomaceous plug; 8) upper flange; 9) copper screens; 10) movable thermocouple; 11) glass for collecting liquid metal; 12) compensating heater.

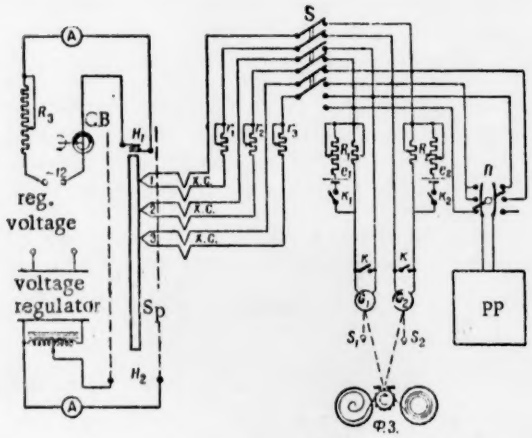

Fig. 17. The measurement circuit. Sp) specimen being investigated; H_1) impulse heater; H_2) tubular electrical oven; C. B.) circuit breaker; A) ammeter; P. R.) photo-recorder; 1, 2, and 3) thermocouples; C. J.) cold junctions of the thermocouples; r_1, r_2 and r_3) ballast resistors 10 × 100 ohms; S) thermocouple switch; R_1 and R_2) variable resistance boxes of 105 ohms; e_1 and e_2) dry cells, 1.4 v; s_1, s_2 and s_3) switches; S) change-over switch; PP) potentiometer; G_1 and G_2) small mirror galvanometers; S_1 and S_2) light sources.

The measurement circuit is shown in Fig. 17. The dc component of the electromotive force of the thermocouples, characterized by the mean temperature level of the experiment, is compensated by the electromotive force of the dry cells e_1 and e_2. The variable components of the thermocouples' electromotive forces are recorded simultaneously on photographic paper through the mirror galvanometers G_1 and G_2 and the photo-recording arrangements. A thermocouple switch S is provided to allow switching of the galvanometers. The dc component of the thermocouples' electromotive force is measured with the potentiometer PP.

Conduct of the Experiments and Data Reduction. With the assistance of the thermocouples, and of the mirror galvanometers, curves of temperature change with time at two different locations in the sample were simultaneously recorded on photographic paper. To eliminate errors associated with differences in the sensitivity and period of the galvanometers always observed in experiments, the galvanometers were interchanged and the recording was repeated. The amplitudes of the first harmonics, and the differences in phase, were calculated from graphical harmonic analyses of each pair of curves.

The apparent values of the coefficient of temperature conduction for the stainless steel tube, filled with the metal being investigated, were calculated according to the well known formula [13].

$$a^* = \frac{\pi L^2 \cdot 4}{T(\Delta\varepsilon_1 + \Delta\varepsilon_2)\ln\frac{A_1 A_1'}{B_1 B_1'}}, \qquad (7)$$

where π = 3.1416; L is the distance between thermocouples, taking into account the temperature lengthening of the tube; T is the period of the fundamental harmonic of the temperature wave; $\Delta\epsilon_1$ and $\Delta\epsilon_2$ are the differences in phase between the first and second curves; A_1 and B_1 are the amplitudes of the fundamental harmonics for the first pair of curves; A_1' and B_1' are the amplitudes of the fundamental harmonics for the second pair of curves.

The coefficient of temperature conduction of the metal studied was calculated according to the formula

$$a = a^*(1+\Delta), \tag{8}$$

where Δ is the correction taking into account the effect of the stainless steel container and dependent on the geometry, thermal properties of the containers and of the metal being investigated, as well as on the numbers Bi which characterize the thermal exchange between the specimen under study and the surrounding medium.

To calculate the correction Δ it was necessary to solve the problem of temperature wave propagation in a two-layer cylinder, taking into account thermal exchange with the surrounding medium. The following expression, correct up to terms of the second order, was obtained for Δ:

$$\Delta = \frac{kR\left(1+\frac{k\cdot Bi}{r}\right)\left(\frac{a_1}{a_2}-1\right)}{(1+kR)(1+2kR)}, \tag{9}$$

where $R = S_2/S_1$; S_1 is the cross-sectional area of the metal being investigated; S is the cross-sectional area of the surrounding container; $k = \frac{\lambda_2}{\lambda_1}$; λ_1 is the heat conductivity of the metal being investigated; λ_2 is the heat conductivity of the container; a_1 is the temperature conductivity of the metal studied; a_2 temperature conductivity of the container, $Bi = \frac{\alpha r}{\lambda_2}$; α is the heat transfer coefficient between the specimen and the surrounding medium; r is the radius of the specimen.

As can be seen from the formula, the effect of measurements of heat exchange between the specimen under study and the surrounding medium, assuming appropriate choice of materials and geometric dimensions of the container, can be made negligibly small.

The values of the corrections Δ in experiments with the alkali metals represented 5-10% of the measured values so that their introduction was essential.

Results of the Measurements. Using the apparatus described, the temperature conduction coefficients were measured for sodium, potassium and a solution of 78% (by weight) potassium and 22% sodium, in the temperature range from 50° to 700-760°C. In this temperature range the apparatus worked satisfactorily. The deviation of the individual results from the average did not exceed 0.5%. The results of the measurements are given in Fig. 18.

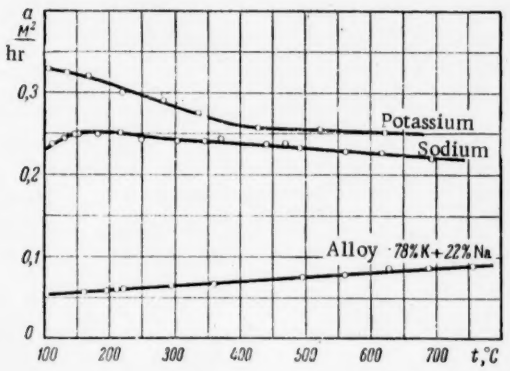

Fig. 18. Temperature conductivity of sodium, potassium and of the solution 22% Na, 78% K.

For comparison of the results obtained with the results of other authors, the coefficients of heat conduction were calculated from the experimental values of temperature conductivity. For this purpose use was made of Lyon's data [18] on the specific heat of sodium, potassium and of the solution of sodium and potassium, as well as data from Lyon's handbook on the density of liquid metals. The calculated values of heat conductivity, and the data of other authors, are given in Fig. 19.

Results for sodium coincide satisfactorily with Ewing's data, and the data of other authors [15 - 18].

The results for potassium agree well with Ewing's data for high temperatures. Deviation at low temperatures is difficult to explain since we had no chemical analysis of the metal used in our experiments.

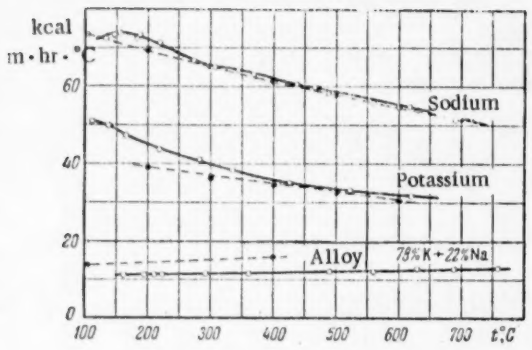

Fig. 19. The thermal conductivity of sodium, potassium and the solution 22% Na + 78% K. O MIFI data, ● Data of Ewing et al (1952) and of Lyon's handbook on liquid metals (L. M. H.), ◑ Hall's data (1938).

On the heat conductivity of solutions of sodium and potassium little data is available [15]. In addition, heat conductivity of the solution near the eutectic composition can depend markedly on the composition; accordingly, for comparison purposes, it is necessary to have an analysis of the alloy being studied.

Density

Existing methods for measuring the density of ordinary liquids, and of the less reactive molten metals, are not applicable for the alkali metals because of their great chemical activity. In conducting experiments with them it is necessary to choose carefully the material of the container, and to isolate the metal from contact with air and water.

For determining the density of molten alkali metals we used a simple and sufficiently accurate method consisting of weighing a weight of known volume in the liquid being investigated, taking the precaution of keeping the surface of the metal protected against contact with air by using a layer of melted paraffin, and by using stainless steel for the container material.

The container was divided into two parts: a "hot" (lower) and a "cold" (upper) (Fig. 20) joined together by a thin-walled tube with a diameter of 10 mm. The outside of the tube was heat insulated by a filling of diatomaceous dust. At not too elevated temperatures, the molten metal occupied the entire lower volume of the container, the joining tube and approximately one-third of the upper volume. The surface of the metal was covered with a layer of melted paraffin. With increasing temperature the level of the metal in the upper volume rose but remained isolated from contact with air.

The lower volume was the working space, and in it was located the suspended weight consisting of a streamlined steel or tungsten cylinder. It was attached to the pan of the analytical balances and suspended on a thin (diameter 0.1 mm) steel filament. To increase the accuracy of measurment the volume of the weight should be large; however, doing so results in a sharp increase in the quantity of metal being studied and of the dimensions of the apparatus. A reasonable optimum turned out to be a volume for the weight of 1-2 cc; we took a weight of 1.6 cc which allowed a small working volume ($\sim$ 130 cc).

The hot part of the container and half the joining tube were placed in the heating oven. Since the upper and lower volumes were united only by a thin-walled tube, while the remainder of the space was filled with heat insulation, heat losses from the hot part of the container were not large. Because of this it is simple to attain a temperature of $\sim$ 900°C in the lower volume at an oven heating power of 0.9 kw, while the temperature along the height of the "hot" volume changed by not more than 3-5°C.

On the other hand, thanks to low heat losses from the "hot" volume, the temperature of the metal and of the paraffin in the upper "cold" volume of the container remained relatively low. To maintain it at a definite level (100-150°C), the upper part of the container was surrounded with a thermostatic jacket containing boiling water. At low temperatures in the working volume, the boiling of the water in the thermostat was maintained by an auxilliary heater. The existence of a large temperature drop along the length of the joining tube should have led to iniation of natural convection; however, its effects could not be detected.

The filling of the apparatus with metal was carried out in the following way. The weight and the filament were placed in the container, the system was hermetically sealed and evacuated. Then, through narrow tubes, the subsequently melted metal and paraffin were sucked into the container. To control the level of the metal being sucked into the container, a contact for an electrical level gauge was introduced. Before entry into the container, the metal passed through a porous glass filter to remove the oxides. After filling, the container was opened and the weight attached to a pan of the analytical balance.

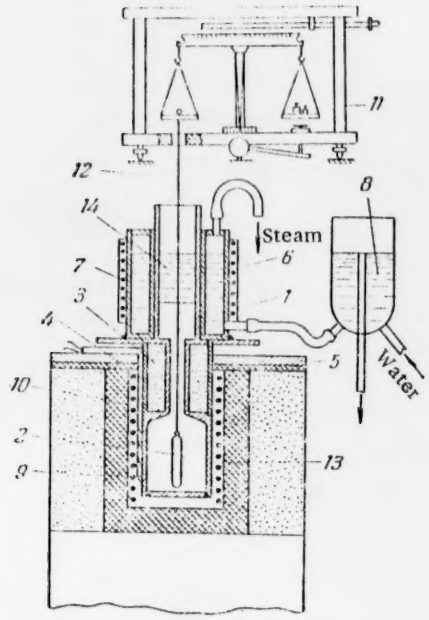

Fig. 20. Experimental arrangements. 1) container; 2) weight; 3) diatomaceous dust filling; 4) casing for the filling; 5) adjusting plate; 6) thermostat containing boiling water; 7) auxiliary heater; 8) level gauge; 9) main heater; 10) thermocouples; 11) analytical balance; 12) suspension filament; 13) the metal being investigated; 14) paraffin.

The measurements were extremely simple, and amounted to weighing the weight placed in the molten metal on an analytical balance as well as measuring the temperature in the working volume. The temperature was measured with the aid of four thermocouples distributed uniformly along the height of the "hot" volume, the value of the density being related to the mean temperature along the height. The volume of the weight at 0°C, and its weight in air, were determined ahead of time; in the calculations a correction was introduced for thermal expansion of the weight.

With the aid of the apparatus described above, the density of sodium was measured from the melting point up to 720°C (Fig. 21). Experiments showed that measurements could be made under steady- and non-steady state conditions. All points, including values obtained with a different weight and while cooling, fall on a single straight line with a maximum deviation of 0.4%. As can be seen from Fig. 21, our data agree fully satisfactorily with data known from the literature [18] (given in the graph by a dashed curve). The maximum deviation, at a temperature of 700°C, does not exceed 1.5%.

The density of potassium from the melting point to 735°C was also measured (Fig. 22). All points, including those obtained while cooling, lie on a single straight line with a maximum deviation of ~ 0.4%. These data agree fully with those known in the literature [18], which are shown on the graph by a dashed line (the maximum deviation, at a temperature of 735°C, does not exceed 0.8%).

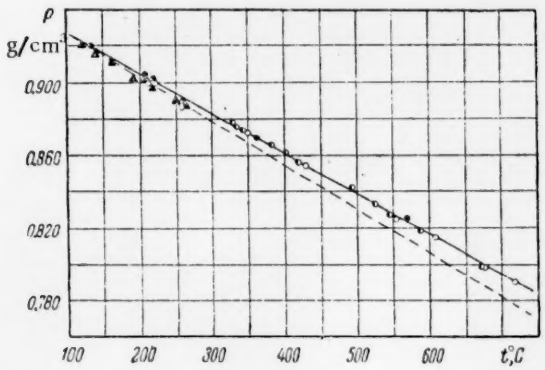

Fig. 21. The density of sodium. ○ ● ◐ Experiments with a tungsten weight in a steady state, while heating and cooling, and in a non-steady state; ▲ experiments with a steel weight; dashed curve is for Lyon's handbook data.

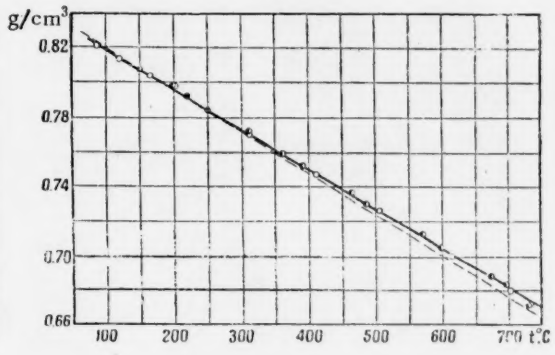

Fig. 22. The density of potassium. ○ The value of density obtained in a stationary regime while heating; ◐ the value of density obtained in a non-stationary regime while heating; ● value of density obtained while cooling.

LITERATURE CITED

[1] M. A. Stirikovitch, and I. E. Semenkover, J. Tech. Phys. USSR 10, 1342 (1940).

[2] R. Lyon, Chem. Eng. Progr. 7, 803 (1951).

[3] M. A. Mikheev, V. A. Baum, K. D. Voskresensky, and O. S. Fedynsky, "Heat transfer by molten metals," Report to the International Conference on the Peaceful Uses of Atomic Energy (Geneva, 1955).

[4] H. A. Johnson, I. P. Hartnett, W. I. Glabauch, Trans. Am. Soc. Mech. Engrs. 75, 1191 (1953) and Trans. Am. Soc. Mech. Engrs. 76, 505 (1954).

[5] H. A. Johnson, I. P. Hartnett, and W. I. Glabauch, Trans. Am. Soc. Mech. Engrs. 76, 513 (1954).

[6] Dwyer, Nucleonics 12, 7, 30 (1954).

[7] J. W. Moyer, W. Riemen, J. Appl. Phys. 1954, No. 3.

[8] E. G. Shvidkovsky, Some Problems in the Viscosity of Liquid Metals (State Tech. Press, Moscow, 1955).

[9] J. S. Chiong, Proc. Roy. Soc. (London) A 157, 264 (1936).

[10] D'Ans and E. Lax, Taschenbuch für Chemiker und Physiker (1943).

[11] E. N. da C. Andrade, E. R. Dobbs, Proc. Roy. Soc. A 212, 1104, 12 (1952).

[12] F. Sauerwald, Z. Metallkunde 11, 259 (1934).

[13] E. G. Shvidkovsky, J. Tech. Phys. (USSR) 10, 8 (1938).

[14] P. H. Sidles, and G. C. Guggenheim, J. Appl. Phys. 25, 1 (1954).

[15] C. Y. Ewing, J. A. Grand, and R. R. Miller, J. Am. Chem. Soc. 74, 1, 11, (1952).

[16] W. C. Hall, Phys. Rev. 53, 1004 (1938).

[17] I. B. Douglas, J. Am. Chem. Soc. 74, 2472 (1952).

[18] R. Lyon, Liquid Metals Handbook, 2 ed., 1952.

Received May 17, 1956.

INVESTIGATION OF SYSTEMS OF FUSED SALTS BASED ON THORIUM FLUORIDE

V. S. Emelyanov and A. I. Evstyukhin

Communication I

INVESTIGATION OF THE SYSTEM ThF_4–NaCl–KCl

The system ThF_4–NaCl–KCL, which is significant in the selection of an electrolyte for the production of thorium by electrolysis, was investigated by thermal and x-ray phase-analytical methods. The salts were melted in an atmosphere of argon. The following structural diagrams were constructed: the system NaCl–ThF_4 – an eutectic type with complete insolubility in the solid state (the eutectic lies at 712°C and 52 mole % ThF_4); the system KCl–ThF_4 – the same type (eutectic at 704°C and 23 mole % ThF_4); and a section of the ternary system NaCl–KCl–ThF_4 along the line (1NaCl: 1KCl)–ThF_4 with the point of intersection with the eutectic crystallization curve at 626°C and 40% (by weight) ThF_4.

Thorium is of interest as one of two forms of a natural raw material for the preparation of nuclear fuel.

Thorium which is used for this purpose must be very pure. The amount of contaminating elements having a greater cross section for the capture of thermal neutrons is not permitted to exceed $1 \cdot 10^{-5}$–$1 \cdot 10^{-6}$ %.

To such dangerous or "forbidden" impurities belong the rare earths (which occur along with thorium in nature and are difficult to separate from it), and certain other elements. The rare earth elements are successfully separated from thorium by electrolysis of the fused halides of sodium, potassium, and thorium. Therefore the production of thorium by electrolysis has an advantage over other possible methods for its production, and is used on an industrial scale. In spite of the long time and widespread use of electrolysis of fused salts for the production of a number of light metals (aluminum, magnesium, potassium, sodium, etc.) and rare, nonreadily fusible metals, thorium among them, this method is comparatively little studied. This fact in particular, is explained by the insufficient study of the physicochemical properties of the fused salts of the rare metals.

The system NaCl–KCl–ThF_4 and the systems NaCl–ThF_4 and KCl–ThF_4 which enter into it are of interest in the selection of the electrolyte for the production of thorium by electrolysis of fused salts. A study of the structural diagrams of these systems was begun by us in 1950 [1]. There is no information on this in the unclassified literature.

Method of Investigation

After a series of preliminary experiments, we selected thermal analysis (with automatic recording of the ordinary and differential curves) of alloys of the salts as the basic method for the investigation of these structural diagrams. Since ThF_4 is easily decomposed by the action of oxygen when melted in air, being converted into the oxyfluoride $ThOF_2$ or the oxide ThO_2, heating and cooling of the alloys were carried out in an atmosphere of argon. Recording of the thermograms was carried out automatically with the recording pyrometer of N. S. Kurnakov [2] while heating and cooling the furnace at a rate of 3° to 6°C per minute. The temperature was

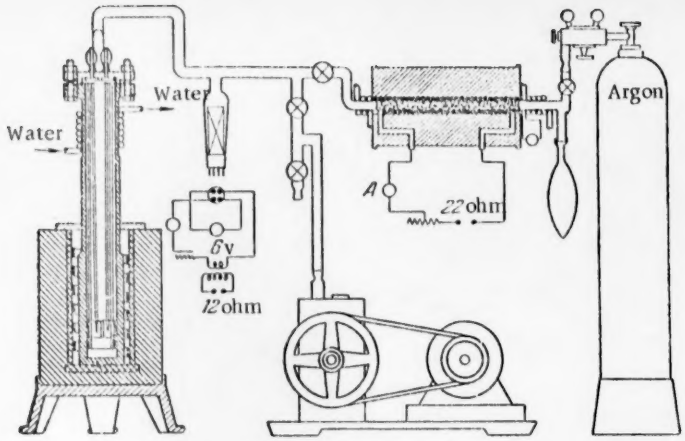

Fig. 1. Diagram of the apparatus for thermal analysis, according to Kurnakov, in an atmosphere of argon.

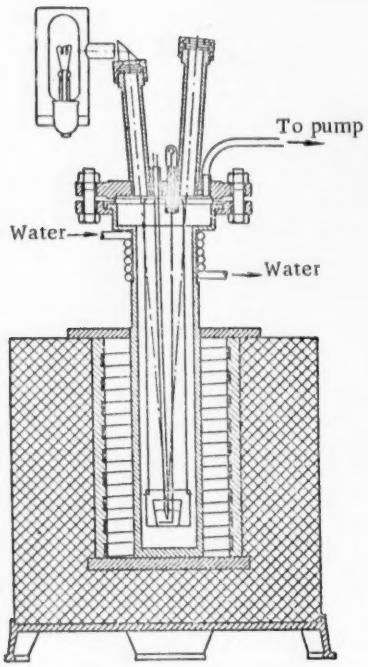

Fig. 2. Diagram of the apparatus for visual thermal analysis in an atmosphere of argon.

regulated by means of a voltage regulator. Melting and cooling of the alloy samples for thermal analysis was carried out in a special metallic cell having the required sturdiness and reliability for the work (Figure 1). It was established that, in a protective atmosphere of argon, nickel crucibles do not react with fused mixtures of the indicated fluorides and chlorides. Therefore, all further work was carried out in crucibles of electrolytic nickel. Standard platinum-platinum -rhodium thermocouples were used for the ordinary and differential recordings. The system was easily pumped out to a residual pressure of $2.0\text{-}3.0 \cdot 10^{-3}$ mm Hg measured by a thermocouple-type manometer. Prior to filling the system with argon, the system was washed several times with this gas. Before entering the system, the argon, which contained up to 0.4% oxygen, was passed over magnesium turnings heated to 400-450°C. Minimum formation of thorium oxides and oxyfluoride, unobservable by the usual analytical methods, occurred during fusion of ThF_4 in an atmosphere of the argon so purified. In certain cases, for the purpose of control, visual thermal analysis was carried out in a special apparatus shown schematically in Figure 2.

X-ray phase analysis was extensively used as an auxilliary method. Radiograms of the alloys were taken with a URS-70 x-ray apparatus with the usual Debye cameras of 9.02 cm diameter using copper K_α-radiation filtered through nickel.

Phase analysis was carried out by direct comparison of the radiograms with radiograms of the pure starting materials: ThF_4, NaCl, and KCl.

In order to facilitate phase analysis of the salt alloys, their phase components were separated prior to exposure of the radiogram. The separation was based on the different solubilities of the phases in water. Upon

washing with water, the NaCl and KCl went into solution, and the ThF_4, which is insoluble in water, remained in the residue. Radiograms were then taken of the insoluble residue and of the soluble phase of the sample of alloy obtained after filtration and evaporation of the solution.

Moreover, during the study of these systems we made partial use of microstructural analysis with preparation of sections of the salt alloys.

Compositions of the alloys were checked by chemical analysis.

Materials

ThF_4. Thorium fluoride with four molecules of water was specially prepared from chemically pure hydrofluoric acid and thorium oxide purified from rare earth elements. It contained a considerable amount of adsorbed hydrofluoric acid which protected the salt from hydrolysis during drying in air or under vacuum. The process of the removal of water of crystallization from $ThF_4 \cdot 4H_2O$ was studied experimentally. The results are illustrated graphically in Figure 3. As seen from the curves obtained, complete dehydration to ThF_4 was not attained, even at 400°C. The dried ThF_4 retained from 1/8 to 1/4 molecule of water per molecule of thorium fluoride. The analysis of the dried fluoride is presented in Table 1.

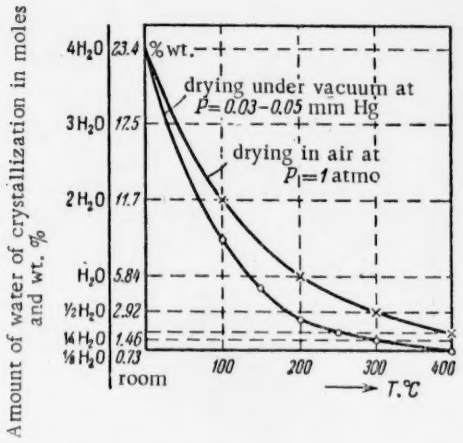

Fig. 3. Graph of the dehydration of $ThF_4 \cdot 4H_2O$ during drying in air and under vacuum (sample weight 0.1-0.3 kg, drying time 4-5 hours).

Moreover, the ThF_4 contained hundredths of a per cent (by weight) organic material, since it was prepared in a rubber-lined dish. For final dehydration of the ThF_4 and the removal from it of organic substances, it was subjected to a preliminary fusion in an atmosphere of purified argon. During this treatment, the organic material floated to the surface of the fused ThF_4 in the form of carbon black, which was easily removed from the surface of the solidified melt.

The amount of carbon black formed during fusion of a fresh portion of ThF_4 was so considerable that the "regulus" of the fused salt was covered with a continuous black layer. In order completely to separate out the carbon on the surface of the melt, the latter was maintained for a certain length of time at a high temperature. The ThF_4, remelted and purified from carbon, was broken up into pieces and ground in an agate mortar to 200 mesh. The fluoride powder was slightly hygroscopic, and was stored in glass jars with ground-glass stoppers. The composition of the remelted fluoride is given in Table 1. It contained less than 0.2% impurities.

TABLE 1

Composition of Thorium Fluoride After Different Treatments

Element	Content in % (by weight)		Analytical method
	After drying	After remelting	
Thorium	73.07	75.25	Gravimetric chemical
Fluorine	23.90	24.56	Gravimetric chemical
Σ of oxides of the rare-earth elements	0.005	0.005	Spectral
Iron	0.015	0.015	Ditto
Phosphorus	0.010	0.010	Chemical
Sulfur	0.015	Not found	Ditto
Water of crystallization	2.90	–	Ditto
Oxygen in thorium oxides and oxyfluoride	–	0.16	By difference
Total	99.915	100.00	

In Table 2 is given the average value of the melting point of the remelted ThF_4, repeatedly determined by the method of thermal analysis. Values of the melting point of ThF_4 determined by other investigators are given in the table for comparison.

TABLE 2

Melting Point of ThF_4 According to Various Data

Authors	Year of the determination	Melting point, °C	Note
Evstyukhin and Bystrov [7]	1949	1060	–
Dergunov and Bergman [8]	1948	1114	–
Brewer [9]	1950	1027	Determined by calculated estimation

As seen from Table 2, the divergence in the values of the melting point of ThF_4, as determined by different authors, is small. Unfortunately, owing to the lack of information on the purity of the preparation used in work [8] and on the method of melting point determination, it is impossible to carry out a comparative evaluation of the data of Table 2.

NaCl and KCl, chemically pure grade. Prior to use, the salts were dried to constant weight and stored in the same manner as the ThF_4. Crystalline powder of NaCl was used for the preparation of the alloys; the KCl, in view of its hygroscopic nature, was used in the form of fused "lumps".

Investigation of the System NaCl – ThF_4

Fifteen alloys were prepared beginning at 10 mole % ThF_4 and continuing at intervals of 10 mole %. In the region of the eutectic, the alloys were prepared at intervals of 2 mole %.

The data from thermal analysis were confirmed by x-ray analysis [3]. In Figure 4 is presented the structural diagram for the system NaCl–ThF_4 constructed from the results of this work. The components of the system were miscible in all proportions in the liquid state. Upon crystallization, they formed a eutectic at 52 mole % ThF_4 and 712°C. Practically complete mutual insolubility of the components was observed in the solid state.

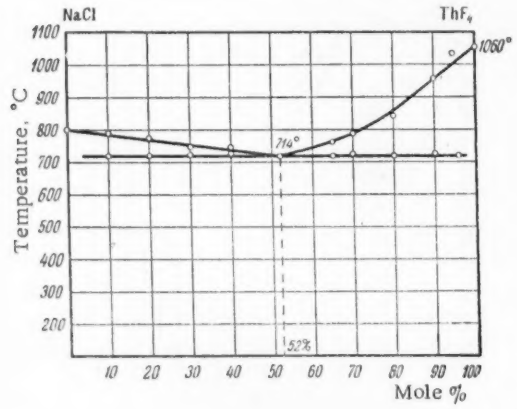

Fig. 4. Structural diagram of the system NaCl–ThF_4.

Investigation of the system KCl – ThF_4

This system was investigated by the method of thermal analysis [4]. The alloys were prepared in intervals of 5 mole %. During the preparation of alloys from KCl powder, an effect in the solid state was observed on the thermograms at a temperature of 504°C in addition to the effects corresponding to the liquidus and solidus lines. The indicated effect was not observed when lumps of fused KCl were used for the preparation of the alloys. X-ray phase analysis of the alloys [3] was carried out to clarify the nature of this effect.

For this purpose, radiograms were taken of the ThF_4 alloys containing 5, 10, 20, and 80% KCl powder and of these same alloys separated into the phase components by washing. Inspection of the radiograms obtained showed that there were two phases in all samples: one was KCl, the other, in samples containing 10, 20, and 80% KCl, had a very complex (but similar in all cases) radiogram which differed from the radiogram of ThF_4. In the radiogram of the alloy with 95% ThF_4, besides KCl, there were observed lines of a phase with another crystalline structure. X-ray analysis involving comparison with specially prepared and chemically analyzed preparations [5] established that both of these phases

were compounds of the type $K_xTh_yF_{x+4y}$. It was shown that a compound having the composition KTh_2F_9 was formed at ThF_4 contents of less than 90%; at ThF_4 contents greater than 90%, another compound having the composition KTh_6F_{25} was formed in the system. Their formation proceeded apparantly as a result of the decomposition of KCl (in the presence of traces of O_2 and H_2O) and the formation of KF, which immediately entered into reaction with ThF_4.

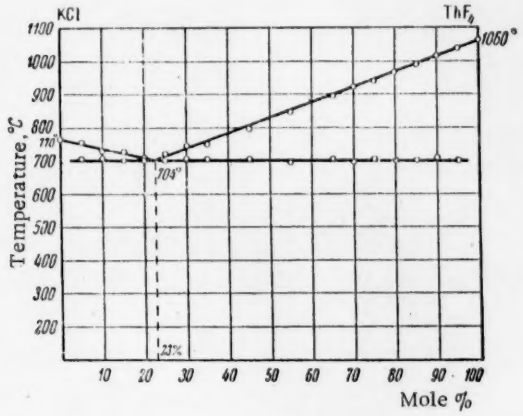

Fig. 5. Structural diagram of the system $KCl-ThF_4$.

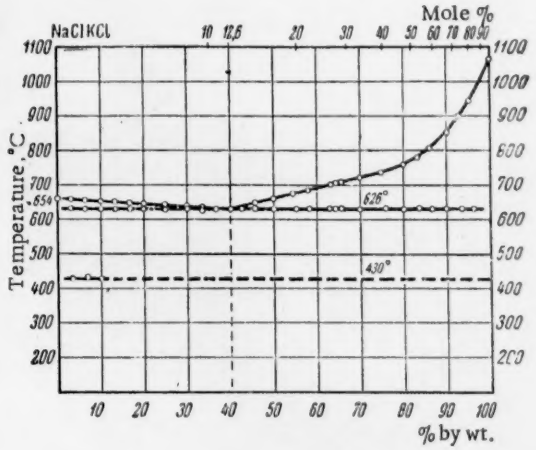

Fig. 6. Polythermal section $1NaCl:1KCl-ThF_4$ of the system $NaCl-KCl-ThF_4$.

X-ray analysis of the alloys prepared from fused lumps of KCl (which were less hygroscopic and adsorbed less water and oxygen) showed that only two phases, KCl and ThF_4, were present in these alloys. On the basis of the data from thermal and x-ray analysis [3, 4], it was established that the structural diagram of the system $KCl-ThF_4$ is a eutectic type (Figure 5) with a eutectic at 23 mole % ThF_4 and 704°C and with practically complete insolubility of the components in the solid state.

Thermal analysis of the systems $KCl-K_xTh_yF_{x+4y}$, where x = 1 and y = 2 or 6, showed that their structural diagrams were similar to the structural diagram of the system $KCl-ThF_4$. At the same time, it was determined that the melting point of the compound KTh_2F_9 is 900°C and that of KTh_6F_{25} is 930°C.

Investigation of the Polythermal Section $1NaCl:1KCl-ThF_4$ of the Ternary System $NaCl-KCl-ThF_4$

The polythermal section $1NaCl:1KCl-ThF_4$ of the ternary system $NaCl-KCl-ThF_4$ was investigated [6], this section being of interest since in it lies the composition of the original electrolyte used for the preparation of thorium.

The study of this section of the ternary diagram $NaCl-KCl-ThF_4$ was facilitated by the fact that all three binary diagrams along the sides of the concentration triangle were known. Two had been constructed from the data of the present work, and the third (NaCl–KCl) had been determined earlier [2]. The components of the latter diagram form a continuous series of solid solutions with a minimum on the liquidus line at 654°C, 50 mole % NaCl, and 50 mole % KCl. Below a temperature of ~ 400°C, the solid solutions of sodium and potassium chlorides decompose forming a mixture of bordering solid solutions.

Thermal analysis of alloys of mixtures of (1NaCl + 1KCl) and ThF_4, which were prepared in intervals of 2-5 mole % ThF_4, laid the foundation of the section shown in Figure 6. X-ray analysis of the alloys with and without separation of the phases by washing showed that they were three-phase alloys and were composed of mixtures of the phases NaCl, KCl, and ThF_4. As seen from Figure 6, the section approximates the structural diagram of a pseudobinary eutectic system. The point of intersection with the line of crystallization of the binary eutectics having the lowest temperature lay at 40% by weight ThF_4 (12.6 mole %) and 626°C. The solid solution NaCl–KCl begins to decompose at 430°C, but, with an increase in the ThF_4 content of the alloy, the heat effect associated with the transition becomes unnoticeable (the transition is represented on the section by a point).

SUMMARY

1. The structural diagram of the system NaCl–ThF_4 was constructed. It is a diagram of the eutectic type with immiscible components in the solid state. The eutectic lies at 52 mole % ThF_4 and 712°C.

2. The structural diagram of the system KCl–ThF_4 is also a eutectic type with a eutectic at 23 mole % ThF_4 and 704°C. The components of this system are practically immiscible in the solid state.

3. Upon fusion of KCl with ThF_4 in the presence of oxygen or moisture, complex compounds of the type $K_xTh_yF_{x+4y}$, where x = 1 and y = 2 or 6, are formed. These complex compounds also give a eutectic type diagram with KCl.

4. The polythermal section (1NaCl : 1KCl)–ThF_4 of the ternary system NaCl–KCl–ThF_4 was constructed in which the lowest point of the line of eutectic crystallization lay at 40% by weight ThF_4 (12.6 mole %) and 626°C.

LITERATURE CITED

[1] A. I. Evstyukhin and E. G. Savelyev, Investigation of the Structural Diagram of the System NaCl–ThF_4 (Reports of the MIFI, 1950) (not published).

[2] L. Ya. Anosov and S. A. Pogodin, Basic Principles of Physicochemical Analysis (Acad. Sci. USSR Press, 1947).

[3] A. I. Evstyukhin and E. A. Orlova, Investigation and Increase in the Precision of the Structural Diagrams of the Binary Systems NaCl–ThF_4 and KCl–ThF_4 (Reports of the MIFI, 1953) (not published).

[4] A. I. Evstyukhin and G. A. Leontyev, Investigation of the Physicochemical Processes in the Electrolysis of Thorium (Reports of the MIFI, 1950) (not published).

[5] W. H. Zachariasen, J. Am. Chem. Soc. 70, 2147 (1948).

[6] A. I. Evstyukhin and R. I. Chernorutskaya, Investigation of a Polythermal Section of the System NaCl–KCl–ThF_4 (Reports of the MIFI, 1952) (not published).

[7] A. I. Evstyukhin and P. D. Bystrov, Investigation of the Structural Diagram of the System NaF–ThF_4 in the Concentration Interval From 0 to 35 mole % ThF_4 (Reports of the MIFI, 1949) (not published).

[8] E. P. Dergunov and A. G. Bergman, Proc. Acad. Sci. USSR, New Series 60, 3, 391 (1948).

[9] "The chemistry and metallurgy of miscellaneous materials," in Thermodynamics, Laurence Quill (ed.) (New York, 1950) p. 200.

Received March 2, 1956

DETERMINATION OF THE SEPARATION COEFFICIENTS OF THE ISOTOPES OF BORON IN THE EQUILIBRIUM EVAPORATION OF BCl_3*

N. N. Sevryugova, O. V. Uvarov, and N. M. Zhavoronkov

The separation coefficients of the isotopes of boron are determined for equilibrium evaporation of boron chloride in the temperature interval 12.7 to 85°C. The methods are described, and the equation relating the dependence of the coefficient on the vaporization temperature is derived.

The stable boron isotope of nuclear mass 10 has met with wide application in neutron research. Compounds enriched with this isotope are used as one of the means for increasing sensitivity of neutron counters.

To obtain substances having a high content of B^{10} it is possible to use a variety of means for separating boron isotopes (thermal diffusion, chemical isotope exchange, fractionation). The simplest and the most productive method, at the present time, is fractionation. For realizing fractionation it is necessary to use liquefied compounds of boron, for example, the halogens: BF_3 (b.p. −101.7°), BCl_3 (b.p. + 12.7°), BBr_3 (b.p. + 91.7°C).

Urey [1] attempted to compute from statistical thermodynamics the separation coefficient for the system $B^{10}Cl_3-B^{11}Cl_3$ and obtained a value at 25°C equal to 1.013.

Green and Martin [2], by fractionation in a glass laboratory column, established that the more volatile component was $B^{11}Cl_3$. The separation coefficient for the normal boiling temperature, according to their data, is 1.0018.

Employment of the fractionating column for determination of the separation coefficient cannot lead to good results since every impairment of the separation capabilities of the column decreases the enrichment and, consequently, distorts the value of the separation coefficient.

For precise determination of the separation coefficient α of the system $B^{11}Cl_3-B^{10}Cl_3$, and for its dependence on temperature, we used Raleigh's distillation method [3].

This method consists of evaporating a large quantity of the substance to a small residue. From the change in the isotope ratios between the beginning and end of the distillation it is possible to determine the separation coefficient [4] from Raleigh's equation.

$$\alpha = \frac{\ln\left(\frac{1-x_0}{1-x_k}\right)\frac{G_0}{G_k}}{\ln\frac{x_0G_0}{x_kG_k}}, \qquad (1)$$

where G_0 and G_k are the initial and final quantities of the liquid, x_0 and x_k, the initial and final concentrations of the more volatile isotope.

As can be seen from the Expression (1), the accuracy of the determination of α depends on the accuracy of measurements of G_0 and G_k and of the isotope concentrations.

*K. I. Sakodynsky and Yu. I. Golovkin took part in the experimental phases of this work.

Taking into account that isotopic analysis can be carried out with a relative accuracy of ± 1%, the ratio G_0/G_k was maintained equal to 3000 to 5000. Under these conditions the magnitude of α was computed up to an accuracy of several parts in the fourth decimal place. For a delivery to analysis of 0.3-0.6 g of BCl_3, the evaporator was loaded with 2000-3000 g of the feed. Such a large quantity could not be evaporated directly to a small residue; accordingly the distillation was carried out in two stages. The first from 2000-3000 g to 50-70 g, and the second from 50-70 g to 0.5-0.6 g.

The separation coefficient could be determined under adherence to the following conditions:

1) At every moment the composition of the liquid must be the same in every part of the volume. This is accomplished by intensive mixing without breaking up the liquid into droplets.

2) The evaporation must be carried out slowly, without violent boiling. The latter leads to droplet formation and, consequently, to a reduction in the value of α.

3) The walls of the evaporator, especially over the liquid, must be somewhat hotter than the temperature of the liquid. If such is not the case, condensation of the liquid can take place, leading to an increase in the value of α.

The first stage of the distillation is accomplished with apparatus whose arrangement is schematically shown in Fig. 1. Its primary part is the evaporator, 1. A mixer with sylphon seal, 8, was attached to an upper cross section of the evaporator. The evaporator had two connecting pipes: one for adding BCl_3, the second for connection to the condenser, 9. During operation, to the connecting tube through which the BCl_3 was introduced, a drying system, 4, was connected together with a manometer and an air line. Condensation of the vapor was accomplished by solid carbon dioxide or by liquid air. To the condenser was connected a drying system, 12, connected to the atmosphere, or with a vacuum, through the manostat, 11. The manostat maintained pressure within ± 1.0 mm Hg [3]. To maintain the distillation regime constant, the evaporator was placed in the cryostat, 2. Before beginning work the entire system was pumped out, the evaporator was cooled to −50°C, after which boron chloride was introduced, the quantity having been weighed to an accuracy of ± 1 g. Ordinarily the temperature in the cryostat was maintained 7-15°C higher than the existing value corresponding to the vapor pressure of BCl_3 in the evaporator.

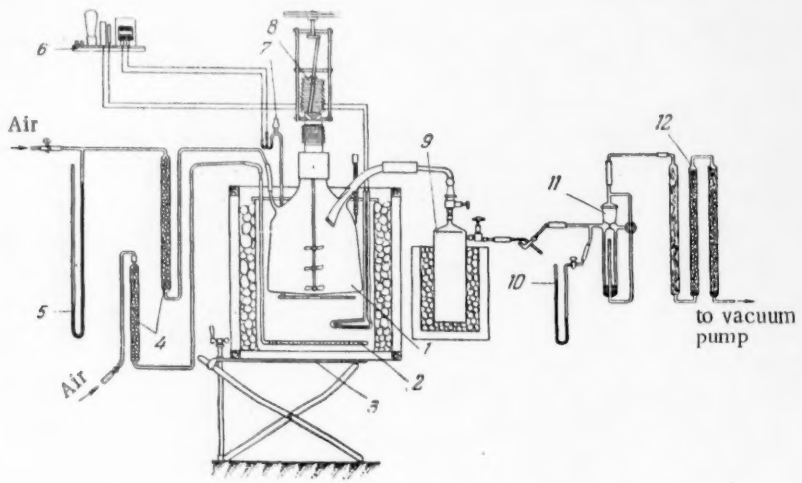

Fig. 1. Arrangement of the apparatus. First distillation stage. 1) evaporator; 2) cryostat; 3) heat insulating box; 4) drying system; 5) manometer; 6) electrical relay; 7) mercury-toluene temperature control; 8) drive for the mixer with sylphon seal; 9) condenser; 10) vacuum gauge; 11) manostat; 12) drying system for the vacuum line.

Evaporation was continued at one and the same rate until the residue was 50-70 g. After this, the small metal flask was disconnected and in its place was introduced the second-stage evaporator. The residue of the liquid from the large evaporator was driven over as a whole, the vapors being driven out by blowing in dry air over a period of several hours.

The second distillation stage. The experimental arrangements are shown schematically in Fig. 2. The evaporator, 2, is equipped with a glass bladed, magnetically actuated mixer. The distillation conditions (pressure, thermostat temperature, speed of evaporation per unit surface of the container cross section, number of mixer revolutions) were the same as in the first stage. The vapors were condensed in a glass trap lowered into a Dewar flask. Distillation was continued until the liquid residue in the evaporator was about 0.5-1.0 g. The weight of the residue was determined by weighing the evaporator on an analytical balance.

The residue was taken up in glass ampules sealed to the evaporator. Air was pumped out as the evaporator was lowered into a Dewar flask containing liquid air. The evaporator was then heated to room temperature, into one of the ampules about 0.3 g of BCl_3 was condensed, and the ampule was then disconnected. The second ampule was filled the same way.

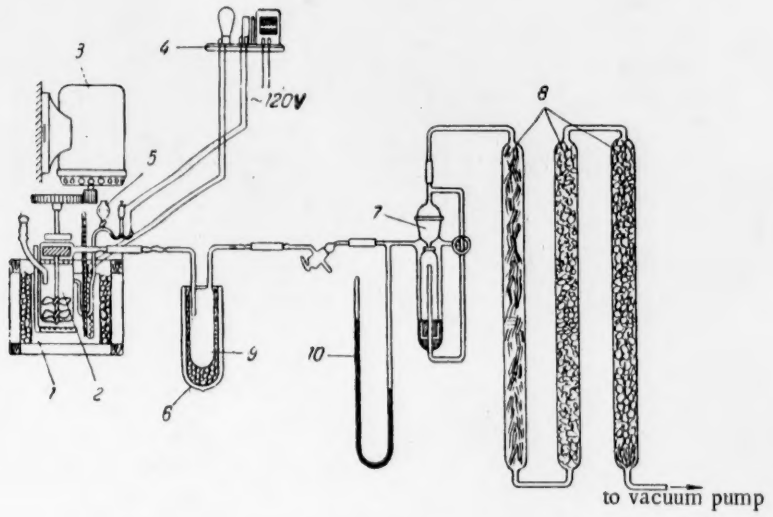

Fig. 2. Apparatus arrangement. Second distillation stage. 1) Cryostat; 2) evaporator with magnetic mixer; 3) electric motor and reducing gear; 4) electrical relay; 5) mercury-toluene temperature control; 6) Dewar flask with cooling agent; 7) Gilmont manostat; 8) drying chamber; 9) condenser; 10) vacuum gauge.

To determine the effect of rate of mixing on the size of the separation coefficient, the rate of rotation of the mixer was varied from 150 to 500 rev/min, while keeping other conditions constant (the value of the coefficient α over the entire range of values of the rotation speed is given in the table).

As is clear from these data, α had a maximum value at 300 rev/min. With further increase in speed of revolution α decreased, probably because of droplet formation in the liquid, evaporation on the hot walls and consequent lack of equilibrium conditions in the evaporation.

The effect of speed of evaporation on the magnitude of the separation coefficient of $B^{10}Cl_3-B^{11}Cl_3$ was studied in the same apparatus (see Figure 1).

In the evaporation speed interval from 1.8 to 4.7 cc/sq·cm·hour, the magnitude of the coefficient remained practically constant.

To determine the temperature dependence of the separation coefficient α, experiments were conducted at 300 mixer rev/min in the temperature range from + 12.7 to −85°C, and with speeds of evaporation no higher than 3.0-3.5 cc/sq.cm. of evaporation area per hour.

The results of the measurements are graphically shown in Fig. 3. The magnitude of α rapidly decreases with the temperature. At −61.7°C the vapor tensions of $B^{10}Cl_3$ and $B^{11}Cl_3$ are equal, while at lower temperatures $B^{10}Cl^3$ becomes the more volatile component. Analytically this dependence can be stated through an equation of the type

$$\alpha = a \cdot e^{\frac{m}{T}}, \qquad (2)$$

where a and m are numerical factors while T is the absolute temperature.

TABLE

Effect of Mixing Speed on the Magnitude of the Separation Coefficient at the Boiling Temperature of BCl_3 (+ 12.7°C)

No. of Expt.	t°C in thermostat	Speed of evaporation, cm³/cm². hr.	Mixer revolutions per min.	$\alpha = \frac{p_{B^{11}Cl_3}^{*})}{p_{B^{10}Cl_3}}$
10	19.5	2.5	150	1.00149
14	18.5	2.7	150	1.00168
16	19.7	2.8	200	1.00262
12	20.0	2.9	300	1.0030
24	20.0	3.5	300	1.0030
23	16.5	2.9	500	1.0023

*) $p_{B^{11}Cl_3}$, $p_{B^{10}Cl_3}$ vapor tensions.

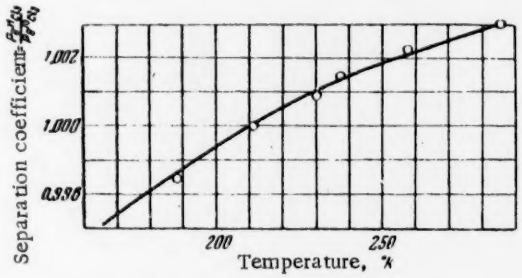

Fig. 3. Dependence of the separation coefficient α on the temperature

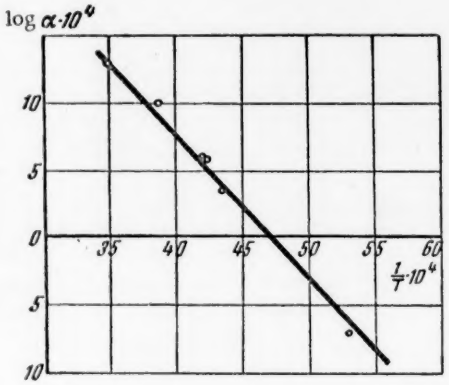

Fig. 4. Dependence of the separation coefficient on the temperature in the coordinates log α, 1/T.

In Fig. 4 the temperature dependence of α is given in terms of the coordinates $(\log \alpha)\,10^4$, $(1/T)\,10^4$.

The values of the numerical coefficients turned out to be equal, respectively, to 1.0112 and −2.33. Thus,

$$\alpha = 1.0112\, e^{-\frac{2.33}{T}} \qquad (2')$$

or

$$\log \alpha = 0.00483 - \frac{1.00757}{T}\,. \qquad (2'')$$

As is known the numerical coefficient m in the Equation (2) represents the ratio of the difference in the heats of vaporization of the isotopic forms of boron chloride to the gas constant:

$$m = \frac{\lambda_{B^{10}Cl_3} - \lambda_{B^{11}Cl_3}}{R} = \frac{\Delta\lambda}{R}\,; \qquad (3)$$

inserting the values of m and R we get $\Delta\lambda$ = 4.6 cal/mol.

Isotopic analysis*. The analysis of the residue for isotopic content was carried out on a type MS-1 mass spectrometer. The apparatus was equipped with an additional magnetic field winding, and with a rapidly acting electronic potentiometer of the type EPP-09 for automatically recording the mass-spectrum traces, as well as with a double metallic system for gas "introduction." This last allowed rapid exchange of the "standard" for the residue being studied. The compound BCl_3 was used for the isotopic analysis of boron. The large reactivity capability of BCl_3 in relation to organic compounds and moisture, as well as its adsorption on the internal surfaces of the apparatus, made the measurements very difficult.

To remove adsorbed BCl_3 from surfaces it is not sufficient merely to prolong pumping, it is necessary to heat well. Because of this a metallic system for gas "introduction" was prepared, from which were excluded all cocks and projections. The ampule with the residue was sealed to the system through a transfer tube made of covar alloy. To compensate for losses through adsorption a considerably larger quantity of it was used than is usually necessary for analysis of other gases on the mass spectrometer. Before each measurement the mass-spectrometer tube and the "introduction" system were heated for about an hour. The process of removing adsorbed gases was continued until complete disappearance of peaks corresponding to $[BCl_2]$. Only after this was it possible to carry out the analysis of a new residue which, before introduction into the system, had been cleaned by distillation.

A series of peaks corresponding to ion currents of B^+, $[BCl]^+$, $[BCl_2]^+$, and $[BCl_3]$ with the masses 10-11, 45-48, 80-85, 115-122, were recorded on the paper tape.

In Fig. 5 is shown a typical mass spectrum for BCl_3. Possible contamination in BCl_3 (basically in HCl) does not impede measurements of these masses.

Relations among the isotope pairs for various masses gave satisfactory agreement. The most intensive were the peaks for $[BCl_2]^+$, while the most stable were $[B]^+$.

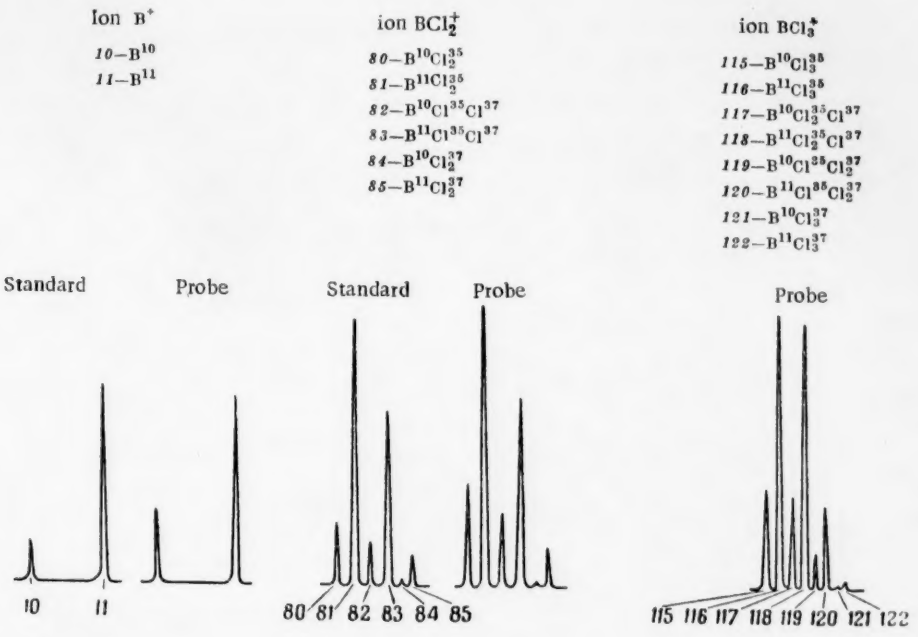

Fig. 5. Mass spectrum of boron chloride.

*Considerable help in fitting out and adjusting the mass-spectrometer was provided by Yu. Orlov.

To obtain greater accuracy in the isotope ratio, each pair was measured not less than 25-30 times. From the results obtained were computed the mean value and the mean square deviation. The maximum deviations of the isotope ratio from the mean value gave differences in the values of α not larger than $\pm$ 0.0001-0.0002, which represented a maximum error in the magnitude of ($\alpha - 1$) of 6-12%. Such fluctuations in isotopic composition were found in measurements of parallel residues. The isotope ratio in the distillate was similarly measured. The mean value of the ratio from several determinations was equal to 4.11 which corresponded to a content of 19.5% of $B^{10}Cl_3$ and 80.5% of $B^{11}Cl_3$. This result agrees well with the data obtained by Aston [6], Osberhaus [5] Shyuttse [7].

CONCLUSIONS

1) The separation coefficient α for the system $B^{10}Cl_3 - B^{11}Cl_3$ is determined by Raleigh's distillation method over the temperature interval + 12.7°C to −85°.

2) The dependence of α on the temperature is obtained

$$\alpha = 1.0112e^{-\frac{2.33}{T}}.$$

It is found that at the temperature −61.7°C the vapors of $B^{10}Cl_3$ and $B^{11}Cl_3$ have the same vapor tension. At lower temperatures the more volatile component is $B^{10}Cl_3$, while at higher, it is $B^{11}Cl_3$.

3) A mass-spectrometric isotopic analysis of the compound BCl_3 is carried out. The isotope ratio in the distillate turned out to be 4.11 which corresponds to a concentration of B^{10} of 19.5% and of B^{11} of 80.5%.

LITERATURE CITED

[1] H. Urey, Chemistry of Isotopes, Collection 1 (Foreign Lit. Press, 1948), p. 86.

[2] M. Green and G. Martin, Trans. Faraday Soc. 48, 5 (1952).

[3] N. M. Zhavoronkov, O. V. Uvarov, and N. N. Sevryugova, Collection: Applications of Tagged Atoms In Analytical Chemistry (Acad. Sci. USSR Press, 1955), p. 223.

[4] A. I. Brodsky, Chemistry of Isotopes (Acad. Sci. USSR Press, 1952), p. 68.

[5] O. Osberhaus, Z. Physik 128, 366 (1950).

[6] F. Aston, Mass Spectra and Isotopes (Foreign Lit. Press, 1948), p. 138.

[7] V. Shyuttse, J. Exptl.-Theoret. Phys. 29, 4, 486 (1955). [Soviet Physics − JETP, 2, 3, 402 (1956)].

Received January 21, 1956.

MINERALS OF URANIUM

V. E. Gerasimovsky

Knowledge about the minerals of uranium is summarized and the conditions of their formation are considered. A table of the physical properties of the most widely distributed minerals of uranium is included.

In recent years the minerals of uranium have attracted great attention, for they are the ore from which uranium, the source of intranuclear energy, is obtained.

Uranium comprises 4×10^{-4}% (A. E. Fersman) [1] or 3×10^{-4} % (A. P. Vinogradov) [2] of the earth's core; that is, considerably more than those elements widely known in the national economy such as silver (1×10^{-5} %), antimony (5×10^{-5} % to 4.1×10^{-5} %), platimum (2×10^{-5} to 5×10^{-7}%), gold (5×10^{-7} %), bismuth (1×10^{-5} to 2×10^{-5} %), and others.

The content of uranium in rocks composing the earth's crust, according to the data of A. P. Vinogradov, is:

a) Magmatic rocks:

Acid rocks (granites, liparites, rhyolites, etc,)	3.5×10^{-4}%
Intermediate rocks (diorites and andesites)	1.8×10^{-4}%
Basic rocks (basalts, gabbroes, diabases)	3×10^{-5}%
Ultrabasic rocks (dunites, peridotites, pyroxenites)	3×10^{-6}%

b) Sedimentary rocks:

Clays and shales	3.2×10^{-4}%

Uranium in nature is met in various forms: 1) It forms uranium minerals (uraninite, pitchblende, autunite, torbernite, carnotite, etc.). 2) It enters into the crystal lattice of nonuranium minerals, isomorphically replacing in them such elements as thorium, zirconium, etc. (thorite, zircon, monazite, etc.). 3) It occurs in a disseminated condition.

According to the ideas of V. E. Vernadsky [4], the bulk of uranium in the earth's crust occurs in a disseminated condition. Vernadsky hypothesized that uranium in igneous rocks "occurs in forms not connected with chemical compounds, and that it is dispersed as atoms, more or less free, penetrating all the material of the earth or dissolved in the capillary water of rocks."

In recent years investigations have been conducted on the interpretation of the forms of occurrence of disseminated uranium in nature, but, in comparison with the propositions of V. E. Vernadsky, they have introduced nothing new in principle to the solution of this question.

According to the data of American investigators [5], uranium in igneous rocks is found in three forms: 1) it forms uranium minerals, 2) it enters into the structure of rock-forming minerals owing to isomorphism;

3) it is maintained in the condition of a cation interchange; 4) it is adsorbed on the surface of crystals and grains; 5) it occurs dissolved in liquid inclusions in rock-forming minerals; and 6) it occurs dissolved in intergranular liquid.

Investigations of Soviet (L. V. Tauson [oral communication]) and foreign [6] scientists, completed in recent years, showed that although the highest composition of uranium in magmatic rocks is found in colored minerals and accessory minerals (micas, amphiboles, orthite, zircon, monazite, apatite, sphene, etc.), nevertheless 30 to 70% of the over-all uranium content is concentrated in the quartzo-feldspathic portion of the rocks.

In natural compounds (minerals) uranium is known in a tetravalent and hexavalent state. The sizes of the radii of the ions of uranium are: U^{4+} = 1.05 A, U^{6+} = 0.79 A. The sizes of the ions of several widely distributed elements are close to the size of the ions of tetravalent uranium, namely: Th^{4+} = 1.10 A, Zr^{+} = 0.87 A, rare earths from La^{3+} = 1.22 A to Lu^{3+} = 0.99 A, Y^{3+} = 1.06 A, Ca = 1.06 A. As uranium in the form of the tetravalent ion is less widespread in the earth's crust, it is often disseminated in the lattices of the minerals of these elements, replacing them isomorphically.

Hexavalent uranium in the form of the ion U^{6+} does not exist freely, and forms the complex bivalent cation uranyl $[UO_2]^{2+}$. The capacity for isomorphic entry into the lattices of other minerals is considered to be slight because of the large size of the radius of the ion $[UO_2]^{2+}$; this limits the possibilities for dissemination of hexavalent uranium. By this also is explained the widespread development of secondary minerals of uranium in the zone of oxidation in the form of separate small crystals, often of microscopic size, in the form of coatings and very thin incrustations in cracks and cavities of rocks.

Uranium minerals are formed in the earth's crust under various conditions. Primary uranium minerals are observed in acid magmatic rocks, in pegmatites, and especially in ore bodies formed by hydrothermal solutions. Uranium minerals are known also in sedimentary and metasedimentary rocks.

Primary uranium minerals of magmatic, pegmatitic, hydrothermal, and sedimentary genesis, when they happen to come to the surface of the earth (into the conditions of the zone of oxidation), become unstable and are easily decomposed – especially minerals of the oxide group (uraninite and pitchblende). With breaking down of the black-colored oxides of uranium in the zone of oxidation, diverse secondary minerals of uranium are formed such as sulfates, carbonates, silicates, phosphates, arsenates, and vanadates, which have a bright color, basically yellow of various hues, yellow-green, and green.

A characteristic feature of natural compounds of uranium is the persistent presence of oxygen. No minerals are known which contain uranium but do not have oxygen in their composition. Uranium minerals of the group of sulfides or halides are not found in nature; uranium also does not occur in the native state.

Uranium-containing minerals are very diverse, and at the present time more than 100 minerals are known. By chemical composition, they are usually subdivided into oxides, hydroxides – simple and complex (uranates), silicates, carbonates, sulfates, sulfate-carbonates, phosphates, arsenates, vanadates, molybdates, organic compounds, and complex oxides (titanates and titano-tantaloniobates). Minerals of the last two groups are usually considered, not as uranium minerals, but as uranium-containing minerals.

Not all minerals of the groups enumerated have commercial interest, but nevertheless they deserve attention since the majority of them (especially the uranium minerals formed in the zone of oxidation) are excellent prospecting signs of uranium mineralization exposed on the surface of the earth.

Of all the natural uranium compounds, minerals of the oxide group incite the greatest interest. They have a black color, resinous luster, high hardness (5-7), and high specific gravity (6-10). Their composition is expressed by the general formula $\underline{1}(U,Th)O_2 \cdot mUO_3 \cdot nPbO$; the greater the age of the uranium minerals, the greater their lead content.

Uranium minerals referred to the oxide group are subdivided into two subgroups – the subgroup of uraninite and the subgroup of pitchblende. Minerals of the uraninite subgroup are observed in the form of crystals of cubic symmetry (cubes, sometimes with faces of octahedrons, rhombododecahedrons, and octahedrons); minerals of the pitchblende subgroup are not found in crystals; they form massive, nodular, stalactitic, and botryoidal aggregates.

Among the minerals of the uraninite subgroup three varieties are distinguished: 1) uraninite – $1\ (U,Th)O_2 \cdot mUO_3 \cdot nPbO$, which usually contains a small amount of thorium (up to 2.8% ThO_2) and rare earths (up to 5.0% RE_2O_3), 2) broeggerite - a variety of uraninite rich in thorium (7.8-11.4% ThO_2) and containing rare earths (to 4.5% RE_2O_3), 3) cleveite (nivenite) – a variety of uraninite with a high content of rare earths (up to 16% RE_2O_3) and containing thorium in the amount of 3.03 to 5.75% ThO_2.

The rare earths in the uraninite subgroup are represented mainly by rare earths of the yttrium group.

In uraninite, broeggerite, and cleveite, the lead content ranges within the limits 0.4 to 20.6% PbO, just as the content of UO_2 ranges from 6.15 to 70.1% and the content of UO_3 from 22 to 60%.

It has been recently revealed [7] that uranium in uraninite may be isomorphically replaced by thorium in any proportion, forming a continuous isomorphic series from uraninite to thorianite (ThO_2). The varieties of thorianite rich in uranium have received the name uranothorianite (the proportion between ThO_2 and UO_2 is 1:1) and aldanite; the latter, by chemical composition occupies an intermediate position between thorianite and uranothorianite.

The minerals of the pitchblende subgroup ($1\ UO_2 \cdot mUO_3 \cdot nPbO$) are distinguished from the minerals of the uraninite subgroup not only by form of deposition but also by chemical composition (content of thorium – up to 1.0% ThO_2, rare earths – up to 3% TR_2O_3). The quantity of tetravalent and hexavalent uranium in pitchblendes, just as the quantity of lead, varies within considerable limits (UO_2 – from 1.5 to 10%, UO_3 – from 53 to 20%, and PbO – from 1.5 to 10%). For minerals of the subgroup under consideration, a continuous series of natural compounds from UO_2 to UO_3 is observed, as a consequence of which an oxygen coefficient, that is, the size of the atomic proportion of oxygen to uranium, is used for the indication of the chemical composition of pitchblendes as proposed by V. G. Melkov.

The general formula of pitchblende may be expressed in the form $UO_{2.17}$ to $_{2.70}$.

In the geologic literature, when deposits of uranium are described, uraninite and pitchblende are often not distinguished and are described under the general name of pitchblende or pitchblende ore. The formulas of uraninite and pitchblende are also often incorrectly written. For uraninite the formula UO_2 is given, and for pitchblende U_3O_8. In nature no mineral with the composition UO_2 has been isolated. In uraninite hexavalent uranium is always contained with tetravalent uranium, often in considerable quantities. In natural pitchblendes the proportion between UO_2 and UO_3 is not only 1:2 (U_3O_8), but, as noted above, ranges within considerable limits – from 5 to 0.44.

Uraninite and pitchblende have diverse origins. They have been established in pegmatites (mainly uraninite and its varieties), in hydrothermal deposits (uraninite and more often pitchblende), in metasomatic deposits (uraninite and pitchblende), and in sedimentary deposits (pitchblende). The geneses of uraninite and pitchblende in conglomerates (Blind River in Canada and Witwaters-Rand in South Africa) is not clear.

Uraninite and pitchblende serve as the basic source for the world production of uranium, composing the prominant type of ore in large commercial deposits (Shinkolobwe in the Belgian Congo, the regions of Big Bear Lake and Lake Athabaska in Canada, Witwaters-Rand in South Africa, etc.) as well as in a great number of intermediate and small sized deposits (Canada, Mexico, Portugal, France, etc.).

In those parts of ore deposits located close to the ground surface (in the zone of cementation and in the zone of oxidation), uraninite and pitchblende are unstable and decompose to form secondary minerals of uranium.

Of the products of decomposition of the primary minerals, we should first pause at those which have received the name uranium blacks. Residual and regenerated uranium blacks are distinguished.

By residual uranium black is understood the products formed primarily in the zone of cementation and in part in the base of the zone of oxidation by decomposition of uraninite or pitchblende. They are amorphous earthy masses of black or dark-grey color, characterized by the absence of the ability to take a polish. Deposits or residual uranium black inherit the exterior form of uraninite or pitchblende (phenocrysts in the form of crystals or their aggregates, grains of irregular forms, nodules, films, incrustations, lenses, streaks, and veins). Between uraninite and pitchblende and residual uranium black formed from them a gradual transition is observed. The properties of these intermediate products change progressively from the properties of uraninite or pitchblende to those of uranium blacks.

The chemical composition of residual uranium black ($U_{2.70-2.92} \cdot m PbO$) is characterized first of all by a high content of UO_3 and by a low content of UO_2.

Regenerated uranium black has a black to dark grey color and is observed in the form of amorphous earthy masses forming coatings, films, more rarely incrustations in cracks and cavities of rocks. It forms in the zone of cementation as a product of the reduction of hexavalent uranium (from sulfate and carbonate solutions of uranium). The chemical composition of regenerated uranium black has not been learned, but hexavalent uranium probably predominates over tetravalent. As distinguished from residual uranium black, regenerated uranium black contains little lead. The quantity of radium in it is always insufficient for radioactive equilibrium (up to 50%).

Often as a result of the alteration of uraninite and pitchblende in conjunction with an alkaline type of weathering, and possibly also under the influence of endogenic hydrothermal solutions, hydroxides of uranium are formed, which are subdivided into simple and complex. In the composition of complex hydroxides, besides the oxide of uranium, oxides of the other metals are found. Certain investigators consider complex oxides as uranates (salts of uranic acid).

To the simple hydroxides are referred the following minerals:

Ianthinite — $2UO_2 \cdot 7H_2O$,
Epiianthinite — $mUO_3 \cdot nH_2O$,
Becquerelite — $3UO_3 \cdot 5H_2O$,
Billietite — a variety of becquerelite containing Ba,
Mineral "X" — $4UO_3 \cdot 7H_2O$ (?),
Skupite — $4UO_3 \cdot 9H_2O$,
Paraskupite — $5UO_3 \cdot 9.5H_2O$,

and to the complex hydroxides (uranates):

Fourmarierite — $PbO \cdot 4UO_3 \cdot 7\text{-}8H_2O$,
Curite — $2PbO \cdot 5UO_3 \cdot 4H_2O$,
Mineral "Y" — close to curite,
Vandenbrandeite — $CuO \cdot UO_3 \cdot 2H_2O$,
Clarkeite — $(Na_2Ca, Pb)(UO_2)^{2+} \cdot (UO_4)_2 \cdot 3H_2O$,
Uranospherite — $Bi_2O_3 \cdot 2UO_3 \cdot 3H_2O$ (?),
Vandendriescheite, Richetite, Masunite — water uranates of lead (?).

In the minerals referred to the hydroxides, uranium is hexavalent, with the exception of Ianthinite in which the uranium may be tetravalent.

Minerals of the group of uranium hydroxides are rarely observed in crystals. More often they are met in the form of pseudomorphs after uraninite and pitchblende, usually originating as a result of their replacement. Therefore, mutual progressive transitions are sometimes observed, from uraninite or pitchblende through hydrated varieties (hydropitchblende *), first to the hydroxides poor in water, then to the water-rich hydroxides, and sometimes to the water silicate of uranium. Inasmuch as pseudomorphs after uraninite and pitchblende are characteristic for hydroxides of uranium, relict protions of undecomposed or partly hydrated uraninite or pitchblende are preserved, and as a rule they can be observed in the interior of the pseudomorph.

Certain investigators erroneously segregate gummite among the hydroxides of uranium. With detailed investigation of gummite it has been revealed that it represents a mixture of hydroxides and silicates of uranium, primarilly curite and soddyite.

In the zone of oxidation, at the time of the decomposition of uraninite, pitchblende, uranium black and hydroxides of uranium, a large number of secondary uranium minerals is formed: they are silicates, sulfates, carbonates, sulfate-carbonates, phosphates, arsenates, and vanadates. The uranium in them is in the hexavalent state. These secondary minerals of uranium are usually characterized by a destruction of the radioactive equilibrium (a deficiency of radium), inasmuch as conditions for its prolonged existence in the zone of oxidation are

*Hydropitchblende ($kUO_2 \cdot lUO_3 \cdot mPbO \cdot nH_2O$), black colored, in thin sections butyl green, brittle, glassy luster.

absent in most cases. This is conditioned by the development of the zone of oxidation and its erosion. Three stages in the development of the zone of oxidation are separated [8]: beginning, intermediate, and ending. In the zone of oxidation are observed not only oxidation of primary minerals and the formation of new ones, but also simultaneously the removal of a series of elements, including uranium. The removal of elements occurs first predominantly in the sulfate form, and then in the carbonate form.

The secondary minerals of uranium, having bright colors (yellow, yellow-green, and green) are excellent prospecting signs for the detection of uranium mineralization and deposits of uranium, since as a rule they are located on the very same areas on which the primary uranium mineralization was located.

Many secondary uranium minerals in the zone of oxidation are observed in considerable quantities and are of commercial interest. To their number relate, for example, silicates (uranophane, beta-uranotile, kasolite), sulfate-carbonates (schroekingerite), phosphates (autunite, torbernite, metatorbernite, parsonsite), vanadates (carnotite, tyuyamunite), sometimes arsenates (zeunerite, metazeunerite), and others.

Of the secondary uranium minerals, the phosphates, arsenates and vanadates, usually known under the title "uranium micas", present the most interest. Minerals referred to the uranium mica group are characterized by thinly laminated (more rarely tabular) fragments of crystals (with the exception of the lead uranyl phosphates) and by a perfect basal (001) cleavage. These minerals are yellow, more rarely green (for minerals having copper in their composition), and extremely rarely some other color.

Uranium micas do not dissolve in water but easily dissolve in the mineral acids: hydrochloric, nitric, and sulfuric. The content of uranium in uranium micas varies within considerable limits, from 20% to 77% UO_3. The radioactive equilibrium in the micas is usually sharply disturbed in favor of uranium, rarely reaching 60% or higher.

In ultraviolet light (200-400 mμ) many uranium micas luminesce with a green-yellow light.

Uranium micas are found in cavities and cracks of rock, most often in association with hydroxides of iron in the form of isolated scales, plates, tablets or their many-formed aggregates, earthy masses, incrustation, films, crusts, and more rarely veinlets consisting of scaly, platy, and tabular segregations of uranium minerals. One must take into consideration that uranium micas are usually rarely met on the ground surface, and they are not found in placers. This is because they are very brittle and mechanically unstable (their hardness is usually 2-3) and because they dissolve even in weakly acid solutions.

Uranium micas are of diverse chemical composition. To the phosphates of uranium are referred the minerals:

phosphuranylite – $Ca_3(UO_2)_5(PO_4)_4(OH)_4 \cdot 10H_2O$,
saleite – $Mg(UO_2)_2(PO_4)_2 \cdot 8H_2O$,
arsenous saleite – $Mg(UO_2)_2 \cdot [(P, As)_2O_4]_2 \cdot nH_2O$,
autunite – $Ca(UO_2)_2(PO_4) \cdot 8\text{-}12H_2O$,
metaautunite – $Ca(UO_2)_2(PO_4)_2 \cdot 2.5\text{-}6H_2O$,
hydrogen autunite – $H_2(UO_2)_2(PO_4)_2 \cdot nH_2O$,
sodium autunite – $Na_2(UO_2)_2(PO_4)_2 \cdot nH_2O$,
uranospathite – $Ca(UO_2)_2(PO_4)_2 \cdot 12H_2O$,
sabugalite – $HAl(UO_2)(PO_4)_4 \cdot 16H_2O$,
uranocircite – $Ba(UO_2)(PO_4)_2 \cdot 8H_2O$,
bassetite – $Fe(UO_2)_2(PO_4)_2 \cdot nH_2O$,
torbernite – $Cu(UO_2)_2(PO_4)_2 \cdot 12H_2O$,
metatorbernite – $Cu(UO_2)_2(PO_4)_2 \cdot 8H_2O$,
lermontovite* – $(U,Ca_2,TR)_3(PO_4)_4 \cdot 6H_2O$, (36.33% UO_2, 14.53% UO_3)
fritzscheite – $Mn(UO_2)_2(PO_4,VO_4)_2 \cdot 8H_2O$,
composite uranium mica – $(Cu, Ca)(UO_2)_2[(P,As)O_4]_2 \cdot 11H_2O$ (?),
przhevalskite – $PbO \cdot 2UO_3P_2O_5 \cdot 4H_2O$ (?), (55.05% UO_3),

*Lermonotovite – a water phosphate of tetravalent uranium, grey-green color, met below the ground water level, unstable in the zone of oxidation.

Mineral name	Formula	Color	Symmetry	Hardness	Spec. gravity	Content of uranium		Genesis (basic)
						UO_2	UO_3	
1	2	3	4	5	6	7	8	9
	OXIDES							
Uraninite	$k(U, Th)O_2 \cdot 1UO_3 \cdot mPbO$	black	cubic	6-7	6.5-10	6-74 (73-93%)	16-60	Pegmatite and hydrothermal deposits
Pitchblende	$kUO_2 \cdot 1UO_3 \cdot mPbO$ (or $UO_{2.17-2.70} \cdot mPbO$)	black	crypto-crystal (cubic)	5-6.5	5-9	25-59 (68-90%)	22-55	Hydrothermal and sedimentary deposits
Uranium black (residual)	$UO_{2.70-2.92} \cdot mPbO$ (?)	black	?	< 4	< 4.5	5.8-11.9	43-67	Base of zone of oxidation and zone of cementation of deposits of various genesis
Uranium black (regenerated)	$kUO_2 \cdot 1UO_3$	black	?	—	—	—	—	
Urano-thorianite	$(Th, U)O_2 \cdot mPbO$	black	cubic	6.5-7.5	8.1-9.7	from several %	to 50% and more	Pegmatites, placers, metasomatic zones
	HYDROXIDES							
Becquerelite	$3UO_3 \cdot 5H_2O$ (?)	brownish-yellow, amber yellow	rhombic	2-3	5.1-5.2	—	88-90	Zones of oxidation and cementation of hydrothermal and pegmatite deposits
Curite	$2PbO \cdot 5UO_3 \cdot 4H_2O$	Orange-yellow	"	4-5	7.2-7.3	—	74	
	SILICATES							
Uranophane (uranotil)	$Ca(UO_2)_2Si_2O_7 \cdot 6H_2O$	yellow, greenish yellow	monoclinic	2-3	3.81-3.96	—	63-67	Zone of oxidation of pegmatite, hydrothermal, and sedimentary deposits
Beta-uranophane	$Ca(UO_2)_2Si_2O_7 \cdot 6H_2O$	lemon yellow, greenish-yellow	"	4-5	3.95	—	66-67	
Kasolite	$Pb(UO_2)SiO_4 \cdot H_2O$	yellow	"	4.5	6.0-6.5	—	48-50	
Coffinite	$U(SiO_4)_{1-x}(OH)_{4x}$	black	tetragonal	—	5.1	—	46-68	Sedimentary deposits
Nenadkevite	$(U^{4+}, Y, Ce, Th)U^{6+}(Ca, Mg, Pb)[SiO_4)_2[OH]_3 \cdot nH_2O$	black	?	—	4.16-4.81	22	31	Hydrothermal deposits
	SULFATES							
Uranopilite	$(UO_2)_6(SO_4)(OH)_{10} \cdot 12H_2O$	light yellow (greenish tinge)	?	?	3.9	—	80-81	Zone of oxidation of hydrothermal and sedimentary deposits
Zippeite	$(UO_2)_2(SO_4)(OH)_2 \cdot 4H_2O$	orange yellow	monoclinic	3	?	—	68-80	

	CARBONATES							
Uranothallite (liebigite)	$Ca_2(UO_2)(CO_3)_3 \cdot 10H_2O$	yellow green	rhombic	2.5-3	2.14-2.43	—	35-37	Zone of oxidation of hydrothermal and sedimentary deposits
	SULFATE-CARBONATES							
Schroekingerite	$NaCa_3(UO_2)(CO_3)_3(SO_4)F \cdot 10H_2O$	yellow, greenish yellow	hexagonal (?)	2.5	2.5	—	30-32	" "
	PHOSPHATES							
Phosphuranylite	$Ca_3(UO_2)_5(PO_4)_4(OH)_4 \cdot 10H_2O$ (?)	yellow	tetragonal (?)	3	3.2	—	72-76	Zone of oxidation of hydrothermal and pegmatite deposits
Autunite	$Ca(UO_2)_2(PO_4)_2 \cdot 8H_2O$	yellow, greenish yellow	tetragonal	2-2.5	3.0-3.2	—	55-62	Zone of oxidation of deposits of various genesis
Torbernite	$Cu(UO_2)_2(PO_4)_2 \cdot 12H_2O$	green, emerald green	"	2-2.5	3.2-3.6	—	57	
Metatorbernite	$Cu(UO_2)_2(PO_4)_2 \cdot 8H_2O$	green	"	2	3.68	—	56-62	
Parsonsite	$Pb(UO_2)_2(PO_4)_2 \cdot 1-2H_2O$	yellow	monoclinic	2.5-3	6.2	—	32-34	Zone of oxidation of hydrothermal deposits
	ARSENATES							
Uranospherite	$Ca(UO_2)_2(AsO_4)_2 \cdot 8H_2O$	yellow, yellow green	tetragonal	2-3	3.0-3.4	—	59	Zone of oxidation of hydrothermal deposits
Zeunerite	$Cu(UO_2)(AsO_4)_2 \cdot 12H_2O$	green, emerald green	"	—	3.2	—	51.0	
Metazeunerite	$Cu(UO_2)_2(AsO_4)_2 \cdot 8H_2O$	"	"	2-2.5	3.7-3.8	—	55-56	
	VANADATES							
Carnotite	$K_2(UO_2)(VO_4) \cdot 3H_2O$	yellow	rhombic	2-2.5	4.4	—	62-65	Zone of oxidation of sedimentary deposits
Tyuyamunite	$Ca(UO_2)_2(VO_4)_2 \cdot 8H_2O$	yellow	"	1-2	3.6-4.3	—	54-65	
	COMPLEX OXIDES							
	Titanates							
Davidite	titanate of Fe, cont. RE and U	black	?	6(?)	4.5(?)	Σ2.25-9.8 (?)		High temperature hydrothermal veins and metasomatic zones
Brannerite	$(U, Y, Th, Ca, Fe)_3Ti_5O_{16}$ (?)	black	tetragonal or rhombic	4.5	4.5-5.4	Σ ~ 44.0		Pegmatites, conglomerates, placers

Mineral name	Formula	Color	Symmetry	Hardness	Spec. gravity	Content of uranium		Genesis (basic)
						UO_2	UO_3	
	Titano-tantaloniobates ABX_4							
Hatchettolite	$(Ca, Fe, U)(Nb, Ta, Ti)_2O_6 \cdot H_2O$	yellow-brown	cubic	5	4.4-4.5	Σ 10.8-21.4		Pegmatites
Elsfordite (Mendeleyevite)	$(U, Ca, Fe)(Nb, Ti, Ta)_2O_6 \cdot 2H_2O$	yellow, dark brown to black	"	4-4.5	3.6-4.7	Σ 18.5-28.9		
Fergusonite	$(Y, Ce, Fe, U)(Nb, Ta)O_4$	brownish black	tetragonal	5.5-6.5	5.6-5.8	Σ 1.5-8.2		
	$\underline{AB_2X_6}$							
Euxenite	$(Y,Ce,U,Ca,Fe,Th)(Nb,Ta,Ti,Sn)_2O_6$	Black, occas. with grn.-brn.	rhombic	5.5-6.5	4.6-5.4	Σ 5.64-14.70		Pegmatites
Polycrase	$(Y,Ce,Ca,U,Th)(Ti,Nb,Ta)_2O_6$	"	"	5.5-6.5	4.7-5.1	Σ 4.32-13.77		
Samarskite	$(Y,Ce,Ca,U,Fe,Th)(Nb,Ta,Ti)_2O_6$	black	"	5-6	5.69	Σ 4.62-18.14		
	$\underline{A_m B_n X_p}$							
Betafite	$(U,Ca)(Nb,Ta,Ti)_3O_9 \cdot nH_2O$	brownish green to black	cubic	4	5	Σ 9.64-28.80		Pegmatites
Ampangabeite	$(Y,U,Ca,Th)_2(Nb,Ta,Fe,Ti)_7O_{15}(?)$	light brown to brownish black	rhombic	4-4.5	3.8-4.9	Σ 6.72-19.40		
	ORGANIC COMPOUNDS							
Thucholite	mixture of hydrocarbons with Th, U, and RE	pitch black, black	?	3.5-4	1.6-2	—	5.8-39.7	Pegmatites, hydrothermal deposits, conglomerates
Carburan			?	—	1.67	—	54.2	

renardite – $Pb(UO_2)_4(PO_4)_2(OH)_4 \cdot 7H_2O$,
dewindtite – $Pb_3(UO_2)_5(PO_4)_4(OH)_4 \cdot 10H_2O$,
dumontite – $Pb_2(UO_2)_3(PO_4)_2(OH)_4 \cdot 3H_2O$,
parsonsite – $Pb_2(UO_2)(PO_4)_2 \cdot H_2O$.

To the arsenates of uranium are referred:

troegerite – $(UO_2)_3(AsO_4)_2 \cdot 12H_2O$,
abernathyite – $K(UO_2)(AsO_4) \cdot 4H_2O$,
novacekite – $Mg(UO_2)_2(AsO_4)_2 \cdot nH_2O$,
uranospinite – $Ca(UO_2)_2(AsO_4)_2 \cdot 8H_2O$,
hydrogen uranospinite – $H_2(UO_2)_2(AsO_4)_2 \cdot 8H_2O$,
zeunerite – $Cu(UO_2)_2(AsO_4)_2 \cdot 12H_2O$,
metazeunerite – $Cu(UO_2)_2(AsO_4)_2 \cdot 8H_2O$,
walpurgite – $UO_3 \cdot 2Bi_2O_3As_2O_5 \cdot 3H_2O$ (?).

To the vanadates of uranium are referred:

ferganite – $(UO_2)_3(VO_4)_2 \cdot 6H_2O$ (?),
uvanite – $(UO_2)_3V_6O_{17} \cdot 15H_2O$,
carnotite – $K_2(UO_2)_2(VO_4)_2 \cdot 3H_2O$,
tyuyamunite – $Ca(UO_2)_2(VO_4)_2 \cdot 8H_2O$,
metatyuyamunite – $Ca(UO_2)_2(VO_4)_2 \cdot 3.5H_2O$,
rauvite – $CaO \cdot 2UO_3 \cdot 6(V_2O_5 + V_2O_4) \cdot 20H_2O$,
sengierite – $Cu_2(UO_2)_2(VO_4)_2(OH)_2 \cdot 9H_2O$.

Not all the minerals of the groups of uranium micas have wide distribution in nature. The most widespread are autunite, torbernite, metatorbernite, carnotite, and tyuyamunite. Phosphates of uranium are most characteristic for the zone of oxidation of deposits of hydrothermal genesis, and vanadates of uranium – for the zone of oxidation of sedimentary deposits of uranium; the latter are also very rarely and in small amounts observed in the zone of oxidation of hydrothermal deposits. Of the arsenates of uranium, the most often observed are uranospinite, zeunerite, and metazeunerite. Arsenates of uranium are met usually in the zone of oxidation of deposits of hydrothermal genesis.

Certain uranium micas sometimes form considerable concentrations, which present commercial interest. For example, autunite, torbernite, autunite-torbernite, carnotite, and carnotite-tyuyamunite ores.

Uranium micas present great interest also as prospecting signs for revealing localities with primary uranium mineralization.

Of the other secondary minerals of uranium characteristic for the zone of oxidation, the uranium silicates present the greatest interest. Among them are:

soddyite – $2UO_3 \cdot SiO_2 \cdot 2H_2O$ (?),
sklodowskite (shinkolobwite) – $Mg(UO_2)_2Si_2O_7 \cdot 7H_2O$,
cuprosklodowskite – $Cu(UO_2)_2Si_2O_7 \cdot 6H_2O$,
uranophane – $Ca(UO_2)_2Si_2O_7 \cdot 6H_2O$,
beta-uranophane – $Ca(UO_2)_2Si_2O_7 \cdot 6H_2O$,
kasolite – $Pb(UO_2)_2SiO_4 \cdot H_2O$,
orlite – $Pb_3(UO_2)_3Si_2O_7 \cdot 6H_2O$ [43.57%UO_3]
and drugmansite (formula not established).

The silicates of uranium have a wide distribution in nature and sometimes are concentrated in considerable quantities, forming commercial ores.

The silicates of uranium are usually yellow-colored (exceptions are sengierite and cuprosklodowskite, which have a green color). The crystals are acicular, finely prismatic. They easily dissolve in dilute hydrochloric acid with the formation of colloidal silica.

Uranium silicates are observed on the walls of cracks and cavities in rocks in the form of separate isolated spicules, radiating aggregates or powder-like incrustations, thin crusts consisting of crystals of acicular or finely-

prismatic appearance, and also in the form of veinlets and dense pseudomorphs of uraninite and pitchblende. The silicates of uranium are often located in close association with the hydroxides of uranium. Sometimes considerable accumulations of the uranium silicates are met contiguous with hydroxides of uranium-forming ores of great interest.

Silicates of uranium are characteristic for the zone of oxidation of pegmatitic, hydrothermal, and sometimes sedimentary ore deposits. The distribution of uranium silicates in the zone of oxidation of uranium deposits is determined by the content of sulfides, first of all pyrite, in primary ores. A high content of sulfides in primary ores produces an acid type of weathering, unfavorable for the formation of uranium silicates. Silicates of uranium are usually observed in this case only close to ground surface.

It has been proposed that silicates of uranium (soddyite and others) may form as the result of endogenic decomposition of uraninite and pitchblende.

To the uranium silicates, besides those described, belong coffinite – $U(SiO_4)_{1-x}(OH)_{4x}$ and nenadkevite – $(U^{4+}, Y, Ce, Th)U^{6+}(Ca, Mg, Pb)_3 \cdot (SiO_4)_2 \cdot (OH)_4 \cdot nH_2O$. These minerals are not characteristic for the zone of oxidation [9].

Coffinite is of tetragonal symmetry, is black colored with a diamond luster, has specific gravity greater than 5.1, has in its composition from 43.37 to 68.29% UO_2 and from 5.20 to 8.5 % SiO_2. It has been revealed in more than 15 non-oxidized uranium deposits in the Triassic and Jurassic of the Colorado Plateau (USA) and in other regions. In deposits of the Colorado Plateau coffinite is found occuring with pitchblende, black vanadium minerals, pyrite, quartz, and organic substances, and is in several ore deposits, along with pitchblende, the basic uranium mineral in nonoxidized ores [10], [11].

Nenadkevite is considered as a mineral of hydrothermal genesis.

The sulfates and carbonates of uranium usually have a limited distribution in nature, and the majority of the minerals in these groups are poorly investigated. The following minerals are referred to the sulfates:

johannite – $Cu(UO_2)_2(SO_4)_2(OH)_2 \cdot 6H_2O$,
uranopilite – $(UO_2)_6(SO_4)(OH)_{10} \cdot 12H_2O$,
beta-uranopilite – $(UO_2)_6(SO_4)(OH)_{10} \cdot 5H_2O$,
zippeite – $(UO_2)_2(SO_4)(OH)_2 \cdot 4H_2O$,
uraconite – $(UO_2)_3(SO_4)(OH)_4 \cdot 12H_2O$, and also the minerals medjidite, uranochalcite, and voglianite, the chemical composition of which has not been learned.

The sulfates of uranium are usually observed in small quantities in the form of powder-like efflorescences and incrustations on the walls of mine workings and in ore tailings. The sulfates of uranium sometimes appear several days after opening of the mine workings. The crystals of the uranium sulfates are usually so small that they may be distinguished only under a binocular magnifier or microscope. The sulfates are yellow colored, and those containing copper (johannite, uranochalcite, voglianite) are green.

The sulfates of uranium dissolve in hydrochloric acid, and several in water (johannite, uranopilite).

The sulfates of uranium are associated with pitchblende and uranium blacks, where they are often met immediately on the surface of the latter minerals, and also with gypsum, jarosite, limonite, etc.

Of the carbonates of uranium, the following are well-known:

rutherfordite (diderichite) – $(UO_2)CO_3$,
sharpite – $(UO_2)_6(CO_3)_5(OH)_2 \cdot 6\text{-}7H_2O$,
uranothallite (liebigite) – $Ca_2(UO_2)(CO_3)_3 \cdot 10H_2O$,
voglite – $Ca_2Cu(UO_2)(CO_3)_4 \cdot 6H_2O$ or $Cu(UO_2)_2(CO_3)_2 \cdot 10H_2O$,
rabbittite – $Ca_3Mg_3(UO_2)_2(CO_3)_6(OH)_4 \cdot 18H_2O$,
andersonite – $Na_2Ca(UO_2)(CO_3)_3 \cdot 6H_3O$,
swartzite – $CaMg(UO_2)(CO_3)_3 \cdot 12H_2O$,
bayleyite – $Mg_2(UO_2)(CO_3)_3 \cdot 18H_2O$, and also the not exactly established minerals shuilingite and studtite (chemical analyses are lacking).

The carbonates of uranium are observed in the form of efflorescences, films, and thin crusts, consisting of very minute crystals usually hardly distinguishable under the binocular magnifier or the microscope. The color of the carbonates is yellow, greenish-yellow, sometimes green (swartzite). The uranium carbonates are easily dissolved in hydrochloric acid with the liberation of bubbles of carbon dioxide, and several carbonates (andersonite and swartzite) are dissolved in water. Of the carbonates of uranium uranothallite (intense deep green luminescence) and swartzite (intense yellowish-green luminescence) luminesce in ultraviolet light.

The carbonates of uranium are developed in the zone of oxidation of hydrothermal and sedimentary deposits from pitchblende in the presence of carbonates.

Of the sulfate-carbonates, only schroekingerite – $Ca_3Na(UO_2)(CO_3)_3(SO_4)F_2 \cdot 10H_2O$ is investigated in detail and described. The color of the mineral is greenish yellow, and the luster is mica-like. It is observed in scaly and spheroidal aggregates, forming incrustations, films, and coatings on the walls of cracks and cavities of rocks. For it an intensive deep green luminescence in ultraviolet light is characteristic. It dissolves easily in hydrochloric acid with profuse liberation of bubbles of CO_2. The mineral is observed in the zone of oxidation of sedimentary and hydrothermal deposits. Characteristic for schroekingerite is a paragenesis with gypsum, calcite, and often with jarosite.

Schroekingerite may serve as a good prospecting sign for revealing uranium mineralization, in conjunction with which it sometimes forms at a greater distance from the locality of the primary uranium mineralization than the other secondary minerals of uranium characteristic for the zone of oxidation.

Besides the minerals of uranium enumerated, two more groups of uranium minerals are known – the molybdates of uranium and the organic compounds with uranium. Minerals of these groups are poorly investigated.

Among the molybdates of uranium three minerals have been established:

umochoite – $(UO_2) \cdot MoO_4 \cdot 4H_2O$ (47.7% U),
moluranite – $UO_2 \cdot 2UO_3 \cdot 5MoO_3 \cdot 12H_2O$ (?),
iriginite – $UO_3 \cdot 2MoO_3 \cdot 4H_2O$.

Umochoite and moluranite are black colored and iriginite is yellow.

Two "minerals" are referred to the organic compounds: thucholite and carburan, which are hydrocarbon complexes containing uranium, thorium, and rare earths. They are considered as a mixture of hydrocarbons with oxides of uranium-uraninite and pitchblende. It should be noted that in several forms of thucholite the uranium is in a dissolved state in the hydrocarbon complex.

Substances referred to thucholite or carburan have a black color, pitchy luster, conchoidal fracture, and low specific gravity (1.6-2.0). They are encountered in pegmatites, hydrothermal deposits, the gold-bearing conglomerates of Witwaters-Rand (South Africa) together with oxides of uranium and with gold, and in the conglomerates of Blind River (Ontario, Canada) in association with brannerite and pitchblende. Occurrence of humate of uranium is possible in natural conditions, but unfortuantely this question has until now not been finally cleared up.

We should pause also at the group of minerals referred to the complex oxides – on the titanates and titanotantaloniobates. In the minerals of this group the content of uranium varies in wide limits, from a hundredth of tenth part of one per cent to several tens of per cent.

Of the titanates, the most important are: brannerite – $(U, Y, Th, Ca, Fe)_3Ti_5O_{16}$ and davidite – a titanate of iron containing uranium, rare earths, etc. – $(Fe, Ce, U)(Ti, Fe, V, Cr)_3(O, OH)_7$ (?).

Brannerite, before its discovery in the ore deposit of Blind River, was considered a rare mineral. It was known as one of the accessory minerals of granites and several greisenizated rocks.

Recently a new mineral close in composition to brannerite was described – absite (found in Australia) – $(2UO_3 \cdot ThO_2 \cdot 7TiO_2 \cdot 5H_2O)$. In absite, according to the data of the chemical analysis, is established 31.83% UO_3 and 12.81% ThO_2 [12].

Davidite is the basic uranium mineral in the Radium Hill deposit (Southern Australia), where it is located with rutile, ilmentite, hematite, biotite, and quartz. Davidite is known also in the Tete deposit (Mozambique in Africa).

Uranium-containing minerals of the titano-tantaloniobate group are very numerous. They are characterized by: 1) black or brownish black, or brown color, more rarely brownish-yellow or greenish-yellow, 2) pitchy luster, more rarely sub-metallic or greasy, 3) conchoidal fracture, 4) high hardness (4-6), and 5) complexity of chemical composition. In them, besides niobium, tantalum, and titanium, are almost always rare earths (sometimes in considerable quantities), and often thorium and other elements.

Among the titano-tantaloniobates containing uranium, the following groups are separated:

a) pyrochlore-microlite (uranic varities: hatchettolite – 10.80 to 21%, mendelyeevite – 19.70 to 28.90%, and elsfordite – 18.50 to 22.00% $UO_2 + UO_3$);

b) fergusonite (in fergusonite – 1.54 to 8.16% $UO_2 + UO_3$);

c) yttrotantalite (yttrotantalite – 1.61 to 5.60% UO_2, ishikawaite – 20 to 24% UO_2);

d) euxenite-polycrase (polycrase – 4.32 to 13.77%, euxenite – 5.64 to 14.70% $UO_2 + UO_3$, chlopinite (khlopinite) – 8.12% UO_2);

e) eschynite-priorite (in priorite 1.75 to 5.35% UO_2);

f) samarskite (samarskite – 4.62 to 18.14%, wiikite – 0.77 to 19.88% $UO_2 + UO_3$);

g) betafite (betafite – 9.64 to 28.80% $UO_2 + UO_3$, blomstrandite – 18.20%, samiresite – 21.20%, ampangabeite – 6.72 to 19.40% UO_2).

The enumerated titano-tantaloniobates are characteristic for granite pegmatites. They do not usually have independent importance as sources of uranium, but they may appear as valuable components in side recovery.

In the review given, certain uranium-containing minerals are not considered since they do not present interest as sources of uranium. They are referred to the following groups: thorosilicates (thorite, uranothorite, hydrothorite, enalite, thorogummite, mackintoshite, maitlandite, nicolayite, pilbarite), zirconosilicates (dyrtolite, malacon, albite, naegite, yamagutilite), silicates of rare earths (orthite, thalenite, rowlandite), phosphates of rare earths (xenotime, monazite).

In the zone of oxidation and zone of cementation of uranium deposits of diverse genesis, uranium is often established in nonuranium minerals, but usually in very small quantities – a thousandth, hundredth, and rarely, tenth part of one percent. Of the nonuranium minerals containing uranium the most widespread are opals and hydroxides of iron, more rarely hydroxides of manganese, gypsum, hypergenic calcite, etc. The form of occurrence of uranium in them is not established with certainty. Besides having increased radioactivity, certain of these minerals (expecially hualite – a clear variety of opal) luminesce splendidly when exposed to ultraviolet light. For this reason they have great importance as prospecting signs for revealing uranium mineralization.

The radioactivity of some minerals is sometimes conditioned, not by uranium or thorium, but by radium. The content of radium in minerals (radiobarite, radiofluorite, radiocalcite, etc.) is very small (less than 1×10^{-7} g/g). Minerals containing radium are not old – no older than 30,000 years (the disintegration period of radium) if the radium enrichment occurred at the moment of their formation.

Having completed a short resume of the minerals of uranium, it should be noted that the process of oxidation of uranium minerals usually leads to the removal of uranium from the zone of oxidation of uranium deposits and to its dispersal.

With formation of zones of oxidation of magmatogenetic, hydrothermal, and sedimentary uranium deposits, simultaneously with decomposition of minerals containing tetravalent uranium, occurs formation of uranium minerals containing hexavalent uranium and removal from the zone of oxidation of a certain part of the hexavalent uranium by waters washing the zone of oxidation. In another geologic circumstance characterized by reducing conditions, hexavalent uranium changes to tetravalent, which favors its concentration and the formation of new deposits of uranium.

In conclusion, it is essential to note that in the USSR great attention is given to the investigation of the minerals of uranium. The appearance at the International Conference on the Peaceful Uses of Atomic Energy in Geneva (August 1955) of the representative of the USSR, V. G. Melkov, who reported on many new uranium

minerals discovered in the USSR, attests to the successes in this field. Among these minerals are: uranium blacks (residual and regenerated); orlite, nenadkevite (silicates); lermontovite, H-autunite, Na-autunite, przhevalskite (phosphates); H-uranospinite (arsenate); uranium micas of mixed composition (phosphate-arsenates); ferganite, tyuyamunite (vanadates); moluranite, iriginite (molybdates); lodochnikovite – $2(U, Th)O_2 \cdot 3UO_3 \cdot 14TiO_2$, uferite – $20FeO \cdot 8Fe_2O_3 \cdot 4TR_2O_3 \cdot UO_2 \cdot 74TiO_2$ (titanates); obruchevite – $(Y, U, Na_2)Ta_2O_6(OH, F)$, mendelyeefite, chlopinite (titano-tantaloniobates); carburan (organic compound).

In the chart the characteristics of the minerals of uranium which have the greatest distribution in nature are briefly cited.

LITERATURE CITED

[1] A. E. Fersman, Geochemistry, Vol. 4 (Scientific-Technical Press for Chemical Literature [USSR], 1939).

[2] A. P. Vinogradov, Geochemistry of Rare and Dispersed Elements In Soils (Acad. Sci. USSR Press, 1950).

[3] A. P. Vinogradov, "Regulating factors of the distribution of chemical elements in the crust of the earth," Geochemistry (USSR) 1956, No. 1.

[4] V. I. Vernadsky, Outlines of Geochemistry (Mining, Geology, and Petroleum Press [USSR], 1934).

[5] G. I. Neuerberg, "Geology of the atomic ore materials," in Reports of Foreign Scientists at the International Conference on Peaceful Uses of Atomic Energy (State Geologic Press, Moscow, 1956), p. 73.

[6] E. S. Larsen, D. Feyer, D. Gottfried, and V. L. Smith, "Geology of the atomic ore materials," in Reports of Foreign Scientists at the International Conference on Peaceful Uses of Atomic Energy, (State Geologic Press, Moscow, 1956), p. 53.

[7] S. C. Robinson and A. P. Sobins, Am. Mineralogist 40, 7, 8 (1955).

[8] S. S. Smirnov, The Zone of Oxidation of Sulfide Ore Deposits (United Sci. Tech. Press, 1936).

[9] V. A. Polikarpova, Atomic Energy (USSR) No. 3,132 (1956) [T. p. 425]*.

[10] L. R. Stieff, T. W. Stern and A. W. Sherwood, Science 121, 3147 (1955).

[11] T. W. Stern, L. R. Stieff and A. W. Sherwood, Geol. Soc. Am. 66, 12, part 2.

[12] A. W. Whittie, Am. Mineralogist 41, 1, 2 (1956).

Received May 26, 1956.

*T. p. = Consultant's Bureau Translation pagination.

INSTALLATION FOR RADIOCHEMICAL INVESTIGATIONS WITH A Co^{60} SOURCE OF GAMMA RADIATION WITH AN ACTIVITY OF 280 g-equiv. RADIUM

A. Kh. Breger, V. A. Belynsky, and S. D. Prokudin

A description is given of an installation in use for irradiation of substances by Co^{60} γ-radiation (280 g-equiv. radium) for radiochemical investigations with the use of a standard Co^{60} preparation. The apparatus was developed on the basis of a critical examination of installations described in the literature which are used for such investigations, and in conformity with the demands made upon modern radiochemical experimental work. The design of the apparatus is such as to permit various physicochemical measurements during irradiation, under safe conditions for the operators. The dose rate in the irradiation of objects 20-30 cc in volume is 120 r/second, and for objects up to 800 cc in volume, 30 r/second.

INTRODUCTION

The radioactive Co^{60} cobalt isotope is now the commonest source of γ-radiation in various branches of science and technology [1-5]. *

Numerous diverse (both in the objects and in the physicochemical methods used) radiochemical investigations have also been carried out with the use of γ-radiation from Co^{60} [6-23].

This wide use of Co^{60} as a source of γ-radiation is explained by the fact that this isotope has a number of properties which make its use especially convenient, particularly for radiochemical investigations.

These properties include: a fairly long half-life period; hard γ-radiation, which makes it possible to carry out radiochemical investigations in thick-walled glass and metal vessels (including autoclaves under pressure); fairly soft β-radiation, easily absorbed by thin layers of materials; high specific activity (up to 50 curie per g [38]), which ensures high dose rates from sources of small dimensions; the relatively simple technology of Co^{60} production, etc.

Installations Described in the Literature for Radiochemical Investigations with Co^{60} Sources of γ-Radiation

The literature contains descriptions of a number of devices used for irradiation of substances by Co^{60} γ-radiation in radiochemical investigations. These installations can be suitably divided into the following groups according to their principal features of importance in the field of interest.

A. Installations with stationary sources of γ-radiation. This group includes the installations used for radiochemical studies described in the publications [6-16] and [18,19], and also the sources described in [25] and [34-36]. The Co^{60} in these installations is in an open channel of a protective lead container [6-16] and [18,19]

*In this paper we examine only sources of γ-radiation made from Co^{60} preparations. Other sources of γ-radiation (Cs^{137}, Ta^{182} Ir^{192} fragments) are not considered in this paper, as they are still not as easily available as Co^{60} at the present time.

or in a well with water, 3-4 meters deep [34-36]. The activity of the source is 40 to 2000 curie Co^{60}. The power of the dose received by the irradiated object is from 10 to 400 r/second (the higher value is obtained for 2-3 cc of irradiated substance).

B. Installations in which the source of γ-radiation is moved from a storage container into the working chamber during the irradiation time. This group may be divided into two subgroups:

a) Installations in which the Co^{60} source is kept in a lead container, while irradiation takes place in a working chamber protected by lead [24, 26, 27].

The activity of the Co^{60} preparations in these installations is from 100 to 500 curie; the dose rate is from 10 to 80 r/second. Large amounts of lead (from 3.5 to 8 tons) were required for the construction of the installations described in these papers.

b) Installations in which the Co^{60} source is kept in a well with water, while irradiation takes place in a large working chamber protected by concrete walls.

The literature contains descriptions of powerful installations with source activities of 3000-4000 curie Co^{60} [28-31],* and also of a small installation [33] with an activity of 25 curie Co^{60}. In one installation [28] the dose rate inside the cylindrical source is from 66 to 83 r/second, and on the exterior of the source, from 60 to 1 r/second (at a distance of 1 meter from the source). The installations [28] and [31] have working chambers 6-8 m^3 in volume, protected by concrete walls.

Within the framework of the present paper it is not possible to give a fuller survey and a detailed discussion of the literature data listed above. However, since a critical examination of known installations (together with other considerations, see below) led to the development of the K-300 installation described here, it was thought necessary to refer to the most important papers.

Installation for Radiochemical Investigations with a Co^{60} Radiation Source with an Activity of 280 g-equiv. Radium (K-300)

A. General requirements. In the design and construction of the installation it was considered necessary to conform to certain basic requirements listed below, characteristic for radiochemical investigations in general, and to take into account the actual conditions for carrying out such investigations in our institute:

a) the use of total valumes of irradiated material up to 1 liter at a dose rate of 20-50 r/second, and of 20-30 ml volumes at dose rates of up to 100 r/second with the use of one standard Co^{60} preparation (nominal activity 400 g-equiv. radium);**

b) possibility and convenience of placing into the working chamber of devices of varying degrees of complexity containing the substances for irradiation (mixers, dilatometers, vessels under pressure and vacuum, various electrochemical cells, thermostatic devices, heaters, coolers, devices for circulation of liquid or gas in the working vessel during irradiation, etc.), without additional irradiation of the operators (irrespective of the complexity of the device), and also the possibility of conducting several experiments simultaneously;

c) the possibility of remote control and observation of the physicochemical conditions and the processes occuring in the objects during irradiation and at the end of the irradiation without any displacement (shaking) of the object;

d) simple and reliable(for long periods) remote control of the movement of the radiation source and container (accessible for precautionary inspection and repairs), with interlocking of the sequence of all the operations to ensure safe working;

e) possibility of charging the γ-radiation source into the container and of replacing it as required (at the factory);

*Only the project of an installation is described in the paper [31].

**The use of the standard preparation considerably facilitates charging and recharging of the installation. At the same time, in view of the need to use a single Co^{60} preparation in this installation, it was necessary to abandon an examination of different variations of activity distribution (for example, in the form of a hollow cylinder) with the aim of obtaining a more regular distribution of the dose rate in the working chamber.

f) possibility of installing the apparatus in an ordinary building (with a height of 4.5-5 meters up to the ceiling and a permissible load of 500-600 kg/m^2 on the ceiling);

g) finally, in the design of the K-300 installation it was taken into account that the experience in the construction and use of this installation may serve as the basis for the development and construction of more powerful installations in our institute.

On the basis of the above considerations, we designed and constructed the K-300 installation, containing Co^{60} with an activity of 280 g-equiv. radium.* K-300 has been in use for about a year. During this time it has been used for more than 500 experiments, which showed that the installation is suitable and convenient for various radiochemical investigations.

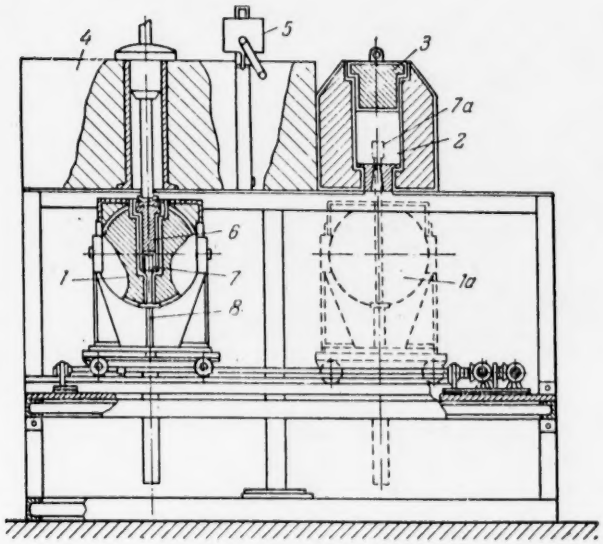

Fig. 1. Scheme of the K-300 installation. 1) Container with the source in the idle position; 1a) container in the working position; 2) working chamber; 3) plug; 4) concrete block; 5) hand jacking mechanism; 6) container plug; 7, 7a) Co^{60} source; 8) rod.

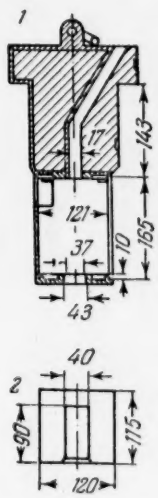

Fig. 2. Device for charging the preparations. 1) Charging device; 2) protective vessel.

B. Description of installation K-300. Installation K-300 consists of the following main parts (Fig. 1): the γ-radiation source 7, the container 1, the working chamber 2, the concrete block 4, the charging devices (Fig. 2 and 4,a) and the control panel (Fig. 3, a).

The installation is mounted in a metal vault surrounded by sheet iron walls; the area of the vault floor is 9 m^2, and the height of the installation is 3 meters.

Working Procedure on the Installation**

The object to be irradiated, contained in one of the charging devices (see Figs. 2 and 4, a) is placed in the working chamber (see Fig. 1 and 4, b). At this time the γ-radiation source is kept in a container closed by means

*According to the data of the manufacturing factory.

**Laid down in a special directive.

of a plug (Fig. 1(6)) so that the charging of the object into the working chamber takes place under perfectly safe conditions (see Fig. 4). All the subsequent operations raising of the container plug, movement of the container with the source below the working chamber, and raising of the source from the container into the working chamber can (because of the interlocking) be performed only with the vault door closed, by remote control. (The control panel is on the front wall of the vault, Fig. 3, a). The start of the raising of the container plug is possible only if the working chamber is closed (see Fig. 1); this is ensured by a special contact indicating device.

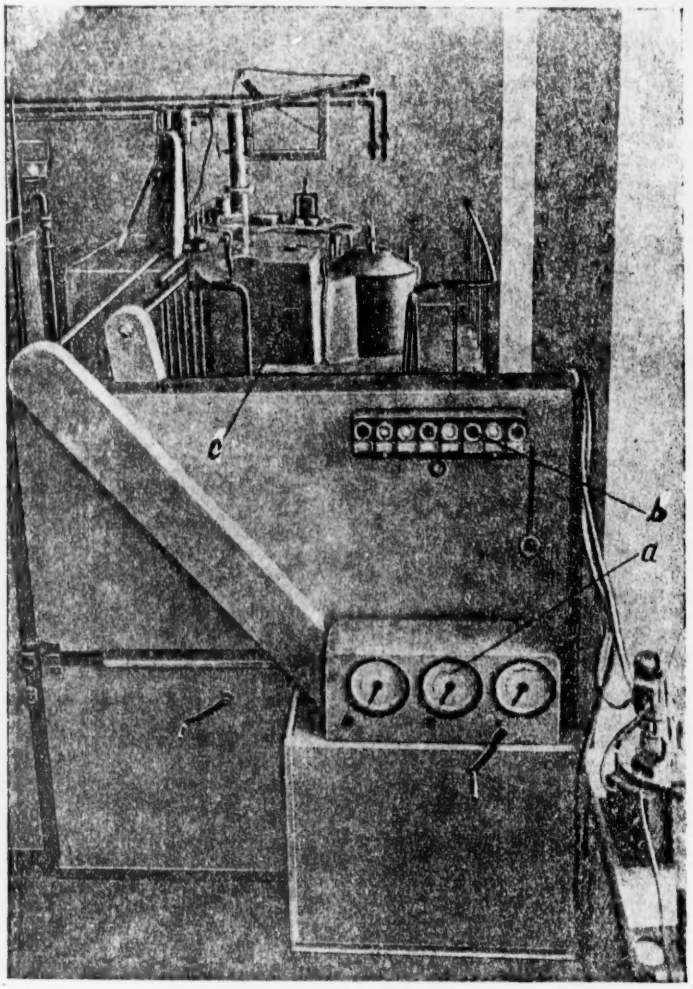

Fig. 3. General view of installation K-300. a) Control panel; b) light signal panel; c) concrete block.

At the end of the irradiation the above operations are performed in reverse sequence, after which the operator can enter the vault to unload the objects from the working chamber.

The installation is operated by one laboratory assistant.

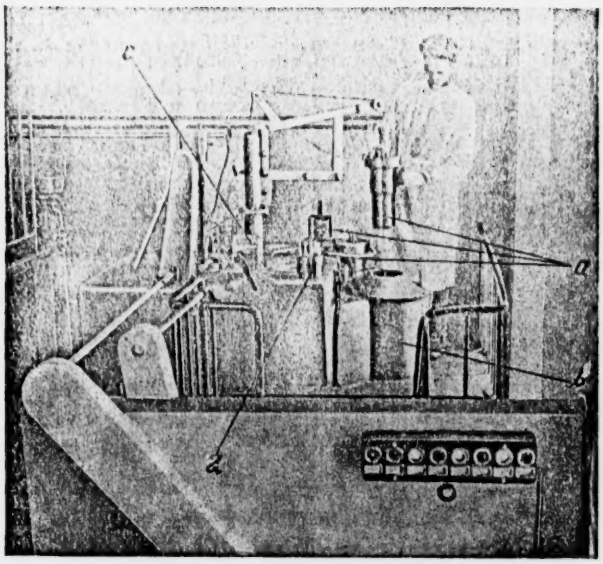

Fig. 4. Charging the objects for irradiation into the working chamber. a) Charging devices; b) working chamber; c) hoist for raising the charging devices; d) stand for charging test tubes into the working chamber.

Short Description of the Principal Parts of the Installation and Their Purpose (see Fig. 1).

The radiation source, a preparation of Co^{60},7, consists of a cobalt cylinder enclosed in an aluminum case. The source is placed at the upper end of the rod 8, which can move freely to a distance of about 50 cm along the vertical cylindrical opening from the center of the lead container 1 to the center of the working chamber 2.

The container 1 is used for storage of the γ-radiation source during removal of the irradiated objects from the working chamber 2, and during loading of the next objects for irradiation, and also to convey the source into the working chamber for irradiation. The container is moved in a small trolley on rails from the left ("idle") into the right ("working") position and back. The thickness of the lead walls* of the container is ~ 20 cm. The weight of the container is ~ 0.8 ton. During storage of the source in the container the latter is closed by the plug 6, which is raised by means of a worm gear into an opening in the concrete block 4 before the container is moved from the idle into the working position.

The working chamber 2 is used for irradiation experiments. The appropriate loading device (see Fig. 2 and 4 a), containing the object to be irradiated and the apparatus demanded by the experimental conditions (mixer, bubbling device, heater, etc.) is placed into the chamber through the upper opening. The thickness of the lead walls of the chamber is 16.5 cm.** The weight of the working chamber is ~ 1 ton. The diameter of the chamber working space is 150 mm, and the height is up to 150 mm. Up to 1 liter of material can be irradiated at one time.

*The wall thickness necessary to ensure safe handling of the container with a preparation having an activity of up to 400 g-equiv. radium was determined by extrapolation from the nomograms given in [32] and [38].

**The thickness of the working chamber walls is so chosen that during irradiation (when the γ-radiation source is introduced into the chamber) the operator is at a distance of about 2 meters from the source. In the course of the working day the operator actually spends on the average about 1 hour at the control panel.

The loading devices (see Figs. 2 and 4, a) are used for placing various objects into the working chamber, and for protection against the stream of radiation which travels upward from the working chamber during the irradiation. The irradiated objects are placed in the protective vessel (Fig. 2,2), in glass or metal ampoules, into the lower part of the charging device, so that when the source is pushed out of the container into the working chamber it enters the central tube of the protective vessel and the central tube of the ampoule with the irradiated liquid (Fig. 5), thus ensuring utilization of the stream of γ-radiation in a solid angle of $\sim 3.7\ \pi$. The upper parts of some of the charging devices have through openings *, through which tubes are passed for removal of gases formed in the objects during irradiation, or for blowing gases through irradiated liquids, and also tubes for holding conductors (for electrical measurements during irradiation). One of the charging devices has a calibrated dilatometer tube passed through the upper lead portion (the observations of the liquid level in the tube are made with the aid of binoculars at a distance of several meters).

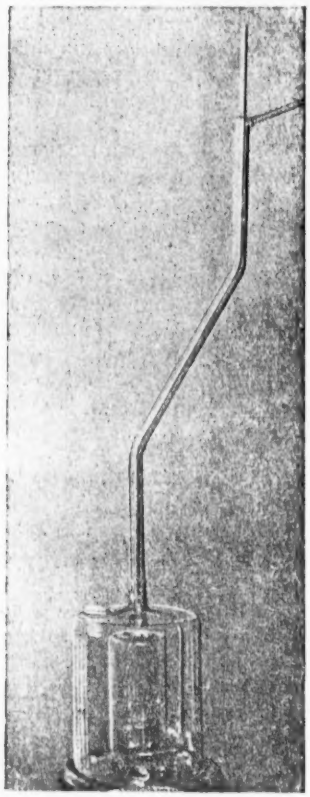

Fig. 5. Glass ampoule for irradiation of liquids.

If several experiments have to be performed simultaneously, the objects for irradiation are fixed in test tubes in a special stand (see Fig. 4, d) around the central tube of the protective vessel. In such cases the working chamber is closed from above by a lead plug (Fig. 1, 3).

A swing hoist fixed on the upper plate of the installation is used for transferring the charging devices and plug from the special stand into the working chamber and back. This hoist is manually operated by means of reducing gear (see Fig. 1, 5 and 4, c) installed on the hoist column.

The control panel (Fig. 3, a) is used for remote control of the movement (up and down) of the container plug, movement of the container from the idle into the working position (and back) and for raising (and lowering) the rod with the γ-radiation source. These movements** are effected by turning handles (by hand, with minimum effort) through a system of shafts and level gears. The front of the panel carries dials with moving pointers indicating the position of the container plug, the container itself, and the γ-radiation source. It was decided to use only mechanical drives, as being the most reliable, in the K-300 installation. Above the control panel is a light signal panel (Fig. 3, b). These signals indicate the positions of the container and source and show whether the working chamber and container are shut or open.

Frame and concrete block (see Fig. 1). All the parts and sections of the installation are mounted on a frame welded out of steel girders. The base of the frame also serves for uniform distribution of the load over the floor of the building (the whole weight of the installation, ~ 3.5 tons, is distributed over about 6 m^2).

In addition to the working chamber, the upper plate carries a concrete block 4, to weaken the stream of γ-radiation which flows up from the container when the latter is moved in the open state from the idle into the working position (and back).

Additional Notes

The design of the installation provides for possible dismounting of the container for charging or recharging it with radioactive cobalt at the works.

*The openings are in zigzag form with 1-2 bends in order to decrease the intensity of γ-radiation escaping through these openings (see Fig. 2).

**An experienced assistant performs the above operations in three minutes.

Control and observations of the physicochemical processes which occur in the irradiated objects during the experiments are performed by special devices (such as ultrathermostats, dilatometers, mixers, etc.) for each individual case. Installation K-300 does not have a special physicochemical panel.

C. Dose rates obtainable in installation K-300 in radiochemical experiments. The dose rates were determined by chemical dosimetry in glass vessels (see Fig. 5) of various capacities. The dosimetric liquid was Mohr's salt solution in 0.8 N sulfuric acid. The Fe^{+++} concentration was determined colorimetrically; the Fe^{++} concentration was determined by potentiometric titrations with $Ce(SO_4)_2$. The yield of the iron oxidation reaction was taken to be 15.6 Fe^{+++} ions per 100 ev of absorbed energy.

In vessels of 800 ml capacity (Fig. 5) the dose rate was 33 ± 3 r/second, in similar vessels 100-120 ml in capacity, up to 80 ± 8, and with a capacity of ~ 30 ml, up to 120 r/second. The dose rates measured in separate test tubes were about 70-80 r/second near the γ-radiation source, and about 20 r/second near the outer wall of the protective vessel.

If it was necessary to carry out radiochemical investigations on liquids in vessels of different shape, or on solids, the dose rate was determined by chemical dosimetry in equivalent geometric conditions. The dimensions of the solid objects irradiated (crystalline powders, films, plates) and the distance from the object to the source were so chosen that the dose rate distribution across the section of the object could be assumed practically uniform. Solid objects were, if necessary, rotated about their axes during exposure.

D. Dosimetric examination of the installation. A dosimetric examination showed that the container, working chamber, and concrete block provide the required protection for the operators. When the project of the installation was worked out it was intended that the question of protection against γ-radiation penetrating through the slit between the upper edge of the container and the plate on which the working chamber is installed during movement of the γ-radiation source from the container into the working chamber and back (1-2 seconds) should be solved when the assembly was completed. To diminish this stream of γ-radiation the dimensions of the slit were diminished (lead sheets were placed on top of the container) and a lead block 12 cm thick was placed in the path of the rays from the slit to the control panel. As a result of these measures the radiation dose at the control panel during the passage of the source past the slit was reduced to the normal value.

Individual dosimetric determinations, carried out with the aid of DK-0.2 dosimeters, showed that with normal use of the K-300 installation the irradiation of the operators is considerably below the permissible level, and is ~ 5 mr per working day.

SUMMARY

1. The installation K-300 for radiochemical investigations, with a Co^{60} source of γ-radiation with activity of 280 g-equiv. radium has been developed and built with regard to the requirements of modern radiochemical research and on the basis of a critical examination of installations described in the literature. A standard industrially available Co^{60} preparation was used in the installation.

2. Various objects from 30 to 800 cc in volume at dose rates from 120 to 30 r/second respectively can be irradiated in the installation. The cylindrical source is placed in the center of the working chamber during irradiation.

3. The use of the K-300 installation over a period of a year showed that it is suitable for radiochemical investigations of varying degrees of complexity (in the physicochemical conditions), and also has demonstrated its convenience, reliability, and safety of operation.

4. On the basis of the design and operating experience of installation K-300 it is possible to develop installations for radiochemical research with more powerful sources of γ-radiation.

In the development of installation K-300 theoretical questions were solved with the participation of V. L. Karpov; much valuable advice was also obtained from M. A. Proskurnin.

Technician M. A. Korotkova took part in the development of the K-300 project. The installation was made in the mechanical workshop of the institute (G. D. Nikolenko, T. F. Evdokunin, I. G. Chinenov, and others). The indicating scheme was constructed in the electrical workshop of the institute (A. F. Lopukhin and A. Ratov).

B. I. Viting took part in the solution of some problems in the assembly and adjustment of the installation. V B. Osipov and G. N. Korolev helped in the operation. The dosimetric inspection of the installation from the aspect of protective efficiency was made by L. A. Vasilyev and V. I. Sinitsyn.

The authors take the opportunity of expressing their gratitude to all these colleagues for their critical comments and participation in the work. Valuable critical comments made on the paper by reviewer A. V. Vibergal are also gratefully acknowledged.

LITERATURE CITED

[1] S. D. Gertstriken and I. Ya. Degtyar, Use of Isotopes in Technology, Biology, and Argiculture, Papers of the Soviet Delegation at the International Conference on the Peaceful Uses of Atomic Energy (Acad. Sci. USSR Press, 1955) p. 39.

[2] S. T. Nazarov, ibid., p.98.

[3] G. G. Iordan, V. B. Brodsky, and B. S. Sotskov, ibid., p.118.

[4] A. V. Kozlova, ibid., p. 204.

[5] A. M. Kuzin, ibid., p. 287.

[6] V. I. Veselovsky, Ts. I. Zalkind, N. B. Miller, and A. A. Aladzhalova, Symposium on Radiation Chemistry (Acad. Sci. USSR Press, 1955) p. 36.

[7] V. I. Veselovsky, N. B. Miller, and D. M. Shub, ibid., p. 49.

[8] V. I. Veselovsky and G. S. Tyurikov, ibid., p. 61.

[9] M. A. Proskurnin, V. D. Orekhov, and A. I. Chernova, ibid., p. 79.

[10] V. D. Orekhov, A. I. Chernova, and M. A. Proskurnin, ibid. pp. 85 and 91.

[11] M. A. Proskurnin and E. V. Barelko, ibid., p. 99.

[12] V. L. Karpov and B. I. Zverev, ibid., p. 215.

[13] N. A. Slovokhotova and V. L. Karpov, ibid., p. 206.

[14] A. V. Zimin and Z. S. Egorova, ibid., p. 241.

[15] A. V. Zimin, S. V. Churmanteev, and A. D. Verina, ibid., p. 249.

[16] V. I. Veselovsky, Investigations in the Fields of Geology, Chemistry, and Metallurgy, Papers of the Soviet Delegation at the International Conference on the Peaceful Uses of Atomic Energy (Acad. Sci. USSR Press, 1955) p. 320.

[17] N. A. Bakh, ibid., p. 346.

[18] V. L. Karpov, Papers at the Session of the Acad. Sci. USSR, Div. Chem. Sci. on the Peaceful Uses of Atomic Energy, July 1-5, 1955, p. 3.

[19] M. A. Proskurnin, V. D. Orekhov, and E. V. Barelko, ibid., p.41.

[20] I. Weiss, Ann. Rev. Phys. Chem. 4, 143 (1953).

[21] E. Hart, Ann. Rev. Phys. Chem. 5, 139 (1954).

[22] Radiation Chemistry, Symposium (Foreign Lit. Press, 1953).

[23] G. H. Kinchin, and R. S. Pease, Repts. Progr. in Phys. 18, 1 (1955).

[24] I. A. Ghormley, and C. I. Hochanadel, Rev. Sci. Instr. 22, 7, 473 (1951).

[25] B. Manowitz, Nucleonics 9, 2, 10 (1951).

[26] M. A. Greenfield, L. B. Silverman, and R. W. Dickinson, Nucleonics 10, 12, 65 (1952).

[27] R. Blomgren, E. Hart, and L. Markheim, Rev. Sci. Instr. 24, 4, 298 (1953).

[28] L. Brownell, W. Meinke, I. V. Nehemias, and E. W. Coleman, Chem. Eng. Progr. 49, 11, 569 (1953).

[29] I. V. Nehemias, L. E. Brownell, W. W. Meinke, and D. E. Harmer, Am. J. Phys. 22, 8, 511 (1954).

[30] I. G. Lewis, I. V. Nehemias, D. E. Harmer, and I. I. Martin, Nucleonics 12, 1, 40 (1954).

[31] W. F. Bland, Petroleum Processing 10, 1, 43 (1955).

[32] Health Regulations and Standards for Work with Radioactive Isotopes (State Medical Press, 1955).

[33] R. F. Obrycki, R. M. Ball, and W. C. Davidson, Nucleonics 11, 7, 52 (1953).

[34] H. A. Schwarz, and A. O. Allen, Nucleonics 12, 2, 58 (1955).

[35] Science 121, 23 (1955).

[36] W. S. Eastwood, Nucleonics 13, 1, 52 (1955).

[37] V. Bochkarev, I. Keirim-Markus, M. Lvova, and Ya. Pruslin, Measurement of the Activity of Sources of Beta and Gamma Radiation(Moscow, 1953).

[38] M. Brucer, Nucleonics 12, 6, 58 (1954).

Received May 9, 1956.

THE ENERGY OF RADIATIONS AND SOME LAWS OF THEIR ACTION ON BIOLOGICAL OBJECTS

E. S. Shchepotyeva

Modern views are presented on the primary physicochemical stage of the mechanism of the biological action of ionizing radiations and on certain laws of their action on biological objects, determined by the space and time distribution of the radiation energy in the organism.

The rapid development of nuclear physics and nuclear technology has made available different types of radiations with a very wide range of energies – from hundredths of an electron-volt (thermal neutrons) to billions of electron-volts. Despite their diversity, all these radiations may have a biological action.

The biological effect is brought about by the energy of the radiations, but depends only on that part of the energy which is absorbed in the organism during the irradiation, termed the integral absorbed dose. Thus, the biological action depends not so much on the total energy of the given radiation, as on the combination of a number of properties of the radiation (particle charge, mass, velocity, etc.) which determine what proportion of the energy of the given radiation will be absorbed by a particular biological object. For example, radiations consisting of particles with relatively high charge and lower velocity (α-particles, recoil nuclei, fragments from nuclear fission of uranium, etc.), by reacting more vigorously with the molecules of the substance through which they penetrate than rapidly moving singly-charged particles (fast electrons, etc.) expend their energy over a considerably shorter path. Thus, one extremely important characteristic of radiation from the viewpoint of its biological effect is the linear absorption of radiation energy in the organism [1]. This value is usually measured in kiloelectron-volts per 1 micron of path through tissues. The linear absorption of radiation energy in the organism varies in very wide limits according to the type of radiation and its energy (Table 1).

On the basis of the data in Table 1 it is possible to estimate the variation of the biological effect with the magnitude of the linear energy absorption in the organism. The last column of this table shows some values of the so-called relative biological effectiveness of radiation, indicating, for equal doses of absorbed radiation, how many times as large (or as small) is the biological action of a given type of radiation relative to the action of ordinary ($\sim$ 200 kv) x-rays. This value greatly depends on the biological object in question, its state, stage of development, method of irradiation, etc., but there is no doubt that for most objects, and in particular for all multicellular objects, the effectiveness of the radiation increases with increase of the linear energy consumption in the organism.

The influence of the linear absorption of the radiation energy in the organism (Tradescantia microspores) on the biological effect is also illustrated by Fig. 1 [7]. The upper part of the figure shows the biological action of one form of radiation, deuterons with energy 190 Mev, but with different linear energy absorption in the organism because on one occasion the action of the radiation in the initial stages of the path was used, and on the second occasion, near the end of the path. It is seen that the biological effect is very different, being much greater at 20 kev/micron than at 0.73 kev/micron. The lower part of the figure shows the biological action of different forms of radiation: x-rays, deuterons with energy 190 Mev, and α-particles with energy 380 Mev, so chosen that the linear energy absorption in the organism was the same in all cases ($\sim$ 3 kev/micron). In this case the biological action was practically the same for all the radiations.

TABLE 1

Linear Energy Absorption and Relative Biological Effectiveness of Various Types of Radiation

Ionizing particle	Radiation	Linear energy absorption, kev per micron	Relative biological effectiveness	Literature references
Electron	β-and x-rays (20-30 mev)	0.3	0.3-1.0	[2], [3], [1]
	Hard β-, γ-rays from natural or artificial radioactive isotopes	0.3-0.4	0.4-1.0	[2], [4], [1]
	Hard x-rays (1000 kv)	0.5	1.0	[2], [1]
	X-rays (200-250 kv)	2.7	1.0	[2], [4]
	Tritium β-rays	5.0	1.3-1.6	[4]
Proton	Fast neutrons (8-14 mev)	6.6-12.8	1.6-5.2	[2], [4], [1]
	Neutrons in some nuclear reactions	28-37	1.3-16	[2], [4], [5], [1]
	Neutron radiation	to 100	–	[6]
Deuteron	190 mev (at beginning of range)	0.73	–	[7]
	190 mev (at end of range)	5-30	–	[7]
α-Particle	Fast helium nuclei (380 mev)	2.9	–	[7]
	Helium nuclei (accelerator)	44	–	[1]
	α-Rays from radioactive isotopes	100-170	up to 10	[2], [8], [9] [4], [1]
	The reaction B(n, α) Li	330	–	[2]
C nuclei	Carbon nuclei, 120 Mev (cyclotron)	220	(1)	[9]
C, N, O, nuclei	Cosmic radiation	1170	–	[10]
Fe nuclei	Cosmic radiation	3340	–	[10]

The fact that the linear energy absorption in the organism is not constant along the path of a moving particle is of great significance in radiobiology. The linear energy absorption increases with retardation of the particles, and reaches a maximum in the so-called "tails", i. e., near the ends of the particle paths [10-12]. Accordingly, radiation has the greatest effect at these places. This property is often used in medical applications of radiations (in particular, in the treatment of malignant tumors) to create directed radiation, such that definite regions of the organism should be irradiated most intensively, while the surrounding tissues receive only little radiation. It is evident that a good knowledge of the physical characteristics of each type of radiation, and of its behavior in the tissues of the organism, is required to produce such radiation. Fig. 2 shows the distribution of the radiation doses (the dose is the energy absorbed by unit mass of the substance) in the organism for three different types of radiation [13]. It is easily seen that with the use of electrons with energy of 16.4 Mev it is possible to obtain fairly uniform irradiation of the layer of tissue to a depth of ~ 5 cm, while with the use of a beam of deuterons with energy 190 Mev it is possible to obtain intensive irradiation of a restricted region at a depth of about 13 cm. with only slight irradiation of the remaining tissues.

However, this characteristic – the amount of radiation energy expended in 1 micron of path through the tissues – does not give a deep enough insight into the nature of the observed effects and does not make it possible to establish a causal relationship between the biological action of radiation and the nature of the microspatial distribution of the radiation energy in the organism. To establish such a relationship it is necessary to examine the phenomena which occur in the organism immediately after the action of radiation on it – the primary physicochemical stage of the long chain of processes which together constitute the biological effect of radiation.

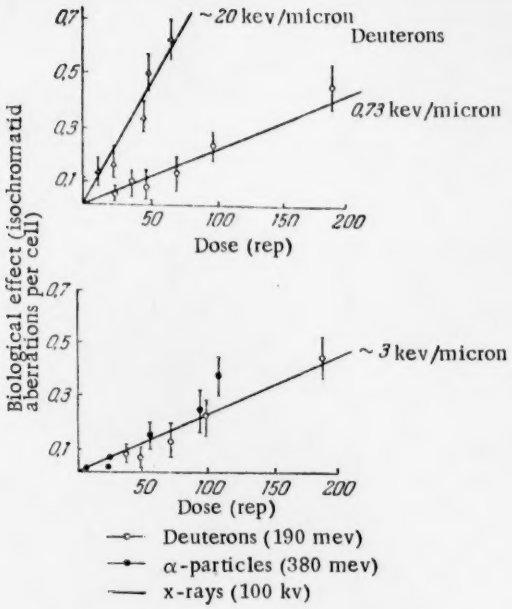

Fig. 1. Variation of biological action with the linear energy absorption in the organism.

It is known that when radiation acts on biological objects, energy is expended for ionization and excitation of the molecules. Each act of ionization and excitation requires the expenditure of a certain amount of radiation energy, and therefore a larger or smaller consumption of radiation energy along 1 micron of path through the organism indicates a larger or smaller density of the ions or excited molecules along the path of the particle. When radiation acts on living objects, either molecules of water or other molecules, some of them biologically important, such as complex protein molecules, enzymes, etc., may be ionized or excited. Since water forms about 3/4 of the total weight of a living organism, the probability of the first process is relatively high. The first route is known as indirect, and the second as direct action. More importance is at present attached to indirect than to direct action in the irradiation of living organisms [14, 15].

In the direct action of radiation, the high density of ionized and excited atoms entering the composition of complex protein molecules probably leads to greater structural disturbances in molecules, which is probably the cause of the greater biological action of radiation with a high linear expenditure of energy [16].

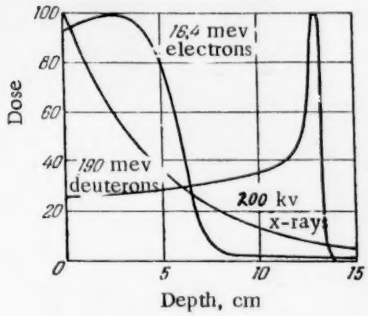

Fig. 2. Distribution of radiation doses in the organism on irradiation by x-rays, electrons with energy 16.4 mev, and deuterons with energy 190 mev.

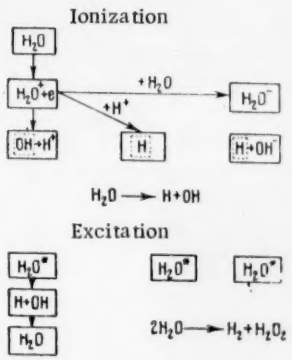

Fig. 3. Scheme for the ionization and excitation of water molecules.

In the ionization and excitation of water molecules which form part of the organism, the radiation energy exerts a biological effect by the indirect route. Ionized water molecules are unstable and decompose to form hydrogen atoms, H, and OH radicals (Fig. 3). The excited water molecules, on colliding, may form so-called molecular decomposition products of water, H_2 and H_2O_2 [17, 18]. Thus, the density of the ionized and excited water molecules present determines in this instance the nature of the distribution of H atoms, OH radicals and the molecular decomposition products of water H_2 and H_2O_2 in the irradiated space, which in turn determines the nature and the probability both of their interaction, and of their reactions with the molecules of complex organic substances.

No methods have as yet been developed for the direct determination of these reactants in biological material, but all the above is confirmed by a number of indirect proofs, and also by direct determinations in solutions by the so-called chemical dosimetry [19].

Table 2 contains data which show that radiations with different linear energy absorptions lead to the formation of different relative amounts of the radicals H and OH, on the one hand, and of the molecular decomposition products of water, H_2 and H_2O_2 on the other[20].

TABLE 2

Yields of Molecular Products (H_2 and H_2O_2) and of Radicals (H and OH) in the Action of Different Types of Ionizing Radiations on Aqueous Solutions

Radiation	Linear energy absorption, kev per micron	% reaction of H and OH radical formation	% reaction of H_2 and H_2O_2 molecular product formation
Ultraviolet radiation < 2000 A	–	100	0
γ-radiation from Co^{60}	0.4	76	24
x-rays, 2 Mev	0.4	77	23
β-rays from H^3	5.0	70	30
α-rays from Po^{210}	150	12	88
α-rays from the reaction B(n, α)Li	330	8	92

Fig. 4, a diagrammatically shows the disposition of ionized and excited molecules along the paths of α-and β-particles, and Fig. 4,b shows the corresponding distribution of radicals and molecular decomposition products of water. The low frequency of ionized and excited molecules along the paths of β-particles (right-hand side of the figure) results in an infrequent and more or less regular distribution of these active reactants, the distances between H atoms and OH radicals being relatively greater and more or less equal to each other. The disposition of the active particles along the paths of the α-particles (left-hand side of the figure) is very irregular [21]: OH radicals and molecular H_2O_2 are densely situated along the particle paths, while the hydrogen atoms, H, are found mainly in the outside regions of the column, where electrons are ejected during ionization (see Fig. 3). The different spatial distribution of the active substances as the result of the action of radiations with high and low linear energy absorptions leads to different probabilities of reactions between them. It is evident that Reactions 1 and 2 (Fig. 4, c) will be more probable under the action of radiations with higher linear energy absorptions, while Reaction 3 will be more probable with low values. The relatively greater probability of the recombination reaction of the H and OH radicals to form water under the action of radiations with low linear energy absorptions partly explains the lower biological effectiveness of such radiations.

The course of the subsequent reactions depends on the probabilities of Reactions 1, 2, and 3 occurring for radiations with different linear energy absorptions. For example, the highly active oxidants HO_2 and H_2O_2 may be formed in appreciable amounts, under the action of radiations with low linear energy absorptions, only in presence of oxygen (see Fig. 4, c on the right), while under the action of radiations with high linear energy absorptions these oxidants are easily formed even in absence of oxygen; moreover, free oxygen may be formed in the tissues under the action of such radiations (Fig. 4, c, on the left).

The powerful oxidants formed, and also the reducing agent H_2, produce changes in the normal oxidation -- reduction processes, influence metabolism, and initiate a whole series of different reactions which ultimately constitute the biological effect. It is therefore not suprising that the nature of the distribution of the ionized and excited molecules determines the various laws of the biological action of radiations.

For example, one of the most important laws of the biological actions of radiation is that the biological effect increases with increase (up to a certain limit) of the oxygen concentration in the irradiated object or in the surrounding medium, and diminishes with decrease of this concentration – the so-called "oxygen effect"

in the action of radiation. However, this is true only for radiations with a low linear energy absorption; for radiation with moderate linear energy absorption (protons, neutrons, etc.) the effect is exhibited slightly, while for radiations with high linear energy absorptions (α-particles, deuterons) it is not found at all. This is understandable in the light of the foregoing: in the action of radiations with low linear energy absorptions the presence of oxygen increases the probability of formation of powerful oxidants, while in the action of radiations with high linear energy absorptions external oxygen is not needed, as in that case it is formed in the tissues in sufficient quantities.

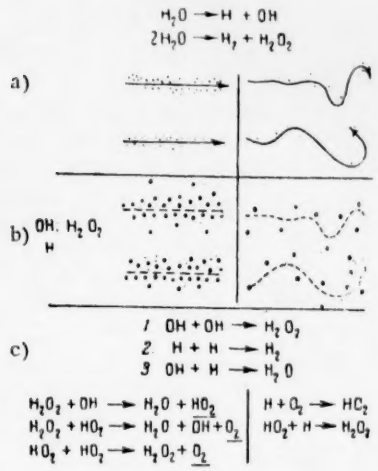

Fig. 4. Distribution of ionized and excited molecules along the paths of α-and β-particles a); the corresponding distribution of radicals and molecular decomposition products of water b); and possible reactions between them c).

The existence of the "oxygen effect" for radiations with a low linear energy absorption, and absence of this effect for radiations with a high linear energy absorption, affects the important question of protection of the organism against the action of radiations. The protective action of certain substances introduced into the organism depends on the fact that they absorb the oxygen present in the organism and so prevent the formation of powerful oxidants in the organism during irradiation. However, while they are protective against the action of radiations with low linear energy absorption, such substances have practically no protective action against radiations with a high linear energy absorption as has been already confirmed by a number of investigations [22].

The routes indicated above for the development of the biological effect under the action of radiation are probably far from the only ones possible. For example the role of the electrons formed as the result of ionization of water or tissues is still not quite clear [23]. While the energy of these electrons is high enough, they can themselves produce ionization and electron excitation of the molecules, but their subsequent behavior, as the so-called subexcitation electrons, i. e., electrons with energy less than the energy of electron excitation of water molecules, is unknown. The number of such electrons is in general large, because each act of ionization leads one way or another to the appearance of a subexcitation electron, and consequently their total energy may be relatively large. It is presumed that the role of these subexcitation electrons may be very considerable if the medium contains a low concentration of some component which requires small amounts of energy for ionization or excitation. It is also possible that the energy of these electrons is used in various relaxation processes (increases of the vibration or rotation energy of the molecules, etc.).

The role, in the biological action of radiation, of the visible or ultraviolet light which excited molecules can emit is also not clear. Radiations with different linear energy absorptions differ in their power of inducing fluorescence in water; in particular, γ-radiation with a linear absorption of 0.3 kev/micron produces a distinct fluorescence spectrum, while soft x-rays with a linear absorption of $\sim$ 3 kev/micron do not produce fluorescence [24]. Nevertheless, the intensity of this luminescence is very low, and it is unlikely that it has a significant effect in the biological action of radiation.

In relation to the question of the routes by which radiation energy can lead to biological effects, particular interest attaches to the possibility of the migration of energy in living matter [25]. The migration of energy is understood to mean the following:

A quantum of electron excitation energy transmitted to one center of an extended system (for example, as the result of absorption of a photon) is transferred without loss to a second center at a considerable intermolecular distance from the first, and there exerts its action. An important feature of the migration of energy is the peculiar directed displacement, observed in some instances, of the quantum toward those centers where its energy can be

utilized [26]. This process has been extensively studied in relation to the fluorescence of crystals, and in a number of other systems [27]. The migration of energy has been demonstrated in complex organic macromolecules, and it has been found that some added substances exert a protective effect under the direct action of radiation, when the irradiation is carried out in absence of water and the indirect effect is excluded [28]. The existence of energy migration in organic macromolecules may play an important part in the biological action of radiations, as this process may lead to a concentration of energy in some special components of these molecules, in appropriate acceptors, where this energy will exert its effects. However, migration of energy directly in the living organism has not yet been convincingly proved, although this question arouses considerable interest and many investigations have been devoted to it.

We have considered the microspatial distribution of radiation energy in organisms, and some laws of the biological action of radiation which depend on this distribution. We see that in a complex multicellular organism the macrospatial distribution of radiation energy should also have a strong influence on the biological effect of radiation. Many investigations show that even with equal radiation doses, different biological effects are produced by irradiations of diverse character – total irradiation, irradiation of different regions of the organism, different organs, etc. [29]. This largely provides the basis for the therapeutic uses of radiations.

For example, in the treatment of malignant tumors it is necessary to carry out local irradiation of isolated regions of the organism, sometimes deeply situated. External irradiation by various forms of hard, penetrating radiation is most commonly used for this purpose: γ-rays, electrons and high-energy deuterons (see Fig. 2). Another device used is the introduction into the malignant tumor of radioactive colloidal gold, or introduction of boron with subsequent irradiation of the tumor by neutrons, so that the nuclear reaction $B^{10} + n \rightarrow Li^7 + He^4$ takes place in the tumor and the latter is subjected to intense irradiation by α-rays, which are highly effective biologically, while the surrounding tissues are practically unharmed.

In the treatment of skin diseases strictly local irradiation of the surface skin layers is also necessary, so that the deeper organs and tissues escape irradiation as far as possible. For such irradiation soft radiations of low penetrating power are used, such as β-radiation from radioactive phosphorus, used as an external application [30], α-rays from radon, used as radon ointments [31, 32], α-rays from thorium X, used in the form of alcoholic solutions, lacquers, and ointments [33, 34], α-rays from thoron disintegration products (thorium C and thorium C'), used as "radioactive bandages" [35], i. e., by application to the affected places of gauze with an active deposit of thoron (radioactive isotopes thorium B, thorium C, thorium C', and thorium C").

This last method of irradiation, by local irradiation by radioactive bandages, has also proved highly effective for the treatment of some diseases involving painful conditions (radiculitis, diseases of the joints, etc.), since such irradiation has pronounced analgesic properties [36].

In the treatment of many other diseases – cardiovascular, nervous, gynecological, metabolic, etc. – the best effects are obtained by total irradiation of the whole organism [37]. Such irradiation is used, in particular, in health resort practice, by means of such procedures as radon baths [38], the inhalation of radon-enriched air in emanatoria [39], etc. [40].

Although the nature of the macro-and microspatial distribution of radiation energy in the organism plays a very important role in the biological action of radiation, the course of the absorption of energy in the organism with time is no less significant. As is known, the organism responds in a particular way to every stimulus, and the course of this reaction with time may vary greatly not only in different organisms but in the same organism according to the stage of its development, functional state, etc., and also according to the nature of the stimulus.

Thus, the observed biological effect is at any given moment the result of two processes – the action of the irradiation itself, and the reaction of the organism. Because of this, a very important characteristic from the aspect of the biological action is the dose rate, which is the amount of radiation energy supplied to the organism in unit time. In most cases the biological effect is greater at higher dose rates (compared for equal integral doses), as in such cases the recovery processes in the organism do not have time to develop fully [41]. Radiations with higher linear energy absorption apparently produce a biological effect less dependent on the dose rate than radiations of low linear energy absorption [5]. In particular, fast electrons with energy 3 Mev, in acting on the human skin (during observations of the appearance of erythema) show a distinct increase of the effect with increasing dose rate, while for soft x-rays the effect is almost independent of the dose rate [42].

A similar influence on the biological effects of radiation is produced by fractionation of the radiation, i. e., irradiation which is not continuous, but given at intervals [41, 43, 44]. In most cases fractionation, by giving the organism a better opportunity of using its adaptation and recuperation powers, results in a smaller biological effect than continuous irradiation. The duration both of the irradiation periods and of the intervals between them, is, of course, very important. In these cases also radiations with different linear energy absorptions produce somewhat different results.

It follows from the foregoing that the distribution of the radiation energy in the organism both in space and in time is of very great importance for the biological action of radiation. However, this question is very complex, and despite the large number of investigations devoted to it the problem cannot be regarded as solved. Much more research is still required on the dependence of biological action on the form of radiation and its distribution in time.

LITERATURE CITED

[1] R. E. Zir* Rad. Biology I, part I (A. Hollaender 1954) p. 315.

[2] W. Dittrich, and G. Schubert, Strahlentherapie 92, 4, 532-554 (1954).

[3] H. Gärtner, Strahlentherapie 96, 3, 378-395 (1955).

[4] J. B. Storer, J. E. Furchner, and A. T. Krebs, J. Aviation Med. 25, 4, 368-377 (1954).

[5] H. H. Vogel, Jr., and S. P. Stearner, Rad. Res. 2, 6, 513-522 (1955).

[6] H. H. Rossi, and W. Rosenzweig, Rad. Res. 2, 5, 417-425 (1955).

[7] N. H. Giles, and C. A. Tobias, Science 120, 3128, 993-994 (1954).

[8] M. M. Elkind, and C. A. Beam, Rad. Res. 3, 1, 88-104 (1954).

[9] J. A. Sayeg, and A. C. Birge, Rad. Res. 1, 6, 560 (1954).

[10] H. J. Schaefer, J. Aviation Med. 25, 4, 338-350, 392-398 (1954).

[11] T. J. Arnason, and M. Morrison, Rad. Res. 2, 1, 91-95 (1955).

[12] M. Lefort, J. chim. phys. 47, 7-8, 624-643 (1950).

[13] C. A. Tobias, H. O. Anger, and J. H. Lawrence, Am. J. Roentgen. Radium Therapy Nuclear Med. 67, 1, 1-27 (1952).

[14] E. Ya. Graevsky, Progr. Mod. Biol. 37, 2, 158-176 (1954).

[15] B. N. Tarusov, Fundamentals of the Biological Action of Radioactive Radiations (State Medical Press, 1954).

[16] R. Setlow, and B. Doyle, Rad. Res. 2, 1, 15-25 (1955).

[17] P. I. Dolin, Symposium on Radiation Chemistry, part 1 (Acad. Sci. USSR Press, 1955) pp. 7-23.

[18] H. A. Dewhurst, A. H. Samuel, and J. L. Magee, Rad. Res. 1, 1, 62-84 (1954).

[19] E. J. Hart, and P. D. Walsh, Rad. Res. 1, 4, 342-346 (1954).

[20] E. J. Hart, Rad. Res. 1, 1, 53-61 (1954).

[21] G. M. Frank, Symposium, The Biological Action of Radiation and Clinical Aspects of Radiation Sickness (State Medical Press, 1954) pp. 50-55.

[22] H. M. Patt, J. W. Clark, and H. H. Vogel, Proc. Soc. Exper. Biology and Medicine 84, 1, 189-193 (1953).

[23] R. L. Platzman, Rad. Res. 2, 1, 1-7 (1955).

---

*[Remainder of name illegible in original – publisher's note].

[24] H. Maier, Strahlentherapie 91, 4, 566-575 (1953).

[25] N. V. Ril, Progr. Phys. Sci. 35, 2, 186-212 (1948).

[26] A. N. Terenin, Progr. Phys. Sci. 43, 3, 347-379 (1951).

[27] A. N. Terenin and V. L. Ermolaev, Progr. Phys. Sci. 58, 1, 37-68 (1956).

[28] P. Alexander, and A. Charlesby, Nature 173, 4404, 578-579 (1954).

[29] M. N. Swift, S. T. Taketa, and V. P. Bond, Rad. Res. 1, 3, 241-252 (1954).

[30] The Use of Radioactive Phosphorus for the Treatment of Skin Diseases (State Medical Press, 1955).

[31] K. Lange, and R. D. Evans, Radiologie 48, 5, 514-516 (1947).

[32] B. V. A. Low-Beer, and R. S. Stone, Radiology 46, 2, 149-158 (1946).

[33] H. Gartmann, Z. arztliche Fortbildung 46, 1/2, 2-7 (1952).

[34] V. H. Witten, E. W. Braker, V. Holmstrom, and R. Loevinger, J. Invest. Dermatol. 21, 4, 249-257 (1953).

[35] G. A. Gusterin, Bull. Roentgenalogy and Radiology (USSR) 1955, No. 3, 107-111.

[36] A. F. Tretyakov, J. Neuropathol. Psychiatry (USSR) 55, 9, 689-694 (1955).

[37] H. Thaler, Radioaktive Isotope in Klinik und Forschung, Sonderbände der Strahlentherapie V. 33 (1955) pp. 56-59.

[38] E. S. Shchepotyeva, Artificial Radon Baths and Methods of Their Preparation (State Medical Press, 1949).

[39] J. Pohl-Rüling, F. Scheminzky, Stranhlentherapie 95, 2, 267-282 (1954).

[40] F. Scheminzky, Radioaktive Isotope in Klinik und Forschung, Sonderbande der Strahlentherapie V. 33 (1955) pp. 43-49.

[41] R. Rugh, and H. Clugston, Rad. Res. 1, 5, 437-447 (1954).

[42] R. K. Kepp, and K. Müller, Strahlentherapie 88, 1, 139-149 (1952).

[43] D. Hofmann, and K. Müller, Strahlentherapie 95, 2, 296-301 (1954).

[44] G. Oehlert, Strahlentherapie 95, 2, 291-295 (1954).

Received May 8, 1956.

LETTERS TO THE EDITOR

BERYLLIUM PHYSICS REACTOR

A. K. Krasin and B. G. Dubovsky

In addition to materials like graphite and heavy and ordinary water it is possible to use beryllium as a neutron moderator in nuclear reactors.

In order to study the physical properties of a reactor with a beryllium moderator, in August of 1954, at the atomic electric-power station of the Academy of Sciences USSR, a BPR reactor with a beryllium-metal moderator was put into operation.

The reactor fuel was a water solution of uranium U_3O_8 with 10% concentration of the U^{235} isotope.

The core of the BPR reactor, composed of beryllium blocks 160 x 160 x 40 mm is a cylinder 960 mm high and 1040 mm in diameter.

The weight of the core is 1200 kg. The beryllium density is 1.78 g/cm^3. Fabrication techniques for beryllium and its physical properties have been described in [1, 2]. The reactor core has vertical channels which form a rectangular lattice with a mesh 107 x 64 mm.

A channel 17 mm in diameter located in the center of each element of the cell is surrounded by six channels 14.5 mm in diameter arranged on a radius of 20 mm. In addition there are 108 horizontal channels 31 mm in diameter.

The fuel is contained in elements of tubular construction. In each element the U_3O_8 solution fills an annular space formed by two thin-walled coaxial steel tubes 13.4 x 0.2 mm and 9.0 x 0.4 mm in diameter.

The height of the solution which fills the gap is 960 mm; 214 grams of U_3O_8 are contained in each element.

The central channels of the elementary cells, the horizontal channels and the inner tubes in the elements are used to study the effects of water on the multiplication parameters of the reactor medium.

The reactor is controlled by two cadmium rods 8.2 mm in diameter and 960 mm long. In addition there are eight cadmium rods of the same dimensions which serve as protection against accidents.

The activity level in the reactor is monitored by boron proportional counters and ionization chambers. A concrete wall 1 m thick serves to protect personnel from radiation.

The critical mass for various modifications of the multiplying medium was achieved by gradually charging the elements from the center toward the periphery. In order to start the reactor safely a Po + Be neutron source with an intensity of $\sim 10^6$ neut./sec is placed inside.

Using the degree of charging and several detection instruments curves were plotted showing the reciprocal of the counting rate $\frac{1}{n} = f(N)$ where n is the number of counts per unit time with N charged uranium elements.

A version of the uranium-beryllium reactor with no water is realized by charging six elements in a cell. Graphite inserts of appropriate dimensions are placed in the center channels of the cells, in the tubes of the elements and the horizontal channels.

The system becomes critical when 366 uranium elements (6.66 kg U^{235}) are charged. In this case beryllium side reflectors 15.5 cm thick were used; there were no front reflectors.

The change over to a nonreflected reactor is accomplished by removing the upper layers of beryllium blocks and charging the elements of all the cells of the core. The critical charge in this case is 11.73 kg U^{235} and the height of the reactor is 89 cm.

Type of reactor	Radius of active zone, cm	Thickness of reflector, cm	Critical mass (kg U^{235})	
			experimental	theoretical (multigroup method)
Bare reactor with side reflectors	36.5	15.5	6.66	7±1.4
Bare reactor without reflectors	52	—	11.73	12±1.6
Bare circular reactor	42	20 *)	12.66	
Reactor with water in the elements	26.2	25.8	3.42	

*) Diameter of the column formed by the uncharged channels.

Under these same conditions (with no water and a charge in six elements of each cell) a reactor in which there is a thermal column at the center can be obtained. With a total height for the beryllium core of 960 mm only the peripheral cells are charged. The system becomes critical when 696 elements are charged and the diameter of the nonactive central is 20 cm.

The data pertaining to these various reactor modifications are presented in the table. For comparison there are also presented data on the critical charge when the inner tubes of the uranium elements are filled with water.

In the version which contains a thermal column at the center the thermal neutron density is four times greater than the average neutron density in the active zone; in the version without the thermal column, which uses reflection, the maximum neutron density is 13% greater than the average density.

The critical charge calculations, based on a multi-group analysis, were carried out by G. I. Marchuk and V. V. Smelov.

E. I. Inyutin, M. N. Lantsov and Yu. Yu. Glazkov participated in this work.

In conclusion we wish to express our thanks to the scientific director of the atomic electric-power station, Prof. D. I. Blokhintsev for his interest and for valuable suggestions and also to M. E. Minashin and Yu. A. Sergeev for participating in the discussion of the results.

Received June 12, 1956

LITERATURE CITED

[1] A. K. Krasin, I. G. Morozov, L. A. Geraseva and A. V. Kamaev, "Physical investigations", Reports of the Soviet Delegation to the International Conference on Peaceful Uses of Atomic Energy (Acad. Sci. USSR Press, 1955), p. 142.

[2] G. A. Meerson, G. E. Kaplan, G. F. Silina and D. D. Sokolov, "Geological, chemical and metallurgical investigations", Reports of the Soviet Delegation to the International Conference on Peaceful Uses of Atomic Energy, (Acad. Sci. USSR Press, 1955), p. 125.

THE CROSS SECTION FOR THE REACTION Li^7 (d, p) Li^8 AS A FUNCTION OF DEUTERON ENERGY IN THE RANGE 1.1-4 MEV.

L. S. Bezrukov, D. A. Panov, D. V. Timoshuk

The dependence of the cross section for the reaction Li^7(d, p) Li^8 on deuteron energy has been investigated in a number of references [1-3] in the region 0.4- 3.3 Mev. In the high energy region the results of these measurements are contradictory and not very accurate. In the present work deuterons with an incident energy of 4.0 ± 0.05 Mev from the 70 cm cyclotron from the Academy of Sciences USSR were used. The energy was varied by degrading the deuterons in a stack of aluminum foils. The final energy was determined from the range-energy relation for aluminum [4 - 6]. The reaction yield was measured by the β-activity in the Li^8. The targets were lithium fluoride deposited by vacuum evaporation. The target thickness was 0.12 g/cm^2. The activity was measured with the beam shut off. The switching cycle, provided by a mechanical commutator, was as follows: after irradiation of the target for one second the cyclotron was shut off and the β counter was successively connected for one second to three detectors. One second after the last detector was cut off the target was again irradiated for 1 sec and the whole cycle was repeated. Using the data from the three counters the β-activity in the Li^8 (λ = 0.824 sec^{-1}) could be reliably separated from the activity due to background contamination. The total integrated deuteron flux was measured while the targets were being irradiated. The Li^8 decay in the target during irradiation was taken into account by introducing a current drain with a time constant equal to the decay constant for Li^8 into the integrating circuit.

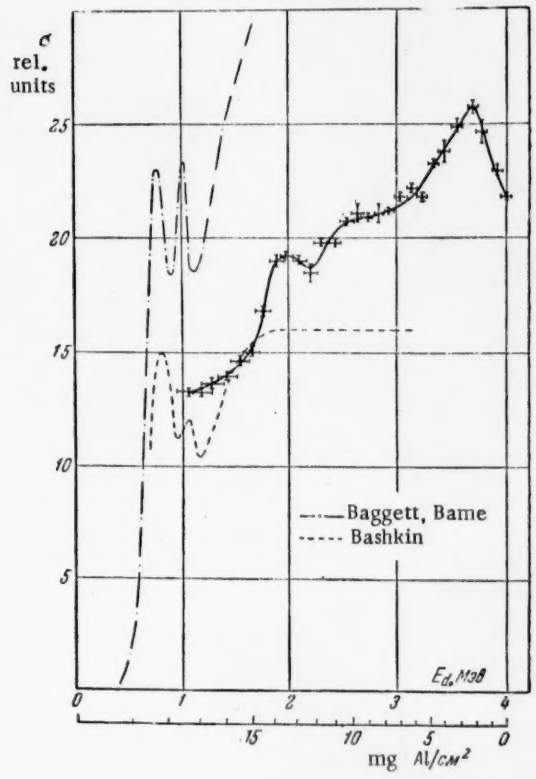

Excitation curve for the reaction Li^7(d, p) Li^8.

The results of the measurements are shown in the graph. The data obtained in [2, 3] are also given. The cross section for this reaction exhibits clear resonances at deuteron energies of 2.0, 2.5 and 3.7 Mev. These resonances correspond to levels in the intermediate nucleus Be^9 having energies of 18.3, 18.7 and 19.6 Mev. These results, which indicate the existence of a level in Be^9 at an energy of 18.3 Mev coincide, within the limits of our accuracy, with the results of a study of the reaction Be^8 given in [2], [7] and [8] in which this level was also found.

We are indebted to N. P. Bondartsev, A. F. Zaitsev, V. L. Mazurov and A. S. Rychev

for providing uninterrupted operation of the cyclotron.

Received March 1, 1956.

LITERATURE CITED

[1] W. E. Bennett, T. W. Bonner, H. T. Richards and B. E. Watt, Phys. Rev. 71, 11 (1947).

[2] L. M. Baggett, S. J. Bame, Phys. Rev. 85, 434 (1952).

[3] S. Bashkin, Phys. Rev. 95, 1012 (1954).

[4] R. R. Wilson, Phys. Rev. 60, 749 (1941).

[5] H. A. Bethe, Rev. Mod. Phys. 22, 213 (1950).

[6] S. K. Allison and S. D. Warshaw, Rev. Mod. Phys. 25, 779 (1953).

[7] W. Whaling, J. E. Evans and T. W. Bonner, Phys. Rev. 75, 688 (1949).

[8] F. Ajzenberg, and T. Lauritsen, Rev. Mod. Phys. 22, 77 (1955).

REMARKS ON MIRROR ASYMMETRY IN NUCLEI

B. M. Strutinsky

An analysis of the experimental data on α-decay in certain heavy even-even nuclei has revealed low-lying states for the daughter nuclei with spin 1 and odd parity (daughter nuclei: Pu^{238}; $Ra^{222, 224, 226}$; $Th^{226, 228}$) [1].

A. Bohr [2] has reported an interpretation of these levels, given by Christie, in which it is assumed that these are excited collective levels associated with the asymmetry of the nuclear shape with respect to reflection in a plane perpendicular to the nuclear symmetry axis ("pear-shaped"). If the shape of the nuclear surface which is asymmetric under reflection is stable, each of the levels for the asymmetric surface oscillations about the equilibrium configuration should be doubly degenerate because there are two stable surface shapes, one of which is the mirror image of the other (Fig. 1). This degeneracy is removed by virtue of the tunnel effect between these these two nuclear configurations (Fig. 1). Thus each level of the asymmetric oscillations is split in two with a spacing between equal to $h\omega_T$ where ω_T is the frequency of the tunnel transition frequency between the two conjugate nuclear shapes (in this connection see [3]). A simple analysis indicates that the parity of the wave functions which describe the asymmetric oscillations should be different in these states with the higher level having the odd parity. The nucleon states are assumed to be the same in both levels, hence the excited collective level of the nucleus should be characterized by a value for the projection of the nuclear spin along the symmetry axis K = 0 and should have a parity which is opposite to that of the ground state. This level should be the first of a series of rotational levels with spin 1, 3, 5, . . . and odd parity.

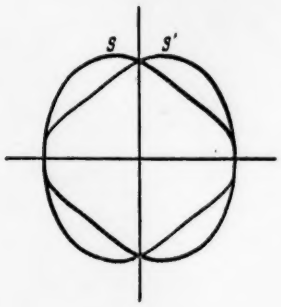

Fig. 1. Pear-shaped nuclear surface and mirror image.

The existence of a system of odd rotational levels displaced with respect to the even spin levels may be explained without recourse to a consideration of the mirror asymmetry of the nuclear shape if these rotational levels are attributed to some excited nucleon state with K = 0 and a parity opposite to that of the ground state (in anology with the theory of diatomic molecules; see, for example, [3]). However the extremely small energy of the 1^- state makes such an interpretation unplausible.

A. Bohr has not indicated a mechanism which would lead to stability for the mirror-asymmetric nuclear shape. Among other things this question is of great importance in connection with the interpretation of effects associated with asymmetric fission with which it is connected in an obvious way. Below are considered one of the possible reasons for the formation of mirror-asymmetric nuclei and the intensity of electric transitions in such nuclei.

Stability for mirror-asymmetric nuclear surfaces. In studying the stability criteria for mirror-asymmetric nuclei we shall consider very small asymmetric deformations in which perturbation theory can be used. For

small deformations the change in the nucleon energy is*

$$\Delta E_N = -\xi^2 \Sigma_n \frac{|M_{an}|^2}{E_n - E_a}, \tag{1}$$

where $\xi M_{ab} = V_{ab}$ is the matrix element; ξ is a small dimensionless parameter which indicates the degree of asymmetry, E_a is the ground state energy for nucleons in the symmetric nucleus, E_n is the energy of the excited state of the nucleons.

The changes in the Coulomb energy and surface energy are given by

$$\Delta E_c = \frac{1}{2} C_\xi \xi^2, \tag{2}$$

where C_ξ is the "liquid-drop" coefficient for nuclear deformation [4]. Comparing Eqs. (1) and (2) it is apparent that the energy of the nucleus is reduced in asymmetric deformation if the symmetric nucleus has a close-lying nucleon level with parity opposite to that of the ground state since then the following condition is satisfied

$$\frac{|M_{ab}|^2}{\Delta E} > \frac{1}{2} C_\xi, \tag{3}$$

where ΔE is the spacing between levels.

For a sufficiently large asymmetric deformation the energy of the nucleus eventually increases; however, the asymmetric deformation parameter corresponding to an equilibrium configuration for the asymmetric nucleus cannot be determined from perturbation theory.

The case of two neighboring levels can be considered by analogy with the intersection of term-levels in molecular theory. Let ψ_a and ψ_b be the wave functions for two nucleon states which have almost the same energy in the symmetric nucleus. E_a and E_b are the energies for the states a and b respectively and $E_b > E_a$. The wave functions ψ_a and ψ_b and the energy depend on parameters which characterize the deformation of the nucleus. The nucleon wave functions in the asymmetric nucleus can be written in the form $\psi_{\alpha,\beta} = C_a^{\alpha,\beta}\psi_a + C_b^{\alpha,\beta}\psi_b$. The energy for the states α and β is

$$E_{\alpha,\beta} = \frac{1}{2}(E_a + E_b) \pm \frac{1}{2}\{(E_a - E_b)^2 + 4|V_{ab}|^2\}^{1/2}, \tag{4}$$

where the indices α and β denote the plus and minus signs for the radical ($E_\alpha < E_\beta$). The nondiagonal matrix elements V_{ab} are different from zero if the a and b states are different in parity. (u and g states in terms of the theory of diatomic molecular spectra). The energy [Eq. (4)] should be considered as a mixture of the "liquid-drop" potential energy of asymmetric surface oscillations. The total potential energy of the asymmetric surface oscillations is

$$W_\alpha = \frac{1}{2} C_\xi \xi^2 - \frac{1}{2}\{(E_a - E_b)^2 + 4|V_{ab}(\xi)|^2\}^{1/2}. \tag{5}$$

It is assumed that only the low-lying states are excited.

---

* The diagonal matrix element vanishes since the perturbation operator is antisymmetric under reflection in the plane perpendicular to the nuclear axis; the off-diagonal elements are different from zero if the parity of the nucleon states is different.

If the deformation is not small, $V_{ab}(\xi) \gtrsim \Delta E$, the nucleon potential energy [Eq.(5)] is almost a linear function of $|\xi|$. Because of this the potential energy W_α has a minimum for a certain value of the parameter ξ which is different from zero. The value of the asymmetric deformation parameter which corresponds to the minimum potential energy is

$$\xi^* = \left\{ (|M_{ab}|/C_\xi)^2 - \frac{1}{4}\left(\frac{E_b - E_a}{|M_{ab}|} \right)^2 \right\}^{1/2} \qquad (6)$$

(for small ξ $V_{ab}(\xi) \approx \xi M_{ab}$). The condition for the existence of ξ^* is the same as Eq. (3). If the energy difference for the nucleon states is large Eq. (4) becomes the usual two-level perturbation-theory formula. If the energy difference between the a and b states is sufficiently large the potential energy Eq. (5) has an extremum only at $\xi = 0$.

To make an estimate of M_{ab} and C_ξ one can use the values calculated for a nuclear surface which is almost spherical [4]. According to the hydrodynamic estimate for octupole surface oscillations and $A \sim 200$, C_ξ is 250-300 Mev. The matrix element M_{ab} can be taken as of the order 20-40 Mev. In the limiting case $E_a = E_b$ (intersection of the nucleon terms) the asymmetric equilibrium deformation is approximately 1/10. The depth to the bottom of the potential well for asymmetric surface oscillations W^* (Fig. 2) is

$$W^* = \frac{1}{2}\frac{|M_{ab}|^2}{C_\xi} - \frac{1}{2}(E_b - E_a) \times \left\{ 1 - \frac{(E_b - E_a)\, C_\xi}{4\,|M_{ab}|^2} \right\}. \qquad (7)$$

For the values of M_{ab} and C_ξ we have indicated, at intersection of the levels ($E_a = E_b$) for W^* we obtain a value of the order of 1-2 Mev. Both W^* and $|\xi|$ are reduced as $E_a - E_b$ increases and become zero for

$$E_b - E_a = \frac{2\,|M_{ab}|^2}{C_\xi}.$$

Hence a nuclear asymmetry of this kind is possible only in those cases for which the spacing between nucleon levels is considerably smaller than $\frac{2\,|M_{ab}|^2}{C_\xi}$ as required by the condition given in Eq. (3).

As has been indicated above the distance between low collective levels in the potential well W_α (Fig. 2) can be very small, in particular it can be so small compared with the distance between nucleon levels that it is possible to satisfy the conditions required for adiabatic excitation of the collective states.

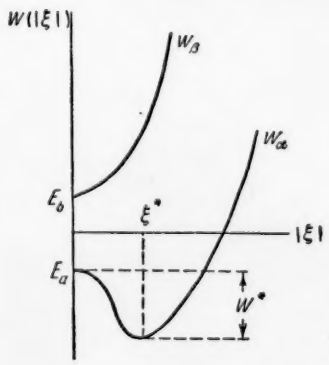

Fig. 2. Total potential energy associated with the asymmetric surface oscillations.

The instability of the symmetric nuclear form upon the intersection of the nuclear terms may be one of the factors which leads to asymmetric fission since there is a high probability for the crossing of the nucleon terms [5] and [6] in the deformation which occurs in fission.

Collective electric transitions in mirror-asymmetric nuclei. Experimentally there have been observed electric dipole radiation transitions from the 1^- state to the low-lying rotational states. Using the intensity ratio for transitions to the rotational states 0^+ and 2^+ the value of the quantum number K in the 1^- state has been determined [7]. In all cases the value K = 0 is in agreement with the experimental data. If one adopts the point of view that the low-lying 1^- states of heavy even-even nuclei are excited collective states the radiative transition which is observed should be a collective dipole transition. A collective dipole transition,

however, can occur only when the center of gravity of the proton does not coincide with the center of gravity of the nucleus [8].

This type of nuclear polarization might arise as a result of the asymmetric internal electric field in an asymmetrically deformed nucleus. Below we present an estimate of the dipole moment of a mirror-asymmetric nucleus, based on this assumption.

The equilibrium distribution of charge in the nucleus is related to the potential of the electric field by the expressions [8]

$$\begin{aligned} 8\beta\rho_z &= -\rho(e\varphi - 4\beta), \\ \Delta\varphi &= -4\pi e\rho_z, \end{aligned} \tag{8}$$

where ρ_Z is the density of protons in the nucleus, φ is the potential of the electric field corresponding to a given charge distribution, ρ is density of particles in the nucleus which is assumed to be constant

$$\left(\rho = \rho_N + \rho_z = \frac{3A}{4\pi R_0^3}\right).$$

In Eq. (8) β is a coefficient in the Weizsäcker formula for the energy of the nucleus:

$$M = \alpha A + \beta\frac{(N-Z)^2}{A} + \gamma A^{2/3} + \frac{3}{5}\frac{Ze^2}{R_0}$$

($\beta \approx 20$ Mev). In calculating the distribution of charge in the nucleus the surface is assumed fixed since the frequency of the charge-density oscillations is large compared with the frequency of the surface oscillations. We also assume that the nuclear deformation is small so that the surface can be described by the equation

$$\begin{aligned} R(\vartheta) &= R_0[1 + \Delta(\vartheta)], \\ \Delta(\vartheta) &= \sum_{l=0}^{3} \alpha_l P_l(\cos\vartheta) \ll 1. \end{aligned} \tag{9}$$

The coefficient α is determined so as to fulfill the condition for a fixed center of gravity

$$\bar{z} = \left(\int z\rho\, dv\right)\Big/\left(\int \rho\, dv\right) = 0. \tag{10}$$

Within an accuracy up to cubic terms in the deformation parameter $\alpha_1 = -\frac{27}{35}\alpha_2\alpha_3$. α_0 is determined from the conservation of nuclear volume. The value of α_0 does not affect the result hence it may be assumed that $\alpha_0 = 0$. Taking into account the relations given in Eq. (8) and (10) the dipole moment of the nucleus along the nuclear axis

$$d_0 = \int z\rho_z\, dv,$$

can be written in the form

$$d_0 = -(e\rho/8\beta)\int \varphi(r)\, r\cos\vartheta\, dv. \tag{11}$$

The integration extends over the volume of the nucleus. We expand the potential φ in a Legendre polynomial series

$$\varphi \approx e\rho_z \int \frac{dv'}{|r-r'|} = \frac{Ze^2}{R_0} \sum_l \gamma_l f_l(x) P_l(\cos\vartheta), \quad x = r/R_0. \tag{12}$$

(To calculate the potential φ as a first approximation the density of protons is assumed constant). Having substituted the expression for the potential Eq. (12) in the integral Eq. (11) and expanding the integral in powers of the deformation parameter, it is easily shown that in calculating the potential with the function $f_1(x)$, excluding the function $f_1(x)$ it is necessary to consider terms in the first power of the deformation parameter α_1, α_2 and α_3. Generally speaking $f_1(x)$ should depend on terms proportional to $\alpha_2\alpha_3$. However, direct calculation shows that $f_1(x)$ does not contain such terms. With an accuracy of the first power in the deformation parameter the function f_1 is

$$\left.\begin{aligned} f_0(x) &= \frac{3}{2} - \frac{1}{2}x^2; \\ f_{l>0} &= x^l; \\ \gamma_0 &= 1; \\ \gamma_{l>0} &= 3\alpha_l/(2l+1). \end{aligned}\right\} \tag{13}$$

Substituting Eq. (12) in the integral Eq. (11) and making use of the relations between α_1, α_2 and α_3, we find *

$$d_0 \approx 0.02 \frac{ZAe^2}{\beta} \alpha_2\alpha_3. \tag{14}$$

As can be seen from Eq. (14) the polarization of the nucleus for asymmetric deformation occurs only for strongly deformed nuclei when the symmetric quadrupole deformation α_2 is large.**

For nuclei with A $\sim$240 and Z $\sim$90 with values of the deformation parameters α_2 and α_3 equal respectively to to 0.3 and 0.1 the nuclear dipole moment is found to be 0.1 R_0. If one assumes for the dipole moment of a single-particle transition the approximate value $\alpha_{part} \sim R_0$ the collective moment should be approximately one hundred times smaller in intensity for the same energy. This difference in the transition probability can be shown to be insufficient for using the transition probability to determine whether or not a given transition is collective. In this connection great interest attaches to the probability of the electric octupole transition, for example the radiative transition $1^- \rightarrow 4^+$ or the transition $0^+ \rightarrow 3^-$ with electric excitation of the nucleus. The collective electric moment of an asymmetrically deformed nucleus is equal to

$$Q^{(3)} = \int r^3 P_3(\cos\vartheta)\, dv = \frac{3}{7} ZR_0^3\alpha_3, \tag{15}$$

and hence the collective octupole transition probability should be approximately $(Z\alpha_3)^2$ times greater than the intensity for a single-particle octupole transition at the same energy.

We wish to express our gratitude to B. T. Geilikman, V. M. Galitskom, V. G. Nosov and D. T. Grechukhin for discussion of the work and valuable suggestions.

Received March 13, 1956

* We are considering the dipole moment of the transition. Eq. (14) is the actual dipole moment operator. The diagonal matrix elements of this operator are zero.

** It is easily shown that the succeeding terms in the expansion of the dipole moment are proportional to $\alpha_2^2\alpha_3$, α_3^3 etc.

LITERATURE CITED

[1] F. Stephens, J. Asaro and I. Perlman, Phys. Rev. 96, 1568 (1954).

[2] A. Bohr, Problems of Contemporary Physics 1956, No. 1.

[3] D. D. Landau and E. M. Lifshits, Quantum Mechanics (State Tech. Press, 1948), p. 208.

[4] A. Bohr, and B. Mottelson, Problems of Contemporary Physics 1955, No. 9.

[5] D. Hill and J. Wheeler, Progr. Phys. Sci. 52, 2 (1954).

[6] J. A. Wheeler, "Fission physics and nuclear theory", Report No. 593 of the U. S. Delegation to the International Conference on Peaceful Uses of Atomic Energy," (1955).

[7] F. Stephens, J. Asaro and I. Perlman, Phys. Rev. 100, 1543 (1955).

[8] A. B. Migdal, J. Exptl.-Theoret. Phys. 15, 3, 81 (1945).

CROSS SECTION FOR INELASTIC INTERACTIONS OF 14.5 MEV NEUTRONS WITH VARIOUS ELEMENTS

N. N. Flerov and V. M. Talyzin

According to the semitransparent model of the nucleus [1-3] the dependence of the cross section for inelastic interactions σ_{in} on the radius of the nucleus for neutrons with energies of several millions of electron volts should have maxima and minima which become less distinct at higher energies [3]. It would be expected that for neutrons with energies of 14 Mev the cross section for inelastic reactions would be a monotonic function of the nuclear radius.

In the majority of experiments the cross sections for inelastic interaction of 14 Mev neutrons with matter have been measured for a small number of elements [4-8]; Strizhak [9] has obtained more complete experimental data but with poor accuracy and with a systematic deviation from the results of other authors.

In [4, ,6, 9] nuclear threshold reactions (usually Cu^{63} (n, 2n) Cu^{62}) were used. However the values for the inelastic cross sections obtained in this manner do not seem to be reliable, especially for light nuclei. In the present work *, a detector with a variable threshold was used – a scintillation counter with a stilbene crystal – and the cross section was measured for 24 elements. The detector was located at a distance of 75 cm from a zirconium-tritium target of an ion accelerator at an angle of 0° to the beam of deuterium ions. The angle of 0° was chosen to eliminate spurious neutron scattering effects in the measurements.

Spherical samples of the materials being investigated (external diameter from 7 to 13 cm and internal diameter from 3.5 to 4 cm) were positioned so that the center of the target coincided with the center of the sample.

In all samples curves were taken which showed the dependence of the ratio of counting rates with and without the sample as a function of detector threshold. In certain parts of these curves the ratios remain constant. In these the detector registers only primary and elastic neutron scattering since it is well known [5, 7, 10, 11] that in elastic scattering and inelastic interactions of 14 Mev neutrons with matter two different energy spectra are found.

A proportional counter was used as a monitor; this instrument registers the α-particles which accompany the 14.5 Mev neutrons over a given solid angle.

The background of scattered neutrons ranged from 1.5% to 0.6% of the primary neutron flux for detector thresholds from 9 to 12 Mev. In this region, because of the stilbene-crystal dimensions in our instrument, the detector was not sensitive to the γ-rays produced in the inelastic neutron interactions. With the high forward directivity of the inelastically scattered neutrons, corrections for the different detector sensitivity for primary and elastically scattered neutrons because of the longer neutron path in the sample due to elastic scattering were not needed for the majority of elements and were only 1-2% for some of the light nuclei.

In the table are shown the cross sections for inelastic interactions of 14.5 Mev neutrons as measured by the authors and others.

* The basic work was completed in 1952 (Report Acad. Sci. 1953). Measurements using a new instrument on a larger number of elements and higher accuracy were carried out in 1955.

Element	Cross sections for inelastic interactions of 14-Mev neutrons —10-24 cm^2			
	Present work	Phillips et.al.[6]	Graves and Davis [8]	Strizhak [9]
Be	0.64±0.02			
B	0.64±0.04	0.69±0.10		
C	0.73±0 02	0.76±0.04	0.601±0.006	0.63±0.05
N	0.82±0.02	0.79±0.05		
O	0.85±0.03			
Mg	0.95±0.04			1.08±0.09
Al	1.02±0.02	1.06±0.05	1.00 ±0.01	1.13±0.07
Si	1.02±0.06			
P	1.13±0,03			
S	1.15±0.03			
KCl	1.20±0,03			
Ca	1.36±0.02			
Fe	1.38±0.02	1.45±0.02	1.27 ±0.04	1.29±0.07
Cu	1.48±0,02	1.51±0.06	1.42 ±0.04	1.35±0.05
Zn	1.58±0.02		1.46 ±0.03	1.37±0.07
Se	1.77±0.06			1.40±0.23
Cd	1.92±0.03	1.89±0.06	1.95 ±0.05	1.83±0.13
Sn	1.85±0.02		1.96 ±0.05	1.81±0.13
Sb	2.06±0.04			1.90±0.16
I	2.11±0.06			1.88±0.16
W	2.48±0.03			2.35±0.14
Hg	2.65±0.04			
Pb	2.54±0.05	2.56±0.05	2.49 ±0.02	2.42±0 09
Bi	2.59±0.03	2.56±0.05	2.53 ±0.02	2.44±0.13

As can be seen from the table the present results, the work of Phillips et.al. [6], and that of Graves and Davis [8] are in good agreement; the results obtained by Strizhak [9], which are of lower accuracy do not contradict the present results. The cross section for inelastic interactions of neutrons with nuclei in almost all the elements measured in the present work is a monotonic function of the atomic weight and is given fairly well by the formula $\sqrt{\frac{\sigma_{in}}{\pi}} = (1.2A^{1/3}+2.1)\cdot 10^{-13}\,c$ (see Figure). The exceptions are the "magnetic" nuclei (tin, lead and bismuth). Apparently even at 20 Mev excitation of the intermediate nuclei , their "magnetic" properties are maintained. An unexpectedly high value for this cross section was found in calcium.*

The total cross section for 14 Mev neutrons exhibits a different dependence on atomic weight. The dashed curve shown in the figure is based on the experimental values of the total cross section obtained by

* Graves and Davis [8] have reported a preliminary value of this cross section in calcium $\sigma_{in} = (1.5 \pm 0.1)\cdot 10^{-24}$ cm^2.

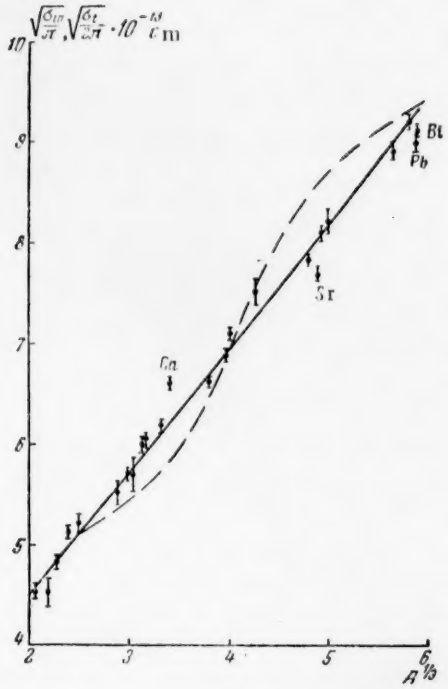

The dependence of the total cross section σ_t and the inelastic cross section σ_{in} on atomic weight (straight line

$$\sqrt{\frac{\sigma_{in}}{\pi}} = (1.2A^{1/3} + 2.1) \cdot 10^{-13} \text{ cm};$$

the dashed line is drawn according to the values of σ_t from [17]).

Coons [17] et al; this curve can not be approximated by a straight line. Consequently it is less likely that the cross section for elastic scattering of 14 Mev would show a linear dependence.

Received April 7, 1956

LITERATURE CITED

[1] H. Feshbach, C. E. Porter, V. F. Weisskopf, Phys. Rev. 90, 166 (1953); 96, 448 (1954).

[2] V. Weisskopf, "The theoretical prediction of neutron cross sections of nonfissionable elements for energies up to 10 Mev", Report No. 830 of the U. S. Delegation to the International Conference on the Peaceful Uses of Atomic Energy (1955).

[3] P. E. Nemirovsky, "Physics investigations" Report of the Soviet Delegation to the International Conference on Peaceful Uses of Atomic Energy (Acad. Sci. USSR Press, 1955), p. 287.

[4] H. T. Gitting, H. H. Barschall and G. G. Everhart, Phys. Rev. 75, 1610 (1949).

[5] B. G. Whitmore and G. E. Dennis, Phys. Rev. 84, 296 (1951).

[6] D. D. Phillips, R. W. Davis and E. R. Graves, Phys. Rev. 88, 600 (1952).

[7] E. R. Graves, and L. Rosen, Phys. Rev. 89, 343 (1953).

[8] E. R. Graves and R. W. Davis, Phys. Rev. 97, 1205 (1955).

[9] M. V. Pasechnik,"Physics research",Report of the Soviet Delegation to the International Conference on Peaceful Uses of Atomic Energy (Acad. Sci. USSR Press, 1955), p. 319.

[10] P. H. Stelson and C. Goodman, Phys. Rev. 82, 69 (1951).

[11] B. G. Whitmore, Phys. Rev. 92, 654 (1953).

[12] J. R. Conner, Phys. Rev. 89, 712 (1953).

[13] J. H. Coon and R. W. Davis, Phys. Rev. 94, 785 (1954).

[14] J. R. Smith, Phys. Rev. 95, 730 (1954).

[15] W. J. Rhein, Phys. Rev. 98, 1300 (1955).

[16] W. G. Cross and R. G. Jarvis, Phys. Rev. 99, 621 (1955).

[17] J. H. Coon, E. R. Graves and H. H. Barschall, Phys. Rev. 88, 562 (1952).

SCIENCE NEWS

ALL-UNION CONFERENCE ON HIGH ENERGY PARTICLE PHYSICS

The All-Union Conference on High Energy Particle Physics, called by the Division of Physical and Mathematical Sciences of the Academy of Sciences of the USSR in Moscow, attracted attention in broad scientific circles not only in the Soviet Union, but also abroad. More than 1000 engineers and physicists from many laboratories and institutes of the Soviet Union convened for an exchange of scientific and technical information and opinions. About 60 foreign scientists from various countries took part in the work of the conference.

The conference began its work with a plenary session, which met on May 14 in the conference hall of the P. N. Lebedev Physical Institute. In opening the session, the chairman of the organization committee, Corresponding Member of the Academy of Sciences of the USSR M. G. Meshcheryakov pointed out the necessity of uniting the efforts of the scientists of different countries for the cooperative solution of the most important problems of the physics of elementary particles.

In the first report* , which was made by A. L. Mints, representing a number of authors, an account was given of the history of the building, basic specifications, and operating experience of the synchrocyclotron of the Institute of Nuclear Problems, now under the direction of the United Institute for Nuclear Investigations. This accelerator, with magnet pole diameter 5 m, was constructed in a short time and began operation in 1949. It was first used with deuterons and alpha particles, and in 1950 protons of energy 500 Mev were obtained. As a result of a reconstruction of the accelerator in 1953 the pole diameter of the electromagnet was increased to 6 m, and the proton energy to 680 Mev. This accelerator also produces intense beams of charged π-mesons with energies up to 400 Mev, and beams of neutrons with energies up to 600 Mev. The magnet pole faces serve as the covers of the vacuum chamber, which occupies the gap of width 60 cm. The 7000 ton magnet produces a field of intensity 16,600 oersteds at the center, and falling off by 4.5% at the periphery. The special construction of the frequency modulator for the accelerating electric field provides variation of the frequency over a range from 26.5 to 13.6 Mc , and the reliability and stability of operation of the high-frequency system makes it possible to dispense with disassembling it for periods of 10,000 working hours. The main measuring devices are placed beyond a concrete wall (of thickness 5 m) containing collimating channels for the beams of particles. The control of the main accelerating apparatus is carried on from a special building. The successful operation of the synchrocyclotron has made it possible to carry out many experimental researches, some of which were reported at the conference.

V. I. Veksler told about the synchrophasotron that is being built at the Electrophysical Laboratory, designed for proton energy 10 Bev. It is also under the direction of the United Institute. This accelerator is intended for the study of the nature of nuclear forces and the properties of mesons, hyperons, antiprotons, etc. The accelerator magnet is of the ring type. It consists of four quadrants of mean radius 28 m, separated by straight-line intervals. The particles move in a vacuum chamber of cross section 200×36 cm^2, in which the pressure is about 10^{-6} mm Hg. The protons are accelerated to an energy of 8.5 Mev in a linear accelerator, and then are turned by a focusing magnet and an electrostatic condenser and introduced into the chamber of the synchrophasotron The accelerating cycle is of 3.3 seconds duration, and there are 5 cycles per minute. The beam intensity is $10^9 - 10^{10}$ protons per pulse. There is a special room for the experimental equipment, separated from the

* This report is published in this issue of this Journal.

accelerator by a concrete wall of thickness 8 m. The current supply for the magnet, the electronic apparatus, and the high-frequency system are located in a separate building. At the present time the final installation work is going on.

The report of V. V. Vladimirsky was devoted to the plans for strong focusing proton synchrotrons for 6 to 7 Bev and 50 to 60 Bev.* At the present time there are still no operating proton accelerators using this principle, but several machines are still under construction, in particular in the Soviet Union, in the USA , and in Switzerland (CERN). In the accelerator for 7 Bev the mean radius of the orbit is 40 m and the maximum magnetic field is 9500 oersteds. The dimensions of the vacuum chamber are $11 \cdot 8$ cm^2. The 2700 ton magnet consists of 98 C-shaped magnets with separate neutral poles and 14 X-shaped compensating magnets. These last decrease the path oscillations, although they somewhat increase the length of the orbit. This machine is to serve to a certain extent as a model for the development of the 50 Bev accelerator, which is intended for the observation of processes of multiple meson production, and also the creation of antiparticles for all known types of elementary particles. The critical energy in the accelerator is eliminated by means of 15 magnets with reversed field. The total weight of all 112 magnets is 22,000 tons. The magnetic field increases from 90 to 10,000 - 12,000 oersteds. The length of the orbit is 1480 m, and the dimensions of the vacuum chamber are 20 x 12 cm^2. A 100 Mev linear accelerator is used for the preliminary acceleration. The permissible error in the field is 0.25%, and the permissible displacement of the magnets is 1 mm. The number of cycles of acceleration is 6 per minute, with the time of growth of the field being 3.8 sec.

The session was concluded by the report of G. Marshall (USA) on the plan for a 15 Bev proton synchrotron, which will be built at the Argonne National Laboratory. This is a machine with weak focusing of the beam. The focusing is to be achieved by shaping of the magnet sections, because the particles will enter a section not at right angles with its side surfaces. The synchrotron magnet, producing a uniform field, will consist of eight sections. The weight of the magnet is 3500 tons. The mean radius of the orbit is about 30 m. The protons will be injected with energy 50 Mev.

On the following days the work of the conference was carried on in three sections: 1) elementary particles and their interactions; 2) accelerators of elementary particles; and 3) theoretical work on the physics of high energy particles.

The first session of the section on elementary particle accelerators was devoted to accelerators of the cyclotron type. Speaking for a number of authors, V. P. Dmitrievsky and V. I. Danilov told about the work done at the Institute for Nuclear Problems on the removal of the beam from the six-meter synchrocyclotron, and also on increasing the density of the external proton beam. The method for removing the beam consists in production at the limiting radius, in the region of the last orbits, of an artificial modification of the magnetic field, which, while maintaining the stability of the ion motion in the vertical plane, increases the amplitude of the radial oscillations. The beam deflected in this way falls into the magnetic exit channel. The new method makes it possible to remove 5 to 7% of the current circulating inside the chamber. Thus the intensity of the beam on emergence from the channel has been brought up to $7 \cdot 10^{10}$ protons per cm^2 sec. The focusing of the external beam was done with the fringing magnetic field, shaped by means of special lenses, located in the otherwise unused region of the accelerator magnet. This made it possible to increase the beam density by about a factor of three. H. Tyren (Sweden) gave a report on a synchrocyclotron giving 185 Mev energy. This accelerator is constructed underground, with the experimental space separated from the accelerator by a two-meter wall. The beam, of intensity $5 \cdot 10^{10}$ protons per second, is focused by two magnets, so that its cross section amounts to a few square centimeters. This accelerator is used for medical purposes, for the production of unstable nuclei, and also for the study of β and γ emission and other investigations.

Other questions were also considered at the first meeting. I. Kh. Nevyazhky told about some particulars of the high-frequency system of the six-meter phasotron, and Prof. Baker (CERN) spoke about the modulation system of the 600 Mev synchrocyclotron being built in Switzerland. Other reports took up particular questions of the motion of particles in accelerators. In the following two meetings of the accelerator section members of the conference heard a number of reports about the synchrophasotron. M. S. Rabinovich, E. G. Komar, S. M. Rubchinsky, I. F. Malyshev, N. A. Monoszon and others told about the physical principles of the 10 Bev

* A report on the plan for the 50 Bev accelerator is published in this issue.

synchrophasotron and its separate components: the magnet and the control system for the magnet and accelerating fields, the injection system, the vacuum system, etc.

Many interesting reports were also given at the meetings devoted to electron accelerators. V. D. Rusanov and Yu. N. Lobanov gave accounts of the results of a series of experimental studies of the process of electron capture in betatron acceleration, of its dependence on various parameters adjusted over a wide range. The report of M. Seidl (Czechoslovakia) was devoted to the same subject. Some questions of the theory of the motion of electrons in accelerators were dealt with in reports by A. A. Sokolov, A. A. Kolomensky and A. N. Matveev.

At a special meeting attention was given to particulars of construction and economic indices of linear accelerators, which are of great importance in connection with the problems of producing large currents in these accelerators. Reports were given by both Soviet and foreign specialists.

In this section there were also presented reports on strong focusing accelerators. I. A. Mozalevsky presented the results of experiments on models of electromagnets prepared in connection with the planning for the 7 Bev accelerator. S. V. Skachkov told about the methods of calculation of C-shaped magnets, which are now regarded as the most suitable. The reports of L. L. Sabsovich and E. K. Tarasov were devoted to questions of the passage of particles in accelerators through the critical energy, and the possibility of eliminating the critical energy in strong focusing accelerators. R. Wilson (USA), who appeared at this meeting, presented the data on the first operating accelerator with such focusing – a 1 Bev electron synchrotron. The diameter of the orbits in the accelerator is about 8 m, the weight of the magnet is 20 tons, and the maximum field is 8800 oersteds. It is proposed to increase the field intensity to 13,000 oersteds and achieve an energy of 1.5 Bev. The electron source is a Van de Graaff generator. The speaker stated that at the present time the accelerator is working very well, giving 30 pulses per second at an intensity of $3 \cdot 10^8$ particles per pulse. Prof. Regenstreif (CERN) told about the 25 Bev proton synchrotron being built in Geneva. It is expected that the proton beam will be obtained in 1960. The accelerator is being built underground, with its foundation resting on 80 columns going down to bed rock. The magnetic field is varied over a range from 140 to 12,000 oersteds in the course of 1 sec, corresponding to an increase of the energy from 50 Mev (the injection energy) to 25 Bev. The accelerator will give one pulse every three seconds. The average orbit radius is about 100 meters, and the dimensions of the vacuum chamber are 16×8 cm^2.

The greatest interest among participants in the conference was aroused by the reports on new methods of acceleration. At the present time these are iron-less construction of accelerators and also ring accelerators with constant magnetic field.

M. Oliphant (Australia) gave an account of the construction of the first 10 Bev proton synchrotron in which large magnetic fields (up to 80,000 oersteds) are produced without the aid of iron cores by a suitable distribution of conductors carrying large currents. Such fields permit the building of the accelerator with orbit diameter about 10 m in all. The enormous currents (1.6 million amperes) will be obtained by the use of a unipolar generator. As injector it is proposed to use a cyclotron with 80 Mev ion energy. The speaker emphasized that the cost of the accelerator is less by a factor of 20 than that of the 6.3 Bev accelerator that has been built in Berkeley.

Theoretical and experimental results of work on the production of large magnetic fields were presented by G. I. Budker. He told about an original idea for producing a closed stabilized electron beam, capable of carrying enormous currents (several thousand amperes), and about the application of the magnetic fields obtained by means of such a beam for the acceleration of particles. A. A. Naumov reported on an experiment on the construction of pulsed iron-less synchrotrons, which is being conducted by the same group of experimental and theoretical workers. At present there has been practically completed a synchrotron of very simple construction, with energy 150 to 200 Mev and equilibrium orbit radius 17 cm. The enormous pulses fields are produced by means of a single massive turn, enclosed in a jacket which serves simultaneously as the return conductor and as the wall of the vacuum chamber. This accelerator is a model for a 1 Bev machine with orbit radius 33 cm and magnetic field intensity 100,000 oersteds. Consideration is also being given to the possibility of building a strong focusing accelerator for 3 Bev.

A. A. Kolomensky, who spoke next, reported on some proposals regarding modifications of constant-field ring accelerators, namely the building of ring accelerators with constant frequency of circulation of the particles, which would permit a considerable increase of the intensity of the beams of accelerated particles.

The last meeting of the section was devoted to experimental methods, both those used in adjusting accelerators and those used in experiments with high energy beams of particles.

P. M. Morozov reported on sources of multiply charged nitrogen ions for the cyclotron, and A. A. Glazov on the use of a cold-cathode ion source in the synchrocyclotron. L. Alvarez (USA) told about the use of counter systems and bubble chambers in the study of "strange" particles. He gave an account of the construction of a hydrogen chamber of 500 liters volume. G. A. Leksin reported on the development of an apparatus for counting high energy neutrons with an efficiency of about 30%.

An interesting idea about the possibility of determining the instant of occurrence of events recorded by means of photographic emulsions was put forward in the report of M. I. Podgoretsky. M. G. Strakhonovsky reported on an arrangement for obtaining pulsed magnetic fields with intensities up to 250,000 oersteds.

The section on elementary particles and their interactions began its work with a discussion of questions connected with the creation of π-mesons by nucleons. Reports were given by M. G. Meshcheryakov, B. S. Neganov, and V. B. Flyagin on the study of the spectra of the π-mesons, nucleons, and deuterons produced in (p, p) collisions and in the bombardment of beryllium nuclei by protons. In collisions of protons with energies of 550 to 660 Mev with protons, the creation of π-mesons occurs mainly in p-states, the contribution of s-states to meson production being small. The calculations showed that the matrix element for production of π-mesons does not depend on the energy of the nucleons, but is a function of the angle of emission and the momentum of the meson, the dependence on the momentum being linear in the interval from 60 to 200 Mev/c.

A study of the spectra of nucleons accompanying meson production in (p, p) collisions showed that protons with momenta greater than 250 Mev/c are emitted predominantly forward and backward; the angular distribution of protons with smaller momenta is nearly isotropic. It was found that transitions leading to the emission of two nucleons with small momenta of relative motion make a small contribution to the cross section of the (p, p) interaction.

A comparison of the spectra of neutrons appearing in the bombardment of beryllium by protons with energies 480 and 660 Mev showed that at the latter energy there appears, besides the maximum lying near the upper limit of the spectrum, an additional maximum lying at lower energies. The position and shape of this maximum agree with the shape of the spectrum of the protons accompanying the production of mesons in the bombardment of beryllium by protons. L. Riddiford (England) told about experiments on the (p, p) interaction at energy 650 Mev. In this report, as in those preceding, the conclusion was drawn that in meson production in (p, p) collisions a considerable part can be played by intermediate states with angular momentum 3/2 and isotopic spin 3/2.

Assuming that all the basic features of the process of meson production in collisions of nucleons are determined by interaction between the π-meson and the nucleon, and taking the matrix element of this interaction from the experiments on the scattering of π-mesons by nucleons, L. M. Soroko calculated the spectra of mesons and nucleons for meson production in (p, p) collisions and obtained satisfactory agreement with experiment.

Reports by Yu. D. Bayukov, A. A. Tyapkin and K. O. Oganesyan were devoted to the study of the creation of π^0-mesons in collisions of high energy protons and neutrons with protons, deuterons, and the nuclei of various elements. When the nuclei of carbon and beryllium are bombarded with protons of energy 470 Mev, π^0-mesons are produced with energy near the maximum possible, and with angular distribution $(0.15 \pm 0.15) + \cos^2\theta$. At 660 Mev proton energy the angular distribution of the π^0-mesons becomes nearly isotropic, and their maximum energy is considerably smaller than the maximum possible energy. The yield of mesons at an angle of 180° in the bombardment of various nuclei is proportional to $A^{2/3}$. The yield at 0° has a weaker dependence on A. These facts are possibly an indication that meson production occurs mainly at the surface nucleons of a nucleus.

In the energy range from 390 to 580 Mev the ratio of the total cross sections for the reactions $p + p \rightarrow \rightarrow \pi^0 + p + p$ and $p + n \rightarrow \pi^0 + p + n$ rises rapidly, and with further increase of the energy the increase of the ratio becomes decidedly slower. The angular distributions become more symmetrical with increase of the energy. The results of these experiments also do not contradict the assumption that the main role in meson production is played by transitions through intermediate states with J = 3/2 and T = 3/2. The cross section for production of π^0-mesons by impacts of neutrons on protons and deuterons were measured at neutron energy 590 Mev. The difference between the cross sections $\sigma^{\pi^0}_{n,d}$ and $\sigma^{\pi^0}_{n,p}$ is close to the cross section for production

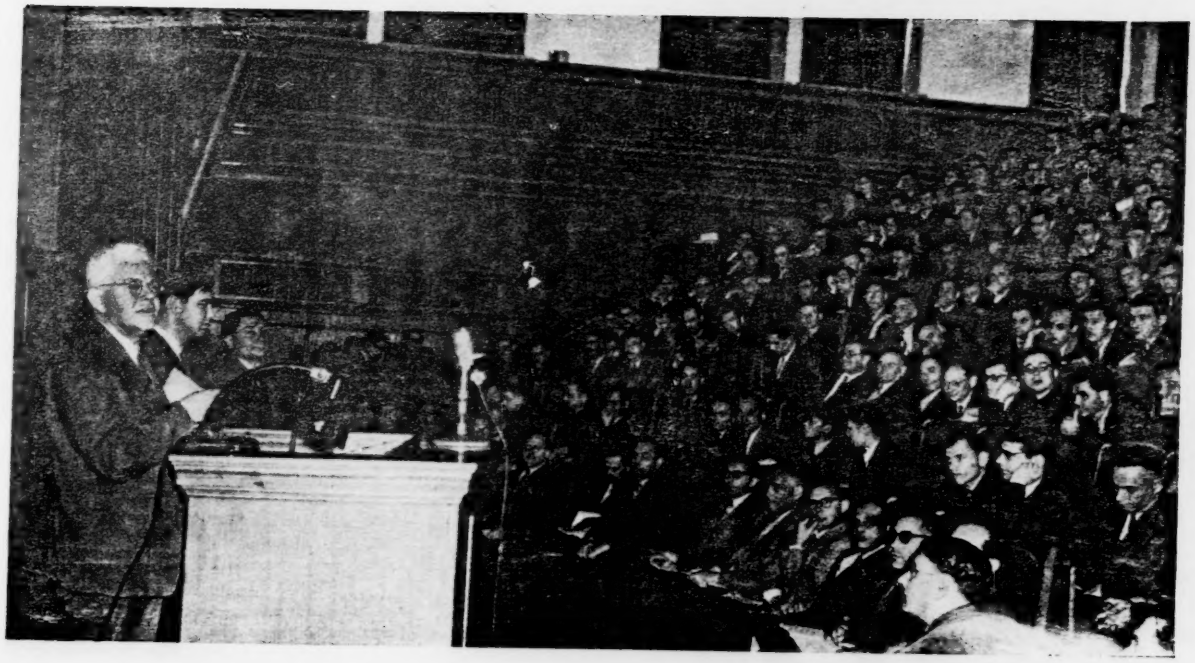

Australian scientist M. Oliphant presents a report at the All-Union Conference on High Energy Particle Physics in Moscow, May 22, 1956.

of π^0-mesons in (n, n) collisions. The experimentally found value of this difference provides evidence that the relatively forbidden character of the production of π^0-mesons found in (n, n) collisions at energy 400 Mev is removed for neutrons with energy 600 Mev.

An account of some results of experiments on the formation of mesons on a nucleus with isotopic spin T = 0 (Li^6), conducted in order to check the correctness of the hypothesis of the charge independence of nuclear forces, was given by R. Marshak (USA).

L. Smith (USA) told about experiments on the interaction of protons with protons in the energy range 1 to 3 Bev. The energy dependencies were found for the production of one, two, and three π-mesons in (p, p) collisions.

S. Z. Belenky pointed out that when account is taken of the interaction between mesons and nucleons in the final state one gets an improved agreement with experiment in calculations carried out on the basis of the statistical theory of the multiple production of particles in the interaction of nucleons with nucleons and of mesons with nucleons, in the range of energies of the order of several Bev.

The discussion of the interaction of nucleons with nucleons was opened by the report of E. Segre (USA), who was greeted with applause. Prof. Segre told about the experiments that led to the discovery of the antiproton and made it possible to obtain an amount of evidence about the interaction of this particle with matter. The total interaction cross sections of antiprotons with beryllium and copper nuclei turned out to be greater by a factor of two than the interaction cross sections of these nuclei with ordinary protons. At 64 Mev energy of the antiprotons, half of them are annihilated in flight and the rest after stopping. In a star appearing on the annihilation of an antiproton, an average of five π-mesons are formed. I. Ya. Pomeranchuk, engaging in the discussion, remarked that in the annihilation of antiprotons on nucleons there is produced a unique system consisting of π-mesons only. The study of such processes will make it possible to find out whether the interaction radii of π-mesons with π-mesons and of nucleons with nucleons are the same.

A survey of the experimental data on the scattering of nucleons by nucleons and an attempt at a theoretical analysis were presented by Ya. A. Smorodinsky. He showed that the available data make it possible to carry out a partition of the cross sections among the isotopic spins. A further problem is the analysis according to the ordinary spins. From this point of view great importance attaches to the carrying out of experiments on the correlation of polarizations. Also important are experiments on triple scattering with a magnetic field applied between scatterer and analyzer, since they will make possible the determination of the size of the longitudinal component of the polarization that arises in the scattering of nucleons by nucleons. Ya. A. Smorodinsky also reported on the results of the work of R. M. Ryndin, who showed that the essential ambiguity of the phase shift analysis, discovered by Minami for the (π, p) scattering, is not present in the analysis of the scattering of nucleons by nucleons.

In his report O. Chamberlain (USA) told about the experiments on the scattering of polarized protons with energy 310 Mev and about the phase analysis of the (p, p) scattering. Besides the ordinary experiments on double scattering, experiments on triple scattering were used to determine the change of the amount and direction of the polarization in (p, p) scattering. Experiments were also performed on triple scattering with a magnetic field located between the first scatterer (polarizer) and the second scatterer (hydrogen). In the carrying out of the phase shift analysis four solutions were found, giving good agreement with the experimental data.

V. P. Dzhelepov reported on experiments on (n, p) and (n, n) scattering at neutron energy 580 to 590 Mev. The differential cross sections for (n, n) scattering were determined from different experiments with scattering of neutrons by deuterons and protons. It was shown that at scattering angles of 30° and 90° in the center of mass system of the two nucleons the cross section for (n, n) scattering is the same as that for (p, p) scattering, and the angular dependence of these cross sections is sharply anisotropic. The analysis of the experiments on (n, p) scattering, carried out on the basis of the hypothesis of charge independence, showed that the total cross sections of the nucleon interactions and the angular and energetic dependencies of the differential cross sections for elastic scattering for T = 0 and T = 1 are decidedly different for energies of about 400 Mev and come closer together with increasing energy. At 580 Mev energy the cross sections for meson production are of nearly the same size for nucleon collisions with both values of the isotopic spin T.

L. I. Lapidus told about the possibility of obtaining additional evidence useful for the phase shift analysis of the data on (n, p) scattering, on the basis of the data on exchange scattering of neutrons by deuterons with small momentum transfers.

The study of the elastic scattering of neutrons and protons by protons and of attempts at phase shift analysis of the results was also the subject of reports by R. Marshak (USA), E. Clementel (Italy) and L. Riddiford (England). The results of experiments on the elastic scattering of protons by protons at energies of 460 to 660 Mev were given in a report by N. P. Bogachev. It was found that anisotropy appeared in the scattering and increased with the energy, and also observations were made on the energy dependence of the differential cross sections for (p, p) scattering. The differential cross sections were measured over a wide range of angles from 5° to 90°. The total elastic cross section for (p, p) scattering remains constant in this energy range at (23-25) $\times 10^{-27}$ cm^2. Included in the report were some data on elastic (p, d) scattering at proton energy 660 Mev.

The report of E. G. Bogomolov was also devoted to experiments on small angle (p, p) scattering at energy 660 Mev.

L. Smith reported on a study of (p, p) scattering at energies from 1 to 3 Bev. The differential cross sections were measured down to 15°; at small angles the cross section reaches values of $(20\text{-}30) \cdot 10^{-27}$ cm^2 / / steradian. A continued increase of the anisotropy of the scattering is observed as the energy increases (at proton energy 3 Bev $\frac{\sigma(15°)}{\sigma(90°)} > 100$). Calculations carried out on the assumption that the scattering at these energies is of purely diffraction character lead to a proton radius of $r_0 \approx 0.7 \cdot 10^{-13}$ cm. A similar analysis carried out by other authors for smaller energies led to a proton radius $r_0 \approx (0.5\text{-}0.7) \cdot 10^{-13}$ cm.

Results of measurements of the total interaction cross sections of nucleons with nucleons and with deuterons were reported by V. I. Moskalev. The total cross section of the (p, p) interaction increases by a factor of 1.5 in the energy range from 380 to 660 Mev. The total cross section of the (n, p) interaction remains constant and equal to $(34\text{-}37) \cdot 10^{-27}$ cm^2. At energies below 580 Mev the (p, d) interaction cross section agrees within the limits of error with the sum of the (n, p) and (p, p) scattering cross sections, and at larger energies is somewhat smaller. This effect can evidently be explained by the screening of the nucleons in the deuteron.

Analyzing the energy dependence of the total cross sections for scattering of nucleons by nucleons, K. Brueckner (USA) came to the conclusion that meson production at energies 500 to 1000 Mev occurs only in collisions of nucleons in states with T = 1. At higher energies, when double meson production begins, mesons are also produced in collisions of nucleons in states with T = 0, and the total cross section of the interaction of nucleons in this state begins to increase. This effect can be explained on the hypothesis that meson production occurs mainly through intermediate states with T = 3/2 and J = 3/2. V. P. Dzhelepov remarked that, according to data obtained by his group, at neutron energy about 600 Mev the meson production occurs equally intensely with T = 1 and with T = 0. The conclusions of Prof. Brueckner are based on the analysis of data relating to the difference between the (p, d) and (p, p) cross sections. The nonadditivity of the (p, d) interaction cross section, which increases with the energy, could thus lead to a lowering of the cross sections found in this way for meson production in states with isotopic spin T = 0.

The morning and evening sessions on May 18 were devoted to the interaction of π-mesons with nucleons and nuclei. In the reports of N. A. Mitin, A. I. Mukhin, and I. V. Sokolova accounts were given of experiments on the scattering of π^+-mesons by nucleons and on the carrying through of the phase-shift analysis of this process. The report of Prof. E. Clementel (Italy) was also devoted to this latter question. The experiments were carried out in the meson energy range from 176 to 310 Mev. The phase-shift analysis was done both with and without the inclusion of $\underline{d}$ waves. It was shown that the contribution of the $\underline{d}$ waves to the scattering is small in comparison with those of the $\underline{s}$ and $\underline{p}$ waves. The dependence of α_3 on the meson momentum was found to be almost linear right up to 307 Mev. From the results obtained it follows that the interaction radius in $\underline{s}$ states with T = 3/2 cannot be appreciably greater than the value $r = 6.5 \cdot 10^{-14}$ cm. At energies larger than 240 Mev it was not possible to obtain agreement of the energy dependence of the phase resonance with the Chew-Low theory. The results of the phase-shift analysis permit one to assert that the conclusions from the dispersion relation agree with experiment right up to 310 Mev energy. R. Marshak told about the scattering of low energy π-mesons by protons. A comparison of the experimental results with the Chew-Low theory led the speaker to the conclusion that the hypothesis of charge independence might be "unjustified" in this energy range, since two effects depending on charge come to be of great importance: the Coulomb interaction and the nucleon mass difference. K. Brueckner stated that the dependence of the total interaction cross sections of π-mesons with

nucleons is not monotonic at high energies. At low energies the meson, as it were, "does not notice" the meson cloud of the nucleon and interacts only with its central core. With increase of the energy the meson cloud becomes transparent and collisions occur at large impact parameters. The resonance nature of the interaction between mesons leads to the nonmonotonic behavior of the energy dependence of the cross sections for interaction of mesons with nucleons.

The interaction of π^--mesons with the nuclei of various elements was the subject of reports by R. M. Sulyaev, N. I. Petrov and A. E. Ignatenko. In collisions of 330 Mev π^--mesons with He^4 nuclei the mesons interact mainly with the separate nucleons of the α particle, but multiple processes also turn out to be important here. The angular dependence of the elastic (π, α) scattering is evidently nonmonotonic in the region of small angles. This fact may possibly be evidence of a difference of sign of the Coulomb and nuclear scatterings, unlike the case of energies below 200 Mev, where the signs are the same. The elastic scattering of π^--mesons by nuclei of carbon and lead is satisfactorily described by means of the optical model. The inelastic collisions mainly have the character of the interaction of mesons with the individual nucleons, the collisions being mostly single for the range of scattering angles from 120° to 180°, while in the scattering at angles from 0 to 60° the mesons make several collisions in the nucleus. The total interaction cross sections and the total inelastic collision cross sections with mesons in the energy range 140 to 400 Mev were determined for a number of nuclei. The experimental results agree well with calculations carried out on the basis of the optical model, with use of the dispersion relation to find the optical parameters of the nuclei. The radii of the nuclei agree well with the expression $R = 1.43 \cdot 10^{-13} A^{1/3}$ cm.

V. V. Krivitsky told about the creation of π^+-mesons by collisions of 308 Mev π^--mesons with carbon nuclei. The total cross section for this process was found to be equal to $\sigma_c = (2.6 \pm 1.3) \cdot 10^{-27}$ cm^2. A rough estimate of the cross section for the similar process in (π^-, p) collisions leads to $\sigma_p \sim 10^{-27}$ cm^2.

In the discussion of questions connected with the interaction of fast particles with nuclei, considerable attention was given to polarization phenomena. G. D. Stoletov reported on the polarization of proton beams arising from the scattering of 660 Mev protons from beryllium nuclei. The experiments were conducted with primary scattering angles of 18° and 9° in the laboratory reference system. The degrees of polarization found here were 33 and 60% respectively. It was found that the maximum value of the degree of polarization in elastic scattering of protons from beryllium nuclei is considerably higher than in the case of quasi-elastic scattering and inelastic collisions. The polarization in elastic scattering at angle 9° does not change perceptibly with increase of the atomic weight of the analyzer. The polarization of proton beams emerging from quasi-elastic collisions and meson formation decreases markedly with increase of atomic weight.

A report by R. Marshak was also devoted to the question of studying the polarization occurring in the scattering of protons by protons and by complex nuclei.

I. I. Levintov told about a determination of the ratio of the real parts of the spin-orbit and central interaction potentials of nucleons with nuclei. This quantity can be found from data on the polarization at high energies, on the basis of information about the levels of certain nuclei and about the scattering at low energies. The values of this ratio found in different ways agree among themselves.

N. A. Guliev told about a calculation of the polarization appearing in the scattering of nucleons by nuclei. In this work the distribution of the nucleons in the nucleus was given and the potential corresponding to this distribution was found by means of scalar meson theory.

Several reports were devoted to the scattering of high energy particles and to the nuclear reactions produced by these particles. In his report L. Rosenfeld (England) discussed the possibilities that the study of the nuclear scattering of fast particles provides for the study of nuclear structure. The data on the scattering of electrons provide evidence that the parameter r_0 in the expression for the nuclear radius must be regarded as dependent on A and equal to $r_0 = 1.4 \cdot 10^{-13}$ cm for heavy nuclei and $r_0 = 1.2 \cdot 10^{-13}$ cm for light nuclei. The calculations show that with further increase of the accuracy of the measurements it will be possible to observe effects due to the fact that the charge is not continuously distributed in the nucleus, but concentrated in the individual protons. On the basis of the results of experiments on the scattering of μ-mesons the conclusion is drawn that the anomalous scattering of these particles either does not exist at all, or else is much smaller than had been expected previously.

M. Levy (France) spoke about the scattering of 550 Mev electrons by protons and deuterons. At large scattering angles the measured cross sections are 10 times greater than the Rutherford values. Better agreement is obtained by taking into account the distribution of charge and magnetic moment in the proton. To explain the data on (e, d) scattering it is necessary to take the neutron radius much smaller than the proton radius, but this contradicts the data on the magnetic moments of nucleons. Better results can be obtained by using a nucleon model with a central core, but here the size of the core has to be taken equal to that of the whole proton. It is possible that the results of these experiments give evidence that the interaction of point charges at small distances ($r \approx 0.5 \cdot 10^{-13}$ cm) departs from the Coulomb law.

V. I. Moskalev reported on measurements of total cross sections and inelastic interaction cross sections of neutrons and protons with nuclei. The total cross sections of light nuclei at energies of 660 Mev for protons and 630 Mev for neutrons are equal to each other, which is evidence for the charge symmetry of nuclear forces. In the range of neutron energies from 380 to 630 Mev a small increase of the cross sections of light nuclei is observed. The total cross sections of the heavy nuclei remain practically constant in this range. The inelastic interaction cross sections of protons with nuclei remain almost constant in a wide range of energies from 150 to 850 Mev.

El-Nadi (Egypt) considered in the Born approximation the theory of reactions in which the incident nucleon captures two nucleons from the nucleus. The results of the calculations agree qualitatively with the experimental data (presence of a maximum in the small angle region). But the further course of the cross section does not agree with the results of the calculation. The carrying out of further experiments will show whether the cause of the discrepancy is the use of the Born approximation.

An account of the elastic and inelastic scattering of high energy neutrons and deuterons by extended semi-transparent nuclei was given by K. A. Ter-Martirosyan. The formulas and curves obtained by his work may be useful in determining the sizes and shapes of nonspherical nuclei.

N. A. Perfilov reported on the emission of fragments with $Z > 4$ in the destruction by protons of the nuclei of an emulsion. In the energy range from 350 to 660 Mev the yield of the fragments increases by a factor of 2.5. The observed effect cannot be explained by the splitting of Ag or Br nuclei, nor by the evaporation of fragments from strongly excited nuclei.

J. Filbert (France) told about a study of the interaction of 1 Bev protons with the nuclei of a photographic emulsion. The total interaction cross sections were studied, and also the yield of α particles from light and heavy nuclei and the probabilities of formation of stars with various numbers of charged particles.

The discussion of the problems connected with photonuclear reactions began with a survey report by A. M. Baldin, devoted to the photoproduction of π-mesons from protons and deuterons. An account of the photoproduction of slow π-mesons from complex nuclei with γ-rays of maximum energy 260 Mev was given by N. G. Semashko. Comparison with the results of the calculations of Baldin and Lebedev showed the necessity of taking into account the finite dimensions of the nucleus. The fact that the cross section for photoproduction of π^- mesons is proportional to $A^{2/3}$ is interpreted as evidence that the formation of mesons occurs mainly at the surfaces of nuclei. The conclusion is drawn that the decrease of the meson yield for small Z is due to the nuclear reaction (repulsion) in the system π-meson-nucleon.

A. A. Abrikosov directed his talk to a consideration of a number of quantum electrodynamical effects at high energies. A. B. Migdal explained that, because of the necessity of taking into account large longitudinal distances in the production of pairs and Bremsstrahlung at high energies the ordinary shower theory turns out to be altogether inapplicable in dense media at energies greater than 10^{13} ev.

In a number of interesting reports W. Panofsky (USA) told about experiments on multiple photoproduction of π-mesons from hydrogen, about the photoproduction of μ-meson pairs, about the direct production of mesons by electrons and about Bremsstrahlung at high energies. At electron energies of 575 Mev the production of pairs of π-mesons was observed with a cross section of 10^{-33} cm^2. The system (π^+, p) is formed mainly in the p state, and the system (π^-, p) in the s state. The distribution of energy between the components of a pair turns out to be extremely uneven: near the threshold the π^+-mesons take up almost all of the energy. The results of the experiments obviously agree with the hypothesis that the production of mesons goes through the intermediate state $J = 3/2$, $T = 3/2$. The results of another series of experiments enable us to conclude that direct creation of pairs of μ-mesons is evidently an existing process. Here the experimental cross sections agree better

with the calculated values if the finite size of the nucleus is taken into account. In these experiments no effects were observed that could be ascribed to the action of nonelectromagnetic coupling of μ-mesons with nuclei.

B. M. Pontecorvo told about attempts to detect a nuclear interaction connected with the interchange of μ-meson pairs. It was shown that if such an interaction exists at all, its contribution to forces does not exceed 10^{-2} % of the contribution due to π-mesons.

Reports by N. B. Delone and V. S. Roganov, and also by R. Wilson (USA) were devoted to various questions connected with the photodisintegration of the deuteron. Studies have been made of the angular distributions and the spectra of the neutrons and protons appearing in this process. It is noted that the angular distributions of the neutrons from the reactions (γ, d) and (γ, C) agree near $\theta = 45°$. It is concluded that with light nuclei reabsorption of mesons is unimportant. The data on the photodisintegration of the deuteron, for energies up to 50 Mev agree in their general features with the theory of Schiff. At larger energies the experimental points lie considerably higher than is predicted by this theory. A simple model is proposed to explain the behavior of the cross section for this process at high energies. Rough agreement with the experimental data can be obtained if one supposes that the production of mesons from the nucleons in the deuteron is the same as from free nucleons. If the production of the mesons occurs at large distances from the nucleon, they escape, and actual meson production is observed. For meson production at small distances, the mesons are emitted and reabsorbed. This effect leads to a rise of the cross section for photodisintegration of the deuteron near the threshold for meson production. Similar conclusions, reached in a study of the photoproduction of π- mesons from deuterons, were reported by M. I. Adamovich.

A. N. Gorbunov reported on experiments on the photodisintegration of helium nuclei at high energies. It was found that the (γ, p) and (γ, n) reactions are of resonance character with a maximum near 27 to 30 Mev. The cross section of the (γ, p) reaction is constant at energies 40 to 75 Mev and falls sharply at the latter energy. In this range the cross section of the (γ, n) reaction decreases monotonically. The angular distributions of the neutrons and protons are identical, and an energy-dependent asymmetry is found around the angle 90°. In the process of absorption of quanta by nuclei of helium higher multipoles play a part even at low energies.

The last session of the section on elementary particles and their interactions was devoted to questions about new particles. M. Menon (India) told about a cloud chamber study of s-particles at a height of about 2500 m.

A. I. Alikhanyan reported on experiments with a mass spectrometer used together with two Wilson cloud chambers. In the composition of the cosmic radiation, besides protons, deuterons, π- and μ-mesons, and positive and negative K-particles, there was observed a group of particles with mass about 560 times the mass of the electron. The intensity of these particles is equal to about 1% of the number of μ-mesons in the same interval of ranges.

V. A. Lyubimov reported on measurements of the spectrum of K-particles at a height of about 3200 m. In the range of momenta up to 450 Mev/c there are far fewer K-particles than π-mesons $\left(\frac{N_K}{N\pi} = 6.5\ \%\right)$; in the interval of momenta up to 900 Mev/c the ratio of the intensities of K-particles and π-mesons rises to 20 %, and in the interval of momenta up to 1200 Mev/c it reaches 40 to 50%. At momenta from 900 to 1000 Mev/c the yield of K-particles is a maximum, and their number exceeds the number of π-mesons. The results of the experiments make it seem possible that K-particles, like π-mesons, are quanta of the nuclear force field. L. Smith reported on experiments with the cosmotron, in which during bombardment of carbon and lead nuclei with 1.9 Bev π-mesons a search was conducted for joint production of Λ- and θ-particles. The lifetimes of θ^0-and τ^0-particles were found to be greater than 10^{-9} sec, and that of K-particles equal to 10^{-9} sec. It was shown that the scattering cross sections for the different kinds of K-particles are the same.

Wang Han-Chang (China) told about some results of work in which heavy mesons and hyperons were studied with a Wilson chamber at a height of 3185 m. In 30,000 exposures 8200 nuclear reactions were found, and 200 heavy mesons and hyperons. Several cases of pair production of these particles were observed.

B. S. Neganov put forward a proposal to consider the nucleon as a system consisting of a hyperon and K-particles. In this case the K-particles must be regarded as structural units entering into the composition of the nucleon, and not as quanta of the nuclear field. On this assumption the process of production of hyperons and K-particles in pairs must be regarded as a process of dissociation of the nucleon.

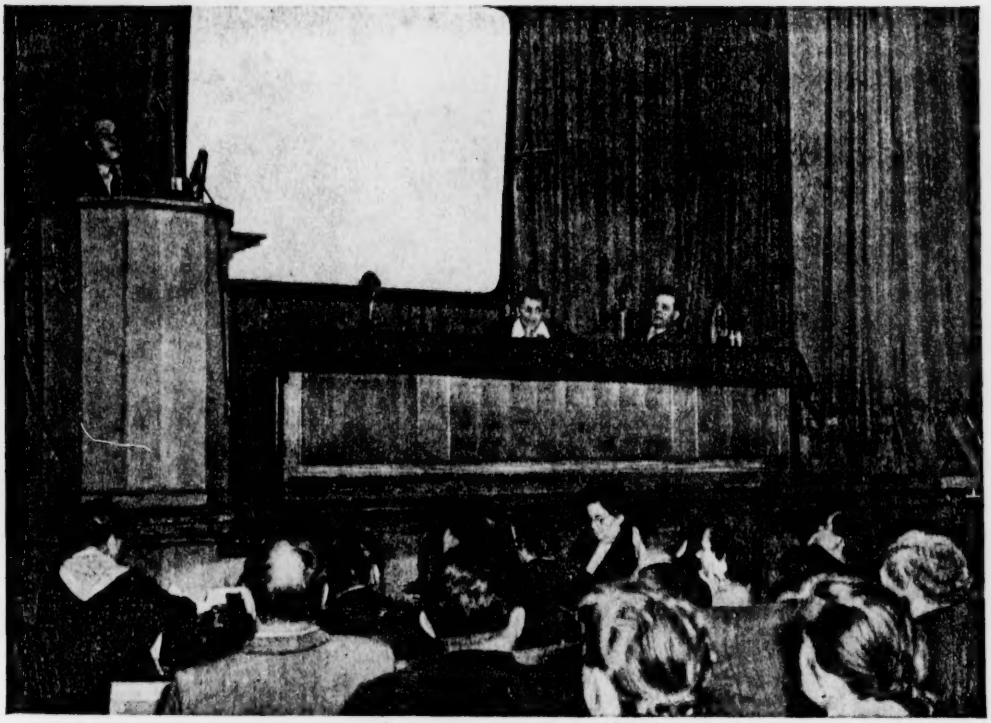

Professor Wang Han-Chang (China) presents a report at the All-Union Conference on High Energy Particle Physics in Moscow, May 22, 1956.

J. Steinberger (USA) presented a report on the production of "strange" particles from hydrogen by 1.3 Bev π-mesons. Decays of Σ^--and K^+-particles were observed, which were due, in the opinion of the speaker, to electromagnetic processes. A considerable number of cases were observed of "unusual" decay of Λ and θ - particles, in which visible tracks of decay particles were absent. The lifetime of Σ^--particles was found to be $1.4 \cdot 10^{-10}$ sec. Analyzing the experimental data, the speaker came to the conclusion that they do not provide an indication of a higher spin for the hyperon.

The report of R. Peierls (England) was devoted to hypernuclei, i.e., nuclear systems in which bound hyperons occur as constituents. Similar questions were discussed in the report of N. N. Kolesnikov at one of the meetings of the theoretical section. Here also L. B. Okun described the results of calculations of the cross sections for exchange collisions of K-particles in hydrogen and deuterium, and also for reactions in which K-particles are captured by deuterium; the purpose is to obtain evidence about the spin and parity of K-particles. The speaker pointed out that the hypothesis of a large value of the spin of the particle is in contradiction with known experimental data on Λ fragments. On the basis of the hypothesis of isotopic invariance these workers obtained relations between the cross sections of processes of production of K-particles, hyperons, and antihyperons in collisions of π-mesons and nucleons with nucleons and deuterons, and also for the scattering and absorption of "strange" particles in collisions with nucleons. Definite limits are established, within which the ratio of the probabilities of the possible decay modes of the Σ-hyperon must lie.

Much attention was given at the conference to the discussion of theoretical problems. They were discussed both at the meetings of the special section and at those of other sections, and also at a number of unofficial meetings not planned ahead of time. The Soviet theorists and their foreign guests held a special meeting

devoted to the work of L. Landau and his collaborators on quantum electrodynamics and the theory of fields. The present state of meson theory was discussed in reports by I. E. Tamm, I. Ya. Pomeranchuk, K. Brueckner and M. Levy. A particularly large amount of discussion was aroused by the report of I. Ya. Pomeranchuk, who expressed the opinion that a consistent treatment of the present quantum electrodynamics and meson theory leads to the conclusion that the renormalized electron charge and the renormalized mesonic charge are equal to zero. This result means that completely new ideas have to be introduced into the theory in order to find a way out of the difficulties in question. The energies at which new physical phenomena involving mesons appear cannot be large in comparison with 10^9 ev. Therefore the present meson theory, in the opinion of the speaker, is incompetent to deal with meson and nuclear processes.

The complexity of the interaction of π-mesons and nucleons makes difficult the unambiguous interpretation of the experiments in question. Therefore it is of interest to arrange experiments at very high energies with weakly interacting particles. By comparing the results of such experiments with the existing theory, one would be able to obtain from them indications about the character of new physical processes.

I. E. Tamm emphasized that meson theory is very successful in the qualitative, and in a number of cases in the quantitative, explanation of phenomena. But even in the most favorable case the construction of a consistent theory requires, in the opinion of the speaker, a reconsideration of a number of basic ideas of present-day quantum theory.

The presence of difficulties of principle in the quantum theory of fields gives a special value to work in which use is made of only such basic ideas of quantum theory as relativistic invariance, the unitary character of operators, and the causality conditions. A discussion of the dispersion relations that follow from these conditions was carried on in a special meeting of the theoretical section. M. K. Polivanov presented a report on the application of the causality principle to problems of scattering. The dispersion relations for the scattering of nucleons by nucleons were discussed in reports by V. Ya. Fainberg and B. Z. Blank, and for the scattering of mesons by nucleons in reports by E. S. Fradkin and B. L. Ioffe. B. L. Ioffe and B. M. Stepanov spoke on the dispersion relation for photoproduction of π-mesons from nucleons.

At the final session of the conference Prof. Tsu (China) told about a possible model in the theory of elementary particles, which includes as two special cases the Fermi-Yang theory and the Heisenberg theory.

At the unofficial meetings of the theoretical section a very wide range of questions was discussed – from "strange" particles and the theory of the interaction of fast deuterons with nuclei to the theory of the solid state. An abundance of unofficial contacts and conversations was characteristic of the conference as a whole.

The conference showed that experimental and theoretical investigations in our country are diversified and deep-going. A considerable part of the interesting results had been obtained by young scientists.

V. A. Biryukov
B. M. Golovin
L. I. Lapidus

INTERNATIONAL NEWS

THE PROPOSAL FOR THE CHARTER OF THE INTERNATIONAL AGENCY FOR ATOMIC ENERGY

From February 27 to June 28, 1956, there took place in Washington a Conference of the representatives of 12 nations (Australia, Belgium, Brazil, Canada, Czechoslovakia, England, France, India, Portugal, the South-African Union, the USA, and the USSR), called for the working out of a proposal for the charter of the International Agency for Atomic Energy.

All of the delegations taking part in the Washington Conference voted for the charter proposal as a whole. The Soviet delegation pointed out, however, that the proposal for the charter suffered from certain essential shortcomings, and took reservations with regard to the articles in question.

One of the most important shortcomings of the proposed charter is the discrimination introduced in regard to those states that are not members of the United Nations Organization or of its special organizations.

In September 1956, in New York, there is to be convened an International Conference for the working out adoption of the final text of the charter of the Agency.

The draft of the charter in the form adopted at the Washington meeting consists of 23 articles.

The basic proposals of the draft charter of the Agency are presented below.

The purpose of the Agency is the achievement of "the more rapid and widespread utilization of atomic energy for the preservation of peace, health, and well-being in the whole world".

The Agency is empowered: a) to cooperate in scientific research work in the field of atomic energy and in the practical application of atomic energy for peaceful purposes throughout the world; b) to serve as an intermediary for the purpose of rendering services to one or another member of the Agency, or the supplying of materials, equipment, or technical aid; c) to carry out any other operations that can assist in the practical application of atomic energy for peaceful purposes, with proper consideration for the needs of the underdeveloped regions of the world; d) to facilitate the exchange of scientific and technical information on the application of atomic energy for peaceful purposes; e) to encourage the exchange of scientific workers and specialists in this field; f) to establish and bring to realization guarantees directed toward assuring that the fissionable and other special materials, services, equipment, technical aid, and information provided by the Agency to its members shall not be used for military purposes; g) to establish standards of safety for the preservation of health and arrangements to minimize dangers to life and property, and to assure the application of these standards both in its own work and in the work in which use is made of the materials, services, equipment, technical aid, and information provided by the Agency; h) to acquire or construct any establishments, plants and equipment necessary for the fulfillment of the functions assigned to it.

The Agency is to carry out its activities "in accordance with the policy established by the UNO of furthering the establishment of agreed guarantees of disarmament throughout the world".

The Agency "will not require for the supplying of aid to its members any political, military, or other conditions incompatible with the conditions of this Charter".

The following structure for the Agency is contemplated in the charter: A General Assembly consisting of representatives of all states that are members of the Agency; A Council of Directors, consisting of 23 members; the personnel of the Agency, headed by a General Director, who will be appointed by the Council of Directors for a term of four years.

The General Assembly, convening in annual sessions, has the following functions: it chooses the members of the Council of Directors; accepts new members; considers the annual report of the Council of Directors; adopts the budget of the Agency; approves reports rendered by the Agency to the UNO; ratifies agreements concluded between the Agency and the UNO and other organizations; ratifies amendments to the Charter.

The General Assembly is empowered to make recommendations to the Council of Directors on any question related to the sphere of activity of the Agency, to present proposals for consideration by the Council, and to require from the Council reports on any matters relating to the functions of the Agency.

In an appendix to the charter there is envisaged the formation of a Preparatory Committee composed of representatives of the 12 states participating in the Washington Conference and representatives of six other states, which will be chosen by the International Conference for the adoption of the charter of the Agency. Tasks of the Preparatory Committee will include preparations for the first session of the General Assembly and the selection of members for the first Council of Directors.

The personnel of the Agency will include the scientists and highly qualified specialists needed to fulfill the functions of the Agency. The staff of the Agency will be selected on the widest possible geographical basis.

Member states of the Agency will provide to the Agency such information as in their opinion can be useful to the Agency. Those states that receive aid from the Agency must provide to the Agency all scientific information obtained as a result of the aid given by the Agency.

It is contemplated that the members of the Agency can provide to the Agency such amounts of special fissionable materials as they consider suitable, and under such conditions as are arranged with the Agency. The fissionable materials assigned to the Agency may be stored either on the territory of the member supplying them or in the custody of the Agency, at the discretion of the member supplying the materials. At the request of the Agency any member of the Agency will without delay supply to another member or group of members such quantity of the materials that it has placed at the disposal of the Agency as the Agency may direct, and will without delay supply to the Agency itself such a quantity of these materials as is actually necessary for operations and scientific research work at Agency establishments.

The Agency must assure such geographical distribution of the materials under its control as will not allow the concentration of large supplies of these materials in any one country, or in any one part of the world. For the reception, storage, and delivery of materials, and for conducting analysis and testing of the fissionable materials it receives, the Agency is empowered to construct or acquire factories, installations, and testing laboratories.

Any member or group of members of the Agency desiring to put into operation any project in the field of scientific research work or practical application of atomic energy for peaceful purposes can ask the Agency to give it assistance in obtaining fissionable and other special materials, services, equipment and technical aid necessary for this purpose. The Agency is empowered to approve such projects and to conclude with the states proposing a project agreements relative to the furnishing of materials and equipment necessary for the carrying out of the project. In these agreements conditions are defined for the furnishing of assistance, including arrangements for payment for the materials, services, equipment, and technical aid furnished by the Agency itself or by its members. These agreements must include the pledge of the states proposing the project not to use the assistance given to them for any sort of military purpose.

To assure the observation of the conditions of agreements, through which the Agency or a member of the Agency gives assistance to other states, the draft charter proposes definite guarantees, and also the rights and duties of the Agency in the field of inspection and control.

The Agency has the right:

to ratify the construction plans of any specialized apparatus and establishments, including nuclear reactors, proposed in a project approved by the Agency;

to require the observation of all measures for health and safety prescribed by the Agency;

to require the submitting of reports on progress in carrying out projects;

to approve the methods of chemical treatment of irradiated materials and determine the distribution of special fissionable materials extracted or produced as by-products;

to send into the territory of receiving states inspectors, who are to have access at any time to all places, all persons, and all data needed for an accounting of the fissionable materials that have been supplied, to establish whether the pledge not to use these materials for military purposes is being observed, and also to check the fulfillment of other conditions of the agreement between the Agency and the state in question.

In case of nonobservance of agreements that have been concluded, the Council of Directors is to inform all members of the Agency of this fact, and also the Security Council and General Assembly of the UNO.

The budget of the Agency is prepared by the General Director, is then considered by the Council of Directors, and is finally presented for adoption by the General Assembly.

The administrative expenses are divided among the members of the Agency in accordance with a scale fixed by the General Assembly. For the storage of materials, and also for the furnishing by the Agency of equipment, services, materials, and technical aid, definite payments will be required, in order to assure an income sufficient to pay to the members of the Agency the cost of the materials, services, equipment, and technical aid supplied by them, and also for the payment of expenses that may be incurred by the Agency itself. Any surplus income over and above the expenses of the Agency, and also any voluntary contributions to the Agency, are to be placed in a general fund, and may be used at the discretion of the Council of Directors with the approval of the General Assembly. The Council of Directors has the right to contract loans in the name of the Agency.

An agreement is to be concluded between the Agency and the UNO, providing for the Agency to present reports to the UNO, and for consideration by the Agency of resolutions regarding it passed by the General Assembly or any of the Councils of the UNO, and the submitting of reports on the measures taken as the result of such consideration.

It is provided that any dispute about the interpretation or application of the Charter of the Agency, which is not settled by consultation, will be submitted to the International Court, if the interested parties do not come to an agreement about some other method of settlement.

The Charter of the Agency is to become effective after it has been ratified by 18 states, including at least three of the following states: Canada, England, France, the USA, and the USSR.

V. Oberemko

NEWS OF FOREIGN SCIENCE AND TECHNOLOGY

HIGH-SPEED IMAGE-TRANSMISSION ELECTRON MULTIPLIER

A new electronic instrument known as the image-transmission electron multiplier [1 - 7] was developed at the Westinghouse Laboratories (USA) during 1955. The instrument, which is a photoelectron multiplier has a time resolution which greatly exceeds that of all existing types. Moreover it can be utilized as an electron-optical image converter (EIC) for image intensification.

Electron multiplication is achieved through the emission of secondary electrons from the "back" of thin plane dynodes. The dynode geometry is extremely simple and eliminates any dependence of the electron motion or amplification on the location of the emission site on the surface of the dynode. The plane-parallel dynodes are disposed in a line with equal spacing between them (see figure). Each dynode is $\sim 5 \cdot 10^{-6}$ cm thick and consists of three layers and a copper screen which makes the structure mechanically stable.

The screen (40-80 mesh per linear cm) gives a transmission of 50%. A substrate consisting of a layer of SiO 100 A thick is applied to the screen.

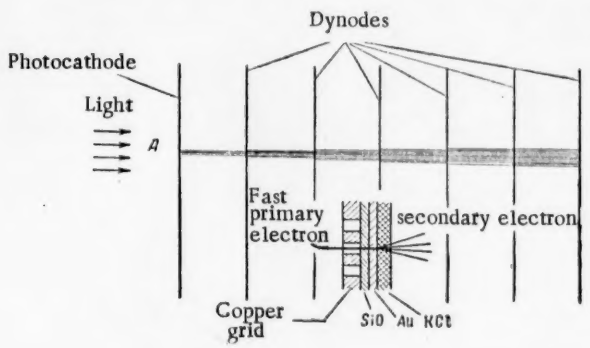

The KCl (300-600 Å) emits the secondary electrons. Preliminary experiments have shown that the secondary electron diffusion length in KCl is 2300 ± 600 A. Thus secondary electrons can traverse the total thickness of the KCl layer.

Between the substrate and the emitting layer there is a thin gold film (20 A). Incident electrons are scattered in this layer and as a result the angle of incidence with which they enter the KCl layer is increased, thereby increasing the effective thickness of the layer for these electrons.

An experimental demountable 7-stage multiplier with an ultraviolet-sensitive gold photocathode at the input has been constructed. The dynodes are 19 mm in diameter and the spacing 5 mm. In order to study the time characteristics a 50-ohm coaxial output was provided. The accelerating voltage was 3 kv per stage.

In order to study the quality of the image a 3-stage instrument was built consisting of two multiplying stages and a luminescent screen. The voltage for each multiplying stage was 3 kv and the voltage between the third dynode and the luminescent screen was 10 kv. To determine the optical resolution the first dynode was covered with an array of gold "dots" opaque to electrons. The different arrays had 4, 16, 32 and 48 dots per linear cm. The image was viewed on the luminescent screen and in each case it was possible to distinguish the dots. The resolving power is three lines per mm.

The measurements indicate that for an incident electron energy from 2.5 to 3.6 kev the secondary-emission coefficient for this material (applied to the interstices of the grid) ranges from 6 to 8. This figure exceeds substantially the secondary-emission coefficient for metals.

With an accelerating voltage of 3 kv the multiplication factor per stage was 4.

In Reference [4] it is indicated that it may be possible to achieve a total gain of 10^6 with a sufficient number of stages.

Using a fast-spark light source the authors have measured the total transit time and the rise time at the output of the multiplier for the 7-stage instrument. These were respectively $(3\pm1)\cdot10^{-9}$ sec and $1\cdot10^{-9}$ sec. For a number of reasons which are explained by the authors, the latter figure arises exclusively from the spread in the electron time of flight through the multiplier which is shown by calculation to be of the order of 10^{-11} sec.

Each stage of this multiplier is essentially a plane condenser, one of the plates of which is the emitting dynode (or photocathode) and the other of which is the output dynode or luminescent screen. There is a uniform electric field between them. All electrons emanating from a given point A on the emitting dynode are accelerated by the field and impinge on the output dynode within the limits of a small "circle of scatter" of radius r. Hence each point of a preceding dynode is reproduced on the next dynode in the form of a small circle and the image is effectively transferred from one dynode to the next. It is apparent that the spread in electron path length through the stage is determined solely by the finite value of the optical resolution and hence is several orders of magnitude smaller than that of the usual photomultiplier.

In principle, a stage of this instrument bears some resemblance to the simple EIC known as the Holst cell (as in [8]). In this instrument the multiplier consists of a number of Holst cells arranged in tandem.

As has been indicated by E. K. Zavoisky and S. D. Fanchenko [9, 10], the fact that the use, in an electron multiplier, of an EIC electrode system improves the time resolution by several orders of magnitude is not accidental. These authors studied the time resolving power of the EIC and have shown that it is determined only by the spread in the initial velocities of the electrons and in the electric field intensity in the region of the cathode (input dynode). The resolving time of a present-day EIC (with a photocathode input) can be as high as 10^{-14} sec. A resolution of $3\cdot10^{-12}$ sec [9] has been achieved experimentally.

There is no doubt that the image-transmission multiplier has an important future. In its application to image intensification the instrument in its present form bears a strong resemblance to the multistage EIC first developed in the Soviet Union by M. M. Butslov [12].* Starting from this it should not be hard to develop electron multipliers with a resolving time of 10^{-11} sec. Such multipliers having an input photocathode or dynode which emits electrons directly upon the impact of a nuclear particle would undoubtedly play an important role in the development of experimental nuclear physics.

S. F.

LITERATURE CITED

[1] E. J. Sternglass and M. M. Wachtel, Phys. Rev. 99, 646 (1955).

[2] E. J. Sternglass and M. M. Wachtel, Bull. Am. Phys. Soc. 30, 7, 11 (1955); Phys. Rev. 100, 1238 (1955).

[3] E. J. Sternglass, Rev. Sci. Instruments 26, 1202 (1955).

[4] Science News Letter 69, 3, 35 (1956).

[5] Science 123, 662 (1956).

[6] E. J. Sternglass and M. M. Wachtel, Bull. Am. Phys. Soc. 1, 1, 38 (1956).

[7] M. M. Wachtel and E. J. Sternglass, Bull. Am. Phys. Soc. 1, 1, 38 (1956). **

[8] Bryukhe and Reknagel, Electronic Apparatus (State Power Press, 1949).

* This instrument has an optical resolution [12] of 10 lines per mm after five stages and makes it possible to detect photographically every electron emitted from the input cathode. It was instrumental in the development of the luminescent chamber in 1952 [11], [12] and has been used in a number of interesting experiments [13], [14].

** References [6] and [7] appear as in the original. – Editor's note.

[9] E. K. Zavoisky and S. D. Fanchenko, Proc. Acad. Sci. USSR 100, 4, 661 (1955).

[10] E. K. Zavoisky and S. D. Fanchenko, Proc. Acad. Sci. USSR 108, 2, 218 (1956).

[11] E. K. Zavoisky, G. E. Smolkin, A. G. Plakhov and M. M. Butslov, Proc. Acad. Sci. USSR 100, 2, 241 (1955).

[12] E. K. Zavoisky, M. M. Butslov, A. G. Plakhov and G. E. Smolkin, J. Atomic Energy 1956, 4, 34.*

[13] M. V. Babykin, A. G. Plakhov, Yu. F. Skachkov and V. V. Shapkin, J. Atomic Energy (USSR) 1956, 4, 38.**

[14] E. K. Zavoisky, and G. E. Smolkin, J. Atomic Energy (USSR) 1956, 4, 46.***

---

* Page 483, this issue.

** Page 487, this issue.

*** Page 495, this issue.

ON THE CALCULATION OF THE ANOMALOUS MAGNETIC MOMENTS OF NUCLEONS BY MEANS OF MESON THEORY

It is found experimentally that the magnetic moments of the proton and the neutron are, respectively

$$\mu_p = 2.79\,\mu_N, \quad \mu_n = -1.91\,\mu_N,$$

where μ_N is the nuclear magneton ($\mu_N = \frac{e\hbar}{2Mc}$, where M is the mass of the proton). These data are in obvious contradiction with "naive" ideas, according to which the magnetic moment of the proton should be equal to μ_N, and the neutron, as a neutral particle, should not have any magnetic moment at all. This contradiction can be qualitatively explained by the fact that the proton and neutron, interacting strongly with the π-meson field of the vacuum, are part of the time, as it were, in a "dissociated" condition.

Part of the time the proton is in the state: neutron + π^+-meson

$$p \rightarrow n + \pi^+$$

and part of the time the neutron is in the state: proton + π^--meson

$$n \rightarrow p + \pi^-.$$

Thus each of the nucleons is, as it were, surrounded by a cloud of virtual charged mesons. The motion of these virtual mesons causes the anomalous magnetic moments of the nucleons, equal to

$$\Delta\mu_p = (2.79 - 1)\,\mu_N = 1.79\,\mu_N$$

and

$$\Delta\mu_n = -1.91\,\mu_N.$$

Despite the fact that such a qualitative explanation has been known for a long time, many attempts to obtain the correct values of the anomalous magnetic moments of the nucleons by means of the known meson theories have been unsuccessful.

For example, the authors of one of the most recent papers [1] devoted to this problem carried out calculations of the magnetic moments of nucleons caused by a meson field satisfying this equation of the fourth order,

$$(\Box^2 - \varkappa^2)^2 \varphi_i = 0.$$

(This equation was proposed in 1950 by Thirring and Bhabha.) In second-order perturbation theory (with the meson field as the perturbation), the calculated value of the ratio $|\Delta\mu_n/\Delta\mu_p|$ proved equal to 2.5 (the experimental value of this ratio is 1.07). In itself this discrepency is large, but the reliability of the result obtained is extremely dubious, since the contribution of higher orders of the perturbation theory (not taken into account by the authors) are by no means small.

There seems to be greater promise in an attempt by Miyazawa [2], based on Chew and Low's very recent [3] development of an approximate nonrelativistic theory of the interaction of π-mesons with nucleons. This

theory contains two parameters – the coupling constant f^2 between meson field and nucleons, and the cut-off momentum K_{max}. The introduction of this latter parameter corresponds to the fact that at distances from the center of the nucleon smaller than $r = \frac{h}{K_{max}}$ the interaction is taken to be "turned off". If this is not done, meaningless infinite quantities turn up in the calculations. It turned out that for the parameter values $f^2 = 0.08$ and $K_{max} \approx 6\mu c$ (where μ is the mass of the π-meson) the theory satisfactorily describes the processes of scattering of π-mesons by nucleons and the formation of π-mesons by high energy photons (photoproduction).

Miyazawa applied the equations of Chew and Low to the problem of the anomalous magnetic moments of nucleons. The results he obtained show that the same values of the constants f^2 and K_{max} that give a correct description of the scattering and photoproduction of π-mesons also give anomalous magnetic moments of the nucleons close to the experimental values. But the ratio $|\Delta\mu_n / \Delta\mu_p|$ calculated by Miyazawa is, as before, somewhat larger than required (~ 1.5).

Of interest in this connection is a note by Sandri [4], who suggests that the K-mesons be brought in for the explanation of the anomalous magnetic moments of nucleons. It is known that at low energies the K^+ and K^- mesons behave unsymmetrically: the energy threshold for the production of K^--mesons lies considerably higher than the threshold for the production of K^+-mesons. This means that the clouds of virtual K-mesons around both proton and neutron must be positively charged. But as was noted above, the cloud of virtual π-mesons around a proton has a positive charge, and around a neutron a negative charge. Consequently, for the neutron the virtual K-mesons neutralize the charges and currents of the virtual π-mesons, and for the proton they reinforce them. In the opinion of Sandri, a consideration of these effects can reduce the anomalous magnetic moment of the neutron, increase the anomalous moment of the proton, and thus secure agreement with the experimental values of these quantities.

L. L.

LITERATURE CITED

[1] S. P. Misra and B. B. Deo, Ind. J. Phys. 30, 16 (1956).

[2] H. Miyazawa, Phys. Rev. 101, 1564 (1956).

[3] G. F. Chew and F. E. Low, Phys. Rev. 101, 1570 (1956).

[4] G. Sandri, Phys. Rev. 101, 1616 (1956).

ESTIMATION OF RESONANCE INTEGRALS

A knowledge of the resonance integrals of a number of elements is extremely important for reactor design. Of interest here is the attempt of Dresner [1] to find a semiempirical relation between the values of the resonance integrals $\int_0^\infty \sigma_r(E)\,dE/E$ and parameters of the resonance levels such as Γ, the total level width, Γ_γ, the local radiation level width averaged over several resonances, Γ_n^0, the local neutron level width averaged over several resonances, D^*, the average separation between levels with the same spin and parity, and E_1, the energy of the first resonance [σ (E) is the cross section for radiative capture as a function of the neutron energy E].

For heavy nuclei ($A \geqslant 100$) with many resonances, a statistical averaging over all resonances leads to the formula

$$\int \sigma_r \frac{dE}{E} = \frac{C}{E_1}\left(\frac{2\pi\overline{\Gamma}_\gamma}{D^*}\right)\frac{\beta - \log(1+\beta)}{\beta^2}, \qquad (1)$$

where $\beta = E_1^{-1/2}\,(\overline{\Gamma}_\gamma/\overline{\Gamma}_n^0)$, and C is a constant.

In the derivation of Eq. (1) it is assumed that $\overline{\Gamma}_\gamma/D^*$ is independent of the energy, as is confirmed by a number of experimental results. The average experimental values of the parameters are $2\pi\,\overline{\Gamma}_\gamma/D^* \approx 0.02$ and $2\pi\overline{\Gamma}_n^0/D^* \approx (5-10)\cdot 10^{-4}\,(\text{ev})^{-1/2}$.

In Fig. 1 the resonance integral is plotted as a function of E_1, according to Eq. (1), for various values of the parameters. The value of the resonance integral is weakly dependent on the choice of $2\pi\overline{\Gamma}_\gamma/D^*$. Experimental values of resonance integrals are plotted as points. For antimony two pairs of values are plotted, corresponding to two possible values of E_1. All of the experimental points lie on curve A (or B) to within a factor of 2 (with the exception of Hf^{180}).

For heavy nuclei ($A \geqslant 100$) with single resonances at energies E_0 separated from the thermal energy E_T by at least several widths Γ, the resonance integral can be correlated with the thermal neutron cross section $\sigma_r(E_T)$ by the following formula:

$$\frac{\int \sigma_r \frac{dE}{E}}{\sigma_r(E_T)} = \frac{2\pi\sqrt{E_T E_0}}{\Gamma}. \qquad (2)$$

In this range of masses $\Gamma \approx \Gamma_\gamma \approx 0.03$-$0.15$ ev.

Figure 2 shows the dependence of $\dfrac{\int \sigma_r\,dE/E}{\sigma_r(E_T)}$ on E_0, as given by Eq. (2), for several values of

Γ_γ. The experimental values are also given. From Fig. 2 it is seen that the accuracy of the estimate of the resonance integral depends on the knowledge of Γ_γ.

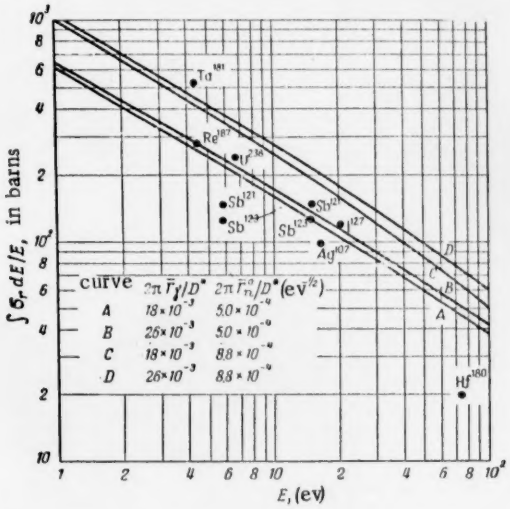

Figure 1. Resonance integral for $A \geq 100$ as a function of E_1, for various values of the parameters (the value $8.8 \cdot 10^{-4}$ ev$^{-1/2}$ is a theoretical value taken from reference [2]).

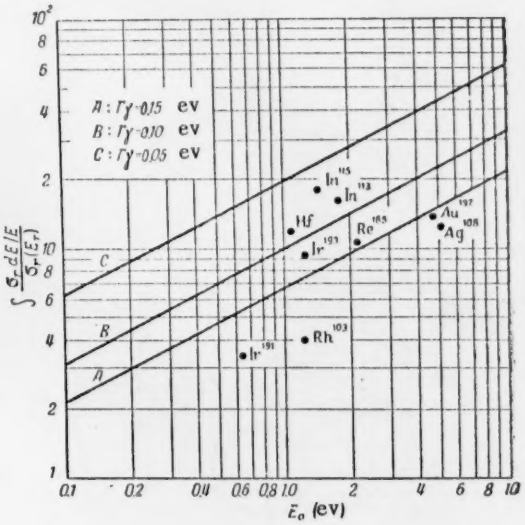

Figure 2. Ratio of the resonance integral to the thermal neutron capture cross section as function of E_0 for various values of Γ_γ.

Light nuclei ($A \leq 50$) as a rule do not have resonances. Their capture cross sections follow the law 1/V. For these nuclei, as is well known [3], the resonance integral taken through the range above the cadmium absorption ($E > 0.4$ ev) is equal to half the capture cross section at thermal energy.

For nuclei of intermediate atomic weight ($50 < A < 100$), contributions are made to the resonance integral both by capture following the 1/V law and by resonance capture. In this range of masses the experimental data agree rather less well with the semiempirical formula.

The so-called magic and near-magic nuclei depart from the regularity that has been noted. They behave like light nuclei. Thus the nuclei Y^{89} and Pr^{141} have capture cross sections varying as 1/V, and Tl^{203} and Tl^{205} have large intervals between their levels.

Thus the formulas that have been presented make it possible to estimate the resonance integrals to within a factor of 2 or 3, from just a knowledge of certain of the resonance parameters.

Of interest here are the recently published [4] new values of the resonance integrals, over the region above the cadmium absorption, for the activation of U^{238} and Th^{232} obtained by comparison with the activation of Au^{197}. When the contribution from the 1/V cross section is removed, these turn out to be 281 ± 20 barns for U^{238} and 67 ± 5 barns for Th^{232}, in good agreement with the estimate in Reference [1].

P. K.

LITERATURE CITED

[1] L. Dresner, J. Nuclear Energy 2, 2, 118 (1955).

[2] J. Blatt and V. Weisskopf, Theoretical Nuclear Physics (Foreign Lit. Press, Moscow, 1954).

[3] D. Hughes, Neutron Researches with Nuclear Piles (Foreign Lit. Press, Moscow, 1954).

[4] R. L. Macklin and H. S. Pomerance, J. Nuclear Energy (in press).

BEHAVIOR OF URANIUM AND CERTAIN OTHER MATERIALS IN FLUORIDIZING MEDIA*

Bromine trifluoride, bromine pentafluoride, and chlorine trifluoride are strong fluoridizing agents, which can be used instead of fluorine for the production of many inorganic fluorides. Since these halogen fluorides can be kept as liquids at room temperatures, they can serve as more compact sources of fluorine than fluorine gas. Under the action of liquid halogen fluorides, metals and oxides can be converted into fluorides at lower temperatures than under the action of gaseous fluorine.

The main purpose of the investigation was to obtain the qualitative characteristic of the behavior of uranium in halogen fluorides and in fluorine at elevated temperatures, and to make a qualitative investigation of the stability of less active materials in these reagents.

Under the action of bromine tri- and pentafluorides and of chlorine trifluoride, metallic uranium is converted into uranium hexafluoride, as is shown by the equations

$$U_{sol} + 2\,BrF_3\ liq \xrightarrow{50\text{-}125^\circ C} UF_6\ liq + Br_2\ liq\,, \qquad (1)$$

$$U_{sol} + 3\,BrF_5\ liq \xrightarrow{50\text{-}75^\circ C} UF_6\ liq + 3\,BrF_3\ liq\,, \qquad (2)$$

$$U_{sol} + 3\,ClF_3\ liq \xrightarrow{25\text{-}75^\circ C} UF_6\ liq + 3\,ClF\ gas\,. \qquad (3)$$

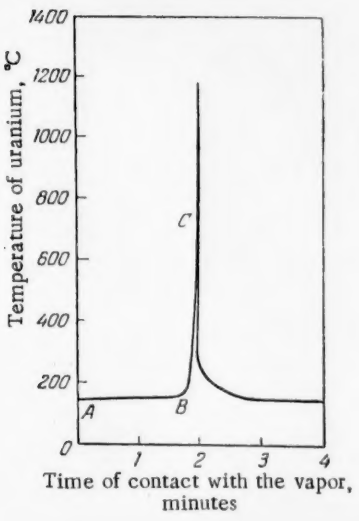

Curve of the ignition temperature of uranium in bromine trifluoride vapor.

This reduction product in the first reaction is shown as bromine, but bromine monofluoride can also be formed. Bromine accelerates the Reaction (1) somewhat, and the intensity of UF_6 formation is appreciably increased. Since these reactions are exothermic, heat must be removed to prevent a rise of the temperature, particularly if the products that accelerate the reaction are not removed. It was found that a slow dissolving of uranium occurs in liquid bromine tri- and pentafluorides at temperatures appreciably exceeding the normal boiling points.

In the action of gaseous halogen fluorides or of fluorine on uranium, a reaction of explosive character occurs. The cause of this phenomenon may be the poor heat transfer in the fluoridizing system solid phase-gas.

The diagram shows the curve of the temperature-time dependence. At the point A the specimen of

* Ind. Eng. Chem. 48, 3, p. 1, 418 (1956).

uranium was exposed to the action of the vapor. Beyond point B the temperature rises abruptly. In the neighborhood of point C the uranium incandesces. The maximum temperature was not determined exactly, since the thermocouple was melted.

Thorium does not react appreciably with any of these reagents under the conditions described above. Experiments to check the stability of certain other materials made it possible to find, in a qualitative way, construction materials that can be used for apparatus or for containers for halogen fluorides.

V. P.

THE PROGRAM OF CONSTRUCTION OF POWER REACTORS IN THE U.S.A.*

The United States of America is setting up a broad program of construction of experimental nuclear power reactors. Table 2 (see pp. 649) gives a summary of the main power installations (operating, in construction, and proposed).

Alongside the construction of the experimental power reactors, the U.S.A. has planned for the period 1957-1962 the construction of atomic electric stations of power 75,000-250,000 kw. Table 1 (see below) shows certain technical and economic indices of these electric stations.

O. Shch.

* Engineer 201, 5231, 425 (1956).

TABLE 1
Proposed Prototypes of Atomic Electric Stations

Company	Westinghouse and Duquesne Light**	Yankee Atomic Electric	Consolidated Edison	Commonwealth Edison and others	Consumers' Public Power District	Power Reactor Development	Westinghouse, and Pennsylvania Power and Light
1	2	3	4	5	6	7	8
Place of construction	Shippingport, Pennsylvania	Western Massachusetts	Indian Point, N. Y.	Near Chicago	Nebraska	Premises of Detroit Edison Co.	Premises of Pennsylvania Power and Light Co.
Type of reactor	with water under pressure (PWR)	with water under pressure	with water under pressure	with boiling water	sodium-graphite	fast neutron, with extended source	homogeneous
Thermal power, kw	236,000	480,000	500,000	682,000	250,000	300,000	–
Electric power, kw	100,000	134,000	250,000***	180,000	75,000	100,000	150,000
Charge of fuel	12 tons natural uranium and 52 kg enriched uranium	28,000 kg	275 kg uranium and 8,100 kg thorium	68,000 kg	24,600 kg	2,100 kg	–

(Continued)

** The reactor is being built by the Atomic Energy Commission of the USA. The firms Westinghouse and Duquesne Light are acting as chief contractors for the Commission.

*** Including 110,000 kw on account of superheating the steam by ordinary means.

TABLE 1 (Continued)

1	2	3	4	5	6	7	8
Enrichment with U^{235} isotope, %	up to 90	2.7	about 90 (for the uranium)	1.1	2.3	20	–
Moderator	H_2O	H_2O	H_2O	H_2O	graphite	none	–
Heat transfer material	H_2O	H_2O	H_2O	H_2O	Na	Na	fuel solution
Av. temp. of transfer material in reactor, °C	282	279	269	249	496	427	–
Pressure in reactor case, atmos	140	140	105	42	21	7 ÷ 14	–
Steam parameters:							
a) pressure, atmos	41	42	30	42	56	42	42
b) temperature, °C	saturated	saturated	saturated	249	441	388	–
Estimated cost of reactor, thousands of dollars •	27,700	17,400	–	34,200	13,500	36,000	–
Estimated cost of turbogenerator installation, thousands of dollars	10,000	16,000	–	10,800	10,800	9,000	–
Estimated cost of whole project, thousands of dollars	37,700	33,400	55,000	45,000	24,300	45,000	–
Cost of plant per kw of power	370	246	230	250	320	540	–
Scheduled time for completion	1957	1959-1960	1960	1960	1958-1959	1959-1960	1962

• Exclusive of expenses for research, preparation of the fuel elements, and special materials for them. The cost of preparing the fuel elements forms part of the cost of the fuel.

TABLE 2
Principal Experimental Power Reactors of the U.S.A.

Name of reactor	EBR-1	EBR-2	HRE-1	HRE-2	BORAX-III •	EBWR	SRE	LAPRE-1	LAPRE-II	LAMPRE	OMRE	LAMPRE
Place of construction	Idaho, National Experimental Base	Idaho, National Experimental Base	Oak Ridge	Oak Ridge	Idaho, National Experimental Base	Argonne	Santa Susanna (California)	Los Alamos	Los Alamos	Los Alamos	Idaho, National Experimental Base	–
Laboratory in charge of project	Argonne	Argonne	Oak Ridge	Oak Ridge	Argonne	Argonne	Atomics International	Los Alamos	Los Alamos	Los Alamos	Atomics International	Brookhaven
Thermal power, kw	1,400	62,500	1,000	5,000–10,000	15,000	20,000	20,000	2,000	1,300	about 1,000	16,000	5,000–10,000
Electric power, kw	150	17,500	150	300	2,400	5,000	7,500	none	none	none	none	none
Cost of reactor ••, thousands of dollars	2,700	15,300	1,100	1,800	600	3,600	5,300	700	100	–	875	–
Cost of entire project•••, thousands of dollars	6,000	39,600••••	12,800	38,800••••	2,800	19,700••••	14,400••••	2,200	280	3,000	1,800	10,000–12,000
Date construction started	Fall, 1949	1956	March, 1951	July, 1954	September, 1954	June, 1955	August, 1954	1955	1955	1958	January, 1956	–
Date reactor reached critical condition	August, 1951	1958	April, 1952	1956	June, 1955	1956	1956	1956	1956	1959	1956	–
Date full power reached	December, 1951	1959	February, 1953	1956	July, 1955	1956	1957	1956	1956	1959	1957	–
Temperature of heat-transfer medium leaving reactor, °C	316	538	249	299	214	253	516	429	316	–	277	–
Pressure (manometric) inside reactor case, atmos	about 7	about 7	70	140	21	42.1	21	about 275	about 56	–	21	–
Charge of uranium, kg	48	150 (or 90 kg Pu)	3	4	15	4,500	2,100	8.4	7.7	Pu alloy	20	–
Enrichment with U-235 isotope, %	about 90	45 (or 24% Pu)	about 90	about 90	about 90	1.4	2.9	about 90	about 90	–	about 90	–
Moderator	none	none	H_2O	D_2O	H_2O	H_2O	graphite	H_2O	H_2O	none	diphenyl	graphite
Heat-transfer medium	NaK	Na	Circulating solution of fuel	Circulating solution of fuel	H_2O	H_2O	Na	H_2O	H_2O	NaK	diphenyl	Circulating solution of fuel in bismuth
Method of controlling reactor	Displacement of source layer and rods of U-238	Displacement of source layer and fuel rods	Change of uranium concentration and temp. coefficient of reactivity	Change of uranium concentration and temp. coefficient of reactivity	Regulating rods and solution of absorber	Regulating rods	Regulating rods	Regulating rods and temp. coefficient of reactivity	Temp. coefficient of reactivity movable reflector, and solution of absorber	Movable reflector	Regulating rods	Change of uranium concentration, temp. coefficient of reactivity, regulating rods
Parameters of steam produced:												
a) pressure, atmos	29	128	15	36.5	21	42	42	250	42	none	none	none
b) temperature, °C	282	482	saturated	saturated	saturated	saturated	441	–	saturated	–	–	–

• The plan for the reactor BORAX-III forms part of the plan for the reactor EBWR.

•• Including cost of reactor and of preparation of fuel elements for first loading (cost of fuel not included).

••• This figure includes the cost of the reactor.

•••• Cost of reactor includes expenses connected with research on the project in question (July 1953 to July 1958).

THE NUCLEAR REACTOR AS A SOURCE OF ENERGY FOR CHEMICAL PROCESSES*

In present-day chemistry a great role is played by processes taking place at high temperatures, to produce which a large amount of energy is expended. For example, in 1947, 11.2% of all the electrical power consumed in the USA was used in industry to provide heat for chemical processes.

The diminishing natural supplies of solid, liquid and gaseous fuels in the USA is leading to a continual increase of prices for these types of fuel. Owing to this, nuclear fuel is becoming more and more promising, and its use is particularly attractive in chemical industry, where direct use can be made of the heat developed in a nuclear reactor. The use of nuclear reactors offers particular advantages in regions that are difficult of access but rich in raw materials for chemical industry.

The Atomic Energy Commission of the USA and the Bureau of Mines of the USA have now begun a study of problems connected with the use of the heat of nuclear reactors for the intensification of a number of chemical processes, for example, the gasification of coal, the production of nitrogen dioxide from the air, the production of acetylene, of hydrocyanic acid, etc.

The most critical problem in the design of such a reactor is that of materials. Uranium dioxide will obviously be used for the fuel elements in such a reactor, and for the construction materials and moderators use will be made of the carbides of beryllium, zirconium, and calcium. There are also other simpler but no less important problems: erosion by the action of solid particles contained in the gas passing through the reactor; the diffusion of fission products through the ceramic coverings of the fuel elements; the problem of controlling the reactor; and many others.

In the agreement concluded between the Atomic Energy Commission and the Bureau of Mines, the putting into operation of the first plant for production of artificial gas by means of atomic energy is set for 1959.

According to the agreement, from one and one half to two years are allowed for the solution of the problems of materials, and about a year for the designing of the reactor.

I. S.

---

* Chem. Engineering 63, 3, 191 (1956).

PYROMETALLURGIC REGENERATION OF NUCLEAR FUEL

To make the reprocessing of nuclear fuel cheaper there have been proposed [1-4] and discussed [5] pyrometallurgic methods analogous to those applied in the metallurgical industry. The advantage of these methods [6] consists in the fact that the expensive operations of dissolving the uranium and then reducing it again are avoided, the volumes to be handled are greatly reduced, and the radioactive wastes are secured in a small volume, which is convenient for their use and storage. The materials employed in the pyrometallurgic processes are relatively stable against irradiation, which makes it possible to regenerate freshly irradiated fuel.

A shortcoming of these methods is the low degree of purification from the fission fragments. Only the main mass of the fragments – the "poisons" absorbing neutrons – is removed. Since the γ-activity is lowered by roughly a factor of 5, there are technical difficulties in carrying out the metallurgical processes, which have to be accomplished behind sufficiently thick shielding.

The following pyrometallurgic processes are regarded as promising:

1. Extraction of plutonium and volatile fission fragments in vacuum at 1600 to 1700° C. The separation of the plutonium from the uranium is based on the fact that the vapor pressure of plutonium at these temperatures is hundreds of times as large as that of uranium. Laboratory experiments have shown [8] that at 1650° C 98.0% of the plutonium is driven off from irradiated uranium containing 0.02% plutonium.

2. Extraction of the plutonium and fragments from liquid fuel by liquid metals (Mg, Ag, Ce). Of interest in this connection is the use of a slight admixture of gold in extraction by silver [9], which under optimal conditions increases the distribution ratio of the plutonium by a factor of 2.5.

3. Extraction of plutonium and rare-earth fragments from the melted fuel by fused salts (UF_4, UCl_3 and others). By an exchange reaction between the salt and the melted fuel the plutonium and rare-earth elements, forming more stable halide compounds, go into the salt phase. The plutonium is displaced from the salt phase by alkaline-earth metals.

4. Melting and settling of the irradiated uranium in crucibles of refractory oxides. In this process the fission fragments – "poisons" – volatilize or are subject to selective oxidation. The plutonium is not separated from the uranium, which can be reused in fast-neutron reactors.

The technical requirements for a pyrometallurgic process for regeneration of the fuel from a reactor (500 megawatt) using natural or slightly enriched uranium, working to burning out of 1% of the fuel, present the following special features. In the regeneration plant there are no liquid radioactive wastes, and it is located in the same building with the reactor. The average amount of uranium regenerated daily (about 50 kg, i.e., 25 l) can be handled readily in a container 0.5 m in diameter and about 1.0 m high. The container is located in a "hot" chamber of width 6 to 7.5 m and height 3 to 4.5 m, of ordinary concrete about 3 m thick, lined on the inside with thin plates of stainless steel to facilitate cleaning. For discharging, repairs and change of equipment a separate shielded area is required. For moving the materials inside the chamber, electric motors or hydraulic devices are used.

The heating is done with high-frequency currents or molybdenum heaters. To cool the chamber, in which a great deal of heat is developed, use is made of liquids that react only weakly with the fuel under treatment, for example hydrocarbons. It must be taken into account that freshly irradiated fuel gives a large amount of heat, which can serve for the melting of the metal.

To protect the molten metal and the vapor from oxidation there must be maintained in the chamber

either an inert atmosphere (helium, argon) or, what is more difficult, a vacuum. Apparatus has to be provided for purifying the medium from radioactive gases.

To test the degree of elimination of the "poison" fragments, a sample of the regenerated fuel is placed in an apparatus in which its reactivity is measured by the multiplication of neutrons. This is considerably more convenient than performing a complete isotopic analysis.

As an example, we describe in outline a process of extraction with liquid silver [6]. The contaminated fuel is melted together with the extraction agent, silver, in a contactor of refractory material. The extraction agent is drawn into a container, and then evaporated, and the plutonium left behind is discharged into a receiver. The purified fuel is drawn out of the contactor and the silver is driven out by distillation. The silver vapor is sent into the contactor, where it condenses and again takes part in the process.

The flow of liquid metal in graphite pipes is regulated by valves operating by freezing and melting the metal in U-shaped bends. The transfer of liquid metal from one vessel to another is by gravity or by means of the pressure of silver vapor – a "vapor pump". The valves and "vapor pump" are actuated by electric heaters.

The temperature conditions in the process must lie between the melting point of the fuel and the boiling point of the extraction agent. The ranges can be seen from the table:

	Mg	Ag	Pu	U	Th
Melting point, °C	650	960	632	1129	1690
Boiling point, °C	1126	2212	3235	3900	> 3000

The greatest difficulty in carrying out this process is in the choice of a refractory material that is stable against corrosion at the high temperatures and capable of withstanding the thermal stresses.

Although the materials used have various defects (graphite forms carbides, the refractory oxides MgO, BeO, ZrO_2, etc. are not sufficiently stable against heat, and the refractory metals Mo, Ta, and Nb are corroded by the liquid fuel), it appears that there are no insurmountable difficulties in the way of solving the problem.

At the beginning of June of the present year a demonstration was given in Harwell of an experimental apparatus for pyrometallurgic regeneration [10]. In the "hot" chamber the irradiated blocks were mechanically removed from their coatings and were melted in a graphite crucible at 1200 to 1300° C. Some of the fission fragments were vaporized, and some were collected in the walls of the crucible and in the slag on the surface of the melt. The molten uranium with a considerable residual activity can be drained off through the bottom and reused for the preparation of fuel elements in the "hot" chamber. It is believed that this process is more economical than the aqueous one, and that it will be semicontinuous.

But the advantage of the pyrometallurgic over the aqueous process can be finally established only after tests in a pilot plant.

The successful development of pyrometallurgic regeneration processes would greatly facilitate the design of an economic nuclear power reactor with liquid metal fuel.

Ya. P.

LITERATURE CITED

[1] E. E. Motta (Report No. 542 at the International Conference on the Peaceful Uses of Atomic Energy, 1955).

[2] H. M. Feder, Report No. 544, ibid.

[3] A. F. Voigt, Report No. 545, ibid.

[4] O. E. Dwyer et al., Report No. 550, ibid.

[5] Reports of Papers Nos. 84-89 of the meeting of the Electrochemical Society, May, 1956, J. Electrochem. Soc. 103, 3, 63c (1956).

[6] R. C. Reid, D. Duffey and J. E. Vivian, Nucleonics 14, 2, 22 (1956).

[7] F. Roberts, Ind. Chem. 32, 272, 15 (1956).

[8] D. E. McKenzie, Can. J. Chem. 34, 515 (1956).

[9] D. E. McKenzie, Can. J. Chem. 34, 749 (1956).

[10] Nucl. Eng. 1, 4, 163 (1956).

USE OF A HELICOPTER FOR URANIUM PROSPECTING

The helicopter is widely used in exploration for mineral deposits in many lands. Recently it has begun to play a leading role also in prospecting for ore deposits of uranium, especially in the U.S.A., in the Colorado Plateau and Rocky Mountain regions.

The possibility of landing a helicopter in a small space and of flying at a low altitude, and also the capability of hovering in the air make it in many instances irreplaceable in the organization and execution of explorations for uranium.

The helicopter makes possible delivery of cargo and personnel to difficultly accessible places in a short time, especially in rugged country. Using a helicopter, a geologist may view, photograph, and sketch craggy, precipitous, and otherwise inaccessible outcrops. In searching for uranium by determination of radioactive anomalies, the helicopter has preference over an airplane since it makes possible flight at a height of 15-20 meters, easy maneuvering in narrow mountain canyons, and landing at the place of an anomaly revealed in the air for investigation immediately on the surface of the ground.

However, the usual helicopters used in the U.S.A. up to recently had a low flight ceiling; as a consequence, many high mountain regions of the western states of the U.S.A. remained unexplored.

Cognizant of this, the Bell Aircraft Corporation released a new helicopter model specially adapted for uranium exploration and calculated for flight at a considerable altitude. In these helicopters the scintillation counter and the auto-recording instruments are located in the pilot's cabin immediately forward of the geologist-observer.

All the equipment, including the scintillation counter, detector, auto-recorder, and panel, may be taken out of the helicopter in several minutes in case it must be used for other purposes.

The Colorado Plateau, with its deep canyons and steep slopes which are often inaccessible for geologic investigation by surface exploration, is a region where the use of the helicopter has proved particularly effective. For investigation of ore-bearing formations which crop out in the walls of canyons, a flight parallel to the rim and 3 to 15 meters from it is used. A flight at such a distance makes possible the separation and tracing of uranium-bearing beds both with the help of a scintillation counter and visually by the characteristic color and other prospecting signs.

Helicopters for uranium prospecting are used by government institutions, various private firms, and also by independent prospectors. In some cases geologists obtain certification as pilots, and when necessary they may make flights themselves.

M. K.

LITERATURE CITED

[1] B. Bower, Mining World 18, 1 (1955).

[2] A. S. MacLaren, Can. Mining J. 76, 4, 55 (1955).

NEW TYPES OF URANIUM ORES

In recent years new mineralogical types of uranium ores have been discovered in a number of countries. If in the past a comparatively small number of minerals (such as pitchblende, uraninite, carnotite, otenite) were considered to be uranium minerals which had industrial importance, it is now true that minerals which did not attract attention earlier or were completely unknown are acquiring ever greater industrial importance.

Thus, brannerite – a uranium titanate – was earlier associated with rare minerals. It was found associated with granites and in certain pegmatites, where it did not assume concentrations of industrial significance. It is now true that in the new uranium-region of Canada – in Blind River – brannerite proved to be the chief uranium mineral which contained large uranium resources [1].

An even less common mineral – davidite – is at the present time being mined in the Australian region called Radium Hill, which is considered a relatively large source of uranium [2]. Davidite is a complex uranium titanate. Besides the Radium Hill location, davidite was discovered in a uranium-rich location near Tete (Mozambique, Africa), where it is also the major uranium mineral. Davidite has also been discovered in the Mount-Ice region (Australia).

Of great interest with regard to industrial applications was the discovery of a new mineral – coffinite – in the Colorado plateau mines [3].

This mineral which belongs to the silicate group is found in dense veins combined with pitchblende in the sandstone of the Big Indian Wash region (in the state of Utah, USA), and is now known to be present in more than fifteen uranium sources of the Colorado plateau region. Recently, a mineral similar to coffinite was found in the state of Nevada in Epic Mine in the vicinity of Austin, where it is found in fissures where it forms coffinite veins [4].

This mineral is evidently one of the members of an isomorphous nenadkevite series which was discovered in the USSR in 1952 [5].

Available data permit us to conclude that a relatively wide distribution of minerals of this series is possible in certain localities and provinces; in individual cases these minerals appear in concentrations which are sufficient for industrial use.

These discoveries verify the fact that in the future it may well be possible to reevaluate the industrial significance of various uranium minerals. Uranium prospectors today cannot limit their knowledge to a small selection of industrial uranium minerals and to those of them which are significant in the sense of present prospecting, but must acquire a broad knowledge of the mineralogy of uranium.

M.K.

LITERATURE CITED

[1] R.I. Trail, Can. Mining J. 75, No. 4, 63-68 (1954).

[2] L. Parkins, Econ. Geol. 48, No. 7 (1953).

[3] L.R. Stieff, T.W. Stern and A.M. Sherwood, Science 121, No. 3147, 608 (1955).

[4] Western Mining and Ind. News, 24, No. 2, 16 (1956).

[5] V.A. Polikarpova, Atomic Energy No. 3, 132 (1956) (T.p. 425). *

*T.p. = C.B. Translation pagination.

ENRICHMENT OF HEAVY WATER BY A BIOLOGICAL METHOD *

In all methods for the enrichment of heavy water the first stage of the process is very expensive, which considerably increases the cost of any final product for whose production heavy water is used. A number of biochemical processes, and such biological production processes as the growing of moulds to obtain penicillin, give only a slight reduction of the volume of the water used, and the amount of enrichment is extremely small.

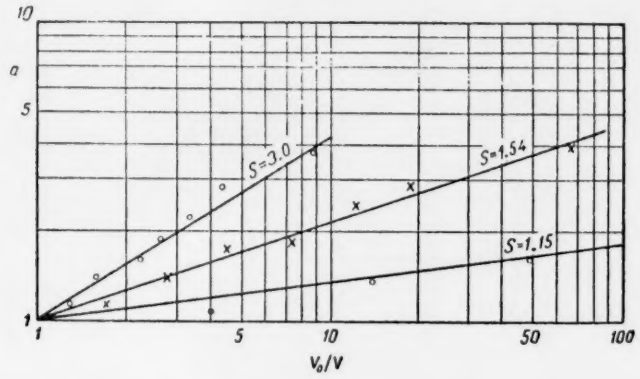

The authors have investigated the heavy hydrogen content in water remaining after the first steeping of grains of barley in the production of malt. In order to obtain a decided reduction of the volume of the water used to steep the barley, the authors tested the water after nine successive steepings. After every third steeping a sample of the water was distilled to remove organic substances leached out of the barley. The experiments were conducted with various proportions of barley and water, but always under fixed conditions of temperature and steeping time. The results of the tests are shown in the diagram, where the enrichment factor α is plotted as a function of the decrease of volume, V_0/V. It is seen from the curves that the percentage of enrichment depends on the conditions of the steeping. For the calculation of the isotopic separation index s the authors use the formula applied in the electrolytic separation of water,

$$\frac{dN_H}{N_H} = s\frac{dN_D}{N_D},$$

where N is the number of molecules of an isotope taking part in the separation process. When the values of the initial volume V_0 and the final volume V are introduced into Eq. (1), we obtain, approximately,

$$s = \frac{\ln V_0/V}{\ln V_0/V - \ln \alpha}.$$

The enrichment factor α is here used as the ratio of the molar concentrations of heavy water in the volumes V and V_0 respectively. In calculating the values of s the authors made use of the fact that the tap water in

* Nature 177, 4517, 988 (1956).

Stockholm contains 0.015% heavy water. The results of the calculations were:

Ratio of weight of barley to weight of water	0.30	0.67	1.33
Isotopic separation index $\underline{s}$	3.0	1.54	1.15

The concentration of the isotope was determined by means of infra-red spectrometry on the absorption band of HDO at 3.83 μ. These measurements were carried out to an accuracy of $\pm$ 0.003% in the absolute scale of D_2O content. The calculations were also confirmed by steeping with water containing 0.5% of heavy water, and by analyzing the isotope content by the method of precision pycnometry.

From these calculations it can be seen that the method of concentration of heavy water by the steeping of germinating barley grains gives a high degree of enrichment as compared with other biological methods.

S. L.

A PORTABLE APPARATUS FOR FREEING WATER FROM RADIOACTIVE CONTAMINATION *

A portable apparatus for the decontamination of reservoirs that have become contaminated with radioactive wastes has been developed in the U.S.A. By processes of coagulation, filtration, and disinfection about 85% of most of the fission products can be removed. This figure can be raised to 93% by a preliminary purification by means of clay, and then by a final ion-exchange treatment to 99.9%.

In continuous 24-hour operation the capacity of the apparatus is (depending on the size) 11,400, 5,700 or 2,280 liters per hour.

The principles for freeing water from radioactive contamination used in this apparatus are basically the same as are used to purify water from ordinary contaminations, since the water being treated is not radioactive, but only contaminated by radioactive substances suspended or dissolved in it.

The sources of contamination of water can be waste water from atomic energy plants, or from laboratories or hospitals using radioactive isotopes, and also radioactive atmospheric fall-out, and other kinds of contamination of the water resulting from atomic fission.

The central part of the apparatus is an "erdlator" (an apparatus developed in Engineer Research and Development Laboratories), which by chemical coagulation removes dirt, bacteria, and other suspended matter, and provides effective decontamination. This part of the apparatus is connected in series with diatomaceous earth filters.

Waste water that has undergone the chemical and physical treatment in this apparatus can be used as drinking water only 20 minutes later.

The apparatus is operated by one man and can work at temperatures down to -40°C. The apparatus is mounted on a motor truck chassis and hauled by a $1\frac{1}{2}$ ton tractor. It has its own electric generator and is equipped with a suitable heater.

S. L.

* Chem. Engineering 63, 4, 130 (1956).

APPLICATION OF LIQUID SCINTILLATORS FOR THE QUANTITATIVE DETERMINATION OF TRITIUM IN URINE*

The increasing use of gaseous tritium and tritium-tagged water for chemical synthesis and other processes has given rise to the necessity of developing a simple, rapid, and sensitive method for checking the safety of persons working with this isotope. The paper describes a method of testing the urine of a given group of workers by means of liquid scintillators.

The urine taken for testing is first clarified by mixing with activated wood charcoal, and is filtered. For the test there is taken 2 ml of the filtrate, 0.1 ml of distilled water, and 20 ml of absolute alcohol. After these have been mixed, 28 ml of toluene is added, and 100 ml of the scintillator – p-diphenyloxazole. Two control specimens are also prepared. One of them serves for the measurement of the background; in it the urine is replaced by distilled water; the second is a standard for determining the counting efficiency; in it 0.1 ml of standard THO is used instead of 0.1 ml distilled water.

The analysis is carried out with a scintillation counter constructed with a coincidence circuit with high resolving power. The counting time must be such that the error of the measurement does not exceed ± 5 %. The radioactivity of the specimen of urine (2 ml) is determined in the following way. First the counting efficiency is found by the formula

$$E_s = \frac{(C_i - C_b) - (C_u - C_b)}{N},$$

where C_i is the number of counts in the measurement with the standard for determining the counting efficiency; C_b is the number of counts in the measurement with the control specimen; C_u is the number of counts in the urine specimen; and N is the number of disintegrations per minute in 0.1 ml of standard THO. The number of disintegrations per minute in 2 ml of urine, D_u is found by the formula

$$D_u = \frac{C_u - C_b}{E_s}.$$

The total radioactivity is given by the expression

$$\frac{D_u \cdot 500}{2.22 \cdot 10^6 \text{ disintegrations/minute}} \quad \text{microcuries/liter}$$

This method makes it possible to determine a concentration of tritium of the order of 0.08 μ curie/l, which corresponds to a total content in the organism of 3 to 4 μ curies of tritium.

S. L.

* G. T. Okita, J. Spratt and G. V. Leroy, Nucleonics 14, 3, 76 (1956).

BIBLIOGRAPHY

RECENT LITERATURE ON THE PEACEFUL UTILIZATION OF ATOMIC ENERGY

Books and Symposia

Beleshinsky, S. V. et al., The Chemistry of Beryllium, Frunze, Acad. Sci. Kirgiz SSR Press, 1955, 201 pages, 10 rubles 45 kopecks.

Budnikov, P. P. and Sukhova, L. A., Determination of the Specific Surface of Mineral Fibers by a Radiometric Method, Industrial Construction Literature Press, 1956, 11 pages (Ministry of Building Materials Industry USSR; Tech. Council and Tech. Admin.; Central Bureau Tech. Information; Information Communications), free.

De Vaucouleurs, G., The Physics of the Planet Mars; Introduction to Aerophysics (Translated from French by Yu. A. Ryabov), V. V. Sharonov, editor. Foreign Literature Press, 1956, 350 pages, 14 rubles 85 kopecks.

Vorobyev, E. I. and Margulis, U. Ya., Atomic Energy and Antiatomic Defense (Lecturer's File) 1955, 13 tables on 7 separate cards in a file (Ministry of Health USSR, Institute of Health Education, Assistance to Lecturers), free.

All-Union Conference on the Use of Isotopes in Catalysis, Summaries of Papers, March-April 1956. (Academy of Sciences USSR, Div. Chem. Sci., Inst. Phys. Chem) Acad. Sci. USSR Press, 1956, 78 pages, free.

Gamma-ray Apparatus for Industrial Irradiation with Co^{60} Preparations (Catalog) Moscow, 1956, 12 pages. (Ministry of Electrotechnical Industry USSR, Central Bureau Tech. Information), free.

Kichkin, I. I., and Kozlov, V. A., Use of Radioactive Isotopes for Control of Saturation of a Dredged Mixture (Acad. Sci. USSR, Inst. Tech.-Econ. Information, Instruments and Equipment), 1955, 19 pages, illustrations, 7 rubles.

Brief Instructions for Inspection of Sites of Useful Minerals and Collections of Rock Materials for Rare and Sparse Elements, State Geol. Tech. Press, 1956, 55 pages (Tech. Admin. All-Union Sci. Res. Inst. Econ. Mineral., Ministry of Geology and Mineral Resources Protection USSR), 1 ruble 75 kopecks.

Kulikov, I. S. and Popov, I. A., Use of Radioactive Isotopes in Metallurgy, Associate Members Acad. Sci. USSR, N. V. Ageev and V. F. Smirnov, Editors, Metallurgy Press, 1956, 20 pages, 9 rubles 35 kopecks.

Kryzhanovsky, V. V., Marking of Cold-Rolled Sheet with the Aid of Radioactive Isotopes, 1956, 8 pages, (Ministry of Ferrous Metallurgy USSR, Paper at All-Union Conference on Automation of Production Processes, Magnitogorsk, 1956), Manuscript, free.

Melentyev, P. V., Atlas of Nomograms for Calculation of the Ages of Minerals by Radioactivity Methods, I. E. Starik, Editor, Moscow-Leningrad, Acad. Sci. USSR Press, 1955, 8 separate sheets (Acad. Sci. USSR, Commission on Determination of the Absolute Age of Geological Formations), 3 rubles 15 kopecks.

Dimensions of Nuclei; Problems of Modern Physics, Collected Translations and Reviews of the Foreign Literature, 1956, No. 5, 181 pages, 10 rubles 50 kopecks.

Conference on Studies of Plant Nutrition and Fertilizer Utilization by Labeled Atom Methods, Moscow, 1956; Summaries of Papers Presented at the Conference, V. M. Klechkovsky et al. Editors, 1956, 77 pages (Academy of Sciences USSR and Ministry of Agriculture), free.

Tishkin, P. E., Some Experimental Methods of Nuclear Physics, 1956, 37 pages, illustrations (All-Union Society for Propagation of Political and Scientific Knowledge, Leningrad Division), 75 kopecks.

Charged Particle Accelerators; Problems of Modern Physics, Collection of Translations and Reviews of the Foreign Periodical Literature, 1956, No. 4, 163 pages, 10 rubles 50 kopecks.

Journal Articles

Abrikosov, A. A., "Scattering of Electrons on Electrons and Positrons on Electrons at High Energies," J. Exptl.-Theoret. Phys. 30, 3 (1956) [Soviet Physics – JETP 3, 3, 379 (1956)].

Aleksandrov, S. N. et al., "Comparison of the Biological Action of X-Rays and Radioactive Cobalt Radiation," Medical Radiology I, No. 2 (1956).

Alimarin, I. P. and Bilimovich, G. N., "Chemical Analysis by the Isotope Addition Method," Chem. Science and Industry I, No. 1 (1956).

Berezin, I. V. et al., "Synthesis of Cyclohexanone and Cyclohexanol Containing a Radioactive Carbon Isotope in the Functional Groups," Bull. Moscow Univ., Phys.-Math. and Nat. Sci. Series 1956, No. 2.

Birger, N. G. et al., "Some Instances of the Generation of Heavy Unstable Particles at Be Nuclei," (letter to the editor), J. Exptl.-Theoret. Phys. 30, No. 3 (1956) [Soviet Physics – JETP 3, 4, 617 (1956)].

Boldyreva, N. V., "Use of Labeled Atoms in Helminthology," Lit. Review, Trans. Helminthol. Lab. (Acad. Sci. USSR) 8 (1956).

Blokh, G. A., "Investigation of the Vulcanization of Rubber by the Labeled Atom Method," Chem. Ind., 1956, No. 2.

Brodsky, A. I. et al., "Study of Metal Corrosion With the Aid of a Heavy Oxygen Isotope," J. Phys. Chem. 30, 3 (1956)

Vanetsian, R. A. and Fedchenko, E. D., "Elastic Scattering of Protons with 18.7 Mev Energy on Nickel and Copper Nuclei," (letter to the editor), J. Exptl.-Theoret. Phys. 30, 3 (1956) [Soviet Physics – JETP 3, 4, 624 (1956)].

Vasilyeva, V. N. and Guryanova, "Synthesis of Mercaptans and Disulfides Labeled with Radioactive Sulfur Isotope," J. Gen. Chem. 26, 3 (1956).

Vysotsky, D. I. and Zavelsky, V. S., "Measurement of the Wear of Engine Parts with the Aid of Radioactive Isotopes," Automobile and Tractor Ind. 1956, 4.

Gracheva, N. D. et al., "Experiments on the Use of Liquid Emulsions in Histoautoradiography," Medical Radiology I, 2 (1956).

Dakhnov, V. N., "Use of Atomic Energy for Investigation of Petroleum and Natural Gas Sources," Petroleum Worker 1956, No. 3.

Domshlak, M. P., "The Therapeutic Use of Radioactive Isotopes," Medical Radiology I, 2 (1956).

Zheludev, I. S. and Yurin, V. A., "Some Physical Properties of Rochelle-salt Crystals Subjected to Radiation," Bull. Acad. Sci. USSR, Phys. Ser. 20, 2 (1956).

Zaslavsky, Yu. S. et al., "Investigation of the Mechanism of the Action of Anticorrosion Additives in Oils by the Tagged Atom Method," Fuel Chemistry and Technology 1956, No. 4.

Zilber, L. A. et al., "The Influence of Ionizing Radiation on the Antigenic Properties of Proteins," Medical Radiology I, 2 (1956).

Kaipov, L. and Takibaev, Zh., "Meson Formation in Nuclei of Pb, Cu, and C Under the Action of Cosmic Rays in the Stratosphere," J. Exptl.-Theoret. Phys. 30, 3 (1956) [Soviet Physics – JETP 3, 3, 385 (1956)].

Kirkina, D. F., Novoselova, A. V. and Simanov, Yu. P., "Polymorphism of Beryllium Fluoride," Proc. Acad. Sci. USSR 107, 6 (1956) [C. B. translation, Proc. Acad. Sci. USSR, Chemistry Section 107, 1-6, 201 (1956)].

Klyucharev, A. P. et al., "Elastic Scattering of Protons with 5.4 Mev Energy by Various Nuclei" (letter to the editor), J. Exptl.-Theoret. Phys. 30, 3 (1956) [Soviet Physics – JETP 3, 3, 463 (1956)].

Konobeevsky, S. T., Levitsky, B. M. and Martynyuk, Yu. A., "A New Method for X-Ray Analysis of Radioactive Materials," J. Tech. Phys. 26, 4 (1956).

Kornev, Yu. V. and Vintaikin, E. Z., "Study of the Sublimation of Silver by the Radioactive Tracer Method and with the Aid of the Mass Spectrometer," Proc. Acad. Sci. USSR 107, 5 (1956) [Soviet Physics – "Doklady" 1, 2, 203 (1956)].

Kocharyan, N. M. et al., "Nuclear Reactions of High-Energy Protons in Copper," Proc. Acad. Sci. USSR 107, 5 (1956) [Soviet Physics – "Doklady" 1, 2, 209 (1956)].

Kravchenko, I., "Atomes" (Review of a French Monthly Popular Scientific Journal), Science and Life 1956, No. 5.

Kunin, P. A. and Taksar, I. M., "Interaction of Nucleons, Including Effects of Isobaric States," Bull. Acad. Sci. Latvian SSR, 1956, No. 2.

Kupriyanov, S. E. et al., "Disintegration of Positive Ions in Collisions with Molecules" (letter to the editor), J. Exptl.-Theoret. Phys. 30, 3 (1956) [Soviet Physics – JETP 3, 3, 459 (1956)].

Larin, S. I., "Angular Momentum Distribution and Spatial Distribution of Nucleons in Nuclei" (letter to the editor), J. Exptl.-Theoret. Phys. 30, 3 (1956) [Soviet Physics – JETP 3, 4, 615 (1956)].

Lvova, E. M. and Moroz, G. S., "Integral Coefficient of Absorption of Solar Radiation by Certain Materials and Coatings," J. Tech. Phys. 26, 4 (1956).

Maksimov, L. A., "Elastic Scattering of Protons by Tritium" (letter to the editor), J. Exptl.-Theoret. Phys. 30, 3 30, 3 (1956) [Soviet Physics – JETP 3, 4, 642 (1956)].

Mikheeva, L. M., Novoselova, A. V. and Bikhtimirov, R., "Determination of the Solubility of Calcium Fluoride and Calcium Fluoberyllate in Water and Hydrochloric Acid Solutions by the Tagged Atom Method," J. Inorg. Chem. (USSR) 1, 3 (1956).

Nemerovsky, P. E., "Cross Sections of Interactions Between Neutrons and Nuclei," J. Exptl.-Theoret. Phys. 30, 3 (1956) [Soviet Physics – JETP 3, 4, 484 (1956)].

Nesmeyanov, A. N. et al., "Investigation of Bromine Isotope Exchange Between Bromides of Elements and Organic Bromine Derivatives," J. Phys. Chem. 30, 3 (1956).

Neiman, M. B. et al., "Investigation of the Influence of Molecular Structure on the Rate of Ionic and Atomic Isotope Exchange Reactions, IV – Investigation of Radical-Chain Reactions in Isotope Exchange Between Alkyl Iodides and Elementary Iodine," J. Phys. Chem. 30, 3 (1956).

Neiman, M. B., "Radioactive Isotopes in Chemical Technology," Chemical Science and Industry 1, 1 (1956).

Nikishov, A. I., "Interaction of Pions with Protons at 1.4 Bev Energy" (letter to the editor), J. Exptl.-Theoret. Phys. 30, 3 (1956) [Soviet Physics – JETP 3, 4, 634 (1956)].

Novozhilov, Yu. V., "The Intermediate Coupling Method in Meson Theory," Bull. Leningrad Univ. Phys. and Chem. Ser. 1956, No. 4.

Orlov, A. S., "Inclusion of Phosphorus in Nucleic Acid in Stable and Labile Combinations with Proteins in Certain Organs of White Rats Under Total X-Ray Irradiation," Medical Radiology 1, 2 (1956).

Peker, L. K., "Isomeric States in Deformed Nuclei" (letter to the editor), J. Exptl.-Theoret. Phys. 30, 3 (1956) [Soviet Physics – JETP 3, 4, 645 (1956)].

Petrov, M. and Vasilyev, V., "Attack on the Nucleus" (Elementary Particle Accelerators; With a Preface by V. I. Veksler), Knowledge is Power 1956, No. 4.

Peshkov, V. P., "Transformation of the λ-Transition in Helium in Presence of Thermal Flow Into a Special Transition of the First Kind," (letter to the editor), J. Exptl.-Theoret. Phys. 30, 3 (1956) [Soviet Physics – JETP 3, 4, 628 (1956)].

Pokrovsky, G. I., "Use of Nuclear Explosions for Industrial Purposes," Mining J. 1956, No. 5.

Rogozhin, Yu. V., "Investigation of the Chemical Stability of Glass in Ferric Chloride Solutions by the Tagged Atom Method," Trans. All-Union Sci. Res. Inst. Glass 1956, No. 36.

Ryzhanov, S. G., "Theory of Asymmetric Fission of Heavy Nuclei" (letter to the editor), J. Exptl.-Theoret. Phys. 30, 3 (1956) [Soviet Physics – JETP 3, 4, 632 (1956)].

Savich, A. V., "Nuclear Shell Structure and Classification of Atomic Nuclei," J. Exptl.-Theoret. Phys. 30, 3 (1956) [Soviet Physics – JETP 3, 3, 400 (1956)].

Spitsyn, V. I., "Application of Tagged Atoms to Studies of the Structure of Certain Isopoly- and Heteropolycompounds," J. Inorg. Chem. 1, 3 (1956).

Starik, I. E., "Pierre Curie (The Role of P. Curie in the History of Fundamental Problems of Radiogeology; On the 50th Anniversary of His Death), Bull. Acad. Sci. USSR, Geol. Ser. 1956, No. 4.

Starik, I. E. and Rozovskaya, N. G., "Study of the State of Microquantities of Radioelements by the Desorption Method," Proc. Acad. Sci. USSR 107, 6 (1956).

Starik, I. E., and Rozovskaya, N. G., "Sorption of Polonium by Glass," J. Inorg. Chem. 1, 3 (1956).

Strutinsky, V. M., "Angular Distribution of Fission Fragments" (letter to the editor), J. Exptl.-Theoret. Phys. 30, 3 (1956). [Soviet Physics – JETP 3, 4, 638 (1956)].

Tarasov, Yu. A. "Reaction Between Nucleons and Antinucleons" (letter to the editor), J. Exptl.-Theoret. Phys. 30, 3 (1956) [Soviet Physics – JETP 3, 4, 636 (1956)].

"Uranium (Structure and Properties)," Review by A. G., Metallurgy and Metal Treatment 1956, No. 4.

Fialkov, Ya. A. and Nazarenko, Yu. P., "Study of Isotope Exchange Reactions in Solutions of Green Modifications of Chromium Salts," J. Inorg. Chem. 1, 3 (1956).

Fogel, Ya. M. and Mitin, R. V., "Formation of Negative Hydrogen Ions in Collisions of Protons with Gas Molecules," J. Exptl.-Theoret. Phys. 30, 3 (1956) [Soviet Physics – JETP 3, 3, 334 (1956)].

Chukhlantsev, V. G. and Stepanov, S. P., "Solubility of Uranyl and Thorium Phosphates," J. Inorg. Chem. 1, 3 (1956).

Shavrova, N. N., "Note on the Radium Content of Lavas From Volcanoes of the Klyuchevskaya Group," Bull. Vulcanol. Station, Acad. Sci. USSR 1956, No. 24.

Shapiro, I. S. and Estulin, I. V., "The Electric Charge of the Neutron" (letter to the editor), J. Exptl.-Theoret. Phys. 30, 3 (1956) [Soviet Physics – JETP 3, 4, 626 (1956)].

V. S.

ERRATA

In issues No. 2 and No. 3 of The Soviet Journal of Atomic Energy, the following mistakes in the original text were repeated in the C. B. translation:

No.	Page	Line	Reads	Should read
2	172	8 from bottom	...for approximately 5% of the total energy ...	...for approximately 50% of the total energy...
3	373	Formula 6	$t_{sing} = z_{sing} t_{sing} \simeq 1.8 t_1$	$t_{sing} = z_{sing} t_1 \approx 1.8 t_1$
		Formula 8	$t_1 = 0.5 a_0 (p_0 \mu)^{1/2} i^{-1/2}$	$t_1 = 0.05 a_0 (p_0 \mu)^{1/4} i^{-1/2}$
		Formula 9	$t_{sing} = 0.09 a_0 (p_0 \mu)^{1/2} i^{-1/2}$	$t_{sing} = 0.09 a_0 (p_0 \mu)^{1/4} i^{-1/2}$
		Formula 10	$I_{sing} = 0.09 a_0 (p_0 \mu)^{1/2} i^{-1/2}$	$I_{sing} = 0.09 a_0 (p_0 \mu)^{1/4} i^{-1/2}$
3	398	7 from top	...discharge current density. But X-radiation...	...discharge current density. In conclusion we will note that S. Cousins and A. Ware [Proc. Phys. Soc. 64 B, 159 (1952)] also observed a sharp change in the structure of the discharge, accompanied by breaks in the current curve, during discharge in various gases. But X-radiation was not observed.
3	383	footnote	blank	The equation below was omitted in the C.B. translation. $\int_0^{t_0} i(t) U(t) dt = W_0.$

CONTENTS (continued)

SOVIET JOURNAL OF ATOMIC ENERGY NUMBER 4, 1956

CONTENTS

(continued on inside back cover)